

UNIVERSITY OF CALIFORNIA  
RIVERSIDE

Sound Localization by the Pallid Bat, *Antrozous pallidus*

A Dissertation submitted in partial satisfaction  
of the requirements for the degree of

Doctor of Philosophy

in

Neuroscience

by

Dustin H Brewton

September 2018

Dissertation Committee:

Dr. Khaleel Abdulrazak, Chairperson

Dr. Jun-Hyeong Cho

Dr. Peter Hickmott

Copyright by  
Dustin H Brewton  
2018

The Dissertation of Dustin H Brewton is approved:

---

---

---

Committee Chairperson

University of California, Riverside

## Acknowledgments

The text of this dissertation, in part, is a reprint of the material as it appears in Brewton *et al.*, 2016. The co-author, Khaleel Razak, directed and supervised the research. Co-author(s) Jamiela Kokash performed experiments, and Jamiela, Oliva Jimenez, and Eloy Rosales-Pena helped with the data analysis. In addition, the figures and text of Chapter 4 are also, in part, a reprint of material as it appears in Razak *et al.* 2015. The co-authors, Khaleel Razak and Stuart Yarrow, directed and supervised the research and performed the data analysis. Figure 1.3B is reprinted from Fuzessery, Z. M. Monaural and binaural spectral cues created by the external ears of the pallid bat. *Hear. Res.* **95**, 1–17 (1996), with permission from Elsevier. Figure 1.6 is reprinted in part from Razak, K. A. Systematic representation of sound locations in the primary auditory cortex. *J. Neurosci.* **31**, 13848–59 (2011), with permission from the Society for Neuroscience. Figure 1.7, 1.8, and 4.1-4.6 are reprinted from Razak, K. A., Yarrow, S. & Brewton, D. Mechanisms of Sound Localization in Two Functionally Distinct Regions of the Auditory Cortex. *J. Neurosci.* **35**, 16105–15 (2015), with permission from the Society for Neuroscience. Chapter 6 is reproduced in its entirety from the publication, Brewton, D., Kokash J., Jimenez O., Pena E. R. and Razak K. A. Age-Related Deterioration of Perineuronal Nets in the Primary Auditory Cortex of Mice. *Front. Aging Neurosci.* **8**, 270 (2016), under the Creative Commons license.

I also want to personally acknowledge several people that were essential to me reaching this goal.

With me every step of the way were all my siblings. Thank you to my older sister, Rachael, for always setting an example to aspire to. And to my younger siblings, Austin and Summer, I hope you can learn half as much from me as I learned from her. Always work hard, be ambitious, and believe in yourself. Good things will come.

To Hailey, thank you for your support through the years, for helping me laugh, especially during the hard times, and for staying by my side through thick and thin.

To my roommates and friends, Teresa and Maggie, thanks for putting up with the late-night practice talks, dealing with/helping take care of FITC, and for binging all of our favorite TV shows together.

To everyone in the Razak lab, Teresa, Kevin, Sarah, Jonny, Anna, Jeff, Brad, Jamiela, Stephen, Katherine, Oliva, Eloy, Victoria, and Max, thanks for the good times. Working with you all made the time fly. It's going to be hard to work anywhere else thanks to how much fun we had in the Razak lab.

When I reflect on my education through the years, I am often dumbstruck by the quality of teachers and mentors I've had. This dissertation is not possible without all of them. I'd like to single out Mr. and Mrs. Alan and Cathy Hays, my high school math and science teachers. Your passions for math and science captivated me and led me down this path. Thank you for sharing that.

Finally, this dissertation wouldn't be complete without the acknowledgement of my advisor, Khaleel Razak. I couldn't ask for more from an advisor. Thank you for including me in this series of fascinating discoveries and for your support throughout.

## Dedication

This dissertation is dedicated to my parents, Shay and Raylene, and to my grandmother, Ula. Thank you for your unending patience, love, and support. Without your constant guidance, I would not have been successful in my pursuit of this degree. The accomplishments represented by this dissertation are yours as much as they are mine.

## ABSTRACT

Sound Localization by the Pallid Bat, *Antrozous pallidus*

by

Dustin H Brewton

Doctor of Philosophy, Graduate Program in Neuroscience  
University of California, Riverside, September 2018  
Dr. Khaleel Abdulrazak, Chairperson

While the auditory cortex is necessary for sound localization, we do not yet know the underlying mechanisms that lead to the behavior. To address this gap, we have designed and executed a series of experiments aimed at describing the neuroethology of sound localization in the pallid bat, an animal which relies on passive hearing of prey-generated noise when foraging. We have made three primary discoveries. First, we have discovered how the external ear filters incoming sounds before they reach the sensory epithelium. Low frequency spectral notches, important for the perception of sound source elevation, depend on the presence of the conspicuous tragus. Second, we developed a sound localization task to test the behavior of the pallid bat. Pallid bats demonstrate remarkable sound localization acuity of  $\sim 4^\circ$  near the midline, and we show that the high frequency range of prey-generated noise (20-30 kHz) is the predominant bandwidth used for azimuth localization. Last, we describe the 2D spatial selectivity of auditory cortex neurons and propose a population code for 2D sound localization. Our data suggests that the extent of active cortex is constrained systematically by the horizontal and elevational sound source direction. We describe preliminary results that indicate the chemogenetic

inhibitory DREADDs system is a viable method for answering questions about the necessity of these auditory cortex populations to sound localization behavior.

Collectively, the research contained in this dissertation provides insight into the way the auditory system is able to compute representations of external space from sound filtered by the external ear and supports the notion of the pallid bat as a viable model from which basic understandings of mammalian sound localization can be obtained.

## Table of Contents

### Chapter 1

#### Introduction

Introduction.....	1
References.....	24

### Chapter 2

#### The Tragus of the Pallid Bat is Necessary for Spectral Cues That Vary with Sound

##### Source Elevation

Abstract.....	30
Introduction.....	31
Methods.....	34
Results.....	40
Discussion.....	59
References.....	67

## Chapter 3

### Accurate sound localization behavior in a gleaning bat, *Antrozous pallidus*

Abstract.....	71
Introduction.....	72
Methods.....	75
Results.....	82
Discussion.....	92
References.....	101

## Chapter 4

### Bicoordinate Space Encoding by Neurons in the Pallid Bat Auditory Cortex Abstract

Abstract.....	105
Introduction.....	106
Methods.....	107
Results.....	113
Discussion.....	114
References.....	125

## Chapter 5

### Preliminary Studies for Validating Chemogenetic DREADDs in the Pallid Bat

Abstract.....	128
Introduction.....	129
Methods.....	131
Results.....	138
Discussion.....	152
References.....	159

## Chapter 6

### Age-Related Deterioration of Perineuronal Nets in the Primary Auditory Cortex of Mice

Abstract.....	164
Introduction.....	165
Methods.....	167
Results.....	174
Discussion.....	189
References.....	195

## Chapter 7

Conclusions.....	201
------------------	-----

## List of Tables

### Chapter 2: The Tragus of the Pallid Bat is Necessary for Spectral Cues That Vary with Sound Source Elevation

Table 2.1: Regression analyses for elevation vs. first notch frequency.....	56
-----------------------------------------------------------------------------	----

### Chapter 3: Accurate sound localization behavior in a gleaning bat, *Antrozous pallidus*

Table 3.1: Percent of correct responses as a function of sound source location...	88
-----------------------------------------------------------------------------------	----

Table 3.2: Mean degrees of error as a function of sound source location.....	88
------------------------------------------------------------------------------	----

### Chapter 6: Age-Related Deterioration of Perineuronal Nets in the Primary Auditory Cortex of Mice

Table 6.1: Mice in each group for the IHC procedure.....	176
----------------------------------------------------------	-----

Table 6.2: Strain specific effects of aging on inhibitory network structures.....	190
-----------------------------------------------------------------------------------	-----

## List of Figures

### Chapter 1: Introduction

Figure 1.1: Pallid bat behavior and auditory cortex organization.....	4
Figure 1.2: Spectral cues generated by the external ear of the pallid bat.....	7
Figure 1.3: IID contours and spectral notches.....	10
Figure 1.4: Auditory pathway for binaural cues.....	11
Figure 1.5: Binaural cluster selectivity.....	13
Figure 1.6: Inhibitory threshold map in the EI cluster.....	14
Figure 1.7: Spatial receptive fields of EI cluster neurons.....	18
Figure 1.8: Model of bicoordinate space encoding in the pallid bat cortex.....	21

### Chapter 2: The Tragus of the Pallid Bat is Necessary for Spectral Cues That Vary with Sound Source Elevation

Figure 2.1: HRTF sound presentation apparatus.....	36
Figure 2.2: HRTF experimental setup and tragus position.....	38
Figure 2.3: Example HRTF.....	41
Figure 2.4: Example DTF-E.....	42
Figure 2.5: DTF-E and DTF-A.....	44
Figure 2.6: Spectral notch maps in the normal condition.....	47

Figure 2.7: DTF-E of the $HRTF_n$ and the $HRTF_{tr}$ .....	48
Figure 2.8: Notch maps of the $HRTF_n$ and the $HRTF_{tr}$ .....	53
Figure 2.9: Correlation between elevation and notch center frequency.....	55
Figure 2.10: The $HRTF_d$ shows the effect of the tragus in the DTF-E.....	57
Figure 2.11: The $HRTF_d$ shows the effect of the tragus in the DTF-E, example 2...58	

### Chapter 3: Accurate sound localization behavior in a gleaning bat, *Antrozous pallidus*

Figure 3.1: The sound localization speaker array and head orientation measures.	83
Figure 3.2: Confusion matrices for individual bats.....	86
Figure 3.3: Pallid bat sound localization performance at the midline.....	87
Figure 3.4: Effects of sound duration on localization behavior.....	89
Figure 3.5: Effect of sound bandwidth on localization behavior.....	91

### Chapter 4: Bicoordinate Space Encoding by Neurons in the Pallid Bat Auditory Cortex

#### Abstract

Figure 4.1: Example SRF of an NSR neuron.....	115
Figure 4.2: NSR SRFs are stable with increasing sound intensity.....	118
Figure 4.3: SRF centroid and gyradius vary with characteristic frequency.....	120
Figure 4.4: Correlations between centroid elevation/azimuth and CF.....	122
Figure 4.5: Proposed model of bicoordinate spatial encoding by NSR neurons.	123

Figure 4.6: Model of 2D space encoding in the pallid bat cortex.....	124
Chapter 5: Preliminary Studies for Validating Chemogenetic DREADDs in the Pallid Bat	
Figure 5.1: rAAV2- and rAAV9-GFP expression in pallid bat auditory cortex..	141
Figure 5.2: rAAV8-GFP expression after two injection volumes.....	143
Figure 5.3: rAAV8-hM4Di-mCherry expression in pallid bat auditory cortex...	144
Figure 5.4: GFAP IHC stain in the pallid bat and mouse auditory cortices.....	146
Figure 5.5: Pallid bat ERP signal.....	151
Figure 5.6: CNO injections do not affect the pallid bat ERP signal.....	153
Figure 5.7: CNO injections do not affect pallid bat behavior.....	155
Chapter 6: Age-Related Deterioration of Perineuronal Nets in the Primary Auditory Cortex of Mice	
Figure 6.1: Example PV+, PNN+, and PV/PNN+ cells.....	177
Figure 6.2: Example cortical images showing the PV and PNN channels.....	179
Figure 6.3: Cell density changes between strains and age groups.....	181
Figure 6.4: Cell density changes with age in deep and superficial layers.....	182
Figure 6.5: Example PNN images for analyzing whole cortex PNN intensity....	184
Figure 6.6: PNN intensity changes with age, strain, and cortical layer.....	186
Figure 6.7: PNN cell intensity changes with age.....	187

Figure 6.8: Cell type specific changes in PNN intensity.....	188
--------------------------------------------------------------	-----

## **Chapter 1**

### **Introduction**

An important function of the auditory system is to localize sound sources. Upon their emergence approximately 200 million years ago as primarily nocturnal organisms, mammals have been especially reliant on sound localization. For most mammals, it is essential for basic survival tasks, such as finding prey, avoiding predation, and locating a mate. Expectedly, sound localization is essential to humans, whether the task is determining dimensions of enclosed spaces or communicating in a crowded and noisy environment<sup>1</sup>. Presently, there is a need to systematically examine sound localization mechanisms underlying the extraction of source location in mammals, as the cortical mechanisms are only beginning to be understood.

Unlike other sensory systems, locations of sound sources in space must be computed at the level of the brain, as a spatial representation does not exist at the output of the sensory epithelium, the cochlea. The mammalian auditory system computes information about sound locations by using the relative intensity and/or onset and ongoing time/phase differences of an impinging sound at the two ears, the location dependent frequency filtering properties of the pinnae, and frequency sensitivity. Thus, investigating the mechanisms of sound localization provides a unique context to study how central and peripheral adaptations interact to shape neural computations. The primary focus of this chapter is on how the external morphology of the auditory system generates the cues relevant to sound source localization and how selectivity for the cues at the level of the auditory cortex is achieved to generate maps of auditory space in the

cortex. We will specifically focus on recent findings in the pallid bat to exhibit how at least one auditory system has solved these issues.

The pallid bat is a desert-dwelling bat, whose range extends from Mexico to British Columbia and as far east as Oklahoma and Cuba. Within this range, pallid bats are often found roosting in rock crevices, in man-made buildings, and beneath bridges. These roosts sites are usually near arid, open environments with a nearby water source. These characteristics are typical for pallid bat foraging grounds<sup>2</sup>. The pallid bat requires open space for foraging, because, unlike most Vespertilionid bats, it relies on prey-generated noise transients (crickets or scorpions walking/rustling on the ground, 5-35 kHz broadband noise (BBN)) to localize and hunt for food (Figure 1.1A). This task is much more difficult in a cluttered environment, hence the desire for an open habitat. Vespertilionid bats are often capable of hunting strictly with echolocation (aerial hawkers). They also have exhibited flexibility in foraging strategy, using either aerial hawking or gleaning when convenient<sup>3</sup>, or combining the behaviors to improve foraging success<sup>4</sup>. In fact, the pallid bat appears to strictly use echolocation (60-30kHz downward FM sweep) for obstacle avoidance and prefers the passive listening for noise transients while hunting<sup>5</sup> (Figure 1.1.1A).

Such gleaning foraging behavior necessitates highly accurate sound localization abilities. But the precision with which the pallid bat localizes sounds in 2D remains unclear and forms a major aim of this dissertation. My studies show that the pallid bats can localize sound sources in the azimuth plane within 2-5 degrees<sup>6,7</sup> (see chapter 3 of this dissertation), placing them among the most accurate sound localizers in the animal

kingdom<sup>8</sup>. Within the pallid bat auditory system, and more specifically within the primary auditory cortex, the neurons selective for echolocation sounds and noise transients are segregated in two different fields<sup>9-11</sup>. Further investigation into the characteristics of the noise selective neurons has revealed specializations for sound source location encoding<sup>12,13</sup> (see chapter 4 of this dissertation). In addition, the filtering properties of the pallid bat external ear have been examined to elucidate cues that the bat may use in localizing sound sources, especially with respect to elevation<sup>14</sup> (see chapter 2 of this dissertation). Together, these studies set the foundational work required to achieving a comprehensive understanding of one mammal's sound localization system, from neuron to behavior.

### **Cues Used in Localizing Sound Sources**

Sound stimuli must first be transferred from the external environment into the cochlea of the listener. This process is accomplished by way of the one-dimensional movement of the tympanum, whether the sound is as simple as a pure tone or as complex as a symphony ensemble. Inputs at each ear are transduced by the hair cells that run along the basilar membrane within the cochlea. This structure is organized such that distinct portions resonate when impacted with distinct frequencies. From nearest the tympanum (base) to furthest from the tympanum (apex), the membrane resonates from high to low frequencies. It is therefore arranged tonotopically. This tonotopic arrangement is maintained throughout the lemniscal auditory pathway, from the cochlea to the primary

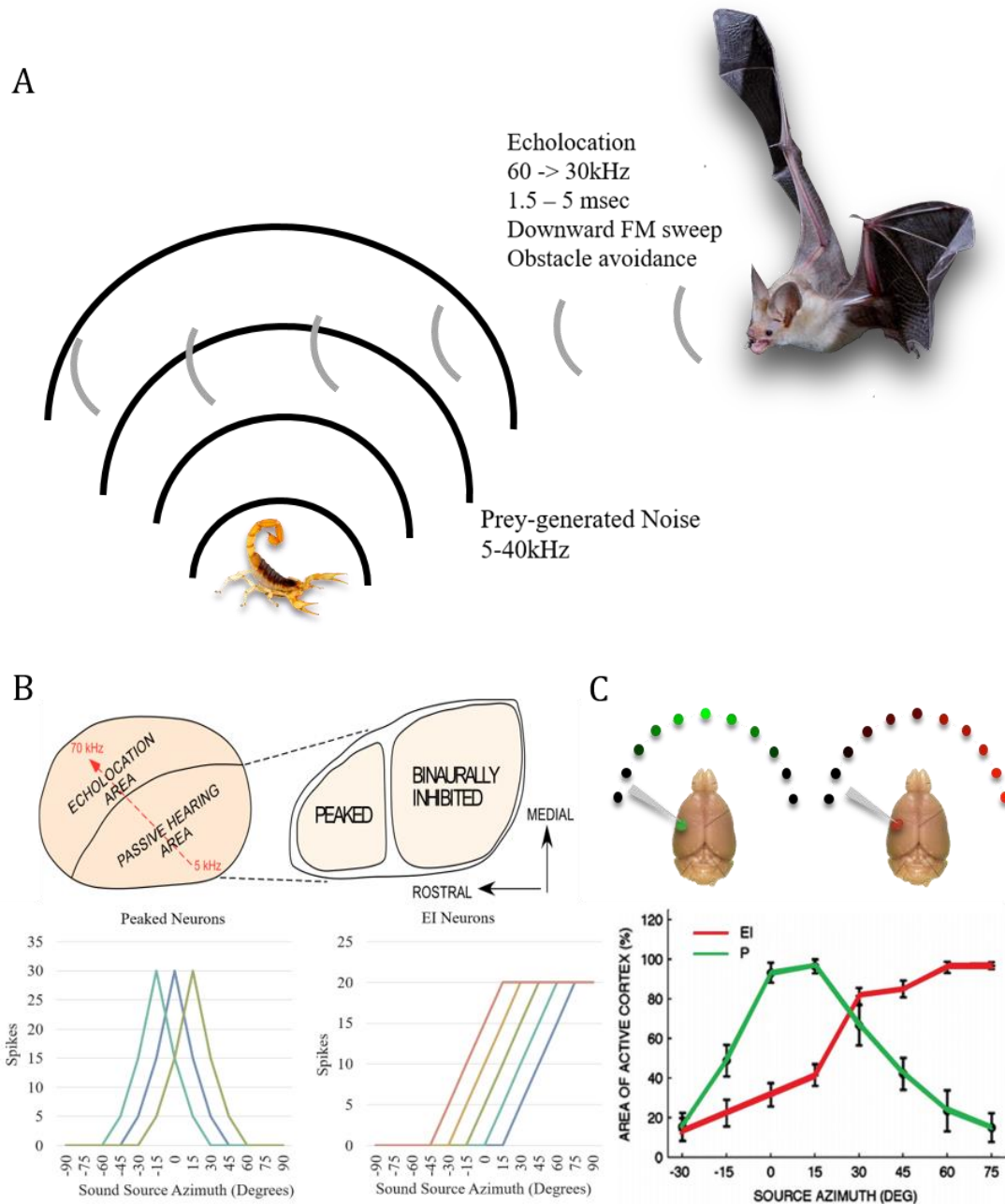


Figure 1.1.<sup>10,12,13</sup> **(A)** Pallid bats echolocate for obstacle avoidance and hunt by listening to prey-generated noise in the low frequency range (5-40kHz). **(B)** The low frequency noise-selective region (NSR) of the pallid bat A1 contains two binaural clusters, distinguished by their IID selectivity. **(C)** The regions are further distinguished by their spatial encoding. The peaked cluster is increasingly active (green) for sound sources near the midline (0° azimuth), while the EI cluster activity (red) increases for sounds in increasingly more contralateral loci.

auditory cortex. Representations of space are then computed in the central auditory system by first integrating inputs from each ear onto neurons residing in the brainstem.

Two main analyses of the waveforms transduced at the cochlea are performed to facilitate sound localization<sup>15</sup> (Figure 1.1.2). The first is the comparison of the differences in the movement of the two tympanums. Timing and intensity differences are encoded this way (Figure 1.1.2A), however, in the case of the mammals that use high frequency sounds, the predominant cue utilized for sound localization on the horizon (or azimuth) is the interaural intensity difference (IID)<sup>16</sup>. At frequencies with wavelengths shorter than the width of the head, the head will attenuate sound such that a difference in the intensity at each ear is present, i.e. the ear further from the sound source will pick up a lower intensity version of the same sound<sup>17</sup>. Dichotic stimulation tasks indicate that IIDs are essential for normal sound localization in the azimuthal plane<sup>18</sup>.

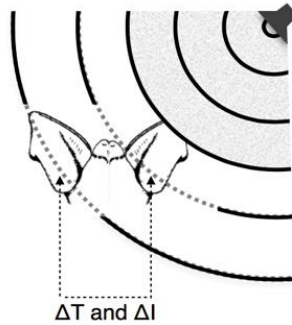
The second cue used for localizing sound sources on the horizontal plane is the interaural phase difference (IPD). When a sound contains mostly low frequencies, the IIDs produced are much less pronounced. IPDs are a useful cue to mammals in such circumstances<sup>16</sup>. This segregation of cues into distinct frequency ranges is the basis of the duplex theory of sound localization, which states that IPDs and IIDs are used for low and high frequencies sounds, respectively<sup>16,17</sup>. An IPD is the measure of the shift the waveform at the near ear must be applied to match the waveform reaching the right ear in time. This is, in effect, the difference in the onset of the sound at either ear, which can theoretically be sampled by the auditory system at various phases throughout the duration of the sound. Maximal usefulness of IPD cues is limited, in part, by head size and

frequencies that can be phase locked to in the auditory system. Only when the distance between the ears is large is there enough time for appreciable IPDs to occur. While IPDs are used in the mammalian localization of sound sources<sup>19</sup>, these cues are thought to be secondary to the IID cues for sound localization for most small mammals that tend to use much higher frequencies. For a bat of similar size to the pallid bat (big brown bat, *Eptesicus fuscus*), the distance between the ears is only enough to produce an IPD of ~50  $\mu$ s at the most peripheral locations. Also, the repertoires of behaviorally relevant sounds bat species are exposed to have relatively high frequency content, including prey generated noises and their echolocation calls, rendering IPDs less useful. For these reasons, mechanisms underlying onset IPD selectivity and their role in encoding acoustic space in mammals are not addressed here (see <sup>16</sup> for review covering IPD processing).

There are obvious limitations to the use of IIDs when considering the localization of sound sources on the vertical plane. Consider a sound source along the median plane, which is the vertical plane intersecting the horizontal plane directly in front of the organism. At any point along this vertical line, IIDs would be approximately constant, and therefore provide no help to the organism's ability to localize the sound accurately. The same can also be said of any single elevational plane intersecting the horizon at a right angle, as IIDs do not vary significantly with elevation or within the "cone of confusion"<sup>20</sup>.

The second analysis performed by the auditory system to build a representation of external space is a comparison of the sound energy across separate bandwidths. This process serves to resolve locations in the vertical axis. When a sound is transferred from

### A. IID and ITD cues



### B. Spectral cues

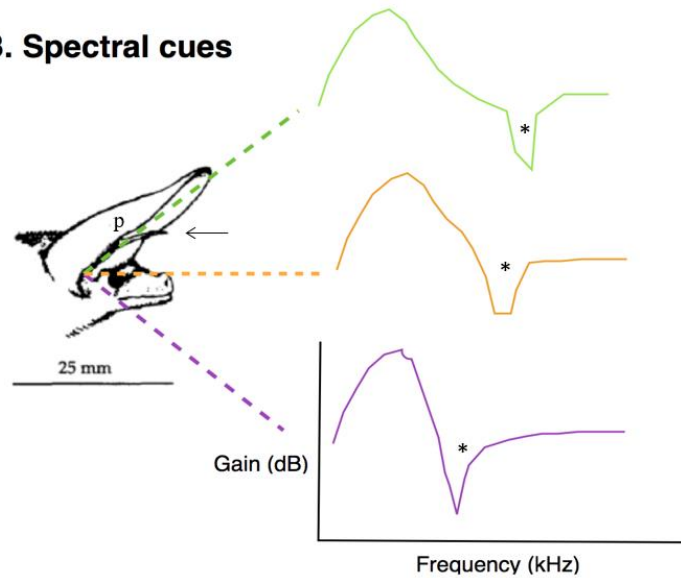


Figure 1.2. The head and external ears create cues indicative of sound source position in the horizontal and vertical planes (**A.**) If a sound source is off the median plane, binaural cues are generated by the difference in the time ( $\Delta T$ ) and intensity ( $\Delta I$ ) of the impinging sound at the two ears. In this example, the right ear of the pallid bat will receive the sound first, while the left ear will receive the sound after some time delay. The left ear will also receive a softer sound, as the head of the animal will attenuate frequencies with wavelengths smaller than the width of the head. (**B.**) Frequency-specific attenuations, or notches, (*asterisks*) are produced by the external ear of the pallid bat. The pinna (p) and tragus (*arrow*) of the external ear can be seen clearly. Gain is the net effect of the ear, and sharp drops in gain are the spectral notches. The center frequency of a notch increases with increasing elevation.

the source to the eardrum, transformations in the spectrum of a sound are generated by the filtering properties of the external ear. This filtering is described by the head-related transfer function (HRTF), and the cues generated are referred to as spectral cues<sup>15,21,22</sup>. It is thought that the predominant spectral cues for localization are notches, or attenuations in a specific frequency range. The center frequency and magnitude of these cues is dependent on the spatial direction (more importantly, elevation) of a sound source<sup>23</sup> (Figure 1.2B). Generally, center frequency of the spectral cues increases with elevation of the sound source<sup>24–27</sup>. Each ear produces these cues individually (monaural), as opposed

to production via the relative sensation at the two ears (binaural). The pinna and the tragus, which form the entire external ear structure (Figure 1.2B), have been implicated in the production of these cues<sup>14,26,28,29</sup>. Importantly, both the external ear structures and the spectral cues they produce are necessary for normal vertical sound localization. The removal of notches from the sound source<sup>30–32</sup> or different parts of the external ear<sup>33–38</sup> impact normal sound localization in the vertical axis.

Much like the other mammals, pallid bat external morphology generates significant IIDs and spectral cues<sup>14</sup>. In this study, a microphone replaced the tympanum of one ear and was sealed into the ear canal. Intensity values picked up by the microphone when pure tones were played across the frontal space in this condition were compared to measurements of the same sounds and locations with only the microphone (without the bat). Measurements of gain due to the head and external ears were made by subtracting the two measured voltages. From these data, estimations of the IIDs and the spectral cues generated by the external ear were calculated. For IID cues, it was found that significant IIDs (>24 dB) were generated at the extremes of the frontal sound field (60 degrees azimuth), while the IID produced reduced as the sound source moved toward the midline (Figure 1.3A). This plot also demonstrates the greater dynamic range and utility of IIDs at higher frequency. Notice the greater number of contours and narrower regions of highest IIDs in the higher frequency plots (20–35 kHz). For each sound source location, the frequency at which the first notch was produced was plotted to demonstrate the spatial distribution of the first notch frequency. In the pallid bat, each ear generates first notch frequency contours, which extend roughly horizontally

from the midline in ipsilateral space (Figure 1.3B). This frequency value shifts upward with increasing elevation, spanning the bandwidth of the typical broadband noise signal these animals are exposed to in the wild while foraging. These data lead to predictions about the frequency dependence of sound localization ability in pallid bats. For instance, we hypothesized pallid bats would localize sounds with high frequency energy better than those with low frequency (see chapter 3 for results).. While the tragus is thought to be important in generating spectral cues, and is quite prominent in the pallid bat, the cues generated by the tragus remain unclear. Therefore, we examined whether the pallid bat tragus would affect the pattern of notches observed in the HRTF (see chapter 2 for results)

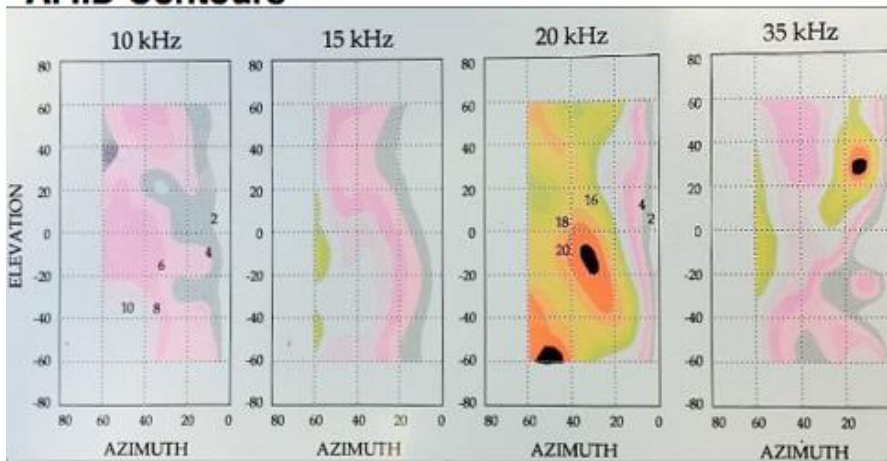
In the following sections, the way the central auditory system processes the cues generated by the external structures is discussed, with an emphasis on cortical involvement and the relevance of recently identified maps therein<sup>12,13,39</sup>.

## **Cortical Mechanisms of Sound Localization**

It is well established that the auditory cortex is necessary for optimally localizing sound sources in both the horizontal and vertical planes<sup>40–45</sup>. Recently, studies of the neurophysiological mechanisms involved in this process have advanced our hypotheses on how the cortex contributes to sound localization behavior.

### *i. IID and Azimuth Selectivity*

## A. IID Contours



## B. Notches

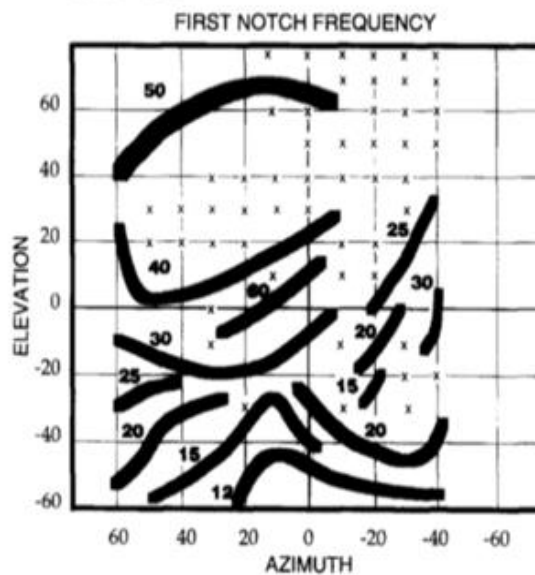


Figure 1.3.<sup>14</sup> Spatial cues generated by the external ears and head of the pallid bat (A.) IID contours of the pallid bat ipsilateral hemifield. Space plots indicate the spatial distribution of IID cues received by the ipsilateral ear. The magnitude of the IID is shown by the color scale, with white values representing minimum values and increasing dark values representing larger IIDs. Adjacent contours are 2 dB difference in IID value, with a general trend of increasing IID value with increasingly peripheral sound source. Darkest spots are areas of maximal IIDs (>24 dB). At higher frequencies (20 and 35 kHz), IID cues shift systematically with elevation as well. (B.) Spectral notches generated by external ear structures are plotted as a function of space. Transfer functions recorded at a single ear tympanum were analyzed to find the frequency at which the first notch occurred in each spatial location. Lines indicate continuity of notches within a range of frequencies (50=50-59 kHz notches). Notches do not appear in every sound location tested (x), though this could be a product of the resolution of testing methods.

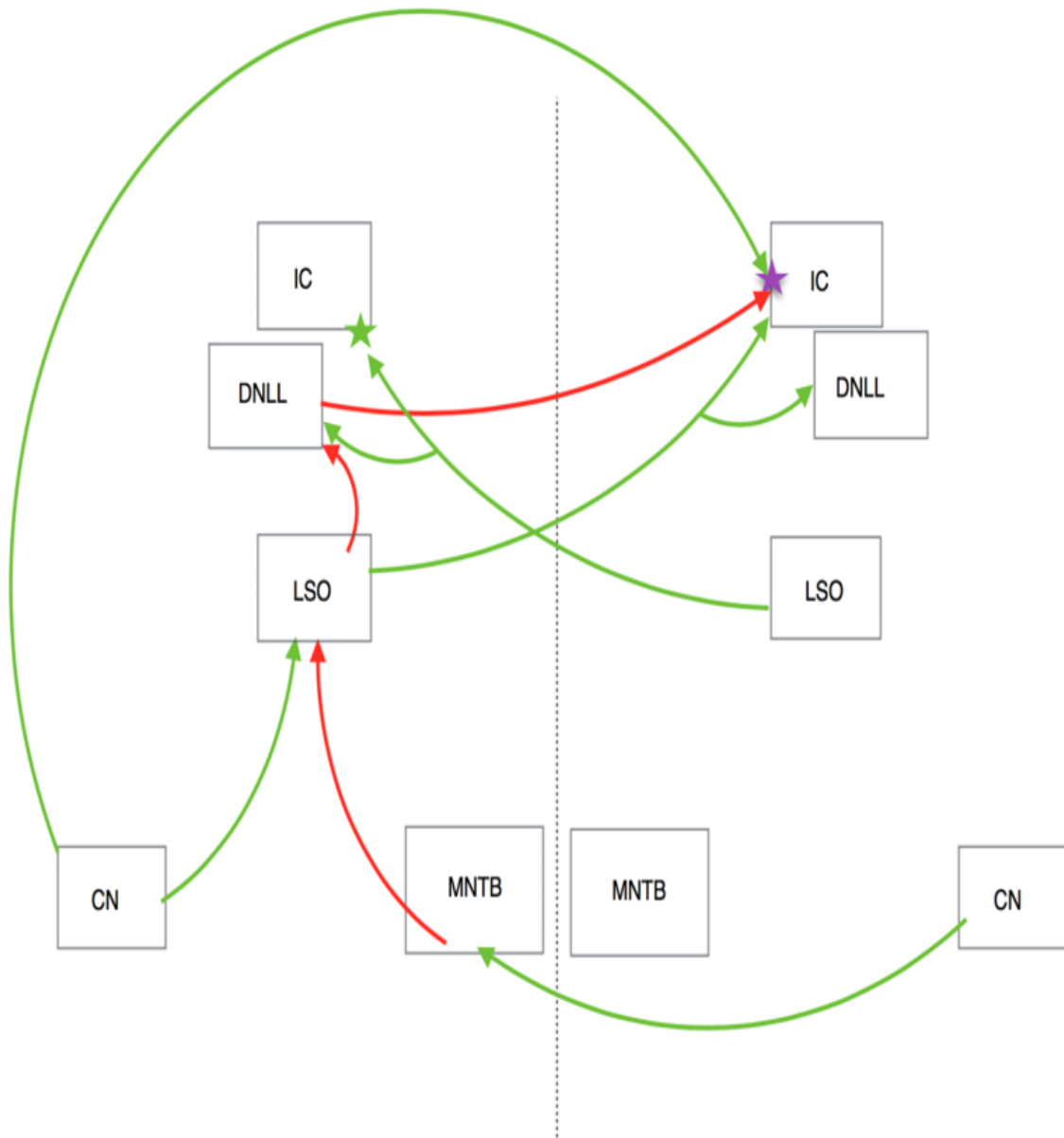


Figure 1.4. Creation of binaurally selective subcortical neurons. Green arrows represent excitatory projections, and red arrows indicate inhibitory projections. The LSO is the initial site of binaural activity, and the IC both inherits (green star) and produces de novo (purple star) binaurally selective neurons, indicating binaural selectivity is generated at more than one location along the auditory pathway. Abbreviations: CN: Cochlear Nucleus; MNTB: Medial Nucleus of the Trapezoid Body; LSO: Lateral Superior Olive; DNLL: Dorsal Nucleus of the Lateral Lemniscus; IC: Inferior Colliculus.

Before discussing the cortical data, let us first briefly address subcortical processing of binaural cues (Figure 1.4). As inputs from either ear are transmitted into the central auditory system, the location at which they are first combined, and therefore the initial site of binaural processing, is in the superior olivary complex (SOC)<sup>16</sup>. Specifically, IID processing is first begun at the lateral SOC (LSO). Here, convergence of excitatory inputs from the ipsilateral cochlear nucleus (CN) and inhibitory inputs from the contralateral CN via the medial nucleus of the trapezoid body (MNTB) create sigmoid shaped selectivity pattern for IIDs in individual neurons. When a sound is louder in the ear ipsilateral to the LSO, the neuron is more active and increasingly less active as IID begins to favor the contralateral ear (excitatory/inhibitory (EI) cells). The IID at which the neuron ceases responding varies from neuron to neuron within the LSO, such that the selectivity of neurons in this region span a range of IIDs, and therefore a range of horizontal space<sup>46,47</sup>. These neurons then relay this response pattern to the contralateral inferior colliculus (IC). About half of the EI neurons in the IC appear to inherit their selectivity pattern directly from the LSO in this way, while the other half enhance IID selectivity via local inhibition<sup>48,49</sup>. Together, these mechanisms generate a systematic arrangement of IID selective neurons. Neurons selective for IIDs favoring the ear contralateral to the IC are located ventrally, and neurons with increasing selectivity for IIDs favoring the ipsilateral ear are located dorsally, making this the likely initial site of a space map for auditory stimuli<sup>47,50</sup>. The superior colliculus contains a precise representation of horizontal space, with specific positions encoded by distinct subpopulations of neurons<sup>51</sup>.

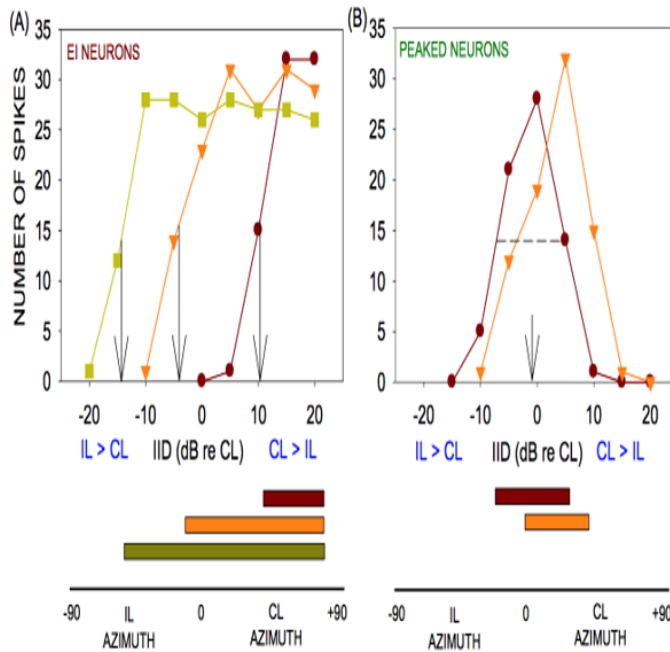


Figure 1.5.<sup>12</sup> Contralateral (CL) and ipsilateral (IL) are relative to the cortical hemisphere recordings took place in. **(A.)** IID selectivity function of three EI neurons. Arrows indicate the inhibitory threshold, the IID at which response is 50% of the max. Stimuli (5-40 kHz BBN) were presented 20 times to give number of spikes. **(B.)** IID selectivity of 2 peaked neurons. Arrow indicates the best IID of one peaked neuron, near 0 dB. The dashed line represents the 50% IID bandwidth. Below the plots, color-matched bars indicate the predicted azimuth selectivity. Positive azimuth indicates CL location, and vice-versa. CF=15kHz for all neurons.

In the primary auditory (A1) cortex of most mammals, no such organization has been discovered<sup>52-54</sup>. Instead, most A1 neurons are broadly tuned to horizontal space<sup>55-57</sup>. This has led to the current view that horizontal space must be represented by a population code in A1, with no systematic representation of azimuth<sup>58</sup>. Studies of the representation of azimuth in the pallid bat A1 challenge this current view.

Across the range of species tested, one common feature of organization within the auditory cortex is the segregation of neurons with similar binaural tuning into distinct clusters (cat<sup>59</sup>; ferret<sup>60</sup>; mustache bat<sup>61</sup>; pallid bat<sup>10</sup>). The pallid bat noise selective region is made up of two clusters based on their selectivity for IIDs (Figure 1.1B)<sup>10</sup>. The binaurally inhibited neurons in the EI cluster respond to monaural stimuli in the contralateral ear, but not the ipsilateral ear. When stimulated binaurally, these neurons

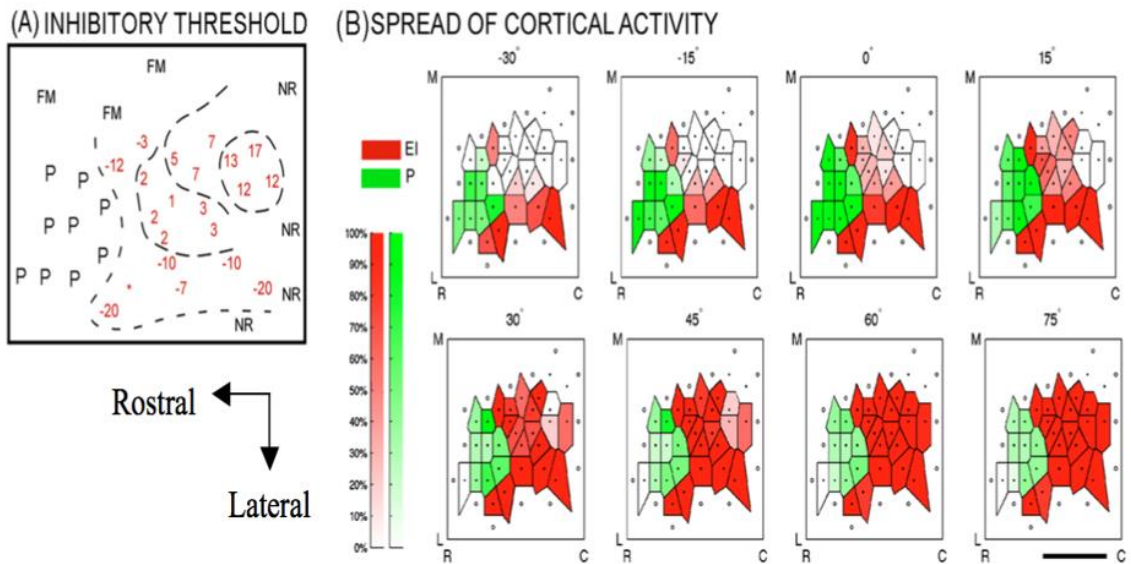


Figure 1.6.<sup>12</sup> (A.) Map of inhibitory thresholds within the NSR of pallid bat A1. Red numbers indicate inhibitory threshold values (dB). Positive (negative) values indicate binaural stimuli that are louder in the CL (IL) ear. Dashed lines delineate the regions of EI neurons with separate inhibitory threshold ranges. FM-echolocation call selective neurons. NR – no response. (B.) Spread of cortical activity when sound is presented in free-field. From top left to bottom right, the panels show the same region of cortex for different sound source locations along the horizon (indicated above the panel). Darker shading indicates more spiking. Green areas are for the peaked cluster neurons, whereas EI cluster neurons are shown in red. M-medial; L-lateral; R-rostral; C-caudal.

spike preferentially to sounds that are louder in the contralateral ear. With increasing

ipsilateral intensity, the response reduces, producing a sigmoid shaped IID selectivity

(Figure 1.5A). The peaked cluster responds best to IIDs near 0 dB (Figure 1.5B), while

responding weakly or not at all to monaural stimuli<sup>62</sup>. Within these binaural clusters,

there are systematic representations of horizontal space<sup>12,39</sup>.

The inhibitory threshold, i.e. the IID value at which neural response falls to 50% of the maximum, can be used to quantify the IID selectivity of EI neurons. At this point, the neuron is providing maximum information about IID<sup>63,64</sup>. Within the EI cluster, there exists a systematic map of inhibitory thresholds, with values decreasing in the

rostromedial direction (Figure 1.6A)<sup>12</sup>. This suggests that when a sound is in the ipsilateral hemifield, a small portion of the rostral EI cluster would be active. If the sound source were to move ipsilateral to contralateral, more neurons in the rostromedial direction would become active while maintaining activity levels in the rostrolateral section. There will be a systematic increase in the active area of the EI cluster. On the other hand, the peaked cluster contains neurons preferentially responding to the midline<sup>65</sup>. As the sound source moves away from the midline, fewer peaked cluster neurons would remain active. This indicates that the peaked cluster may act as an additional representation of midline azimuth.

These findings led to the novel hypothesis that systematic changes in the area of activated cortex within binaural clusters could represent horizontal position of sound sources. Predictions that IID and azimuth selectivity would correlate well were tested and supported<sup>12,39</sup>. In the EI cluster, systematic changes in azimuth from ipsilateral to contralateral locations resulted in systematic increases in the area of activated cortex (Figure 1.6B, red). In the peaked cluster, area of activity increased for azimuths closer to the midline and decreased as the sound source moved to more peripheral locations (Figure 1.6B, green). These data provided the first evidence for the nature of azimuth representation in the cortex.

## *ii. Spectral Cues and Vertical Space Selectivity*

Our knowledge of the mechanisms involved in generating vertical sound localization behavior is relatively limited when compared to mechanisms of horizontal

localization. Most of the literature on subcortical mechanisms for sound localization on the vertical plane and selectivity for spectral cues describes the dorsal cochlear nucleus (DCN) to IC pathway. Type IV neurons of the DCN provide input into the IC onto the type O neurons there. Type IV neurons have a unique response selectivity to auditory stimuli. These cells show a small island of response around their characteristic frequency at or near the threshold intensity. Louder sounds inhibit the cells over a broad frequency range<sup>66,67</sup>. Type II DCN neurons provide this inhibitory input onto the Type IV neurons, while the excitatory inputs are provided by the auditory nerve fibers. Convergence of these inputs results in sensitivity of the Type IV neurons to notched noise, specifically being inhibited by notched noise when the notch center frequency matches the characteristic frequency of the neuron<sup>66</sup>. Type O neurons of the IC receive input from their respective Type IV DCN neurons when stimulated by tones, and thus show the same near-threshold island of activation. However, the response profile of the Type O neuron to notched noise is flipped, with the cells being activated only when notch center frequency is just off the characteristic frequency<sup>66</sup>. The interpretation of this result is that a source of inhibition is present at the level of the IC, but this source requires energy in the just below CF range in order to suppress activity. Due to the pattern of selectivity at the type O unit, it is argued that this pathway is the center for processing the spatially dependent spectral cues generated by the external ear. This selectivity for spectral contrast appears to remain functionally segregated up to the medial geniculate body<sup>68</sup>.

Recent neurophysiological data has provided evidence for a vertical space code in the noise selective region (NSR) of the pallid bat A1<sup>13</sup>. Spatial receptive fields (SRF) of

single units were measured in the NSR by presenting BBN from 55 locations in space and recording the elicited activity. SRF centroid, a measure of the geometric center of the SRF in vertical and horizontal degrees, varies along the tonotopic axis. As the characteristic frequency of a neuron increases, the center of the SRF shifts upward in elevation. Also, for low characteristic frequency neurons, the area of the SRF is greater (Figure 1.7). This suggests that, just as the map in the EI cluster results in a greater active area with movement from IL to CL space, more of the tonotopic map in the noise region is recruited as sound sources move from low to higher elevations.

It is currently unknown how the pallid bat auditory cortex achieves selectivity for vertical space. Because of the spectral cues apparent in the pallid bat head-related transfer function (Figure 1.3B), the assumption is that these cues are essential to maintaining the spatial selectivity. Working under the assumption that the pallid bat central auditory system has a similar pathway for spectral cue processing to the cat Type IV DCN – Type O IC connection, one can hypothesize about how selectivity for vertical spatial positions can be achieved at the level of the cortex, while being guided by the external morphology of the listener. Consider a sound source located below the horizontal midline. At this position, a spectral notch will be generated at a relatively low frequency. The Type O IC neurons with CFs just above this spectral notch center frequency would be activated by this stimulus, leading to the prediction that the corresponding tonotopic region of A1 is being activated, i.e. neurons with CFs just above the generated spectral cue. For a sound coming from above the midline, a higher frequency spectral cue will be generated resulting in a relatively high frequency region of the tonotopic gradient being activated.

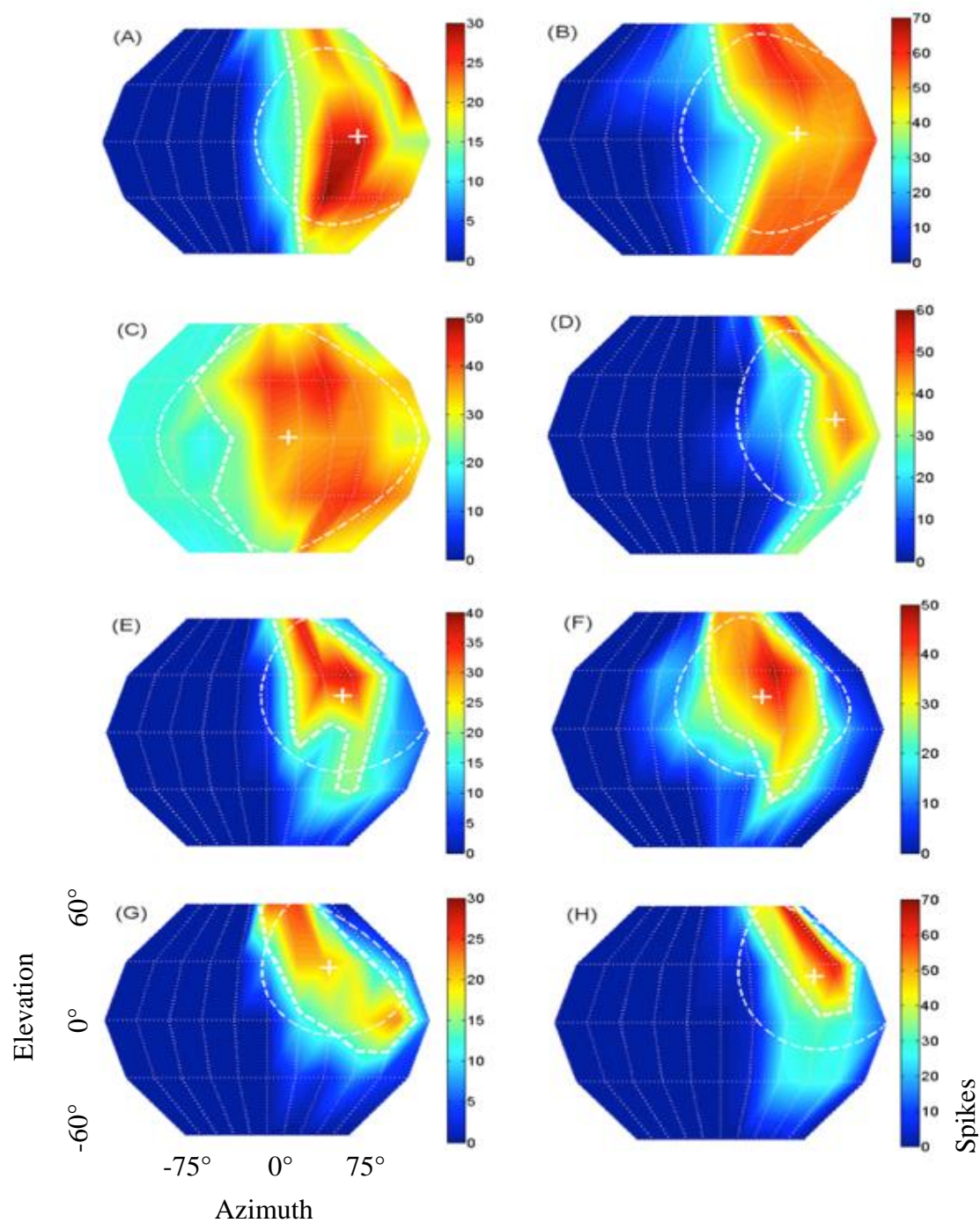


Figure 1.7.<sup>13</sup> SRFs of single unit neurons in pallid bat NSR. From A-H, characteristic frequency is progressively greater. For the low frequency neurons (**A-D**): 12, 18, 18, and 20 kHz CF, respectively), centroid (white +) is relatively low and gyradius (dotted line), a measure of the size of the SRF, is relatively large. For high frequency neurons (**E-H**): 24, 24, 29, and 29 kHz, respectively) the centroid is high and the gyradius is constrained.

Razak et al, 2015 demonstrates that the low frequency neurons are active at the lower elevations and maintain their activity as a sound source moves upward in elevation. At the higher elevations, the entire tonotopic representation in the NSR is recruited into the activity. Combined with the azimuth selectivity data, a more comprehensive picture of cortical selectivity for spatial positions begins to emerge (Figure 1.8). Azimuth selectivity does not vary with characteristic frequency, indicating that the active area of the cortex when a broadband sound is present in the bat's frontal environment is constrained predominantly by sound position<sup>12</sup>. In contrast, the vertical position of the sound source will further constrain activity based on the region of the tonotopic axis that sound source activates. These data predict that elevation, compared to azimuth localization, will suffer more if narrowband noise stimuli are presented.

## **Conclusions and Future Directions**

The study of central auditory system mechanisms underlying sound localization in pallid bats represents a model system that could provide fundamental insight into general mammalian mechanisms of sound localization, as well as general mechanisms of brain processing. While the generation of sound localization cues appears to represent a general feature of mammalian auditory systems, it is unknown how generalizable the cortical mechanisms underlying spatial selectivity are. The IID selectivity exhibited in the

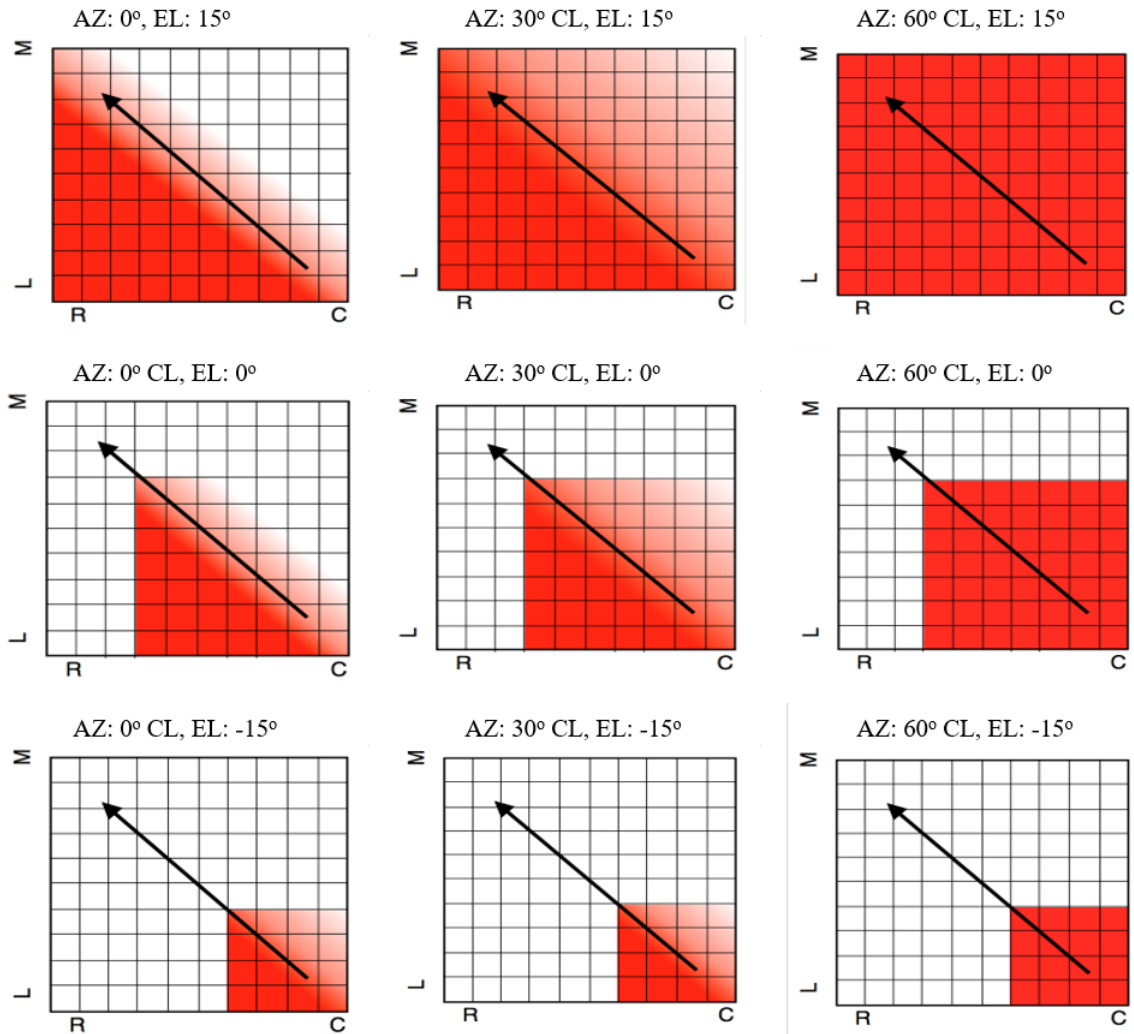


Figure 1.8. Model of a systematic representation of 2-dimensional space via the extent of cortical activity in pallid bat low frequency region EI cluster. Each box is a schematic of the same cortical space activated by the same broadband noise stimulus from different points in space. The location of the sound source is indicated above each box; AZ=azimuth, CL=contralateral, and EL=elevation. L and M indicate the medial-lateral axis. R and C indicate the rostral-caudal axis. Tonotopic axis (diagonal black arrow) extends and increases from the caudal-lateral corner to the rostral-medial corner. Red cells indicate active areas, with the darkest shades of red representing conditions of peak activity for that region of the cortex. From left to right, on any given row, the extent of activity increases perpendicular to the frequency axis (isofrequency axis). From top to bottom, on any given column, one can see that the extent of activity decreases along the tonotopic axis. Thus, the extent of activity in the isofrequency axis indicates sound source in the azimuthal plane (Razak, 2011, 2012), but this activity is further constrained by the vertical location of the sound, indicating a systematic representation of 2-dimensional space.

mustache bat IC indicates that a similar map of acoustic space may exist here <sup>50,69</sup>.

Although conclusions about the presence of systematic representations of space in other mammals differ from those in the pallid bat, these conclusions are based on different methodologies. Until studies on the organization of binaural selectivity are carried out across isofrequency contours, as opposed to within them in other species, one can only speculate about the generality of these mechanisms<sup>12</sup>.

Major gaps in our understanding of sound localization behavior and mechanisms remain to be filled. In the case of the pallid bat, sound localization behavior remains to be explored in detail. Analysis of the localization acuity on an open-loop task has been performed<sup>6,7</sup>, but the approximate cues the bat was receiving during these tasks was unknown, as the head position was unaccounted for. Understanding basic sound localization behavior under more controlled conditions is necessary for subsequent investigations into the specific roles the distinct cortical clusters contribute to sound localization. This was the main goal of chapter 3 in the dissertation. Tests for the necessity of the peaked cluster to localizing sounds arriving from near the midline and for the EI cluster to accurate localization of peripheral sounds can be performed by lesioning or inactivating individual clusters.

Additionally, the mechanisms underlying the pallid bat's representation of vertical space are relatively unexplored. HRTFs of the pallid bat frontal sound field need to be generated with external ear structures intact and removed to fully understand the specific contributions they are making to the generation of these cues. This was the main aim of chapter 2 in the dissertation. Even knowing that spectral cues are systematic across the

vertical axis and generated by the external ear features will not determine whether the bat relies on these cues for accurate localization behavior. Assessment of vertical localization behavior following external ear morphology manipulations or filtering of the stimulus will inform about the necessity of these cues. Subsequent investigations into cortical spatial receptive fields following the same manipulations will give insight into the way in which external morphology can shape neural processing. Because we know that external ear morphology generates cues on the vertical plane, and that a representation of space exists along the systematic tonotopic axis, this area of exploration provides for very specific hypotheses to be tested from the level of cortical selectivity to behavioral performance. This connection between structure and function of the auditory system represents a general model system through which broader understanding of brain function can be obtained.

Based on this short review of the literature, the main aims of my dissertation were to learn the spatial cues generated by the external ear features of the pallid bat (Chapter 2), demonstrate behavioral accuracy on sound localization tasks (Chapter 3), and measure the 2D spatial selectivity of auditory cortex neurons (Chapter 4). A minor aim of this dissertation focused on the development of genetic manipulation techniques in pallid bats, serving to further our goals of determining the role of the auditory cortex in sound localization behavior (Chapter 5). In addition to the primary objectives of this dissertation, I describe the changes to inhibitory structures in the auditory cortex of normal aged mice (CBA) and mice aged with accelerated hearing loss (C57) (Chapter 6).

1. Blauert, J. Spatial hearing with multiple sound sources and in enclosed spaces. in *Spatial Hearing: The Psychophysics of Human Sound Localization* 201–287 (MIT Press, 1997).
2. Orr, R. T. Natural history of the pallid bat, *Antrozous pallidus*. *Acad.* (1954).
3. Hackett, T. D., Korine, C. & Holderied, M. W. A whispering bat that screams: bimodal switch of foraging guild from gleaning to aerial hawking in the desert long-eared bat. *J. Exp. Biol.* **217**, 3028–32 (2014).
4. Faure, P. A. & Barclay, R. M. Substrate-gleaning versus aerial-hawking: plasticity in the foraging and echolocation behaviour of the long-eared bat, *Myotis evotis*. *J. Comp. Physiol. A.* **174**, 651–60 (1994).
5. Bell, G. P. Behavioral and ecological aspects of gleaning by a desert insectivorous bat *Antrozous pallidus* (Chiroptera: Vespertilionidae). *Behav. Ecol. Sociobiol.* **10**, 217–223 (1982).
6. Barber, J. R., Razak, K. A. & Fuzessery, Z. M. Can two streams of auditory information be processed simultaneously? Evidence from the gleaning bat *Antrozous pallidus*. *J. Comp. Physiol. A Sensory, Neural, Behav. Physiol.* **189**, 843–855 (2003).
7. Fuzessery, Z. M., Buitenhoff, P., Andrews, B. & Kennedy, J. M. Passive sound localization of prey by the pallid bat (*Antrozous p. pallidus*). *J. Comp. Physiol. A* **171**, 767–777 (1993).
8. Koay, G., Kearns, D., Heffner, H. E. & Heffner, R. S. Passive sound-localization ability of the big brown bat (*Eptesicus fuscus*). *Hear. Res.* **119**, 37–48 (1998).
9. Fuzessery, Z. M. Response selectivity for multiple dimensions of frequency sweeps in the pallid bat inferior colliculus. *J. Neurophysiol.* **72**, 1061–79 (1994).
10. Razak, K. A. & Fuzessery, Z. M. Functional Organization of the Pallid Bat Auditory Cortex: Emphasis on Binaural Organization. *J. Neurophysiol.* **87**, 72–86 (2002).
11. Razak, K. A., Shen, W., Zumsteg, T. & Fuzessery, Z. M. Parallel thalamocortical pathways for echolocation and passive sound localization in a gleaning bat, *Antrozous pallidus*. *J. Comp. Neurol.* **500**, 322–338 (2007).
12. Razak, K. A. Systematic representation of sound locations in the primary auditory cortex. *J. Neurosci.* **31**, 13848–59 (2011).

13. Razak, K. A., Yarrow, S. & Brewton, D. Mechanisms of Sound Localization in Two Functionally Distinct Regions of the Auditory Cortex. *J. Neurosci.* **35**, 16105–15 (2015).
14. Fuzessery, Z. M. Monaural and binaural spectral cues created by the external ears of the pallid bat. *Hear. Res.* **95**, 1–17 (1996).
15. Blauert, J. Spatial hearing with one sound source. in *Spatial Hearing: The Psychophysics of Human Sound Localization* 36–200 (MIT Press, 1997).
16. Grothe, B., Pecka, M. & McAlpine, D. Mechanisms of Sound Localization in Mammals. *Physiol. Rev.* **90**, 983–1012 (2010).
17. Rayleigh, L. On our perception of sound direction. *Philos Mag.* **13**, 214–232 (1907).
18. King, A. J., Schnupp, J. W. H. & Doubell, T. P. The shape of ears to come: dynamic coding of auditory space. *Trends Cogn. Sci.* **5**, 261–270 (2001).
19. Masterton, B., Thompson, G. C., Bechtold, J. K. & RoBards, M. J. Neuroanatomical basis of binaural phase-difference analysis for sound localization: A comparative study. *J. Comp. Physiol. Psychol.* **89**, 379–386 (1975).
20. Woodworth, R. *Experimental Psychology*. (Holt, 1938).
21. Blauert, J. Sound localization in the median plane. *Acta Acust. united with Acust.* **22**, 205–213 (1969).
22. Butler, R. A. An analysis of the monaural displacement of sound in space. *Percept. Psychophys.* **41**, 1–7 (1987).
23. Brown, C. H. & May, B. J. Comparative mammalian sound localization. in *Sound source localization* 124–178 (Springer, 2005).
24. Aytekin, M., Grassi, E., Sahota, M. & Moss, C. F. The bat head-related transfer function reveals binaural cues for sound localization in azimuth and elevation. *J. Acoust. Soc. Am.* **116**, 3594–3605 (2004).
25. Koka, K., Jones, H. G., Thornton, J. L., Lupo, J. E. & Tollin, D. J. Sound pressure transformations by the head and pinnae of the adult Chinchilla (*Chinchilla lanigera*). *Hear. Res.* **272**, 135–147 (2011).
26. Rice, J. J., May, B. J., Spirou, G. A. & Young, E. D. Pinna-based spectral cues for sound localization in cat. *Hear. Res.* **58**, 132–152 (1992).

27. Hebrank, J. & Wright, D. Spectral cues used in the localization of sound sources on the median plane. *J. Acoust. Soc. Am.* **56**, 1829–1834 (1974).
28. Firzlaff, U. & Schuller, G. Spectral directionality of the external ear of the lesser spear-nosed bat, *Phyllostomus discolor*. *Hear. Res.* **185**, 110–122 (2003).
29. Wotton, J. M., Haresign, T. & Simmons, J. A. Spatially dependent acoustic cues generated by the external ear of the big brown bat, *Eptesicus fuscus*. *J. Acoust. Soc. Am.* **98**, 1423–1445 (1995).
30. Searle, C. L., Braida, L. D., Cuddy, D. R. & Davis, M. F. Binaural pinna disparity: another auditory localization cue. *J. Acoust. Soc. Am.* **57**, 448–455 (1975).
31. Tollin, D. J., Ruhland, J. L. & Yin, T. C. T. The role of spectral composition of sounds on the localization of sound sources by cats. *J. Neurophysiol.* **109**, 1658–1668 (2013).
32. Wotton, J. M., Haresign, T., Ferragamo, M. J. & Simmons, J. A. Sound source elevation and external ear cues influence the discrimination of spectral notches by the big brown bat, *Eptesicus fuscus*. *J. Acoust. Soc. Am.* **100**, 1764–1776 (1996).
33. Roffler, S. K. & Butler, R. A. Factors That Influence the Localization of Sound in the Vertical Plane. *J. Acoust. Soc. Am.* **43**, 1255–1259 (1968).
34. Heffner, R. S., Koay, G. & Heffner, H. E. Sound localization in chinchillas III: Effect of pinna removal. *Hear. Res.* **99**, 13–21 (1996).
35. Chiu, C. & Moss, C. F. The role of the external ear in vertical sound localization in the free flying bat, *Eptesicus fuscus*. *J. Acoust. Soc. Am.* **121**, 2227–2235 (2007).
36. Lawrence, B. D. & Simmons, J. A. Echolocation in bats: the external ear and perception of the vertical positions of targets. *Science* **218**, 481–3 (1982).
37. Wotton, J. M. & Simmons, J. A. Spectral cues and perception of the vertical position of targets by the big brown bat, *Eptesicus fuscus*. *J. Acoust. Soc. Am.* **107**, 1034 (2000).
38. Fisher, G. & Freeman, S. The role of the pinna in auditory localization. *J. Aud. Res.* (1968).
39. Razak, K. A. Mechanisms underlying azimuth selectivity in the auditory cortex of the pallid bat. *Hear. Res.* **290**, 1–12 (2012).

40. Whitfield, I. Auditory space and the role of the cortex in sound localization. in *Psychophysics and Physiology of Hearing* (eds. Evans, E. & Wilson, J.) 1–9 (Academic, 1977).
41. Jenkins, W. M. & Masterton, R. B. Sound localization: effects of unilateral lesions in central auditory system. *J. Neurophysiol.* **47**, 987–1016 (1982).
42. Heffner, H. E. The Role of Macaque Auditory Cortex in Sound Localization. *Acta Otolaryngol* **532**, 22–27 (1997).
43. Malhotra, S., Hall, A. J. & Lomber, S. G. Cortical Control of Sound Localization in the Cat: Unilateral Cooling Deactivation of 19 Cerebral Areas. *J. Neurophysiol.* **92**, 1625–1643 (2004).
44. Jenkins, W. M. & Merzenich, M. M. Role of cat primary auditory cortex for sound-localization behavior. *J. Neurophysiol.* **52**, 819–47 (1984).
45. Bizley, J. K., Nodal, F. R., Parsons, C. H. & King, A. J. Role of Auditory Cortex in Sound Localization in the Midsagittal Plane. *J. Neurophysiol.* **98**, 1763–1774 (2007).
46. Boudreau, J. C. & Tsuchitani, C. Binaural interaction in the cat superior olive S segment. *J. Neurophysiol.* **31**, 442–54 (1968).
47. Park, T. J., Grothe, B., Pollak, G. D., Schuller, G. & Koch, U. Neural delays shape selectivity to interaural intensity differences in the lateral superior olive. *J. Neurosci.* **16**, 6554–66 (1996).
48. Klug, A., Park, T. J. & Pollak, G. D. Glycine and GABA influence binaural processing in the inferior colliculus of the mustache bat. *J. Neurophysiol.* **74**, 1701–13 (1995).
49. Park, T. J. & Pollak, G. D. GABA shapes sensitivity to interaural intensity disparities in the mustache bat's inferior colliculus: implications for encoding sound location. *J. Neurosci.* **13**, 2050–67 (1993).
50. Wenstrup, J. J., Ross, L. S. & Pollak, G. D. Binaural response organization within a frequency-band representation of the inferior colliculus: implications for sound localization. *J. Neurosci.* **6**, 962–73 (1986).
51. Palmer, A. R. & King, A. J. The representation of auditory space in the mammalian superior colliculus. *Nature* **299**, 248–249 (1982).
52. Middlebrooks, J. C. & Pettigrew, J. D. Functional classes of neurons in primary

- auditory cortex of the cat distinguished by sensitivity to sound location. *J. Neurosci.* **1**, 107–120 (1981).
53. Rajan, R., Aitkin, L. M. & Irvine, D. R. Azimuthal sensitivity of neurons in primary auditory cortex of cats. II. Organization along frequency-band strips. *J. Neurophysiol.* **64**, 888–902 (1990).
  54. Imig, T. J., Irons, W. A. & Samson, F. R. Single-unit selectivity to azimuthal direction and sound pressure level of noise bursts in cat high-frequency primary auditory cortex. *J. Neurophysiol.* **63**, 1448–66 (1990).
  55. Stecker, G. C., Harrington, I. A. & Middlebrooks, J. C. Location Coding by Opponent Neural Populations in the Auditory Cortex. *PLoS Biol.* **3**, e78 (2005).
  56. Furukawa, S., Xu, L. & Middlebrooks, J. C. Coding of sound-source location by ensembles of cortical neurons. *J. Neurosci.* **20**, 1216–1228 (2000).
  57. Nakamoto, K. T., Zhang, J. & Kitzes, L. M. Response Patterns Along an Isofrequency Contour in Cat Primary Auditory Cortex (AI) to Stimuli Varying in Average and Interaural Levels. *J. Neurophysiol.* **91**, 118–135 (2004).
  58. Miller, L. M. & Recanzone, G. H. Populations of auditory cortical neurons can accurately encode acoustic space across stimulus intensity. *Proc. Natl. Acad. Sci. U. S. A.* **106**, 5931–5 (2009).
  59. Imig, T. J. & Adria'n, H. O. Binaural columns in the primary field (A1) of cat auditory cortex. *Brain Res.* **138**, 241–257 (1977).
  60. Kelly, J. B. & Judge, P. W. Binaural organization of primary auditory cortex in the ferret (*Mustela putorius*). *J. Neurophysiol.* **71**, 904–13 (1994).
  61. Liu, W. & Suga, N. Binaural and commissural organization of the primary auditory cortex of the mustached bat. *J. Comp. Physiol. A Sensory, Neural, Behav. Physiol.* **181**, 599–605 (1997).
  62. Semple, M. N. & Kitzes, L. M. Binaural processing of sound pressure level in cat primary auditory cortex: evidence for a representation based on absolute levels rather than interaural level differences. *J. Neurophysiol.* **69**, 449–61 (1993).
  63. Harper, N. S. & McAlpine, D. Optimal neural population coding of an auditory spatial cue. *Nature* **430**, 682–686 (2004).
  64. Tollin, D. J., Koka, K. & Tsai, J. J. Interaural Level Difference Discrimination Thresholds for Single Neurons in the Lateral Superior Olive. *J. Neurosci.* **28**,

4848–4860 (2008).

65. Razak, K. A. & Fuzessery, Z. M. GABA Shapes a Systematic Map of Binaural Sensitivity in the Auditory Cortex. *J. Neurophysiol.* **104**, 517–528 (2010).
66. Davis, K. A., Ramachandran, R. & May, B. J. Auditory Processing of Spectral Cues for Sound Localization in the Inferior Colliculus. *JARO - J. Assoc. Res. Otolaryngol.* **4**, 148–163 (2003).
67. Imig, T. J., Bibikov, N. G., Poirier, P. & Samson, F. K. Directionality Derived From Pinna-Cue Spectral Notches in Cat Dorsal Cochlear Nucleus. *J. Neurophysiol.* **83**, 907–925 (2000).
68. Imig, T. J., Poirier, P., Irons, W. A. & Samson, F. K. Monaural Spectral Contrast Mechanism for Neural Sensitivity to Sound Direction in the Medial Geniculate Body of the Cat. *J. Neurophysiol.* **78**, 2754–2771 (1997).
69. Wise, L. Z. & Irvine, D. R. Topographic organization of interaural intensity difference sensitivity in deep layers of cat superior colliculus: implications for auditory spatial representation. *J. Neurophysiol.* **54**, 185–211 (1985).

## **Chapter 2**

### **The Tragus of the Pallid Bat is Necessary for Spectral Cues That Vary with Sound Source Elevation**

**Abstract.** The mechanisms by which the auditory system is able to compute the source of incoming sounds is only partially understood. One canvas upon which directional cues are generated is at the external ear before even reaching the sensory epithelium. Sound is filtered by the external ear structures of animals. These structures (pinna and tragus) vary to an outstanding degree across mammals. Here, we tested the dependence of the directional cues generated by the large external ear of the pallid bat on the presence of the animal's conspicuous tragus. A microphone was situated at the tympanum of the pallid bat ear canal to record incoming sounds played from various positions in frontal space after it had passed through the external ear. We then compared these recordings to similar recordings following the removal of the tragus. We find that a typical directional cue imparted by the external ear, the spectral notch, loses significant directionality after the tragus is removed in the pallid bat. This loss was observed in the low frequency band of pallid bat hearing (5-40 kHz) and corresponded only to locations below the horizon. Furthermore, we find evidence of an attenuating effect of the tragus on the high frequency band of pallid bat hearing (30-60 kHz). Together, these results suggest a potential bimodal role for the tragus in an animal that must navigate its environment while simultaneously localizing sounds in both frequency bandwidths.

## Introduction

Animals rely on their ability to accurately localize the direction of a sound source for essential tasks, such as foraging, general orientation, finding mates, and predator avoidance. Furthermore, accurate localization is an important and often underappreciated function for humans, playing an essential role in our ability to communicate in a noisy environment, for example<sup>1</sup>. Unlike the visual or somatosensory sensory epithelia, there is no direct representation of space in the cochlea. Instead, the cochlea is organized from base to apex in a high-to-low frequency gradient within the hearing range of the animal. The information brought into the central auditory system from the two ears must be combined to compute source direction. Auditory localization, therefore, represents an ideal behavior to gain insights into neural computations derived from unique external morphology.

In mammals, different cues are used to localize sound sources in the azimuthal versus the elevation planes<sup>2,3</sup>. In the former case, interaural intensity differences (IIDs) and interaural time differences (ITDs) are used to distinguish sound sources. The range of possible interaural cues depends on head size and sound frequency<sup>2-4</sup>. For vertical localization, mammals use monaural spectral cues, the frequency-specific filtering properties of the external ear (pinna and tragus)<sup>4-7</sup>. The filter applied to a broadband sound is described by the head-related transfer function (HRTF). In addition to the distance between the ears, the pinna provides gains at various frequencies and spatial locations, contributing to IIDs the animal will experience. The frequency-specific filtering also often produces sharp attenuations in a limited frequency band, known as

spectral notches. The frequency of spectral notches increases with elevation<sup>4,7-12</sup>, and thus may serve in elevation detection. The tragus is an additional external ear structure for the production of these cues, specifically in bats<sup>6,13,14</sup>, but the functional role of tragus is not fully understood.

One group of bats is particularly suited for an analysis of sound localization abilities, due to their foraging strategy, known as gleaning. Like many other Microchiropteran bats, gleaning bats forage at night<sup>15</sup>. However, gleaning bats exhibit a few unique foraging strategies. Instead of relying on echolocation in flight to detect, localize and hunt prey, gleaners rely on prey-generated noise caused by prey walking and rustling noise on substrate (e.g., leaves, ground<sup>16</sup>). Another behavioral technique employed by most gleaners is the reduction of the echolocation call intensity while foraging<sup>17,18</sup>. These whispering bats are thought to drop their echolocation call intensities to avoid detection by eared prey, thereby increasing prey capture rates. Gleaners also typically have remarkably large external ears, with an exaggerated tragus. This foraging strategy must exert strong selective pressure for accurate sound localization.

A gleaning bat that has been the focus of several neuroethological studies is the pallid bat, *Antrozous pallidus*<sup>16</sup>. Pallid bats are obligate gleaners<sup>16</sup>, have pronounced external ear structures, and produce low intensity echolocation calls<sup>18</sup>. Pallid bat sound localization behavior<sup>19,20</sup> (also see chapter 3 of this dissertation), cortical mechanisms<sup>21-25</sup> (Chapter 4 of this dissertation), and HRTFs<sup>4</sup> have been described. Due to their small head sizes and high frequency hearing, phase-dependent ITDs are rendered less useful as a localization cue in these bats. Thus, azimuth localization is likely achieved through IID

encoding<sup>22,25</sup>. In previous HRTF experiments, the extent to which the external ear shapes IIDs and the spectral notches were examined<sup>4</sup>, however, the role of the tragus in shaping these cues is still unclear.

To my knowledge, no comprehensive analysis of tragus size across bat species has been completed. However, one differentiating factor between bats that hunt on the wing and gleaners is much larger external ear structures in gleaning bats. This has been characterized in at least one genus (*Myotis*), where it was found that gleaning bats do have a wider, more prominent tragus<sup>26</sup>. Therefore, it is of particular interest to compare role of the tragus on sound pressure transformations received at the ear canal across bat species.

Most investigations of the role of the tragus have been performed on *Eptesicus fuscus*. The tragus is an important structure of this bat, both for the generation of spectral cues and for localization behavior<sup>13,14,27-30</sup>. In addition, the directionality of the higher frequency range of hearing (60-90kHz) is altered by the removal of the tragus, while the removal of the pinna causes changes in gain across most of the hearing range (20-90kHz)<sup>29</sup>. In one gleaner bat, *Phyllostomus discolor*, tragus deflection disrupted spectral notches and IIDs in the low frequency range (35-40kHz), while the pinna provided a low frequency gain (20-50kHz)<sup>6</sup>. Several other ear directionality studies in gleaner bats have characterized a similar low frequency (10-30 kHz) gain but did not examine the function of the tragus<sup>4,31-33</sup>.

Due to the conspicuous nature of the pallid bat tragus (Figure 2.2B), we aimed to describe the pallid bat HRTF for potentially relevant sound localization cues that are altered by the tragus removal. We find the tragus to be involved in the coherent pattern of low frequency (10-40 kHz) spectral notches across frontal space, specifically below the horizon (0° elevation). We also find a high-frequency (40-60 kHz) attenuation caused by the tragus, indicating that the tragus may play a role in prey-generated noise and echolocation detection. Combined with previous literature on pallid bat localization, these data can help fill the gap in our knowledge of how external ears and auditory circuits cooperate to form spatial percepts in the auditory system.

## **Methods**

*Animal Use Statement.* Data were collected from 4 bats. The aim of our methods was to position the microphone in place of the bat's tympanum. Bats were perfused and decapitated, leaving as much tissue as possible above the shoulders. The tissue between the skin and skull behind the animals' right ears was carefully removed until the ear canal was exposed. An intersecting cut was made behind the tympanum, followed by careful removal of the tympanic membrane with forceps. The bat head was then taken into the testing chamber to be mounted into position for sound presentation.

*Apparatus.* A 75x110 (W x H) cm metal frame (Figure 2.1, arrow) was secured to a vibration isolation table with clamps inside of an anechoic sound attenuating chamber

(Gretch-Ken, Inc). The center of the top and bottom bars of this frame contained two posts extending 3 inches directly forward (Figure 2.1, red arrows). A semicircular metal bar was then secured to these pivot points on either end, creating a surface that was consistently between 0.9-1m from the center of the metal frame. A speaker mount was customized to hold the speaker ((LCY-K100, Madisound, WI)) on the metal bar (Figure 2.1, red star). This mount was detachable and could easily slide around the entire length of the semicircular bar. The bar was labeled in 15° increments from 75° above the midline to 75° below, marking 11 positions along the elevation axis. The bar itself could be loosened from its connection to the frame and rotated through the azimuth plane continuously. A protractor with 15° angles between markings was secured between the connection of the bottom of this bar and the bottom piece of the metal frame so that azimuthal position of the bar could be measured accurately. Azimuths between 90° on either side of the midline were sampled with 15° resolution giving a total of 13 positions along the horizontal axis. Together, this setup allowed for the sampling of 143 positions across the frontal hemisphere of the bats.

From the bottom center of the apparatus, a large heavy rod was secured and extended straight upward towards the center of the metal frame. Both the recording microphone and the bat head was secured to this rod (Figure 2.1, dotted red arrow). First, cadaver bat head was secured to a wire frame, shaped to fit a typical bat's dimensions.

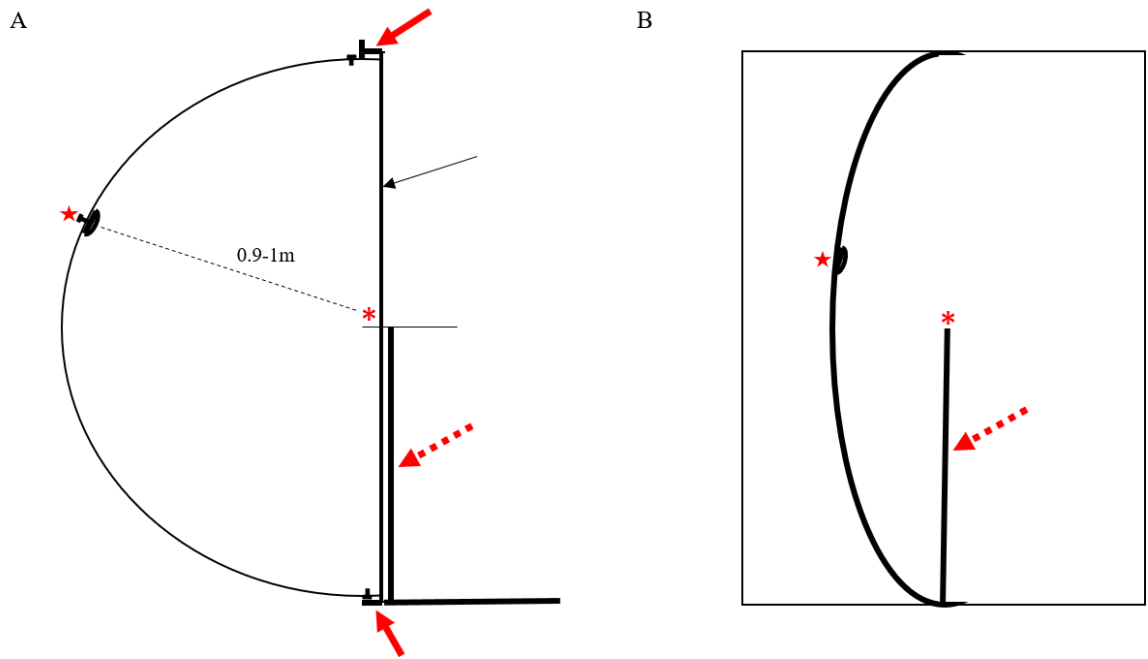


Figure 2.1. The sound presentation apparatus frame (black arrow) mounted inside of an anechoic chamber with the bat head in place (asterisk), is schematized from the side view (**A**) and from the view directly in front (**B**). In this example, the speaker (star) is situated at  $\sim 15^\circ$  above the midline and  $\sim 30^\circ$  to the ipsilateral side of the recording microphone placed at the position of the bat's tympanum. Ipsilateral data is denoted by a positive sign for the data figures. The screws for securing and loosening the semicircular bar to and from the frame are at the top and bottom of the semicircular bar (red arrows).

The frame was shaped so that the wire traced the bat's chin, supporting it from below. An extension of this wire was secured to a metal rod, extending directly upward from the larger metal frame. The height of the metal rod and the extension were designed so that the bat's nose was positioned at the middle of the semicircular bar. The tip of the nose was aligned more precisely by mounting lasers to project the lines between the two extremes of azimuth and elevation ( $+90^\circ$  and  $-90^\circ$  elevations are the points where the semicircular bar connects to the apparatus) and moving the bat head until the nose just intersected both.

A microphone (Sokolich Ultrasonic Probe Microphone System) was clamped into a micromanipulator secured to the same vertical metal rod that the head was attached to. The skin on the right side of the bat's head was positioned so that the ear canal could be accessed, and the microphone was carefully situated in the approximate location of the removed tympanic membrane. The microphone tip was sealed to the ear canal behind the tympanum with super glue, and the skin tissue was positioned back to normal, so that the ear of the animal rested naturally with the microphone now in place of the tympanum. A layer of foam and a blanket were then used to cover all equipment on the lower half of the apparatus and the table to reduce the impact of reflections on measurements.

*Data collection.* With the bat's head properly positioned, sound was presented from each of the 143 locations in sequence. Broadband noise (1 second duration) with a frequency response profile extending from 3-96 kHz were generated through the TDT RZ6 system (Tucker Davis Technologies, FL). Measurements taken from the microphone were represented in a time series waveform in SpectraPlusSC via the SpectraDaq200 external sound converter (Pioneer Hill Software, WA). FFTs were obtained from these waveforms, and the resulting 2-dimensional data (Frequency (kHz) x Gain (dB V)) were saved to a spreadsheet. This procedure was performed for three conditions. The first condition was with the microphone in place of the tympanum, as described above. The second condition was the same as the first condition, except for the tragus of the right ear being removed. The tragus was removed with scissors as close to the base of the structure

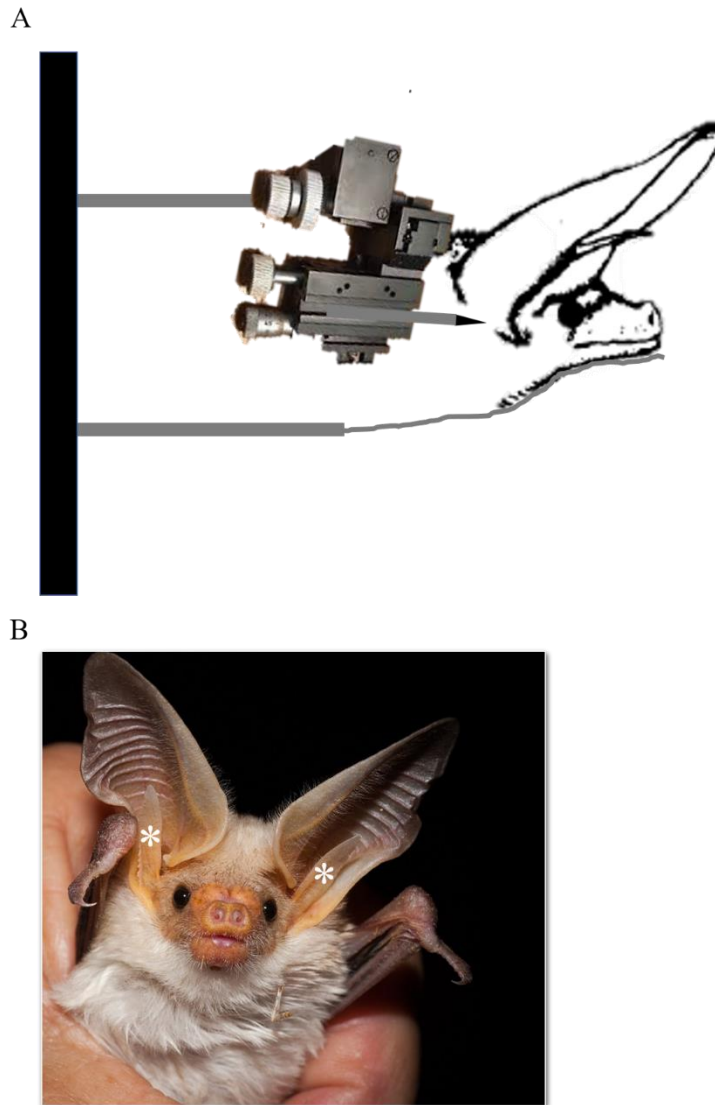


Figure 2.2. **(A)** Schematic of the bat head with intact tragus in position for data collection. The wire frame on which the chin is superglued can be seen under the chin of the bat. This connects to a solid bar that can be extended to position the bat's head appropriately. The Sokolich microphone is positioned at the tympanum using a micromanipulator. This setup is also attached to a bar that can be extended or retracted. The bars holding the bat head and the microphone are solidly anchored to the large post extending upwards from the apparatus frame (black bar, far left). **(B)** The pallid bat tragi (asterisks) protrude upward from the center of the base of the ear. Both the tragi and the pinnae are large relative to the pallid bat head size, compared to other, mostly non-gleaning, bat species.

as possible. This allowed for the determination of the contribution of the tragus to the HRTF. The third condition was a measurement of speaker output across all positions with the microphone only (no bat), as a reference signal. This required careful removal of the bat's head while maintaining the position of the microphone. Because the microphone tip was fitted with a plastic cone, onto which the super glue was applied, the head could be removed easily, with the plastic tip sliding off the microphone tip along with it. Bat tissue was removed from the cone and the cone was repositioned before recordings took place.

For each position, the reference Fourier transform values (dB V) were subtracted from the normal and tragus-removed values across the sampled frequency range. The resulting data were plotted against frequency to generate the standard HRTF. These plots demonstrate the gain of frequency bands at one specific azimuth and elevation pair for each HRTF (Figure 2.3). In this manuscript, the HRTF obtained by subtracting the reference signal from the signals measured from a normal bat head is the normal HRTF ( $HRTF_n$ ). HRTF obtained by subtracting the reference from the bat head minus the tragus is the tragus-removed HRTF ( $HRTF_{tr}$ ). Spectral notches were identified in these plots as any transient attenuation that fell and rose by 6 dB V within a 6 kHz bandwidth. One last data set was calculated by taking the difference between  $HRTF_n$  and  $HRTF_{tr}$  (mathematically,  $HRTF_n - HRTF_{tr}$ ). This difference HRTF ( $HRTF_d$ ) was used to show the magnitude of changes caused by tragus removal.

Directional transfer functions (DTF) were used to show a sequence of HRTFs through the entire elevation range at a constant azimuth (DTF-E), or through the entire azimuth range at a constant elevation (DTF-A). HRTF were plotted with their dB V values on a color scale (as in Figure 2.4E). All identified spectral notches were plotted as scatter plots on top of the DTFs. The first identified spectral notch was also plotted onto a 2-dimensional space map, with the center frequency of the notch indicated on a color scale (as in Figure 2.2.6). Regression analyses were carried out in MATLAB to determine the significance of the relationship between elevation and notch frequency. Custom MATLAB scripts were used to generate all HRTF plots, spectral notches, DTFs, and space maps, and are available upon request.

## Results

### *i. The HRTF and spectral notches*

Figure 2.3 shows an example  $HRTF_n$  plot. This example trace was recorded from Bat1 during stimulus presentation from  $-15^\circ$  azimuth (negative denotes contralateral side) of the recorded ear and at  $75^\circ$  below the midline. Any deviation of the graph above 0 dB is a gain provided by the ear. Deviation below is an attenuation. Characteristic features of these plots are the gain (up to 15 dB) at low frequencies, followed by a relatively constant decrease in gain interrupted by sharp notches. In all traces, the HRTF drops below the 0 dBV value at some point along the frequency axis. These gains and attenuations measure the effects of the external ear on sound input into the auditory system in a frequency-specific manner. Spatial location also influences these gains and attenuations as can be seen in figures below. Periodically, sharp drops in the gain value within a relatively narrow bandwidth appear. These are called spectral notches, thought to be important for distinguishing sound sources from various vertical positions<sup>5,11,34–36</sup>. Vertical lines on the  $HRTF_n$  and all HRTFs presented here denote the presence of a notch, as identified by the custom MATLAB script. Notches are denoted by their center frequency for the rest of the results.

In many species, the frequency of the first spectral notch of the  $HRTF_n$  increases with a corresponding increase in elevation<sup>4,12,34,36,37</sup>. In the pallid bat, we find

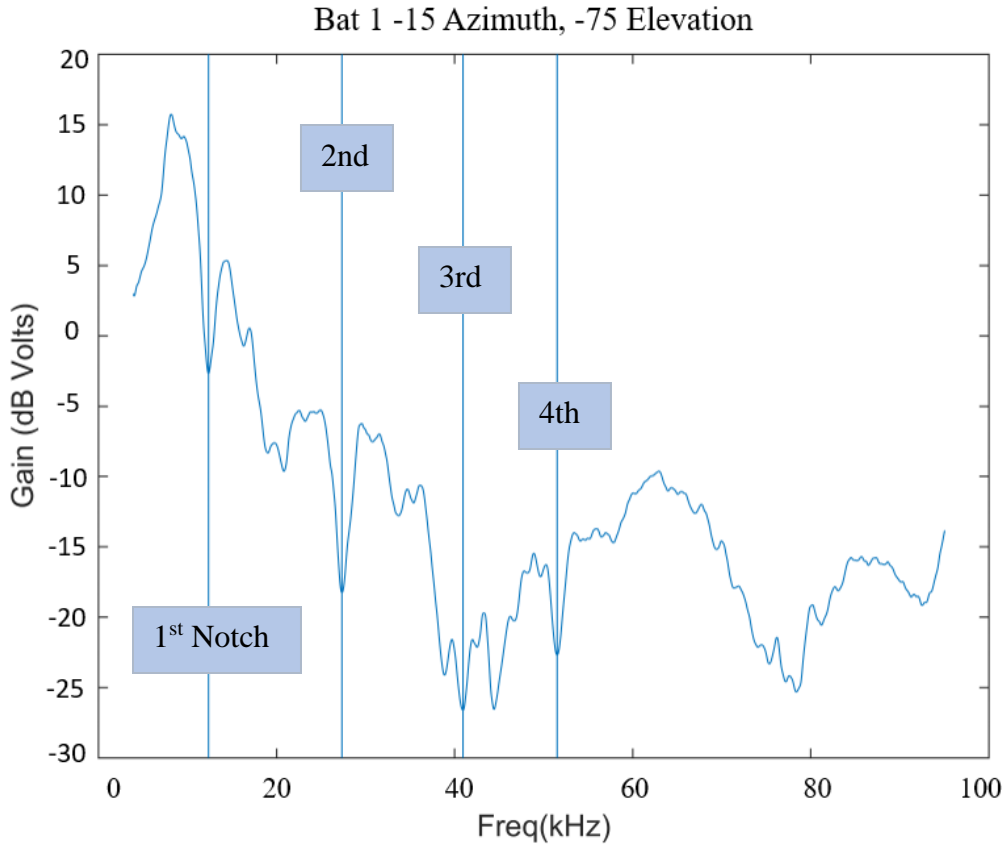


Figure 2.3. Example HRTF<sub>n</sub> of Bat1 measured at spatial position -15° azimuth and -75° elevation. Vertical lines represent identified spectral notches, numbered as they appear across the frequency axis.

this to be the case in all bats tested, especially for locations below the horizon (0° elevation). Figure 2.4A-D shows a series of HRTF<sub>n</sub> plots of decreasing elevation from top to bottom. As expected, the first notch frequency drops along with the decrease in elevation. However, this is only true for elevations at or below 0°.

Figure 2.4E demonstrates this pattern of notch frequency in a DTF-E. The DTF-E shows a series of HRTF<sub>n</sub> measured at different elevations (plotted along the y-axis), at a single azimuth. Lines on the DTF-E connect similar notches (i.e. 1<sup>st</sup>, 2<sup>nd</sup>, 3<sup>rd</sup>, etc.) in HRTF<sub>n</sub> from all the elevations where they appear. In this case, HRTF<sub>n</sub> plots from

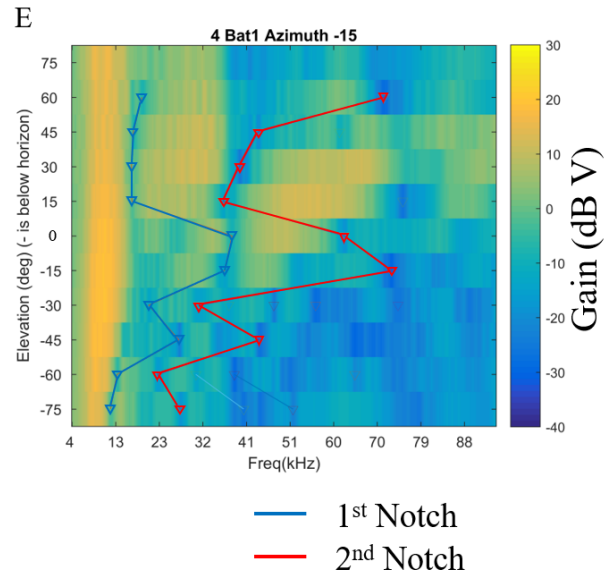
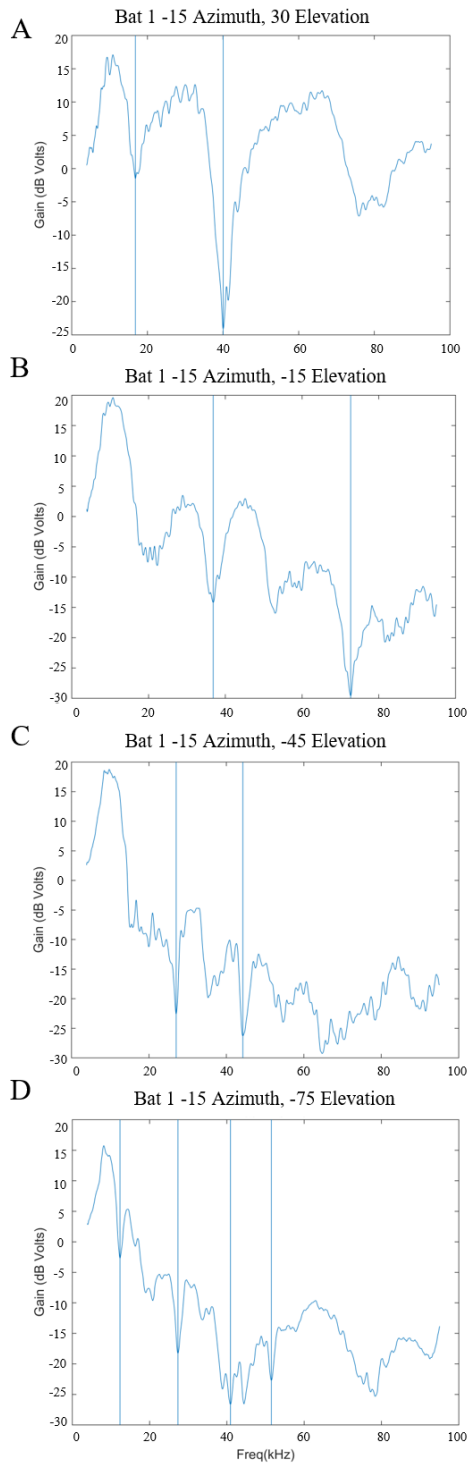


Figure 2.4. (A-D): The increase in identified notch frequency with increasing elevation of the sound source is demonstrated in 4 example HRTF<sub>n</sub> of Bat1 measured at various elevations at -15° azimuth. (E): The DTF-E is a simplified way of demonstrating this. All elevations in -15° azimuth are represented ascending the ordinate, with frequency represented on the abscissa. The color scale displays the magnitude of the HRTF filtering effect relative to the reference signal. Lines connect 1<sup>st</sup>, 2<sup>nd</sup>, 3<sup>rd</sup>, or 4<sup>th</sup> identified notches from different elevations so that the increase in notch frequency is seen in the rightward shift of the line as it moves higher up the elevation plane.

HRTF<sub>n</sub> from all the elevations where they appear. In this case, HRTF<sub>n</sub> plots from all elevations at a constant azimuth (-15°) demonstrate how the first notch frequency migrates to the right side of the plot as the elevation increases, until 0° elevation, at which point, the first notch frequency becomes a constant of ~18kHz (Figure 2.4E; note the shift in the red line towards lower frequencies suddenly at 15° elevation). This constant notch is noticeable as the lowest frequency notch in Figure 2.4A. Similarly, this pattern carries over to the second notch at this azimuth.

Observing multiple DTF-Es side by side gives a picture of trends (Figure 2.5). For instance, there is an elevation dependent gain across the low frequency bandwidth of the signal (5-32kHz). The brighter yellow portion of the plot broadens in frequency as the elevation of the sound source increases, regardless of the azimuth. This usually terminated in a region of attenuation (blue), and is typically the presence of the first notch (Figure 2.5A-D), corresponding with previous reports of the pallid bat monaural cues<sup>4</sup>.

The pattern of notches seen in Figure 2.4 emerges consistently when the azimuth is near the midsagittal plane (0° azimuth). When the azimuthal position is more eccentric, the first notch at higher elevations is no longer present (Figure 2.5A-D). The first notch frequency is not thought to be an essential cue to the perception of sound source azimuthal position, due to the lack of significant change in these values with azimuth<sup>4</sup> and due to the azimuthal localization ability of animals not changing when these notches are removed<sup>38</sup>. To determine whether pallid bat external ears produce a significant alteration in first notch frequency with azimuth, DTF-As at constant elevations were generated (Figure 2.5E-H). Like the DTF-E, the DTF-A shows a series of HRTF<sub>n</sub>. The

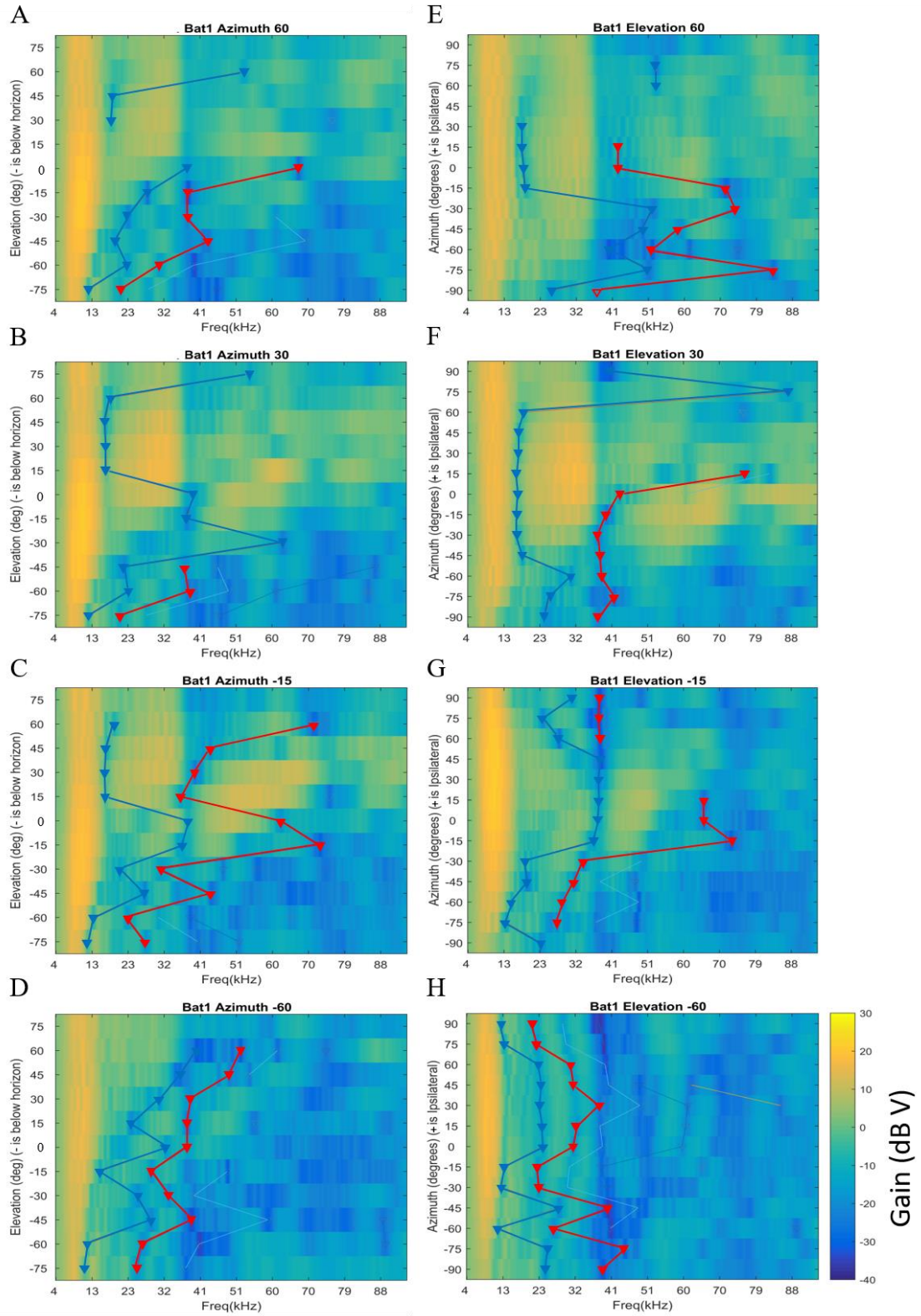


Figure 2.5. (A-D): DTF-Es with a constant azimuth show spectral notches shift to higher frequencies with increasing elevation. Solid lines connect 1<sup>st</sup> (blue) or 2<sup>nd</sup> (red) notch across elevations. (E-H): DTF-As with a constant elevation show that notches do not shift systematically with shifting azimuth. All data were obtained from Bat1. Gain is indicated by the color scale in dB V units. Positive gains are yellow, and negative gains are blue.

DTF-A, however, displays the  $\text{HRTF}_n$  measured at different azimuths (plotted along the y-axis), at a single elevation. As in Figure 2.4E, lines on the DTF-A connect similar notches (i.e. 1<sup>st</sup>, 2<sup>nd</sup>, 3<sup>rd</sup>, etc.) in  $\text{HRTF}_n$  from all the elevations where they appear. As previously reported in the pallid bat<sup>4</sup>, we find a stable first notch frequency across azimuth at various elevations, as indicated by the lack of consistent change in notch frequency with azimuth (mostly vertical lines, Figure 2.5E-H).

The first notch frequency can be plotted at each of the 143 positions sampled to get a picture of how this feature varies across frontal space (Figure 2.6). In all 4 pallid bat  $\text{HRTFs}$  measured, there is a relative increase in the first notch frequency with increasing elevation. In almost all cases, this trend is strongest between the midsagittal plane and 75° IL and spans a bandwidth that the pallid bat uses for foraging (5-40kHz). Higher frequency notches begin to appear at higher elevations, including positions above the horizon. However, in 3/4 bats the pattern is disrupted near the midsagittal plane by the large region with a low frequency notch (10-20 kHz). This resulted in a disruption of the expected 1<sup>st</sup> notch frequency gradient. Bat 3 was an exception to this rule, exhibiting a relatively linear increasing 1<sup>st</sup> notch frequency with elevation, extending above 0° elevation. Thus, we surmised that the first notch frequency of the pallid bat systematically increases with increasing elevation of the sound source, specifically at low elevations in ipsilateral space. Consistent with the interpretation, a linear regression

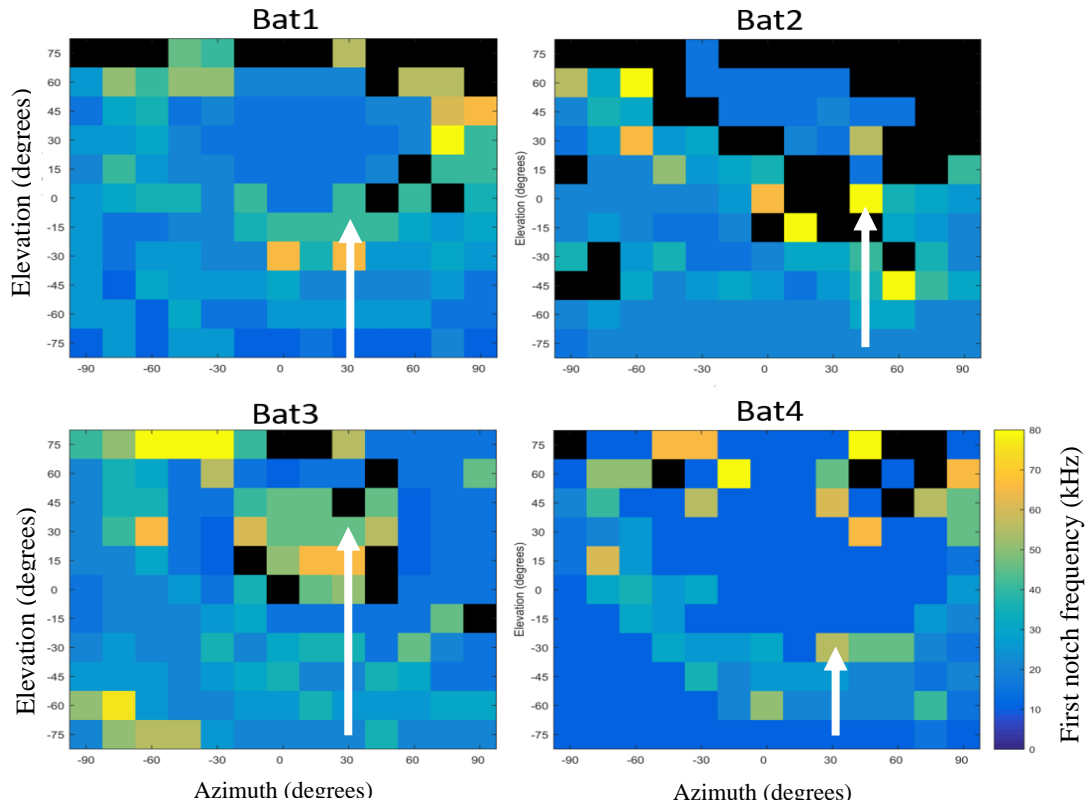


Figure 2.6. 2D space maps with first notch center frequency represented on the color scale demonstrate the upward notch frequency shift with increasing elevations. White arrows are used to point out azimuths where this trend was observed. The white arrow in the space plot for Bat 1 indicates the notches plotted in Figure 2.5C.

analysis indicates a significant relationship of first notch frequency measured from all 4 bats and elevations ranging from  $0^\circ$  to  $-75^\circ$  (below the horizon) at most azimuths in ipsilateral space (Table 2.1).

*ii. The pallid bat tragus contributes to the spectral notch pattern*

The role of the tragus in shaping these ear directionality cues is not yet known. In other bat species, removal of the tragus resulted in the disruption of the elevation-related increase in first notch frequency<sup>6,13</sup>. Therefore, we removed the tragus and recorded the  $HRTF_{tr}$ . The resulting DTF-Es of these  $HRTF_{tr}$  demonstrate an effect on the first notch

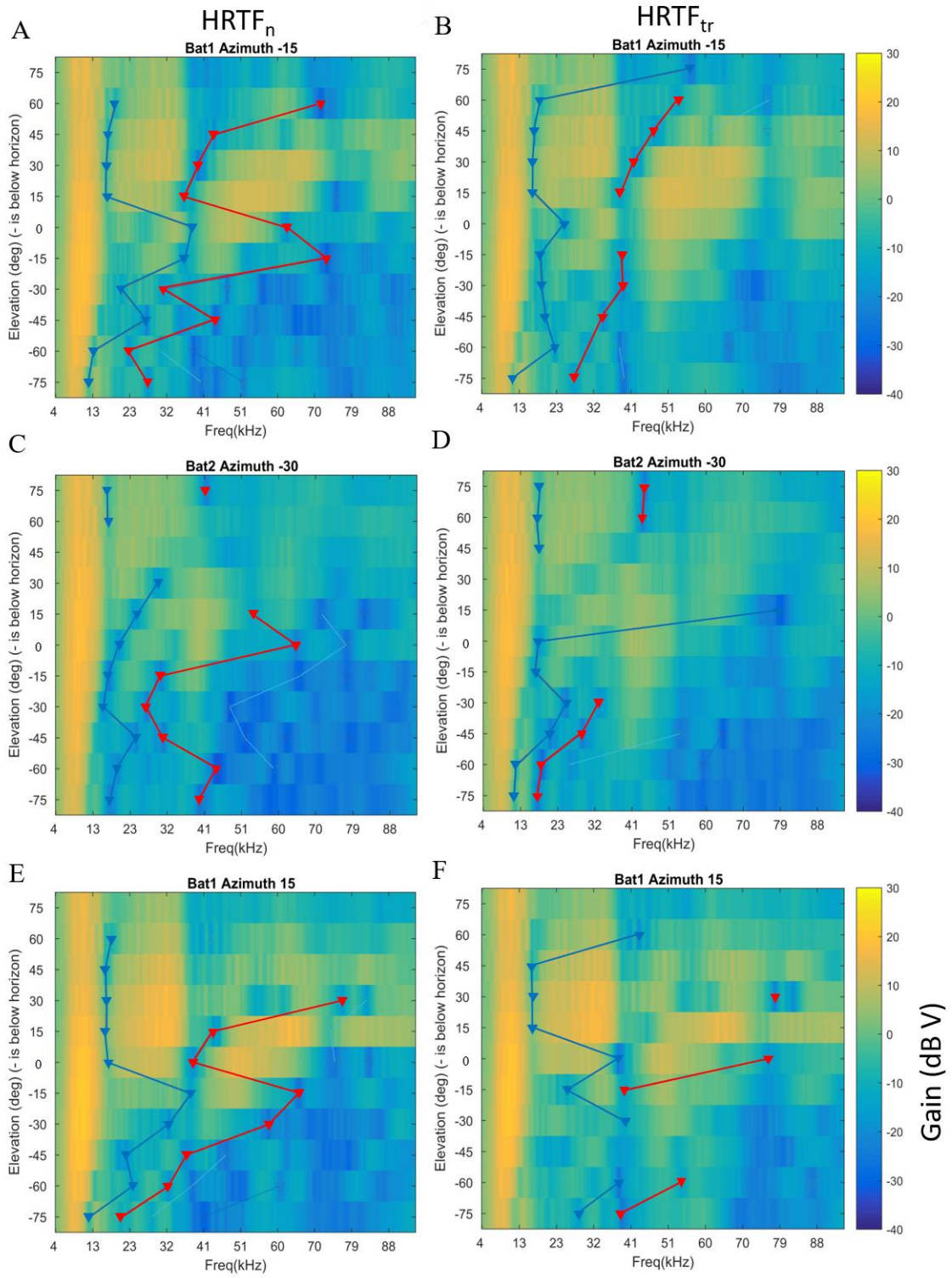


Figure 2.7. Removal of the pallid bat tragus results in disrupted notch patterns on the DTF-Es. The left column shows normal HRTF plots, with the full ear intact, from various animals and azimuthal positions. The right column shows the corresponding plots for those positions when the animal's tragus was removed. The color scale is represented as in Figure 2.5.

frequency gradient similar to prior studies on other bat species. With tragus removal, notches are still present in the DTF-E plots, but the gradients discussed previously are no longer apparent (Figure 2.7B). In some cases, the notches are absent, although these cases are rare, and the notches that are the most affected appear to be in the lower elevation range (Figure 2.7E-F). This suggests that the tragus has little to do with the consistent low frequency notch at higher elevations but may be shaping low elevation cues.

Next, we looked at whether the first notch frequency map across frontal space was altered in any notable way by the removal of the tragus (Figure 2.8). As expected based on the DTF-E results, there was little change in the number of notches. Also corresponding to the DTF-E results of Figure 2.7, there is an apparent smoothing of the first notch frequency gradient from low to high elevations (Figure 2.8, white arrows). The magnitude of this smoothing varies between bats, with some bats exhibiting a stark contrast (Bat1, Figure 2.8A-B), while others exhibit little to no change (Bat3, Figure 2.8E-F).

To determine whether this observed effect of the tragus was significant, linear regressions were performed in the first notch frequency vs. elevation data obtained from the  $HRTF_{tr}$  as it was from the  $HRTF_n$ . An example regression plot demonstrates the change in regression slope observed following removal of the tragus (Figure 2.9). Data from all 4 bats consolidated onto one plot allowed us to observe the pattern of notch frequency change with elevation. The blue data points and trend line are data derived from the intact ear condition ( $HRTF_n$ ), while the orange data points are from the tragus

removed condition ( $HRTF_{tr}$ ). The orange trend line has a less steep slope, caused by the appearance of more low frequency notches following tragus removal.

Table 2.1 shows that unlike the observed significant relationship between elevation and first notch in the intact ear condition, there were no azimuths at which the relationship was significant after removal of the tragus, as indicated by all p-values being greater than 0.05. A further observation supporting the conclusion that the tragus shapes low elevation notch frequency gradients is shown in column 4 of Table 2.1. This column shows p-values testing the hypothesis that the slopes obtained from regressions of the elevation vs. notch data in the intact ear and tragus removed conditions were equal. According to the individual example in Figure 2.9, we expected this hypothesis would be rejected. P-values less than 0.05 indicate a significant difference in the slope of the regression caused by the removal of the tragus relative to the same regression slope obtained from data for the intact ear. At 4 locations throughout ipsilateral space, the null hypothesis was rejected or trending closely towards that conclusion ( $p < 0.07$ ). Thus, tragus removal significantly reduced the correlation between first notch frequency and elevation below the horizon within the ipsilateral hemisphere of frontal space.

*iii. The  $HRTF_d$  demonstrates location specific contributions of the tragus to the  $HRTF_n$*

Consistent changes in the difference between  $HRTF_n$  and  $HRTF_{tr}$ , which shows the magnitude of the influence of the tragus on the  $HRTF_n$ , are seen in the  $HRTF_d$  plots. Positive gain (yellow) in this plot indicates that the net effect of the tragus is one of amplification for that location and frequency pairing. In the pallid bat, most effects of the

tragus occur at or below the horizon (Figures 2.10 and 2.11). There was virtually no influence of the tragus on the positive gain in the low frequency bandwidth of higher elevations, as evidenced by the lack of any amplifications or attenuations in the top left of each plot. This included the low frequency notch that was often present in this range of frequencies and spatial locations, consistent with the conclusions made from the notch maps (Figure 2.8). The tragus influences the rest of the notches in this frequency range that are present at lower elevations (Figure 2.10 and 2.11, white ovals). The tragus also has a net attenuating effect across a broad range of elevations and azimuths in the echolocation frequency range (30-60kHz; Figure 2.10 and 2.11, black ovals).

Together, these data support the conclusion reached in several other mammalian species; that the tragus is an external structure involved in the construction of spatially dependent spectral cues. We find evidence for the involvement of the tragus in the first notch frequency vs. elevation relationship, cues that largely reside in the low frequency range (5-40 kHz). In addition, the HRTF<sub>d</sub> suggests the tragus is involved in attenuating the echolocation frequencies (30-60 kHz).

## Tragus Effect on Identified First Notch Frequency Maps

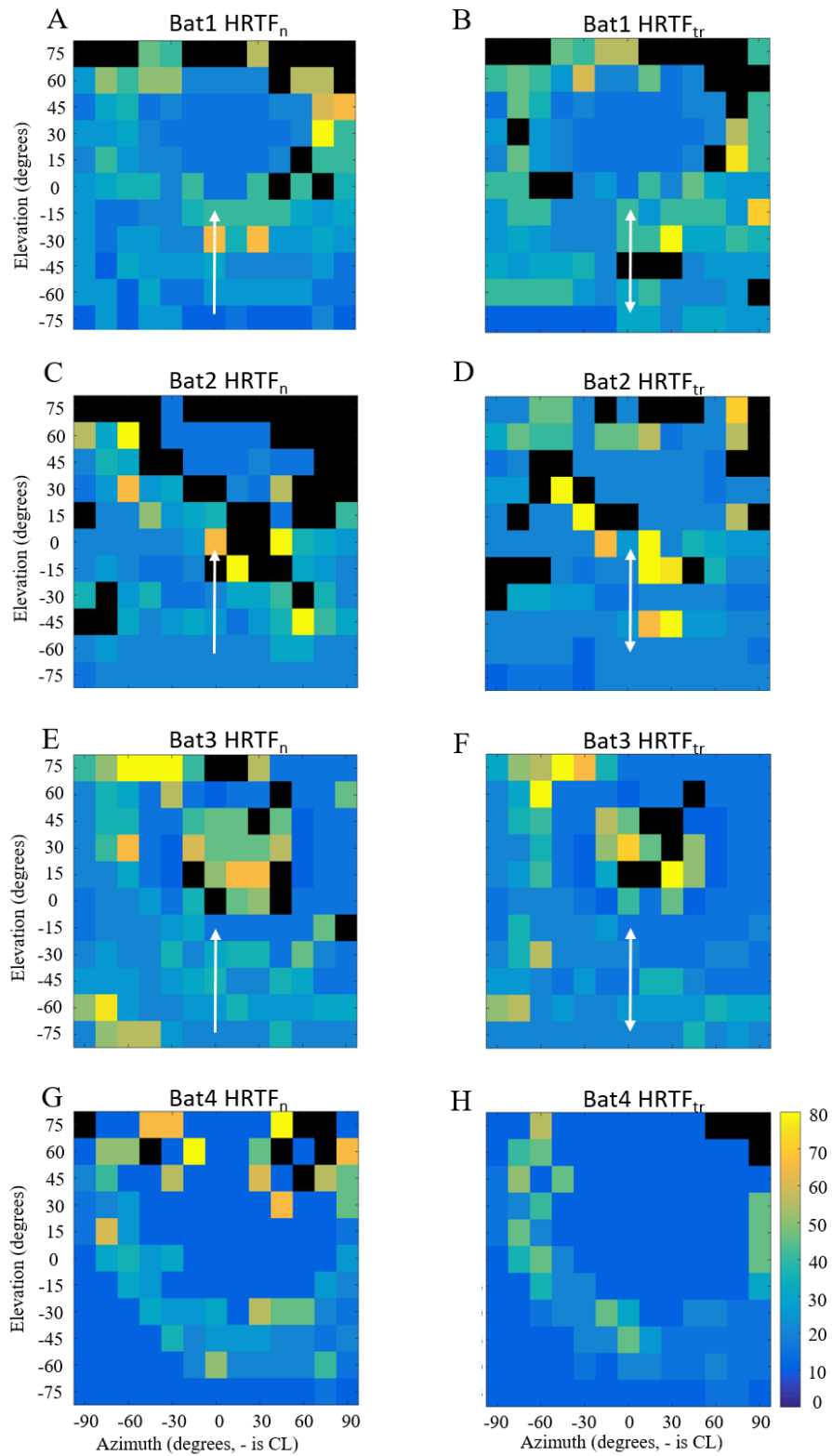


Figure 2.8. Tragus removal caused disruption in the pattern of identified first notch frequency in elevation. 2D space maps with identified first notch frequency represented on the color scale are presented for comparison of  $HRTF_n$  (left column, replications from Figure 2.6) and  $HRTF_{tr}$  (right column) conditions. In line with predictions based on Figure 2.7, the removal of the tragus affected the pattern of first notch frequencies in frontal space. White arrows in the left column are examples where notch gradient is systematically increasing with increasing elevation, indicated by the arrow direction. This directionality is lost when removing the tragus, indicated by the bidirectional arrows in the right column. The low frequency notch at higher elevations obfuscated too much of Bat 4's map to discern any details regarding notch gradients up the elevation axis.

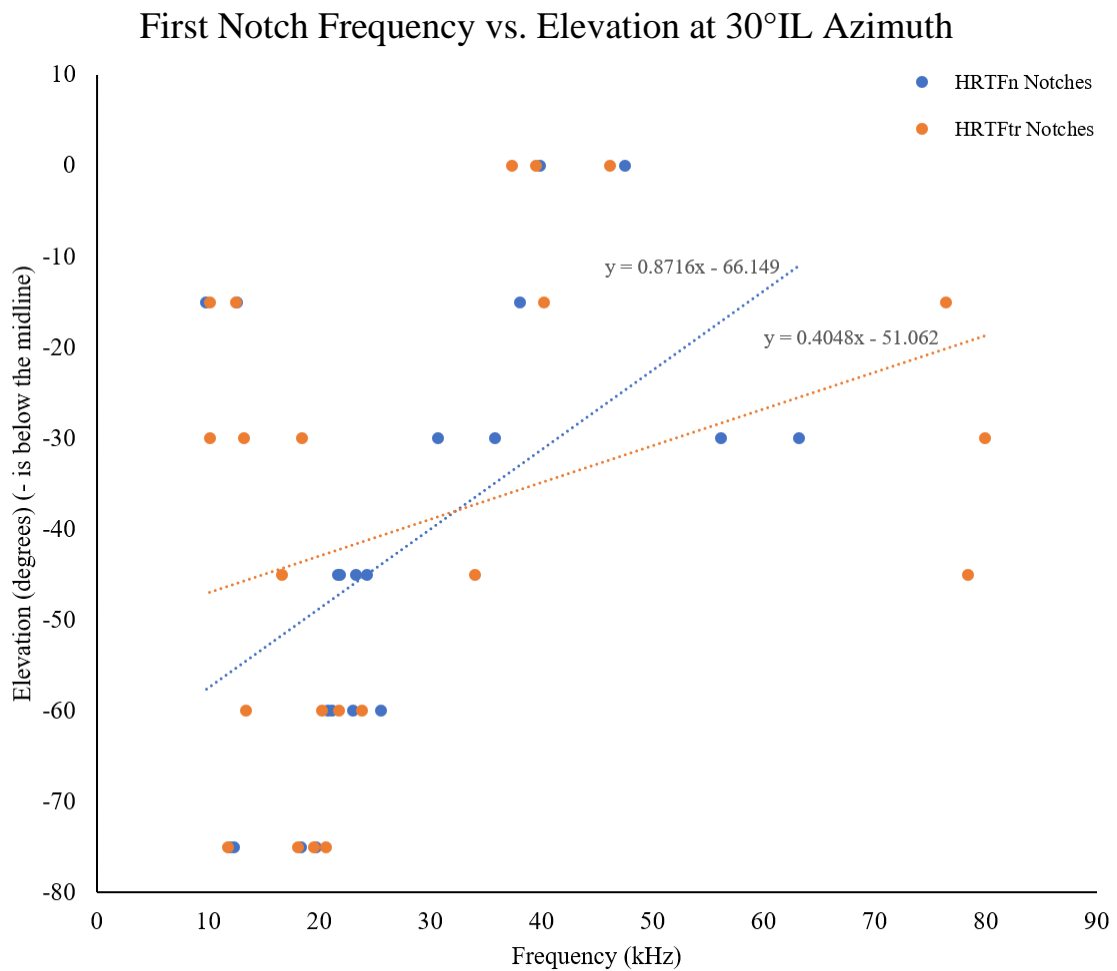
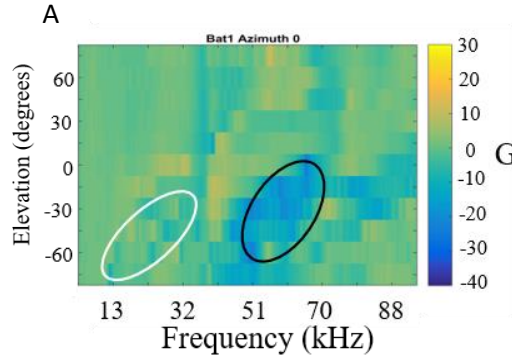


Figure 2.9. Example regression plot showing the reduced slope of the trendline plotted for the first notch frequency and elevation with (blue data points and trendline) and without (orange) the tragus. Data are from all 4 bats, pooled into one data set, and were measured from 30°IL azimuth.

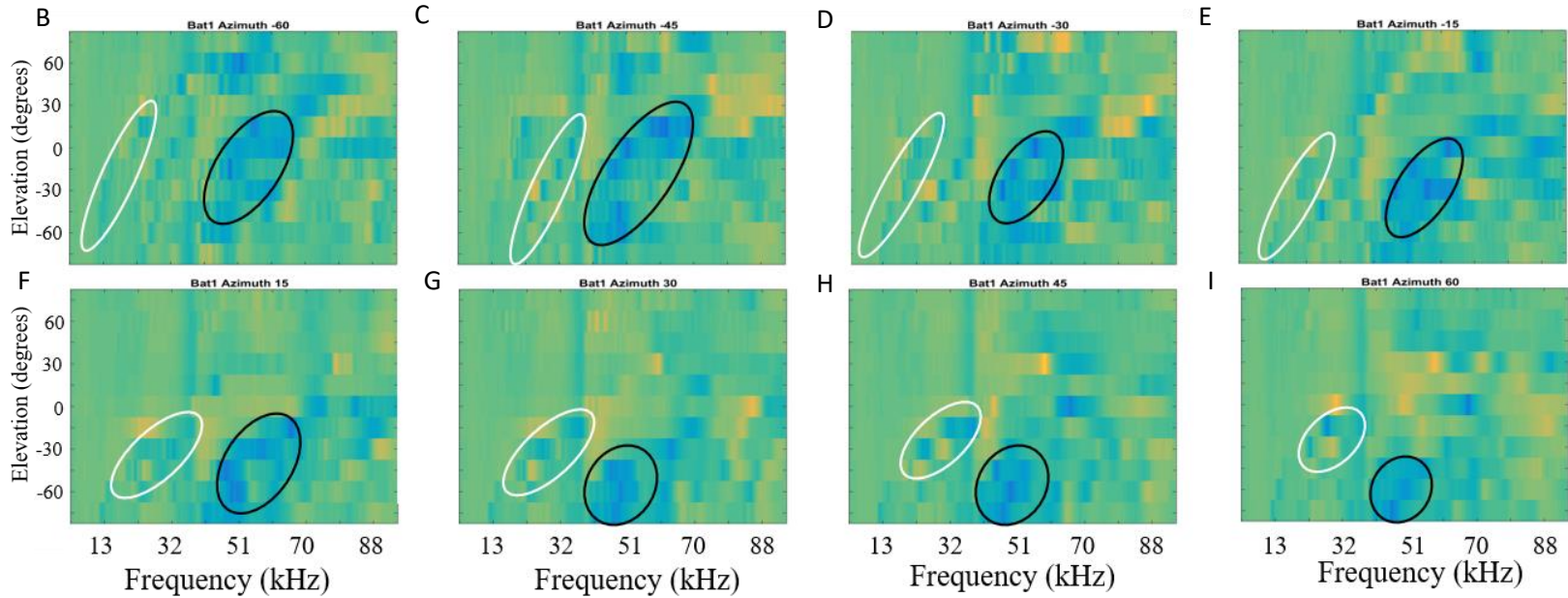
Azimuth	Significance ( $p < 0.05$ )		
	HRTF <sub>n</sub>	HRTF <sub>tr</sub>	H: HRTF <sub>n</sub> = HRTF <sub>tr</sub>
0	0.13	0.64	0.320608
15	0.06	0.66	0.038866
30	0.05	0.97	0.045199
45	0.05	0.45	0.054622
60	0.49	0.25	0.211855
75	0.05	0.91	0.069157
90	0.08	0.25	0.291674

Table 2.1. Removal of the tragus abolishes the significant relationship between notch frequency and elevation at all IL azimuths where the trend was observed (columns 2 and 3). The slopes of both trends are significantly different from one another (red highlight,  $p \leq 0.05$ ) or trending towards significance (yellow highlight,  $0.05 < p < 0.07$ ) at most IL azimuths (column 4).



Gain (dB V)

Figure 2.10. DTF-Es generated from the HRTF<sub>d</sub> of Bat 1. (A). DTF-E of 0° azimuth. Gain values are plotted as in Figure 2.5, and the scale is conserved across all panels. Two regions of tragus influence are apparent. The low frequency spectral notches are shifted, indicated by the pattern of amplifications and attenuations (white ovals). The high frequency (40-60kHz) band is attenuated (black ovals). (B-I) First notches are affected across azimuths. The elevational spread of high frequency attenuation is azimuth dependent, becoming smaller as azimuth is more ipsilateral.



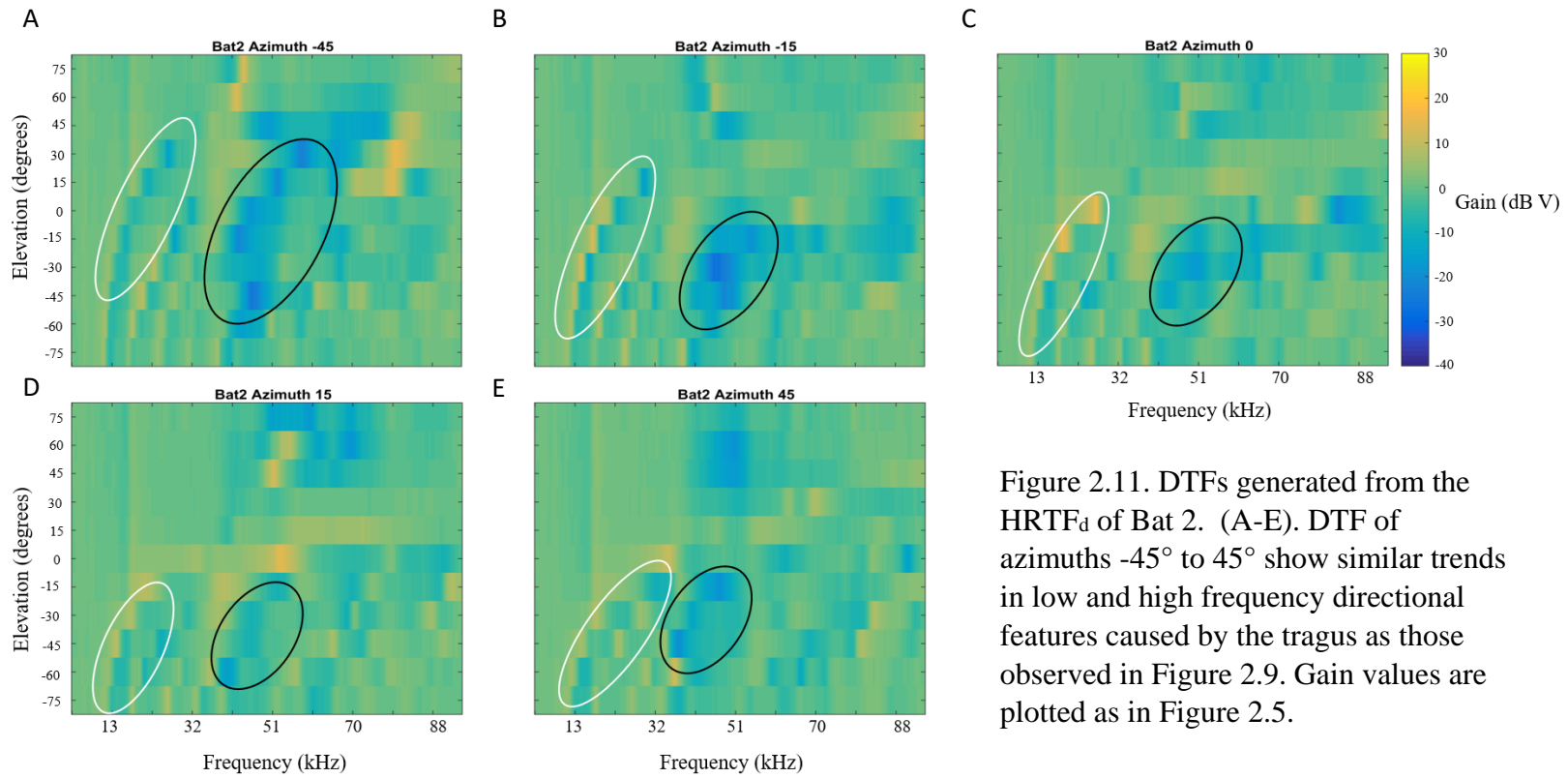


Figure 2.11. DTFs generated from the HRTF<sub>d</sub> of Bat 2. (A-E). DTF of azimuths  $-45^{\circ}$  to  $45^{\circ}$  show similar trends in low and high frequency directional features caused by the tragus as those observed in Figure 2.9. Gain values are plotted as in Figure 2.5.

## Discussion

In the HRTFs of 4 pallid bats, we have identified several potentially important cues for accurate performance when localizing broadband sounds (see Chapter 3 of this dissertation for a description of these behavioral results). As in other species of mammals examined, we report that the frequency of the first notch is dependent on the elevation of the sound source. Removal of the tragus resulted in a significant reduction in this observed correlation. The pallid bat HRTF<sub>n</sub> measured here both corroborates previous reports<sup>4</sup> and expands their findings. The increases in low frequency gain and first notch frequency with increasing elevation are consistent across the two studies (Figure 2.5). A unique feature observed here was in the low frequency notch that appeared at many continuous locations on or above the horizon, centered on the midsagittal plane (Figure 2.5-7). It is unclear whether this feature is an artifact introduced by our preparation or a true representation of the frequency-filtering properties of the head and ears. In any event, the removal of the tragus had virtually no effect on this notch, contrary to most other notches observed (Figures 2.8, 2.9, 2.10, 2.11, and Table 2.1). Removal of the tragus affected the elevation trends in notch frequency at elevations below the horizon and ipsilateral azimuths, though it did not remove the notches (Figure 2.9). Additionally, we provide evidence that the termination frequency of the low frequency gain, which is often the location of the first notch, is dependent on an intact tragus (Figures 2.9 and 2.10). The tragus also attenuates echolocation frequencies (40-60kHz) across a range of elevations.

*i. A potential bimodal role for the tragus*

The first notch frequency maps, (Figures 2.8), correlations (Figure 2.9) and the HRTF<sub>d</sub> (Figure 2.10 and 2.11) reported here build on previous examinations of tragus function in other bat species<sup>6,13</sup>. In the big brown bat (*Eptesicus fuscus*), removal of the tragus severely disrupted the pattern of notch frequency change with sound source elevation<sup>13</sup>, and this translated to an altered perceptual and behavioral avoidance ability<sup>14,39</sup>. These cues fell within the echolocation range of the bat (30-50 kHz), implicating the tragus in perception of returning echoes while avoiding obstacles or hunting<sup>13</sup>. Although the big brown bat is an aerial hawking forager, its low frequency hearing is considerably well-developed<sup>40-42</sup>. Despite this, the tragus appears to play little role in shaping non-echolocation frequency spectral cues.

That the tragus affects only the echolocation range of spectral notches in the big brown bat is an interesting species difference in the observed range of first notch frequencies in the pallid bat (10-80 kHz, Figures 2.6 and 2.8). A likely explanation for these species differences in tragus function resides in the differences in foraging behavior. Because the gleaning pallid bat relies on the perception of sound sources across the 5-40kHz bandwidth, it is reasonable to consider that they make use of most of the spectral notches in that bandwidth. The morphology of the tragus in aerial hawking bats and gleaners also differs, with the gleaning bat species often exhibiting a larger tragus<sup>26</sup>. The larger tragus may have been adapted in gleaners to shape spectral cues in the lower bandwidth of their hearing range (5-40kHz), corresponding to the frequency range of prey-generated noise<sup>43</sup>. Since the pallid bat is listening for prey-generated noise along the

ground as it flies, most of the sound sources are likely below 0° elevation. At these elevations, the pallid bat external ear produces many low frequency spectral notches, and the pattern is tragus-dependent.

The presence of a notch will greatly enhance the intensity difference between the two ears at that bandwidth, making it much quieter in the ear that generated the notch, and thus represents a potentially important cue for accurate azimuthal localization. Pallid bats are accurate at localizing peripheral sound sources containing energy in the same range as the observed notches. When these sound sources are restricted to low frequency (<20 kHz) energy only, their performance drops significantly (see chapter 3 of this dissertation). The pallid bat will experience very few spectral notch center frequencies below 20 kHz. Therefore, excluding all frequency content above 20 kHz is filtering out most of the spectral notches. If spectral notch gradients in elevation are important for localization ability, it is expected that pallid bat sound localization performance would suffer when the tragus is deflected. Future studies aim to address this line of reasoning by testing elevation localization accuracy.

Perhaps another important feature of the tragus, is the attenuating effect of the tragus on echolocation frequencies (40-60kHz) (Figures 2.9 and 2.10). The functional significance of this feature is not certain. However, two speculations arise based on previous neurophysiological and behavioral data from the pallid bat. The first is that the azimuth-dependent attenuation could serve to enhance detection of the laterality of echoes. Cortical neurons that respond selectively to echolocation calls are mostly monaural, and their spatial receptive fields broaden to include much of the frontal space

for sounds above threshold<sup>21,44</sup>. The pallid bat navigating through a cluttered environment with large objects, like trees, will experience loudly reflected echoes. It is unclear how such neurons could lateralize this sound source without inhibition, as both hemispheres of echolocation selective neurons would become activated<sup>21,44</sup>. Therefore, the animal may rely on “inhibition” to come in the form of attenuation of the echoes by the contralateral tragus. Having a tragus to suppress contralateral echolocation frequencies would reduce detectability in that ear, favoring activity driven through the ipsilateral ear. In such a system, the code informing the animal of sound lateralization could be a cross-hemisphere comparator located downstream from the auditory cortex.

Of course, there is still some attenuation at the echolocation frequencies for midline and ipsilateral sound locations (Figures 2.9 and 2.10). However, at 0° azimuth the attenuating effect drops below the midline. This attenuation adjacent to (just below) the middle of frontal space could serve as a contrast enhancement mechanism for the detection of incoming echoes. A similar contrast enhancement mechanism has been proposed as the relevant directional cue of the spectral notch<sup>4,45</sup>. As a whispering bat, pallid bats will preferentially alter their outgoing echolocation pulses to maintain the returning echo intensity in a sensitive range of 30-50 dB SPL while approaching a target<sup>18</sup>. Accurate detection of these low intensity sounds is essential for obstacle avoidance and successfully approaching a landing area, and the attenuating effect of the tragus could assist the pallid bat in attending only to the most relevant returning echoes during these behaviors: those echoes returning from directly along the flight path of the bat.

Collectively, these data suggest a potential bimodal function of the conspicuous external ear structure of the pallid bat, wherein the tragus shapes low frequency notches (5-40kHz) in the peripheral space and modifies echolocation frequencies near the midline. This implies the tragus is an important structure in sound source localization in two dimensions of frontal space (azimuth and elevation), and in general orientation and obstacle avoidance through returning echoes of self-emitted echolocation calls. Future studies can examine the necessity of the tragus-dependent cues in noise localization and wire avoidance behavioral tasks.

*ii. Spectral cues and spatial selectivity of the central nervous system*

In consideration of spectral cue processing in the central auditory system, relatively little is known compared to the processing of interaural cues. Most literature focuses on subcortical mechanisms of sound localization for vertical sound source. These studies have searched for selectivity for spectral cues in the dorsal cochlear nucleus (DCN to inferior colliculus (IC) pathway. Type IV neurons in the DCN project to the IC and synapse onto Type O neurons. The Type IV cell is distinguished based on a unique response to auditory stimuli. Instead of the more standard V-shaped frequency tuning curve, where the bandwidth of activation increases with higher intensity stimuli, Type IV neurons exhibit a small island of response near their characteristic frequency, only at or near the threshold. Louder sounds will inhibit the Type IV neurons over a broad range of frequencies<sup>34,46</sup>. Type II DCN cells are the source of this inhibitory input. Excitation is provided directly from the auditory nerve fiber projections into the cochlear nucleus. Convergence of the excitation and inhibition results in sensitivity to broadband noise

containing a spectral notch. More specifically, noise containing a notch centered at the characteristic frequency will inhibit these Type IV DCN neurons, prohibiting the output to Type O neurons of the IC. Type O neurons exhibit the same near threshold activation as Type IV neurons of the DCN when stimulated by tones, supporting the notion that they are coupled by a direct connection. However, they are inhibited by all notch frequencies except for a narrow range just below the characteristic frequency of the neuron<sup>46</sup>. This results in a scenario wherein there is wideband inhibition projected onto the Type O cell in the IC that is released when a narrow bandwidth notch is present within a noise stimulus. Such a network is thought to be the neural correlate explaining spectral notch necessity for accurate sound source perception<sup>9,11,36,47</sup>. This mechanism also supports the hypothesis that it is the contrast in energy between the spectral notch and adjacent frequencies that is the relevant directional cue<sup>45</sup>.

In the pallid bat auditory cortex, putative mechanisms underlying vertical sound source localization have been identified<sup>21</sup>. Importantly, all noise-selective neurons in the pallid bat auditory cortex are activated by a range of sound sources within the two-dimensional region of frontal space. Center points of these response areas increase in elevation with increasing characteristic frequency (CF), and the higher the CF, the smaller the response area of the neuron. This suggests that more of the tonotopic axis is recruited into a population response as a sound source moves from low to high elevations. The spectral notch is a theoretical cue by which this population is modified. Notches would activate cells with CFs adjacent to the notch frequency, through a similar mechanism to that shaping Type O IC neuron selectivity, or perhaps even by inheriting

the activity of the Type O IC neurons themselves. Future studies should aim to evaluate changes in both neural spatial selectivity and behavioral performance when the tragus is deflected away. Both phenotypes should be disrupted compared to the natural state if the tragus removal effects observed in the data presented here are consequential.

### *iii. Methodological considerations*

Our apparatus was designed to obtain measurements from cadaver bat heads, detached from the torso and shoulders. One primary methodological consideration is that there are significant influences on the low frequency range of the HRTF by these excluded morphologies<sup>8,48</sup>. It is not clear whether these low frequency alterations would be of consequence to the bat, especially when considering the differences in body orientation while active. In flight, the body of the bat will be behind the interaural axis, and any interactions causing shifts in the frequency content of a sound source would not likely interfere with the initial sensation of the sound as it is filtered by the ears first. Nonetheless, a future study of pallid bat HRTFs would benefit from the inclusion of a whole-body condition to control for this possibility. Considerable differences were found when data were collected from a whole bat condition versus a head only condition in the big brown bat, most importantly in the tragus-notch relationship<sup>12,13</sup>.

Additionally, our apparatus was setup to wrap the entire bottom half of the metal frame in sound attenuating materials, to reduce reflections (Figure 2.1). Due to the orientation of the semicircular array, this likely had a much greater effect of reducing reflections for sound sources below 0° elevations. Situating the bat's head and the

microphone in place required open space above the midline, and afterward, we had to make sure the head was not moved. Therefore, we decided not to wrap the top half with sound attenuating materials. This discrepancy could explain the sudden appearance of the low frequency notch for higher elevations.

#### *iv. Conclusions*

The HRTF measurements of the pallid bat head with a normal, intact ear and with tragus removed allowed us to determine contributions of the conspicuous structure to the sound localization ability of the bat. We have discovered a gradient of spectral notches that shifts with changing source elevation. Furthermore, we have found evidence for the involvement of the tragus in the detection and localization of both archetypes of sound most relevant for pallid bat behavior, prey-generated noise and echolocation frequencies. These myriad spectral cues generated by the external ear of the pallid bat call for several future studies which will attempt to determine their relevance to the encoding of spatial information and the perception of sound sources.

1. Blauert, J. Spatial hearing with multiple sound sources and in enclosed spaces. in *Spatial Hearing: The Psychophysics of Human Sound Localization* 201–287 (MIT Press, 1997).
2. Grothe, B., Pecka, M. & McAlpine, D. Mechanisms of Sound Localization in Mammals. *Physiol. Rev.* **90**, 983–1012 (2010).
3. Brown, C. H. & May, B. J. Comparative mammalian sound localization. in *Sound source localization* 124–178 (Springer, 2005).
4. Fuzessery, Z. M. Monaural and binaural spectral cues created by the external ears of the pallid bat. *Hear. Res.* **95**, 1–17 (1996).
5. Huang, A. Y. & May, B. J. Spectral cues for sound localization in cats: Effects of frequency domain on minimum audible angles in the median and horizontal planes. *J. Acoust. Soc. Am.* **100**, 2341–2348 (1996).
6. Firzlaff, U. & Schuller, G. Spectral directionality of the external ear of the lesser spear-nosed bat, *Phyllostomus discolor*. *Hear. Res.* **185**, 110–122 (2003).
7. Rice, J. J., May, B. J., Spirou, G. A. & Young, E. D. Pinna-based spectral cues for sound localization in cat. *Hear. Res.* **58**, 132–152 (1992).
8. Blauert, J. Spatial hearing with one sound source. in *Spatial Hearing: The Psychophysics of Human Sound Localization I* 36–200 (MIT Press, 1997).
9. Blauert, J. Sound localization in the median plane. *Acta Acust. united with Acust.* **22**, 205–213 (1969).
10. Butler, R. A. An analysis of the monaural displacement of sound in space. *Percept. Psychophys.* **41**, 1–7 (1987).
11. Roffler, S. K. & Butler, R. A. Factors That Influence the Localization of Sound in the Vertical Plane. *J. Acoust. Soc. Am.* **43**, 1255–1259 (1968).
12. Aytekin, M., Grassi, E., Sahota, M. & Moss, C. F. The bat head-related transfer function reveals binaural cues for sound localization in azimuth and elevation. *J. Acoust. Soc. Am.* **116**, 3594–3605 (2004).
13. Wotton, J. M., Haresign, T. & Simmons, J. A. Spatially dependent acoustic cues generated by the external ear of the big brown bat, *Eptesicus fuscus*. *J. Acoust. Soc. Am.* **98**, 1423–1445 (1995).
14. Wotton, J. M., Haresign, T., Ferragamo, M. J. & Simmons, J. A. Sound source

- elevation and external ear cues influence the discrimination of spectral notches by the big brown bat, *Eptesicus fuscus*. *J. Acoust. Soc. Am.* **100**, 1764–1776 (1996).
15. Neuweiler, G. Foraging ecology and audition in echolocating bats. *Trends Ecol. Evol.* **4**, 160–166 (1989).
  16. Bell, G. P. Behavioral and ecological aspects of gleaning by a desert insectivorous bat *Antrozous pallidus* (Chiroptera: Vespertilionidae). *Behav. Ecol. Sociobiol.* **10**, 217–223 (1982).
  17. Hackett, T. D., Korine, C. & Holderied, M. W. A whispering bat that screams: bimodal switch of foraging guild from gleaning to aerial hawking in the desert long-eared bat. *J. Exp. Biol.* **217**, 3028–32 (2014).
  18. Measor, K. R. *et al.* Matched Behavioral and Neural Adaptations for Low Sound Level Echolocation in a Gleaning Bat, *Antrozous pallidus*. *eneuro* **4**, ENEURO.0018-17.2017 (2017).
  19. Fuzessery, Z. M., Buitenhoff, P., Andrews, B. & Kennedy, J. M. Passive sound localization of prey by the pallid bat (*Antrozous p. pallidus*). *J. Comp. Physiol. A* **171**, 767–777 (1993).
  20. Barber, J. R., Razak, K. A. & Fuzessery, Z. M. Can two streams of auditory information be processed simultaneously? Evidence from the gleaning bat *Antrozous pallidus*. *J. Comp. Physiol. A Sensory, Neural, Behav. Physiol.* **189**, 843–855 (2003).
  21. Razak, K. A., Yarrow, S. & Brewton, D. Mechanisms of Sound Localization in Two Functionally Distinct Regions of the Auditory Cortex. *J. Neurosci.* **35**, 16105–15 (2015).
  22. Razak, K. A. & Fuzessery, Z. M. Functional Organization of the Pallid Bat Auditory Cortex: Emphasis on Binaural Organization. *J. Neurophysiol.* **87**, 72–86 (2002).
  23. Razak, K. A. & Fuzessery, Z. M. GABA Shapes a Systematic Map of Binaural Sensitivity in the Auditory Cortex. *J. Neurophysiol.* **104**, 517–528 (2010).
  24. Razak, K. A. Systematic representation of sound locations in the primary auditory cortex. *J. Neurosci.* **31**, 13848–59 (2011).
  25. Razak, K. A. Mechanisms underlying azimuth selectivity in the auditory cortex of the pallid bat. *Hear. Res.* **290**, 1–12 (2012).

26. Fenton, M. B. & Bogdanowicz, W. Relationships between external morphology and foraging behaviour: bats in the genus *Myotis*. *Can. J. Zool.* **80**, 1004–1013 (2002).
27. Wotton, J. M. & Simmons, J. A. Spectral cues and perception of the vertical position of targets by the big brown bat, *Eptesicus fuscus*. *J. Acoust. Soc. Am.* **107**, 1034 (2000).
28. Chiu, C. & Moss, C. F. The role of the external ear in vertical sound localization in the free flying bat, *Eptesicus fuscus*. *J. Acoust. Soc. Am.* **121**, 2227–2235 (2007).
29. Aytekin, M., Grassi, E., Sahota, M. & Moss, C. F. The bat head-related transfer function reveals binaural cues for sound localization in azimuth and elevation. *J. Acoust. Soc. Am.* **116**, 3594–3605 (2004).
30. Lawrence, B. D. & Simmons, J. A. Echolocation in bats: the external ear and perception of the vertical positions of targets. *Science* **218**, 481–3 (1982).
31. Guppy, A. & Coles, R. B. Acoustical and neural aspects of hearing in the Australian gleaning bats, *Macroderma gigas* and *Nyctophilus gouldi*. *J. Comp. Physiol. A* **162**, 653–668 (1988).
32. Coles, R. B., Guppy, A., Anderson, M. E. & Schlegel, P. Frequency sensitivity and directional hearing in the gleaning bat, *Plecotus auritus* (Linnaeus 1758). *J. Comp. Physiol. A* **165**, 269–280 (1989).
33. Obrist, M. K., Fenton, M. B., Eger, J. L. & Schlegel, P. A. What ears do for bats: a comparative study of pinna sound pressure transformation in chiroptera. *J. Exp. Biol.* **180**, (1993).
34. Imig, T. J., Bibikov, N. G., Poirier, P. & Samson, F. K. Directionality Derived From Pinna-Cue Spectral Notches in Cat Dorsal Cochlear Nucleus. *J. Neurophysiol.* **83**, 907–925 (2000).
35. Tollin, D. J., Ruhland, J. L. & Yin, T. C. T. The role of spectral composition of sounds on the localization of sound sources by cats. *J. Neurophysiol.* **109**, 1658–1668 (2013).
36. Butler, R. A. & Belendiuk, K. Spectral cues utilized in the localization of sound in the median sagittal plane. *J. Acoust. Soc. Am.* **61**, 1264–1269 (1977).
37. Rice, J. J., May, B. J., Spirou, G. A. & Young, E. D. Pinna-based spectral cues for sound localization in cat. *Hear. Res.* **58**, 132–152 (1992).

38. Tollin, D. J., Ruhland, J. L. & Yin, T. C. T. The role of spectral composition of sounds on the localization of sound sources by cats. *J. Neurophysiol.* **109**, 1658–1668 (2013).
39. Wotton, J. M. & Simmons, J. A. Spectral cues and perception of the vertical position of targets by the big brown bat, *Eptesicus fuscus*. *J. Acoust. Soc. Am.* **107**, 1034 (2000).
40. Dalland, J. I. Hearing Sensitivity in Bats. *Science (80-. )*. **150**, 1185–1186 (1965).
41. Koay, G., Heffner, H. E. & Heffner, R. S. Audiogram of the big brown bat (*Eptesicus fuscus*). *Hear. Res.* **105**, 202–210 (1997).
42. Koay, G., Kearns, D., Heffner, H. E. & Heffner, R. S. Passive sound-localization ability of the big brown bat (*Eptesicus fuscus*). *Hear. Res.* **119**, 37–48 (1998).
43. Goerlitz, H. R., Greif, S. & Siemers, B. M. Cues for acoustic detection of prey: insect rustling sounds and the influence of walking substrate. *J. Exp. Biol.* **211**, 2799–806 (2008).
44. Razak, K. A. Functional segregation of monaural and binaural selectivity in the pallid bat auditory cortex. *Hear. Res.* **337**, 35–45 (2016).
45. Musicant, A. D., Chan, J. C. K. & Hind, J. E. Direction-dependent spectral properties of cat external ear: New data and cross-species comparisons. *J. Acoust. Soc. Am.* **87**, 757–781 (1990).
46. Davis, K. A., Ramachandran, R. & May, B. J. Auditory Processing of Spectral Cues for Sound Localization in the Inferior Colliculus. *JARO - J. Assoc. Res. Otolaryngol.* **4**, 148–163 (2003).
47. Tollin, D. J. & Yin, T. C. T. Spectral Cues Explain Illusory Elevation Effects With Stereo Sounds in Cats. *J. Neurophysiol.* **90**, 525–530 (2003).
48. Algazi, V. R., Avendano, C. & Duda, R. O. Elevation localization and head-related transfer function analysis at low frequencies. *J. Acoust. Soc. Am.* **109**, 1110–1122 (2001).

## Chapter 3

### Accurate sound localization behavior in a gleaning bat, *Antrozous pallidus*

#### Abstract

Acute auditory processing in bats is typically associated with echolocation. A subset of bats, called gleaners, listens to prey-generated noise to hunt surface-dwelling prey. Gleaners depend less on echolocation to hunt and, therefore, accurate localization of prey-generated noise is necessary for foraging success. Here we studied azimuth sound localization behavior in the pallid bat, a gleaning bat in which spatial encoding has been studied extensively. We tested pallid bats on a relatively difficult open loop task (single sound, duration  $\leq 200$  ms). The bats were trained to face the midline when stimulus was presented, and this was confirmed with video analysis. Bats localized broadband noise (5-30 kHz) from 1 out of 11 speakers spaced evenly across the horizontal plane of the frontal sound field. Approach to the correct speaker was rewarded. Pallid bats show accurate localization near the midline with mean errors between 3-6°. Remarkably, the accuracy does not decline significantly at peripheral locations with bats averaging  $< \sim 7^\circ$  error up to 72° off midline. Manipulation of stimulus bandwidth shows that higher frequencies (20-30 kHz) are necessary for accurate localization. Comparative studies of gleaning bats will reveal convergent adaptations across auditory systems for non-echolocation-based behaviors in bats.

## Introduction

Sound localization is a primary function of the auditory system. The ability to localize sounds is important for successful foraging, avoiding predation, and locating a mate. Most bat species use echolocation for general orientation and foraging<sup>1-5</sup>. A small group of bat species have evolved another foraging strategy, called surface gleaning, in which prey-generated sounds are localized to hunt prey from a substrate (ground, foliage, etc.). The term ‘passive localization’ is used to describe the dependence of gleaning bats on prey-generated sounds to hunt. While gleaners can use a combination of passive localization, active echolocation and vision to hunt, the greater dependence on prey-generated noise distinguishes this group of bats from those that depend on echolocation for foraging<sup>1,6-9</sup>. Indeed, gleaning bats often reduce echolocation rates and intensities when closing in on prey<sup>1,10,11</sup>. Gleaning bats are present across multiple families, suggesting convergent evolution of this foraging strategy, but the neural specializations that support gleaning behavior across species are unclear. Given the dependence of gleaning bats on localizing relatively low intensity, prey-generated noise in the dark, it is likely that they have specializations for sound localization. However, few studies have examined the sound localization performance of gleaning bats. Here, we studied sound localization in the pallid bat (*Antrozous pallidus*), a gleaner, and report one of the most accurate localization performance across the frontal azimuth plane amongst vertebrates.

The pallid bat depends on prey-generated noise to hunt terrestrial prey such as crickets and scorpions<sup>12,13</sup>. Previous observations of sound localization behaviors in the pallid bat were performed in a manner that mimicked natural hunting behaviors wherein

the bat was in flight or on a perch when the sound was presented<sup>10,13</sup>. Therefore, the head orientation in relation to the sound source was unknown. These studies reported localization accuracy of  $\sim 2\text{-}4^\circ$ , but it remains unclear if and how the accuracy of localization is related to the eccentricity of source location. It is also unclear if properties of sound, such as duration and bandwidth show interactions with eccentricity of source location in determining accuracy. Therefore, it has not been possible to link behavioral outcomes to predictions from known cortical maps to examine the neuroethology of sound localization in the pallid bat.

Recent electrophysiological studies have suggested a cortical population code for the representation of 2D source locations<sup>14–17</sup>. The auditory cortex of the pallid bat contains a region selective for broadband noise with spectral energy present in prey-generated noise. Approximately a third of this noise-selective region contains neurons with peaked azimuth selectivity functions with preferred azimuth at  $\sim 0\text{-}15^\circ$ . This suggests the presence of a cortical region specialized for midline azimuth localization. A second cluster within the noise-selective region contains neurons with sigmoid-shaped azimuth functions, with strong responses to contralateral locations. The intrinsic organization of this binaural cluster is such that the area of active cortex increases systematically as the sound moves from midline to more contralateral locations. Previous studies also indicated that azimuth selectivity is predicted by interaural intensity difference (IID) selectivity<sup>16</sup>. Ear directionality of the pallid bat is broad for frequencies below 15 kHz, and begins to sharpen and generate increasing IIDs for frequencies above 15 kHz<sup>18</sup>.

These studies make several predictions regarding azimuth localization by the pallid bat. First, the presence of a midline sensitive binaural cluster suggests that the bat should be most accurate near the midline. While this is not surprising given the comparative literature<sup>19–22</sup>, the electrophysiology data also suggests that the bat should be accurate at more eccentric locations. In the cluster of neurons with sigmoidal azimuth functions, the slopes of these functions are found across the frontal space, including peripheral locations. Slopes of approximately 40% of neurons course the midline. The remaining neurons have their azimuth slopes at more peripheral locations, including a sizable number with slopes located at  $>30^\circ$  from midline<sup>16</sup>. The notion that azimuth function slopes are where neurons provide maximal information for spatial discrimination leads to the prediction that the bat should perform relatively accurately at peripheral locations. The ear directionality and IID/azimuth correlation results indicate that azimuth localization accuracy should improve with inclusion of frequencies  $>15$  kHz<sup>14,16,18</sup>.

Here, we tested these predictions in a set up that allowed for the measurement of head position when a single, short noise burst was presented from 1 out of 11 speakers distributed evenly on the ground in front of the bat. This is an open loop task in that the sound was presented just once and with a duration that likely precluded head movements to update information. Thus, we tested the limits of azimuth localization accuracy in the pallid bat. The task for the bat was to localize the sound and crawl to the speaker for a reward. This allowed a measurement of absolute sound localization accuracy across frontal space.

## Methods

*Animals.* Pallid bats were netted in California, Arizona, and New Mexico and housed in an 11 X 14 feet flight room at the University of California, Riverside. The room was maintained on a reversed 12-hour light/dark cycle. Bats involved in the experiments were paired and housed in standard mouse cages with *ad libitum* access to water. The bats were moved to a different room (13W x 14L x 9H feet) for training and testing. This room contained the speaker array at one corner and was anechoic (Sonex, 3in foam). The bats were returned to the flight room and left overnight in their cages at the end of trials each day. All experimental procedures used were approved by the Institutional Animal Care and Use Committee (AUP20160044). A total of 8 bats were used for this study. Bats were fed only in the room where testing occurred for the duration of the experiments. Weights of the bats were monitored daily and maintained above 80% of the starting weight.

*Apparatus.* 11 holes were cut out of a plywood board, distributed in a semicircular pattern with each hole separated by 18° from the next. The radius of the semicircle was 0.9 m. Speakers were mounted to the underside of each hole in the plywood board (Figure 3.1A). The plywood board was placed horizontally on the floor such that the speakers faced upwards. A wire mesh was affixed on top of each hole to allow placement of freshly killed mealworms as reward for accurate localization. The wire mesh was ~5 mm below the surface of the platform. All non-target locations contained dummy mealworms made of clay and with similar dimensions as real worms. A 10.5 x 19 x 8in (L x W x H)

box was secured to the middle of the semicircular array of speakers (Fostex FT17H), such that an opening at one end of the box was equidistant (0.9m) from all speakers. The bat entered the speaker arena through this opening. Two infrared video cameras (XA10 Professional, Canon) were mounted directly above the opening in the box. One camera was angled such that the entire array was visible to analyze the approach behavior. The second camera was zoomed into the opening in the box from which the bats would initiate their localization trials. The recordings from this camera were used to analyze head position at sound presentation (see *Head Orientation Measurements*). All trials were recorded under infrared light illumination (IRLamp6; Bat Management IR Kit). The experimenter also wore a headlamp with red light to observe the bats during all trials.

*Sound localization training.* Bats were conditioned to associate noise bursts with food reward. Pallid bats do not readily approach speakers generating noise<sup>13</sup>. Therefore, a specific sequence of training was used on each bat. To begin, each bat fed on freshly killed mealworms *ad libitum* for 30 minutes per day in the testing arena, until they became comfortable enough to remain in the testing arena voluntarily for the entire duration. No measures were taken to keep animals in the arena, and the bats could fly away at will. After a few days, the bats would remain foraging for the entire 30-minute duration. Mealworms were then moved to a random speaker location from which a broadband noise (5-30 kHz, 200 ms white noise) was repeated continuously at a rate of 1 Hz. Eventually, the bats would readily localize the sound, move to the speaker, and

obtain food reward. At this point, only the sound-producing speaker contained a single mealworm, while all other speakers contained clay mealworm models.

To ensure relatively consistent head positions at the time of sound presentation, bats were trained to walk through a plastic box with holes cut out on each end to enter the arena before foraging. Sound presentation only began when the bat emerged from the box. The noise was played less frequently each day, until the bats attempted to localize only one sound presentation consistently. Bats were then trained to wait at the same location just outside the box with their heads facing forward until the sound was played. If they tried to approach a speaker or turned their heads off center, the bats were given a brief time out before being allowed to try the task again. A running average of degrees of error at the midline speakers over five days was calculated to determine when testing should begin. A correct response is counted as an error = 0°. If the bat missed the target by one speaker, the result was 18° error, and so on. Most mammals tested on sound localization ability exhibit less than 18° of error when localizing broadband sounds from directly ahead<sup>23</sup>. Therefore, we used this as the criterion performance before moving to the testing phase. When bats were successfully localizing broadband sounds at the midline speakers (Figure 3.1A, black boxes) with less than 18° error, data collection commenced. The bats rarely required more than the initial five days to demonstrate an average of less than 18° of error for sounds from the midline speakers. Between 20-30 trials were completed each day, so the bats reached this criterion within 150 trials.

*Stimulus and data collection protocol.* The 200 ms broadband noise was generated using Audacity software. To confirm signal fidelity over the course of the experiments, the frequency response of all speakers was periodically measured with an ultrasonic microphone (Sokolich Ultrasonic Probe Microphone System). Speaker output was relatively flat (within 6 dB) across the 5-30 kHz range for the duration of the experiments. The possibility of bats using variation in intensity from speaker to speaker to identify the sound source was addressed by randomizing the intensity on each trial, between 60 and 70 dB SPL, measured 10cm above the speakers.

Another potential cue that the bats may use to their advantage in this task is the noise generated by the experimenter in preparation for the next trial. Reward placement cues between trials are of particular concern. To ensure our bats were not able to use this information, they were placed in a holding cage in the opposite side of the experiment room between trials. Thus, visual observation of reward placement was impossible. In addition, the experimenter intentionally replaced the dummy clay worms at multiple speakers before each trial. This ensured that ‘reward placement sounds’ were present from multiple locations before each trial.

Data were obtained for various duration and band-limited stimuli. 50, 100, and 200ms duration broadband noise and 200ms duration 20 kHz low-pass-filtered noise (20LP) were tested first. Subsequently, 200ms duration, 15 kHz and 20 kHz high-pass-filtered noise (15HP and 20HP) and 15 kHz low-pass-filtered noise (15LP) were tested. An external filter (Model 3364, Krohn-Hite Corporation) was used to generate filtered noise. Sounds were presented pseudo-randomly from different locations, up to a

maximum of 30 trials per day per bat, to maintain motivation for the bats to participate on consecutive days. Data collection was considered complete when bats had localized each stimulus (different bandwidths and durations) 15 times at every speaker location. An incomplete data set was collected from 2 bats localizing a 15-kHz tone, but the data collection was stopped before completion due to the inability of the bats to localize the pure tone stimulus (see Results).

*Head Orientation Measurements.* All trials were video recorded to ensure head orientation towards the midline speakers when the sound was presented. We randomly picked 60% of the trials to determine head orientation distribution. We assumed this would reflect the distribution present in the entire data set. To find the video frame corresponding to the moment of sound onset, the stimulus was split at the output of the external data acquisition card (Spectra DAQ-200, SpectraPLUS). One path led to the external filter and then on to the speakers. The other path was fed into the microphone input of the overhead camera zoomed in to view the task start point, such that the only sound present in these video files were the stimuli themselves. The resulting audio was extracted from these video files, and a custom Matlab script was used to extract the time points of sound onset from these audio files. Time points were then converted back to frame numbers, and these frames were manually examined in the video files. The Kinovea video analysis software package was used to measure the head orientation of the bats in these frames. The native protractor tool was used to determine the angle of the bat's head relative to the midline speaker. The front of the box was aligned perpendicular

to the midline, and therefore served as consistent feature for alignment of the frame to the midline speaker. The protractor was aligned with this perpendicular plane and its swivel point was positioned on the center of the region between the base of each of the bats' ears. One end of the protractor would then be turned to intersect the nose of the bat. The corresponding angle from the midline, or the head orientation, was simply the absolute value of a subtraction of this protractor reading from 270 degrees.

*Data analysis and statistical methods.* Sound localization accuracy was quantified as the percentage of correct trials, average error, and the mutual information between sound source location and response location. Percent correct data was calculated as the percentage of correct responses for each bat and stimulus condition. Error was calculated as the average error for each bat and stimulus condition. Mutual information was calculated from the equation:

$$I(X;Y) = \sum_{y \in Y} \sum_{x \in X} p(x,y) \log \left( \frac{p(x,y)}{p(x)p(y)} \right) \quad (1);$$

where X and Y are the sound location and response location, respectively,  $p(x,y)$  is the probability of the joint occurrence of X and Y, and  $p(x)$  and  $p(y)$  are the probabilities of X and Y independently occurring, respectively. As in the percent correct and average error calculations, a mutual information value was calculated for each bat under each stimulus condition. For example, one bat would localize a 200ms broadband noise sound

(5-30kHz) at each of the peripheral speakers (Figure 3.1A, filled black circles) at least 15 times. Every trial, the bat receives a score based on the degrees of error away from the target speaker. These 90 data points are averaged to give the error estimate for the bat localizing 200ms broadband noise in the periphery. Each bat contributed a single value of each data type (percent correct, error, and mutual information) for each experiment, giving a total N of 4 to 7 per dataset, excluding tests of performance localizing the 15-kHz tone stimulus (N=2).

Means of percentage correct and degrees of error measurements on behavioral performance across various bandwidths, locations, and durations were compared with the Repeated Measures Two-Way ANOVA statistical test (IBM SPSS Statistics 24), unless specified otherwise, to determine the effect of each factor. Outliers were identified and removed using the boxplot function in SPSS (IBM SPSS Statistics 24). Outliers were identified based on the data that reside outside the 1.5XIQR (interquartile range). Only two data points were excluded based on this criterion (degrees of error obtained from bat A1 at peripheral locations for 50 and 100ms duration sounds). Data were tested for normal distribution with the Kolmogorov-Smirnov test prior to hypothesis testing. Based on the outcome of this analysis, all statistics are reported with the F-test statistic for main effects. All pairwise multiple comparison procedures were run after finding a main effect ( $p < 0.05$ ). P-values for each comparison of the *post hoc* tests are reported. The datasets of the current study are available from the corresponding author on reasonable request.

## Results

The main goal of this study was to quantify azimuth localization performance across the frontal hemifield and test the influence of duration and bandwidth on localization accuracy. Experiments were designed to identify potential interactions between location and duration or bandwidth in determining accuracy. Data were collected on an approach-to-speaker task (Figure 3.1A). The 90° speaker data were not analyzed. The 90° positions represented the extremes of the array. Each of the 90° speakers only contained one adjacent speaker (the 72° location). This makes the 90° locations different from all other speakers, which contained two neighboring speakers. The 90° speakers were utilized in the study to maintain symmetry of speakers for the most eccentric locations (72°) that were quantified. Bats were trained to face the midline for sound presentation. The head position was analyzed off-line using video recordings to establish trial inclusion criteria.

### *i. Validation of head orientation at sound presentation*

We performed offline video analyses of head position to ensure that the bats were facing the midline speakers when the stimulus was presented. For this purpose, we randomly selected ~60% of all trials (3099/5164 trials) to quantify the bat's head position in the video frame at which the sound was presented. Our inclusion criterion was that the bat's head should be oriented within  $\pm 18^\circ$  of the midline at the time of sound presentation. This criterion was satisfied in the vast majority of the trials (93%) (Figure 3.1B). There was no difference in statistical significance of reported results if the 7% of

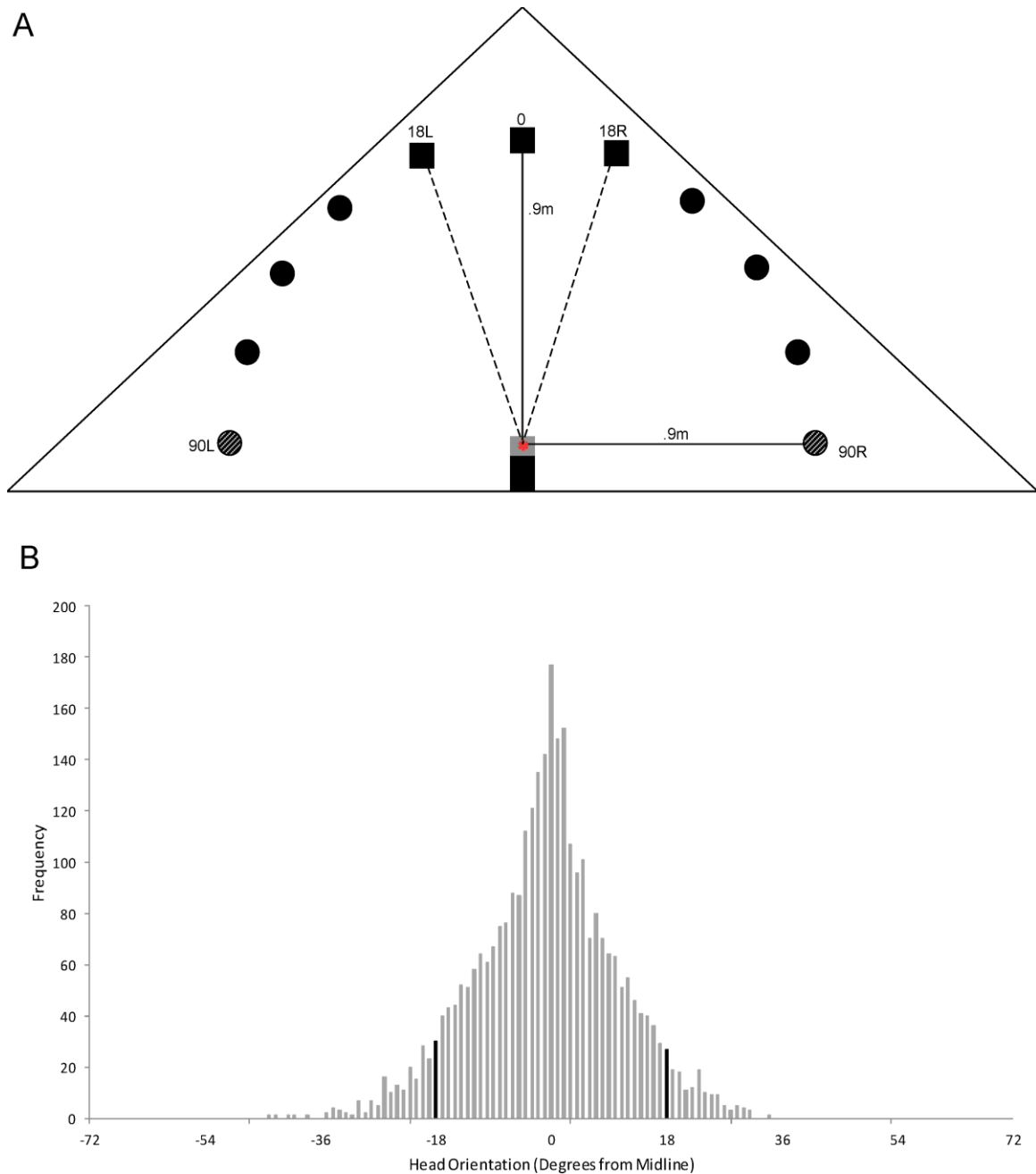


Figure 3.1. **(A)** A schematic of the speaker array used to test pallid bat azimuth localization accuracy. Eleven speakers (circles and boxes) were mounted ( $18^\circ$  separation between speakers) to sample across  $180^\circ$  of frontal azimuth space. Bats were trained to crawl out of a cage (black box,  $42 \times 21 \times 20$  cm) and position themselves in a consistent location (grey box and asterisk). The bats were also trained to orient towards the midline (between the two dashed lines) for the stimulus to be presented. For two-way ANOVA analyses, speakers were grouped into midline (black squares) and peripheral (black circles) locations. The two most peripheral speakers (striped circles at  $90^\circ$ ) were excluded from data analysis. **(B)** Distribution of measured head orientation relative to the midline. Data are separated into  $1^\circ$  bins. Black bars represent the criterion  $-18^\circ$  to  $18^\circ$  window.

trials (for which the head position did not meet criterion) were included or not. Based on the observation that head position was within criterion in 93% of the randomly chosen 3099 trials, we assume a similar distribution across all 5164 trials. Therefore, we present data from all 5164 trials below.

## *ii. Localization of Broadband Noise*

Confusion matrices are often used to show sound localization accuracy<sup>20,22,24</sup>. The confusion matrix displays the actual location of the sound on the abscissa and the bat's trial, all circles would be of maximum size and centered on the diagonal. A qualitative examination of each confusion matrix (Figure 3.2A-G, each panel shows data from an individual bat, n=7) shows that the bats were accurate to within one speaker location on most trials. This is further demonstrated by the composite performance matrix (Figure 3.2H), which shows that on average, pallid bats rarely missed by more than 1 speaker away from the target.

Three measures were calculated from confusion matrices to quantify sound localization accuracy: mutual information (MI), percent correct (PC), and degree error (DE) (Figure 3.3). Localization of a 200ms broadband noise (5-30kHz) was quantified for the midline speaker (0°) and the two adjacent speakers (see Figure 3.1, black squares for speaker locations). On average, pallid bats approached the correct speaker accurately ~80% of the time. The average localization error for these midline locations is ~4°. Mutual information is an additional measure that indicates performance accuracy. This value represents the predictability of unknown data (response location), given known data

(stimulus location). This unit of information is measured in bits and is maximized by perfect performance. On average, the MI for broadband localization in pallid bats is 1.10 (maximum possible in this task is 1.59). Taken together, these data show that even with a relatively difficult open loop task, the pallid bat shows quite accurate localization of broadband noise near the midline.

*iii. Localization accuracy does not deteriorate significantly, even at eccentric locations*

Tables 1 and 2 show the performance of pallid bats localizing the 200ms broadband noise across the entire speaker array. Localization is relatively accurate throughout the frontal azimuth plane. Comparison of performance from midline to peripheral space shows that the average percent correct changes from ~78% to 67% and the average degree error changes from ~4° to 7°. However, these trends were not statistically significant (One-Way Repeated Measures ANOVA: Percent Correct:  $F_{(4, 7)} = 1.490$ ,  $p = 0.236$ ; Error:  $F_{(4, 7)} = 1.795$ ,  $p = 0.163$ ), indicating that pallid bat sound localization ability does not decline even at relatively eccentric locations when localizing broadband noise. All subsequent analyses combine speakers into midline or peripheral groups (Figure 3.1; filled boxes and circles, respectively) to determine interactions between the location and the duration or bandwidth of the stimulus.

*iv. Influence of sound duration on azimuth localization*

To determine if performance deteriorates for shorter sound durations<sup>20–23</sup> in an azimuth dependent manner in the pallid bat, we tested two additional durations (50, 100

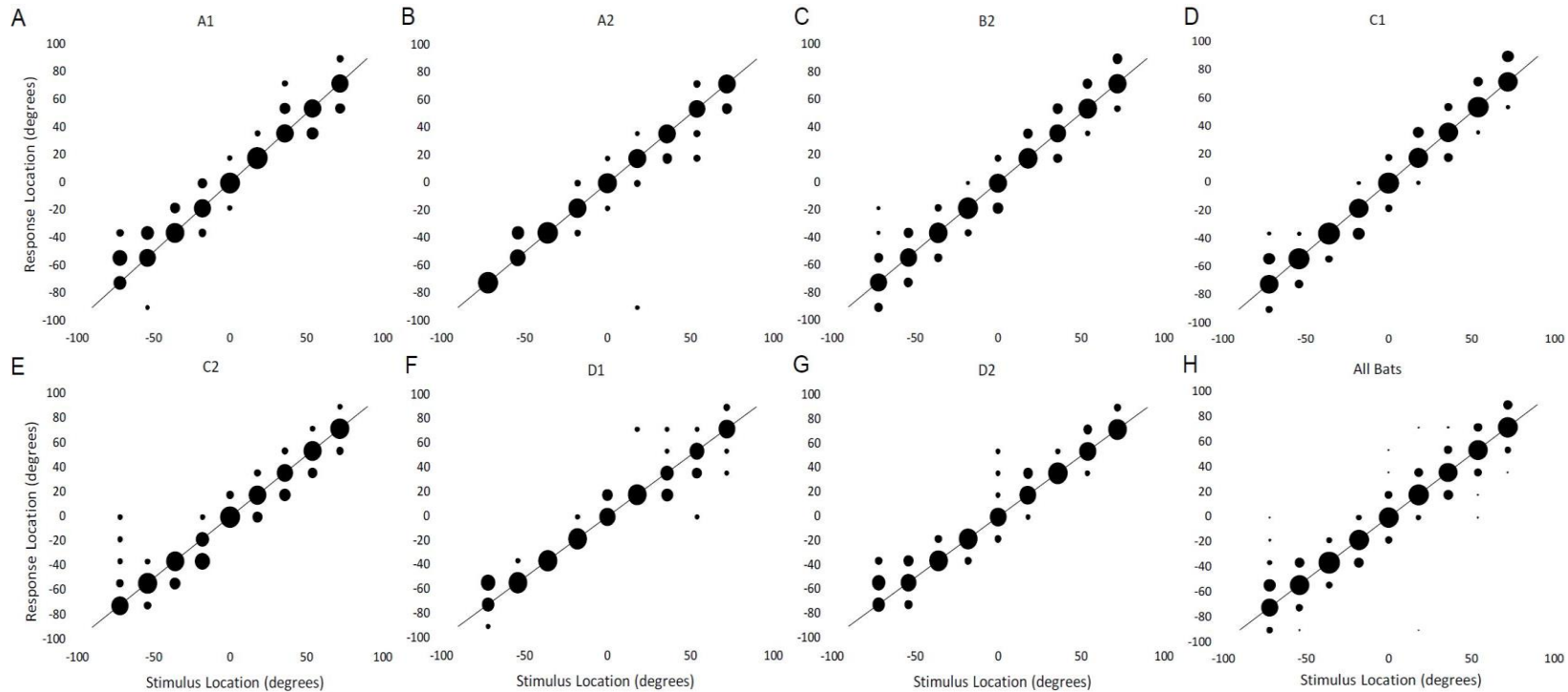


Figure 3.2. Confusion matrices demonstrate the performance of individual bats (A-G) and average performance (H). These data are for the 200ms broadband noise stimulus. Circle position indicates the response location for a given stimulus location. The size of the circle indicates the percentage of trials on which the bat responded to a given speaker location. When a circle falls along the diagonal line, it is representative of  $0^\circ$  error. Circles falling above or below the diagonal by one position indicate  $18^\circ$  of error, and so on. A qualitative examination of the confusion matrices shows that the bats approached the correct speaker on the majority of trials, and mistakes were rarely more than one speaker away from the correct location.

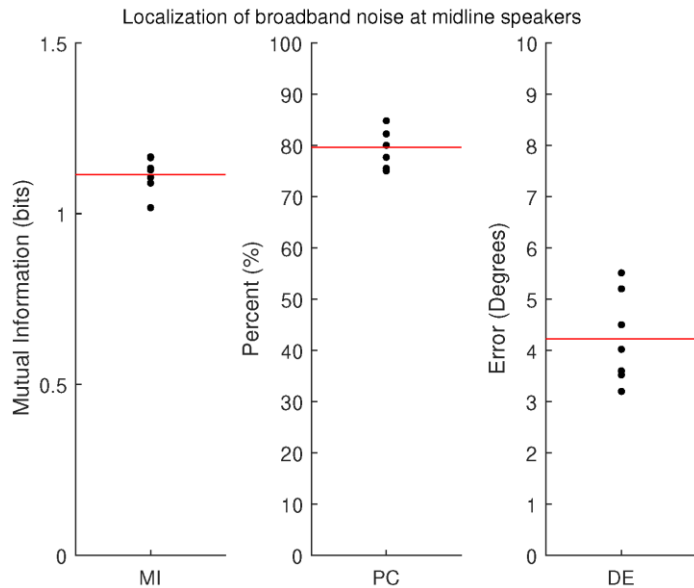


Figure 3.3. Performance of 7 pallid bats on the broadband noise (5-30kHz, 200ms) localization task, quantified using three separate measures: Mutual Information (A), Percent Correct (B), and Error (C). The solid red line in each plot indicates means of each measure. The theoretical maximum mutual information bit value is 1.59.

ms). Confusion matrices indicate better performance when the sound source duration is 200ms compared to 50ms (Figure 3.4A-C). There is a main effect of sound source duration when measured by mutual information (Figure 3.4D;  $F_{(2, 4)} = 7.295$ ,  $p = 0.03$ ) and the percent of correct responses (Figure 3.4E;  $F_{(2, 4)} = 4.957$ ,  $p = 0.05$ ), but not when measured by degrees of error (Figure 3.4F;  $F_{(2, 4)} = 4.066$ ,  $p = 0.11$ ). The mutual information between the perceived sound source and the location of the actual sound source is significantly greater when the sound source is 200 ms compared to 50 ms, but not 100ms (Figure 3.4D; *post-hoc*: 200 vs. 50ms:  $p = 0.05$ , 200 vs. 100ms:  $p = 0.20$ , 100 vs. 50ms:  $p = 0.11$ ). Post-hoc tests show comparable results for percent of correct trials (Figure 3.4E; *post-hoc*: 200 vs. 50ms:  $p = 0.01$ , 200 vs. 100ms:  $p = 0.50$ , 100 vs. 50ms:  $p = 0.15$ ). There was no interaction between duration and location (two-way repeated measures ANOVA,  $F_{(2, 4)} = 4.066$ ,  $p = 0.11$ ), indicating that the longer duration sounds do not provide an advantage at specific locations. These data demonstrate that pallid bats are more accurate when localizing sounds of 200 and 100ms duration, compared to 50ms.

Animal ID	Location (Degrees from Midline)					
	0	18	36	54	72	90
A1	87.50	79.31	72.00	63.64	52.94	35.14
A2	86.67	80.00	86.96	64.71	90.00	18.18
B2	67.65	83.33	68.85	68.85	66.18	53.13
C1	80.65	72.13	80.00	81.36	67.19	56.25
C2	87.50	55.88	65.71	77.42	74.19	29.03
D1	68.75	93.33	74.19	76.67	58.06	35.48
D2	70.59	78.13	90.00	65.63	63.33	47.06
<b>Means <math>\pm</math> S.E.</b>	<b>78.47 <math>\pm</math> 3.48</b>	<b>77.45 <math>\pm</math> 4.34</b>	<b>76.82 <math>\pm</math> 3.46</b>	<b>71.18 <math>\pm</math> 2.70</b>	<b>67.41 <math>\pm</math> 4.55</b>	<b>39.18 <math>\pm</math> 5.17</b>

Table 1. Percent of correct responses when localizing 200ms broadband noise across the separate possible sound source locations of the speaker array are shown for each of the 7 tested bats. Data are combined for each speaker equidistant to the left and right of the midline speaker. Therefore, data are approximately doubled for locations 18-72° off midline, compared to the midline (0°). Means and standard error are reported in bold on the last row.

Animal ID	Location (Degrees from Midline)					
	0	18	36	54	72	90
A1	2.25	3.72	5.76	7.09	9.53	27.73
A2	2.40	6.60	2.35	7.41	1.80	30.27
B2	5.82	3.00	5.61	5.61	6.88	11.53
C1	3.48	5.02	3.60	3.36	6.19	10.13
C2	2.25	7.94	6.17	4.06	8.13	45.87
D1	5.63	2.40	5.23	5.40	8.13	22.06
D2	8.47	3.94	1.80	6.19	7.80	22.76
<b>Means <math>\pm</math> S.E.</b>	<b>4.33 <math>\pm</math> 0.90</b>	<b>4.66 <math>\pm</math> 0.75</b>	<b>4.36 <math>\pm</math> 0.67</b>	<b>5.59 <math>\pm</math> 0.56</b>	<b>6.92 <math>\pm</math> 0.94</b>	<b>24.34 <math>\pm</math> 4.59</b>

Table 2. Average error for 7 bats across the speaker array. All data are displayed as in Table 1.

While pallid bats miss more often when localizing 50ms duration sounds, the performance is still quite accurate for these short duration sounds.

*v. Pallid bat azimuth localization accuracy improves when noise includes 20-30 kHz*

To test whether the bandwidth of the target sound affects azimuth localization performance, we first tested two pallid bats on their ability to localize a 15-kHz pure

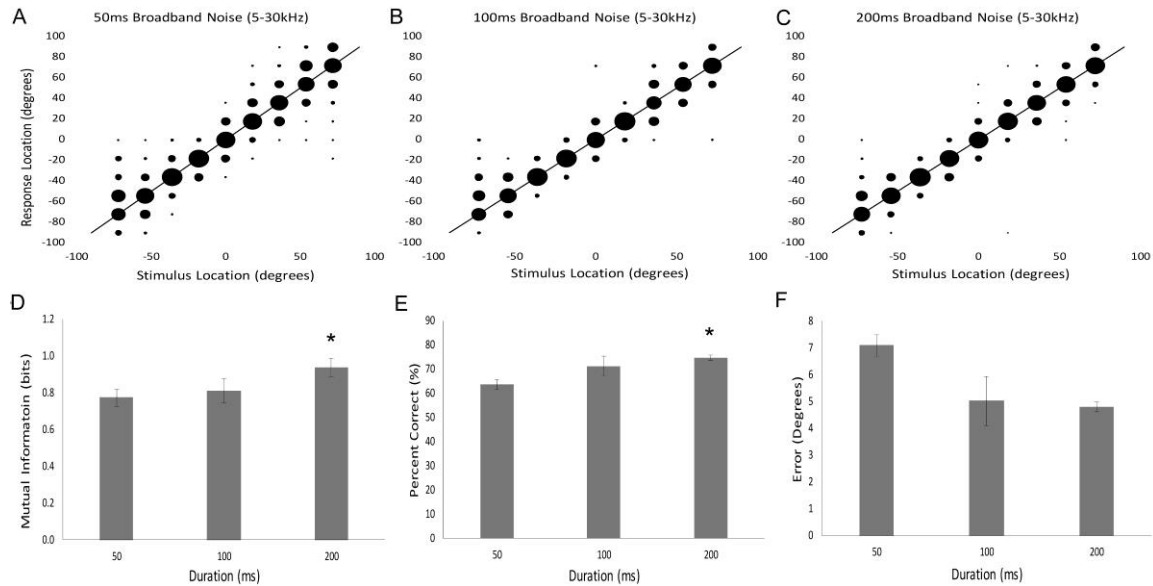


Figure 3.4. Effects of sound duration on localization behavior. Data are represented qualitatively in confusion matrices (A-C) and quantitatively in bar graphs (D-F). Bar graphs allow a comparison of group means (error bars denote s.e.) across the three different durations tested: 50, 100 and 200ms. Asterisks indicate a significant difference from the 50ms duration stimulus. \*  $p < 0.05$ .

tone. While these bats approached a speaker in response to a sound presentation, the data show that they were unable to localize, or even lateralize, these sound sources. The bats showed a response bias toward the left side of the speaker array, regardless of the sound source (Figure 3.5A). Due to the inability to localize pure tones by these two bats, we did not test additional bats and did not include tone localization performance in any further statistical comparisons.

Based on ear directionality studies that showed increasing IID values for frequencies  $>15$  kHz, it has been hypothesized that the high frequencies in prey-generated noise would be necessary for accurate localization<sup>18</sup>. This hypothesis was supported (Figure 3.5G-I). Confusion matrices demonstrate better performance for the HP noise (both 15kHz HP and 20kHz HP, termed HP15 and HP20, respectively)

compared to LP noise (cut-off at 15 and 20 kHz, termed LP15 and LP20, respectively) across all locations (Figure 3.5). Pallid bats demonstrated a significant increase in the percent of correct responses (Figure 3.5H;  $F_{(4, 4)} = 98.599$ ,  $p = 0.001$ ), and a significant decrease in degrees of error (Figure 3.5I;  $F_{(4, 4)} = 44.721$ ,  $p = 0.001$ ) for HP and broadband noise compared to LP noise. The percent of correct responses is significantly reduced for LP15 compared to the other sounds tested (Figure 3.5H; *post-hoc*: LP15 vs. HP15:  $p = 0.03$ , LP15-HP20:  $p = 0.01$ , LP15 vs. BBN:  $p = 0.002$ ). Post-hoc tests show a similar result for average error when comparing LP15 to the other sounds (Figure 3.5I; *post-hoc*: LP15 vs. HP15:  $p = 0.01$ , LP15 vs. HP20:  $p = 0.01$ , LP15 vs. BBN:  $p = 0.01$ ). When LP20 is compared to the HP and broadband noise, there is a trend for decreased accuracy (percentage correct, *post-hoc*: LP20 vs. HP15:  $p = 0.084$ , LP20 vs. HP20:  $p = 0.05$ , LP20 vs. BBN:  $p = 0.08$ ; degree of error, *post-hoc*: LP20-HP15:  $p = 0.091$ , LP20-HP20:  $p = 0.109$ , LP20-BBN:  $p = 0.116$ ), but no significant differences. When mutual information was used as measurement metric, there was no main effect of bandwidth, although there was a trend (Figure 3.5G;  $F_{(4, 4)} = 4.440$ ,  $p = 0.089$ ). Additionally, there was no significant difference in performance when localizing HP15 noise compared to broadband noise on all 3 measurements (Mutual Information (MI):  $p = 0.92$ , Percent Correct (PC):  $p = 0.12$ , and Error (E):  $p = 0.12$ ). Paradoxically, performance improved when localizing HP20 noise compared to broadband noise (MI:  $p = 0.03$ , PC:  $p = 0.03$ , E:  $p = 0.05$ ). There was no interaction between bandwidth and location (2way rpt-measures ANOVA), indicating that these observations are true across the entire frontal hemisphere.

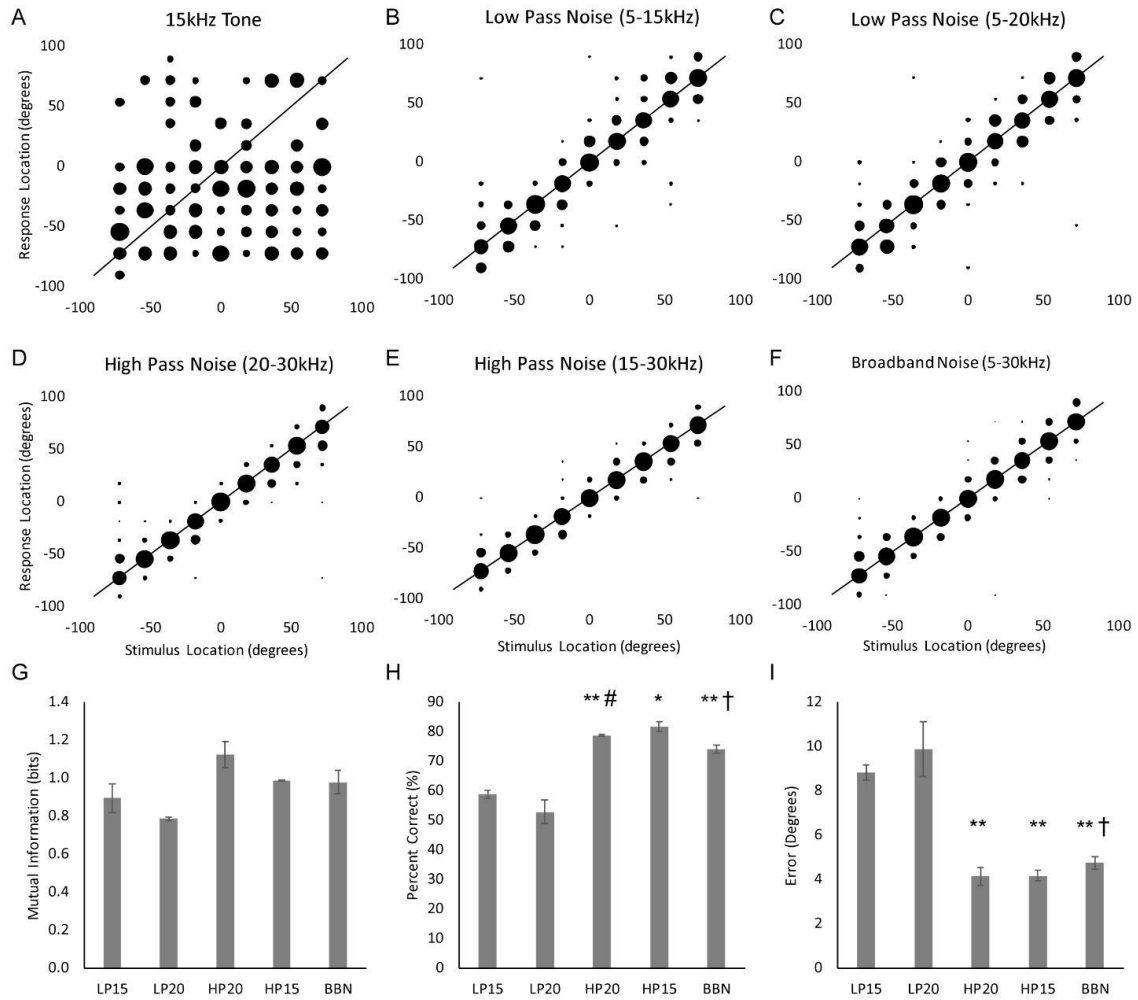


Figure 3.5. The presence of high frequencies in the stimulus is necessary for accurate localization performance. Data are represented qualitatively in confusion matrices (A-F) and quantitatively in bar graphs using the three data types: mutual information (G), percent of correct responses (H), and degrees of error (I). Bar graphs allow a comparison of group means (error bars denote s.e.) across the five different bandwidth conditions. Asterisks indicate a significant difference from the 15kHz low-pass stimulus, pound signs indicate a significant difference from the 20kHz low-pass stimulus, and crosses indicate a significant difference from the 20kHz high-pass stimulus. \*  $p<0.05$ , \*\*  $p<0.01$ .

Taken together, these data demonstrate that the pallid bat performs better with azimuth localization when the noise stimulus is broadband and includes frequencies >15 kHz.

## **Discussion**

The pallid bat exhibits a localization accuracy of  $\sim 4^\circ$  near the azimuth midline. Perhaps the more remarkable finding of this study is that the accuracy does not decline significantly at increasing azimuth angles, even up to  $72^\circ$  away from the midline. Most accurate localization was seen when frequencies >15 kHz were included in the stimulus, while the performance on the only pure tone tested was quite inaccurate.

### *i. Comparison of azimuth localization across species*

Humans, carnivores (cats and ferrets) and the barn owl have been best studied for absolute localization performance. The pallid bat is on par with these other vertebrates in midline localization. The performance of the bat at more peripheral locations is at least on par if not better (depending on the study) than the other animals tested. Comparison of sound localization estimates across species must consider the differences in task (pointing, approach, head orientation), stimulus used (tones versus noise), number of speakers tested and whether the task was absolute localization or relative localization (minimum audible angle). In general, localization is more accurate for broadband sounds than pure tones. Therefore, only studies that used broadband noise are compared here. One of the first assessments of human sound localization ability reported an average error of  $4.6^\circ$  when tasked with pointing to the location of a click<sup>19</sup>. A different study, using a

head orientation task and a 150ms, 1.8-16 kHz noise stimulus, reported  $< \sim 8^\circ$  error across the frontal hemifield, with the best performance near the midline ( $\sim 2-3^\circ$ )<sup>21</sup>. Although the standard deviation increased for more eccentric locations, the mean error was still  $< \sim 8^\circ$  even at  $80^\circ$  azimuth. Carlile and colleagues showed similar results in their study of human sound localization<sup>25</sup>.

In cats, the accuracy estimates vary considerably according to the outcome measure used. Localization measurements using head orientation showed errors  $< \sim 5^\circ$  in midline azimuth, but errors increase to  $\sim 30^\circ$  for eccentric locations (e.g.,  $75^\circ$ )<sup>26</sup>. Cats also exhibit increased errors at eccentric locations when localization of a 100ms noise burst was measured with head orientation<sup>27</sup>. There are systematic undershoot errors in head orientation<sup>26</sup> and saccades<sup>28</sup> in cats and head orientation in ferrets<sup>22</sup> for eccentric locations that may contribute to increased error in peripheral space. When minimum audible angles are used to measure spatial acuity, cats show excellent resolution ( $\sim 4^\circ$ ) near the midline, which declines to  $\sim 9^\circ$  in peripheral space<sup>29</sup>. When an approach to speaker task is used, the cat performs quite accurately<sup>20,30-32</sup>. The exact error calculations are not known from these papers, but the confusion matrices show performance akin to the pallid bat.

Ferrets show  $\sim 50-70\%$  correct response on average when durations  $< 200$  ms were used in an approach to speaker task<sup>22,33</sup>. Performance is typically much better for midline locations compared to lateral locations. There is a considerable difference in percentage correct in approach to speaker tasks between the two carnivores tested, with the cat showing superior performance. Barn owls studied using head orienting behavior exhibit  $\sim 2^\circ$  of error when localizing sounds near the midline. The performance drops off to

between 6-10° at lateral azimuths<sup>34</sup>. The pallid bat data demonstrate that there is virtually no change in the percent of correct responses or mean error between 0° and 36° from the midline (-1.65% and +0.03° change, respectively). A significant change is not seen even when the sound is presented 72° away from the midline. When considering sound source locations that are in the range of 45-72° from the midline, pallid bats perform with accuracy better than or equal to human and barn owl localization and better than carnivores<sup>21,23,34,35</sup>. This is interesting when considering that the head size of the pallid bat is much smaller compared to the carnivores studied while using relatively similar frequency range (<35 kHz) for localization and points to both peripheral and central specializations that need to be further explored.

*ii. Possible neural mechanisms of accurate azimuth localization behavior in the pallid bat*

The auditory cortex is necessary for sound localization behavior in every species tested, particularly in approach-to-target tasks<sup>20,31,36,37</sup>. Previous electrophysiological studies of the pallid bat auditory cortex have led to the proposal of a population code for representation of 2D source locations<sup>16,17</sup>. Such a population code is found in the noise selective region, part of the primary auditory cortex of the pallid bat that represents frequencies between 5-35 kHz and is selective for broadband noise<sup>14,38</sup>. The noise selective region contains two clusters of neurons, distinguished by their interaural intensity difference (IID) and azimuth selectivity<sup>14-16</sup>. One cluster contains neurons with

peaked IID selectivity, with best IID  $\sim 0$  dB in most neurons. These neurons respond best to sources directly in front of the bat<sup>15</sup>.

The second cluster consists of neurons with sigmoidal IID selectivity functions (binaurally inhibited neurons). The binaurally inhibited neurons respond best to contralateral azimuth angles and show an inhibition of response as the source moves to relatively more ipsilateral loci<sup>15</sup>. The slope of the sigmoidal response can be centered at different azimuth locations (termed the 50% azimuth cutoff angle or simply ‘50% azimuth’). There is a diversity of 50% azimuth angles in the cluster of binaurally inhibited neurons. The topographical organization within this cluster depends on each neuron’s 50% azimuth angle. The organization is such that when sound moves from ipsilateral to contralateral locations, there is a systematic increase in the area of active cortex<sup>16</sup>. This idea is similar to hypotheses on spatial encoding in the inferior colliculus of the mustached bat<sup>39</sup> and the superior colliculus of the cat<sup>40</sup>.

The accurate midline localization performance of the pallid bat may arise due to the over-representation of midline locations in the cluster of neurons with peaked IID selectivity. In addition, the forward facing large ears may enhance spatial sensitivity near the midline. The peaked cluster occupies  $\sim 25$ -30% of the noise selective region in the pallid bat auditory cortex. Similar midline preferring neurons are also seen in other mammals<sup>41,42</sup> and may explain the generally better localization accuracy near midline compared to more eccentric locations across species. The main difference between the pallid bat and other species studied is the presence of a separate cluster of neurons whose response is maximal for sounds directly in front of the bat.

The accuracy of the pallid bat at eccentric sound locations may arise due to specializations in the cluster of binaurally inhibited neurons. First, there is a diversity of 50% azimuth in this cluster. Across neurons, these values cover a wide range of the contralateral hemifield. To the extent that the slopes of azimuth selectivity functions bear relevant localization information<sup>43,44</sup>, previous data from the cat cortex suggests that accurate midline performance arises through the preponderance of azimuth function slopes that transverse the midline<sup>42</sup>. A corollary of this hypothesis is the reduced performance expected at more eccentric locations because the sigmoidal functions tend to be flat (less informative) at increasingly contralateral locations. These predictions are met behaviorally in cats when tested with head orientation<sup>26,27</sup>. In the pallid bat, more neurons tend to have slopes between 0° – 30°, but a substantial number of neurons have slopes between 30° – 75°. Indeed, the area of active cortex within the cluster of binaurally inhibited neurons continues to increase linearly as the sound moves more from 30° to 60° azimuth and saturates past 60°. Thus, the activated area of this cluster contains information for azimuth discrimination even at peripheral locations<sup>16</sup>, and may explain the accurate performance of the bat at peripheral locations.

The fact that a number of cortical neurons have azimuth function slopes in peripheral space (>30°) is consistent with sharp changes in IID-azimuth relationships in lateral locations<sup>18</sup>. Neuronal IID responses are sensitive to such changes<sup>15</sup>. Ear directionality of the pallid bat is such that for frequencies <15 kHz, the maximum IID generated is ~10 dB. For frequencies >15 kHz, the ear becomes more directional and maximum IIDs increase up to 20-25 dB, particularly at peripheral azimuths. The rate of

change of IIDs with azimuth increases with frequencies  $>15$  kHz<sup>18</sup>. The availability of a broader range of IIDs at the higher frequencies likely explains the improved localization accuracy for sounds that include frequencies  $>15$  kHz. Under free field conditions, only the high frequency tuned neurons will be sensitive to azimuth changes that generate IID changes in the 15-25 dB range. These neurons will be less activated by LP noise explaining the difference in performance for low-pass versus high-pass noise.

The bats were unable to localize a 15 kHz pure tone. In other mammals, reported accuracy of tone localization varies widely in the literature<sup>19,20,45-49</sup>. Given the description of the binaural clusters above, wherein the extent of active neurons represents locations, it is not surprising that the pallid bat performed poorly in tone localization tasks. In individual bats, 50% azimuth map in the cluster of binaurally inhibited neurons cuts across multiple isofrequency bands. When a narrowband sound is presented, only a part of the map will be activated and the spatial information will be ambiguous<sup>45</sup>. As the sound includes more frequencies, the full map can be utilized. It is unlikely the results are specific to the 15 kHz tone used here, because only part of the map will be activated at any single tone frequency used as stimulus.

### *iii. Methodological issues*

A number of methodological issues need to be considered in interpreting the accuracy of sound localization behaviors reported here. We eliminated movement related cues from the mealworms by killing them first. To reduce the probability that the bats echolocated the worms, we provided dummy clay worms in non-target speakers. There was also a  $\sim 5$  mm dip between the top of the platform and the wire mesh on which

worms were placed reducing the probability that echolocation was used to detect worms from the bat's starting position. We assume that the bats would have a more difficult time distinguishing a clay worm shape from a real worm, than a real worm from an empty speaker mesh. Moreover, trained bats rarely performed stop and search behaviors while approaching speakers.

These data were obtained with a relatively difficult open loop task in which the bats identified absolute location of a single, short duration (200 ms or less) stimulus. The latency from sound onset to the beginning of the head orienting behavior is unknown from this data set but has been estimated in other species. Cats demonstrate an orientation onset of ~50ms following sound onset<sup>46</sup>, while big brown bat latency to head orienting stimuli is 60-100ms<sup>47</sup>. Pinna movements likely have shorter latencies. Assuming the pallid bat head orienting response is similar, it is possible that the bats were able to update spatial information during presentation of the 100 and 200 ms duration sounds. The moderately improved performance for sounds with 200 msec duration compared to the 50msec duration suggests that this may be the case. Alternately, the difference in performance between 50 and 200 msec could arise due to the different energy content of stimuli with different durations. We consider this unlikely because we randomly varied stimulus intensity between 60 and 70 dB SPL across trials, more than the 3-6 dB energy differences expected in stimuli with durations between 50 -200 msec. The performance is only likely to improve if the sounds were longer or repeated allowing the bats to update information with pinna and head movements<sup>21,26,27</sup>. Given that the bat had to approach

the target for reward, errors in remembering the location may also contribute to the overall accuracy.

The speakers in this study were separated by  $18^\circ$ . It is unclear if such quantization over- or under-estimates accuracy. On the one hand, *a priori* knowledge of speaker distribution may provide an advantage in localization. On the other, the accuracy may be an underestimate because even a single mistake by one speaker introduces an  $18^\circ$  error to the average error estimate. A previous study of the pallid bat sound localization was performed by dropping crickets on the floor<sup>13</sup>. While this approach avoided fixed speaker locations, the head position of the bats when crickets were dropped was not known, precluding a comparison of midline versus peripheral locations. Nevertheless, this study found an accuracy  $\sim 2\text{-}3^\circ$  with this task. The sound durations of the stimuli were  $<25$  msec. Here, we report accuracy  $\sim 4^\circ$ . The relative consistency of the reported results, regardless of the differences in study design, suggest that quantization played a minimal role in error estimates reported here.

#### *iv. Conclusions*

The behavioral performance and the cortical mechanisms identified suggest that the specializations for sound localization in the pallid bat may provide insight into general mechanisms of mammalian sound localization. Comparative sound localization studies of gleaners will reveal constraints and adaptations in the auditory systems of bats to improve acuity in non-echolocation-based behaviors. Despite the information that the binaurally inhibited cluster of neurons may provide at peripheral locations, the overall

organization of the auditory cortex emphasizes midline azimuths. While we predicted accurate performance in the periphery, the similarity in peripheral and midline performance is a surprising finding. It is possible that, in a single source task in relatively quiet background conditions, the system was not pushed to reveal differential responses at midline and peripheral locations. Future experiments with masking will be performed to determine possible differences in midline and peripheral accuracy. Future studies will also examine the relative contributions of the two different binaural clusters to sound localization accuracy in the pallid bat using targeted chemical manipulations.

1. Neuweiler, G. Foraging ecology and audition in echolocating bats. *Trends Ecol. Evol.* **4**, 160–166 (1989).
2. Moss, C. F. & Surlykke, A. Probing the natural scene by echolocation in bats. *Front. Behav. Neurosci.* **4**, 33 (2010).
3. Simmons, J. A., Fenton, M. B. & O’Farrell, M. J. Echolocation and pursuit of prey by bats. *Science* **203**, 16–21 (1979).
4. Griffin, D. R. *Listening in the dark*. (Yale University Press, 1958).
5. Schnitzler, H.-U., Moss, C. F. & Denzinger, A. From spatial orientation to food acquisition in echolocating bats. *Trends Ecol. Evol.* **18**, 386–394 (2003).
6. Faure, P. A. & Barclay, R. M. Substrate-gleaning versus aerial-hawking: plasticity in the foraging and echolocation behaviour of the long-eared bat, *Myotis evotis*. *J. Comp. Physiol. A.* **174**, 651–60 (1994).
7. Bell, G. P. & Fenton, M. B. Visual acuity, sensitivity and binocularity in a gleaning insectivorous bat, *Macrotus californicus* (Chiroptera: Phyllostomidae). *Anim. Behav.* **34**, 409–414 (1986).
8. Fenton, M. B. Echolocation: Implications for Ecology and Evolution of Bats. *Q. Rev. Biol.* **59**, 33–53 (1984).
9. Arlettaz, R., Jones, G. & Racey, P. A. Effect of acoustic clutter on prey detection by bats. *Nature* **414**, 742–745 (2001).
10. Barber, J. R., Razak, K. A. & Fuzessery, Z. M. Can two streams of auditory information be processed simultaneously? Evidence from the gleaning bat *Antrozous pallidus*. *J. Comp. Physiol. A Sensory, Neural, Behav. Physiol.* **189**, 843–855 (2003).
11. Measor, K. R. *et al.* Matched Behavioral and Neural Adaptations for Low Sound Level Echolocation in a Gleaning Bat, *Antrozous pallidus*. *eneuro* **4**, ENEURO.0018-17.2017 (2017).
12. Bell, G. P. Behavioral and ecological aspects of gleaning by a desert insectivorous bat *Antrozous pallidus* (Chiroptera: Vespertilionidae). *Behav. Ecol. Sociobiol.* **10**, 217–223 (1982).
13. Fuzessery, Z. M., Buitenhoff, P., Andrews, B. & Kennedy, J. M. Passive sound localization of prey by the pallid bat (*Antrozous p. pallidus*). *J. Comp. Physiol. A* **171**, 767–777 (1993).

14. Razak, K. A. & Fuzessery, Z. M. Functional Organization of the Pallid Bat Auditory Cortex: Emphasis on Binaural Organization. *J. Neurophysiol.* **87**, 72–86 (2002).
15. Razak, K. A. & Fuzessery, Z. M. GABA Shapes a Systematic Map of Binaural Sensitivity in the Auditory Cortex. *J. Neurophysiol.* **104**, 517–528 (2010).
16. Razak, K. A. Systematic representation of sound locations in the primary auditory cortex. *J. Neurosci.* **31**, 13848–59 (2011).
17. Razak, K. A., Yarrow, S. & Brewton, D. Mechanisms of Sound Localization in Two Functionally Distinct Regions of the Auditory Cortex. *J. Neurosci.* **35**, 16105–15 (2015).
18. Fuzessery, Z. M. Monaural and binaural spectral cues created by the external ears of the pallid bat. *Hear. Res.* **95**, 1–17 (1996).
19. Stevens, S. S. & Newman, E. B. The Localization of Actual Sources of Sound. *Am. J. Psychol.* **48**, 297 (1936).
20. Jenkins, W. M. & Merzenich, M. M. Role of cat primary auditory cortex for sound-localization behavior. *J. Neurophysiol.* **52**, 819–47 (1984).
21. Makous, J. C. & Middlebrooks, J. C. Two-dimensional sound localization by human listeners. *J. Acoust. Soc. Am.* **87**, 2188–2200 (1990).
22. Nodal, F. R., Bajo, V. M., Parsons, C. H., Schnupp, J. W. & King, A. J. Sound localization behavior in ferrets: Comparison of acoustic orientation and approach-to-target responses. *Neuroscience* **154**, 397–408 (2008).
23. Koay, G., Kearns, D., Heffner, H. E. & Heffner, R. S. Passive sound-localization ability of the big brown bat (*Eptesicus fuscus*). *Hear. Res.* **119**, 37–48 (1998).
24. Sabin, A. T., Macpherson, E. A. & Middlebrooks, J. C. Human sound localization at near-threshold levels. *Hear. Res.* **199**, 124–134 (2005).
25. Carlile, S., Leong, P. & Hyams, S. The nature and distribution of errors in sound localization by human listeners. *Hear. Res.* **114**, 179–196 (1997).
26. May, B. J. & Huang, A. Y. Sound orientation behavior in cats. I. Localization of broadband noise. *J. Acoust. Soc. Am.* **100**, 1059–1069 (1996).
27. Beitel, R. E. & Kaas, J. H. Effects of bilateral and unilateral ablation of auditory

- cortex in cats on the unconditioned head orienting response to acoustic stimuli. *J. Neurophysiol.* **70**, 351–69 (1993).
28. Populin, L. C. & Yin, T. C. Behavioral studies of sound localization in the cat. *J. Neurosci.* **18**, 2147–60 (1998).
  29. Heffner, R. S. & Heffner, H. E. Sound localization acuity in the cat: Effect of azimuth, signal duration, and test procedure. *Hear. Res.* **36**, 221–232 (1988).
  30. Jenkins, W. M. & Masterton, R. B. Sound localization: effects of unilateral lesions in central auditory system. *J. Neurophysiol.* **47**, 987–1016 (1982).
  31. Malhotra, S., Hall, A. J. & Lomber, S. G. Cortical Control of Sound Localization in the Cat: Unilateral Cooling Deactivation of 19 Cerebral Areas. *J. Neurophysiol.* **92**, 1625–1643 (2004).
  32. Malhotra, S. & Lomber, S. G. Sound Localization During Homotopic and Heterotopic Bilateral Cooling Deactivation of Primary and Nonprimary Auditory Cortical Areas in the Cat. *J. Neurophysiol.* **97**, 26–43 (2007).
  33. Parsons, C. H., Lanyon, R. G., Schnupp, J. W. H. & King, A. J. Effects of Altering Spectral Cues in Infancy on Horizontal and Vertical Sound Localization by Adult Ferrets. *J. Neurophysiol.* **82**, 2294–2309 (1999).
  34. Knudsen, E. I., Blasdel, G. G. & Konishi, M. Sound localization by the barn owl (*Tyto alba*) measured with the search coil technique. *J. Comp. Physiol. ? A* **133**, 1–11 (1979).
  35. Kavanagh, G. L. & Kelly, J. B. Contribution of auditory cortex to sound localization by the ferret (*Mustela putorius*). *J. Neurophysiol.* **57**, 1746–66 (1987).
  36. Smith, A. L. *et al.* An investigation of the role of auditory cortex in sound localization using muscimol-releasing Elvax. *Eur. J. Neurosci.* **19**, 3059–3072 (2004).
  37. Heffner, H. E. The Role of Macaque Auditory Cortex in Sound Localization. *Acta Otolaryngol* **532**, 22–27 (1997).
  38. Razak, K. A., Shen, W., Zumsteg, T. & Fuzessery, Z. M. Parallel thalamocortical pathways for echolocation and passive sound localization in a gleaner bat, *Antrozous pallidus*. *J. Comp. Neurol.* **500**, 322–338 (2007).
  39. Fuzessery, Z. M., Wenstrup, J. J. & Pollak, G. D. A representation of horizontal sound location in the inferior colliculus of the mustache bat (*Pteronotus p.*

- parnellii). *Hear. Res.* **20**, 85–89 (1985).
40. Wise, L. Z. & Irvine, D. R. Topographic organization of interaural intensity difference sensitivity in deep layers of cat superior colliculus: implications for auditory spatial representation. *J. Neurophysiol.* **54**, 185–211 (1985).
  41. Higgins, N. C., Storace, D. A., Escabí, M. A. & Read, H. L. Specialization of binaural responses in ventral auditory cortices. *J. Neurosci.* **30**, 14522–32 (2010).
  42. Stecker, G. C., Harrington, I. A. & Middlebrooks, J. C. Location Coding by Opponent Neural Populations in the Auditory Cortex. *PLoS Biol.* **3**, e78 (2005).
  43. Harper, N. S. & McAlpine, D. Optimal neural population coding of an auditory spatial cue. *Nature* **430**, 682–686 (2004).
  44. Tollin, D. J., Koka, K. & Tsai, J. J. Interaural Level Difference Discrimination Thresholds for Single Neurons in the Lateral Superior Olive. *J. Neurosci.* **28**, 4848–4860 (2008).
  45. Brainard, M. S., Knudsen, E. I. & Esterly, S. D. Neural derivation of sound source location: Resolution of spatial ambiguities in binaural cues. *J. Acoust. Soc. Am.* **91**, 1015–1027 (1992).
  46. Tollin, D. J., Ruhland, J. L. & Yin, T. C. T. The Vestibulo-Auricular Reflex. *J. Neurophysiol.* **101**, 1258–1266 (2009).
  47. Valentine, D. E., Sinha, S. R. & Moss, C. F. Orienting responses and vocalizations produced by microstimulation in the superior colliculus of the echolocating bat, *Eptesicus fuscus*. *J. Comp. Physiol. A* **188**, 89–108 (2002).

## **Chapter 4**

### **Bicoordinate Space Encoding by Neurons in the Pallid Bat Auditory Cortex**

#### **Abstract**

The auditory cortex is necessary for sound localization in both the azimuthal and elevational planes. The mechanisms that lead to the encoding of spatial representations in the auditory cortex are unclear. We have characterized the spatial receptive fields (SRFs) in the noise-selective region (NSR) of the auditory cortex of the pallid bat to address this gap in the field. The pallid bat must rely on passive listening for prey-generated noise to localize prey. The region of the cortex that responds to these noise sounds is the NSR. Within the NSR, neurons are selective for azimuthal sound source position. Here, we sought to determine how the NSR neurons' selectivity is shaped in 2D (azimuth and elevation) by measuring the SRF. We find that NSR neurons represent a broad region of contralateral space and that SRF size and centroid elevation covary with the characteristic frequency of the NSR neuron. These data show that NSR neurons contain overlapping maps of azimuth and elevation selectivity, suggesting a novel model for bicoordinate space encoding.

## Introduction

Unlike the visual and somatosensory systems, the auditory system does not encode space information at the sensory epithelia. Instead, space encoding is achieved through central nervous system (CNS) computations, making the auditory system an ideal system to gain insights into mechanisms underlying brain computations. The auditory cortex is a necessary structure for sound localization in the azimuth<sup>1-6</sup> and elevation<sup>7</sup> planes. Importantly, most studies of spatial encoding mechanisms have demonstrated a lack of any “one-to-one” space map in the cortex, leading to hypotheses of azimuth encoding by populations of cortical neurons<sup>8-11</sup>. Our understanding of the details of this population code is incomplete, but beginning to be understood<sup>12,13</sup>. In comparison, even less is known about the coding of sound source elevation<sup>14-16</sup>. Therefore, the field lacks models of the neural mechanisms that achieve 2D space encoding. In this study, we examine neurons in the noise-selective region (NSR) of the pallid bat primary auditory cortex (A1) and find evidence supporting a new model for 2D space encoding in the auditory system.

The pallid bat, *Antrozous pallidus*, depends on passive hearing to localize and hunt their prey, based on the prey-generated noise caused by walking, rustling leaves, etc<sup>17</sup>. The energy content of this prey-generated noise falls within the 5-30kHz range<sup>18</sup>. In the pallid bat A1, neurons selective for these noise sounds are segregated into the NSR and distinctive from the rest of the A1, which contains neurons tuned to the echolocation frequency range (30-60kHz)<sup>19,20</sup>. Mapping studies have outlined further functional separation of neurons within the NSR into binaural clusters<sup>19</sup>. One cluster responds best

to interaural intensity differences (IIDs) near 0 dB and 0-15° azimuth for free field sounds<sup>13,21</sup>. The second cluster contains binaurally inhibited neurons (EI), which respond best to contralateral (CL) stimulation and are inhibited by increasingly ipsilateral (IL) favoring IIDs and azimuths. The IID/azimuth at which the response decreases to 50% of the maximum is known as the inhibitory threshold, and the EI cluster neurons are organized topographically by their inhibitory thresholds, resulting in azimuth-dependent systematic activations of the cluster<sup>13</sup>. This encoding is similar to the model proposed in the superior<sup>22</sup> and inferior colliculi<sup>23</sup>. Currently, there are no known mechanisms of elevation selectivity within these NSR neuron populations. To determine potential 2D encoding strategies of the pallid bat cortical neurons, this study has characterized the 2D spatial receptive fields (SRFs) of EI cluster neurons, by playing sounds free-field from various azimuths and elevations.

## **Methods**

Methods on surgical procedures, recording and stimulus protocols, stimuli, and quantification of SRF properties have been reported previously<sup>24</sup> and are reproduced here briefly.

Pallid bats netted from various sites in Arizona, California, and New Mexico were used in this study according to the procedures outlined in the animal welfare guidelines required by the National Institutes of Health and the Institutional Animal Care and Use Committee. Bats were housed in an 11x14 foot room at the University of California,

Riverside. Bats were able to fly and were provided mealworms/crickets and water ad libitum, except for bats going through the behavior experiments. The room was maintained on a reversed 12 h light/dark cycle.

*Surgical procedures.* Adult aged, male and female pallid bats (n=14) were anesthetized with isoflurane inhalation followed by an injection of sodium pentobarbital (30  $\mu$ g/g body weight) and acepromazine (2  $\mu$ g/g body weight). For a detailed report of the surgical and recording process, see <sup>13,19</sup>. The head was placed into a custom designed bite bar, a midline incision was made on the scalp, and the temporal muscles were deflected. Bats were held in a Plexiglas device, custom designed for a typical pallid bat. A head pin was inserted through a bar stationed overhead, and dental cement attached the bar to the front of the skull. The cement and pin held the bat's head still for the duration of the recording session. A1 location was determined based on the relative position of the midsagittal sinus and the location of the lateral blood vessel. An approximately 2mm exposure was made in the skull above this location with a scalpel and the exposed surface was covered with paraffin oil to deter drying out. Each exposure, and therefore, recording session, was made over the right A1.

*Recording and stimulus protocols.* All experiments were carried out in an anechoic sound attenuation chamber (Gretch-Ken Industries) at ~80°F. Bats were maintained at a stable anesthetized state with supplemental sodium pentobarbital. Custom software was used to carry out stimulation and data acquisition (Batlab, Dr. Don Gans, Kent State University, Kent, OH) and a Microstar digital signal processing (DSP) board. Prior to amplification by a stereo power amplifier (HCA1100, Parasound or AX430, Yamaha), sound levels

were controlled by programmable attenuators (Tucker-Davis Technologies).

Extracellular, single-unit recordings were obtained with glass capillaries (1 M NaCl, 2-10 M $\Omega$  impedance) at cortical depths between 200-600  $\mu$ m. This falls within the range of layers III-V, since the pallid bat A1 is 800  $\mu$ m deep, the 55% depth position marks the layer IV/V boundary<sup>25</sup>, and layer V resides ~450  $\mu$ m deep. Action potentials recorded were amplified by an extracellular preamplifier (2400A, Dagan) and spike signal enhancer (FHC) and band-pass filtered (0.3-3 kHz, Krohn-Hite). Batlab was used to store waveforms and peristimulus time histograms. All presented data are from single-unit recordings, identified by action potential and waveform consistency, displayed on an oscilloscope. All responses reported are based on the total number of spikes after 20 stimulus presentations at a 1 Hz repetition rate.

In order to obtain 2D SRFs from these neurons, sound stimuli were played free field with an LCY-K100 speaker, manually positioned between 75° CL and 75° IL with 15° of resolution in the azimuthal plane on a semicircular loop (40 cm radius around the bat's head). The bat, recording equipment, and the loop were mounted onto a vibration isolation table (TMC). The loop was rotatable to 5 different elevations (60° above and below the bat's head, with 30° resolution), giving 55 total spatial locations to test each neuron's response at.

The amplifier-speaker frequency response curve was measured with a 1/4-inch microphone (Bruel and Kjaer). This response curve was flat within  $\pm 3$  dB between 8-35 kHz. From 35-80 kHz, the falloff was gradual, ~20 dB/octave. The nose of the bat was oriented such that it faced directly at 0° azimuth and elevation.

*Stimuli.* The NSR neurons were stimulated with noise that mimicked the broadband noise (BBN) of prey-generated sounds. NSR neurons were distinguishable by their selective response to white noise. Other neurons in the high frequency region (HFR) of the pallid bat A1 respond selectively to downward frequency-modulated sweeps, which mimic echolocation calls<sup>13,19,21,26,27</sup>. Therefore, NSR is easily identifiable. The characteristic frequency of these neurons, which is the frequency that elicits activity at the lowest intensity, is between 7-35 kHz. Most NSR neurons prefer broadband noise to narrowband noise or tones. The NSR is determined to be in the A1 of the pallid bat based on short latencies, narrow tuning, and presence within a tonotopic gradient.

The NSR contains two functionally distinct clusters, based on their IID selectivities<sup>13,19,21,28</sup>. They are arranged so that the peaked neurons are rostral to the EI neurons. The EI neurons respond with a sigmoid pattern, becoming more activated by more CL ear stimulation. The EI neurons are inhibited as the sound intensity increases into the IL ear. Peaked neurons are inhibited when sound intensity becomes too unbalanced to favor either ear. These neurons are inhibited by monaural stimuli but facilitated by binaural input. Since we aim here to determine how elevation restrains cortical activity spread within the EI cluster, we focused only on these neurons when measuring SRFs. Broadband noise (5-40 kHz, 5-10 ms duration, 20-70 dB SPL) was presented free-field at CL 15° or 60° azimuths. An EI neuron that responds to 15° will remain activated as the sound source is moved to 60°<sup>13,28</sup>. We could eliminate neurons quickly this way if they stopped responding at 60° azimuth, as these are the peaked neurons.

Best azimuths were obtained from isolated EI neurons by moving the speaker between  $-15^{\circ}$  and  $+75^{\circ}$  azimuth locations. The position yielding the greatest number of spikes after 20 repetitions was determined to be the best azimuth. The CF of the neurons was determined as the tone frequency (5-40 kHz, 5 kHz steps, 20-70 dB SPL, 5-10 ms duration, 1 ms rise/fall time, 1 Hz repetition rate) that gave responses to five stimuli in a row at the lowest sound level tested. The minimum threshold for noise (MT) was determined by increasing SPL from 20-70 dB SPL (5 dB steps to begin and 1 dB steps closer to threshold) and noting the lowest intensity at which responses were elicited to five stimuli in a row. The response was then measured from each of the 55 different spatial locations with the sound level at 10 dB above MT.

For most neurons, another level was tested at each location (15-30 dB SPL), in order to determine the effect of sound intensity on the SRF measurements. While not a large range, this span of sound levels replicates the sound intensity range a hunting pallid bat might experience, as the sounds made by small insects as they walk will not vary so much. The walking of a ~1 g (body weight) scorpion on desert soil generated 55-60 dB peak equivalent SPL, 10 cm away from the recording device<sup>29</sup>. While a pallid bat is foraging 0.5-2.5 m from the ground<sup>30</sup>, they would be unlikely to experience a range of >20 dB SPL. Any prey smaller than 1 g will produce an even smaller range of intensities. Much of the pallid bat diet consists of crickets and beetles that will weigh <1 g, so this range of noise sounds tested on cortical neurons is likely behaviorally relevant.

*Quantification of SRF properties.* SRFS were coded and analyzed in MATLAB in collaboration with Dr. Stuart Yarrow (University of Edinburgh). The SRFs were

quantified using the centroid, the 50% SRF, and the polar radius of gyration (gyradius).

The centroid and gyradius can be understood by considering a physical analogy. The SRF can be thought of as a large mountain on the surface of a globe, where the response firing rate is equivalent to surface elevation, azimuth is equivalent to longitude, and elevation is equivalent to latitude. The centroid of the SRF is equivalent to the position (latitude and longitude) of the center of gravity of the mountain. To understand the gyradius, consider the globe rotating about an axis that passes through the center of gravity of the mountain. If the mass of the mountain is distributed far from the axis, it will have greater rotational inertia than if the mass is concentrated close to the axis. If the entire mass of the mountain is concentrated at a single point, the gyradius quantifies the distance that this point must be from the axis of rotation to maintain the same rotational inertia. Thus, the gyradius of the SRF quantifies the angular size of the SRF in a way that takes the entire response into account and is not sensitive to the level of activity in any particular region of the SRF.

Each SRF was defined by N data, each of which was composed of measurements of azimuth ( $i$  for the  $i$ th datum), elevation ( $\phi_i$ ), and response spike count ( $r_i$ ). The centroid of the SRF was found by taking moments about the origin; this discounts the circular nature of the azimuth dimension but does not result in loss of accuracy as all data were located in the frontal hemisphere. The azimuth of the centroid was defined as follows:

$$\phi_{centroid} = \frac{\sum \phi_i r_i}{\sum r_i}$$

and the elevation of the centroid as follows:

$$\theta_{centroid} = \frac{\sum \theta_i r_i}{\sum r_i}$$

To find the gyradius about the centroid, we first needed to find the total angle between the centroid and each datum. Total angle was given by the law of cosines, as follows:

$$\Phi = \arccos(\sin(\theta_{centroid}) \sin(\theta_i) + \cos(\theta_{centroid}) \cos(\theta_i) \times \cos(\varphi_{centroid} - \varphi_i))$$

The gyradius  $R_g$  of the SRF was then given by the following:

$$R_g = \sqrt{\frac{\sum \Phi_i^2 r_i}{\sum r_i}}$$

## Results

### *i. SRF properties of NSR neurons*

Recordings from 104 neurons in the NSR were used to generate SRFs. 81 of these units were sampled at 2 different sound levels. Figure 4.1 shows an example SRF and demonstrates the various properties of the SRF that were quantified. In the left column of Figure 4.2, the SRFs of four NSR neurons recorded at 10 dB above threshold is shown. The right column of Figure 4.2 shows the SRFs of the same 4 neurons at 20 dB above threshold for comparison. In these plots, three observations are demonstrated. The first is that NSR neurons are more selective for sound source azimuth than elevation. The second is that the SRF is continuous and resides mostly in the CL region of frontal space at both

tested sound levels. The last observation is that the SRFs of these neurons are stable with increasing sound level.

Centroid elevation and gyradius correlate with the NSR neuron's CF. 8 example NSR neurons of varying CF demonstrate this point (Figure 4.3). As the CF of the NSR neuron increases, the centroid elevation increases. This is true at both MT + 10 dB (Figure 4.4A) and MT + 20 dB (Figure 4.4B). This correlation does not occur when considering centroid azimuth in place of elevation (Figure 4.4C, D), consistent with previous reports showing a lack of correlation between azimuth selectivity and CF<sup>13,28</sup>. In addition, the gyradius of NSR neurons decreases as the CF of the neuron increases at both MT + 10 dB and + 20 dB (Figure 4.5A-B). Together, these data indicate a significant correlation between NSR elevation and frequency selectivity.

## **Discussion**

### *i. NSR neuron SRFs suggest a 2D space code in the extent of active cortex*

Three main findings relating to the SRFs of NSR neurons are that the SRFs represent a broad region of CL space, the neurons are level-tolerant, and the centroid and gyradius are correlated with CF. These findings, considered along with previously described azimuth encoding from the same region<sup>13,28</sup>, suggest a bicoordinate code for sound localization in the NSR of pallid bat A1 (Figure 4.6).

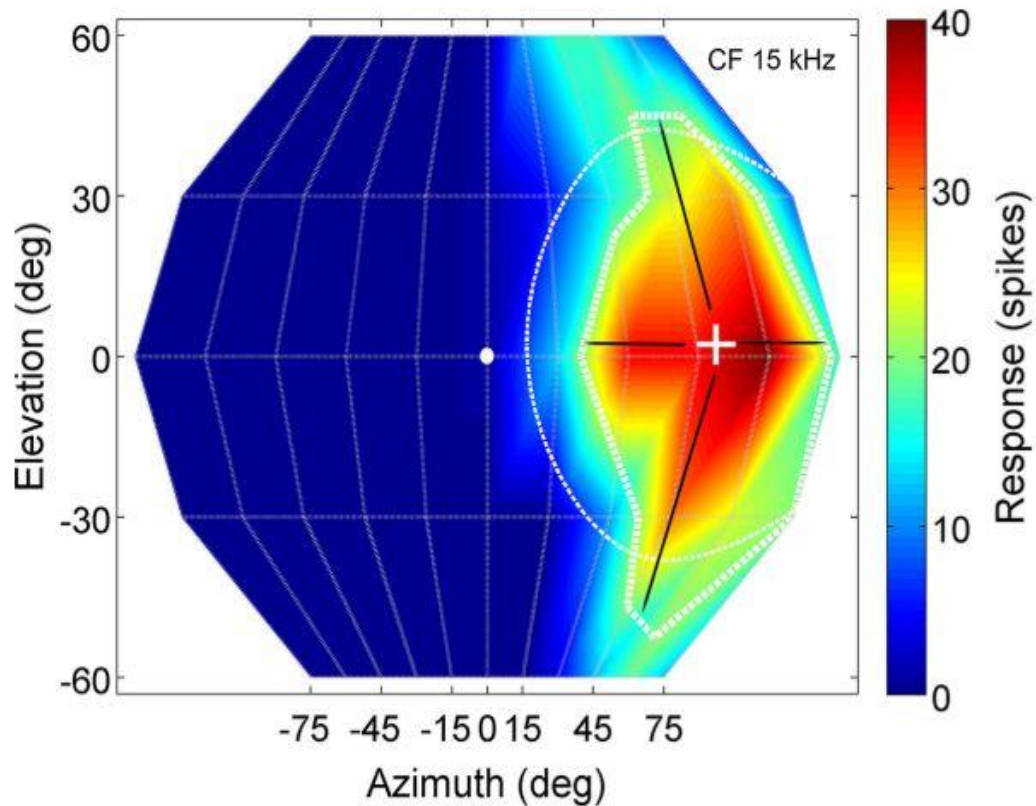


Figure 4.1. SRF of a NSR neuron recorded at MT + 10 dB shows the measurements taken from a single cell. The nose of the bat is directed at 0°azimuth/elevation (white dot). Azimuth is represented on the x-axis and ranges from 75°IL (negative values) and 75°CL (positive values). The resolution of this axis is 15°. Elevation is represented on the y-axis and ranges from 60°above to 60°below the bat's nose in 30°increments. The color scale represents the number of spikes following 20 stimulus repetitions (response magnitude). The gyradius is marked by the thin dashed white line, and the thicker dashed line indicates the 50% SRF, defined as the contour along which response magnitude decreased to 50% of the maximum response. The white plus sign indicates the centroid location of the SRF. The x and y coordinates of this position are the centroid azimuth and elevation, respectively. The black arrows emanating from the centroid position provide measures of the 50% SRF azimuth and elevation based on where they intersect the thicker dashed white line. (Figure 1 from <sup>35</sup>).

There is a map of azimuth selectivity in the EI cluster of the pallid bat NSR, represented in the systematic recruitment of more neurons as the sound source moves more CL. Previous work established a map of binaural cue selectivity in this region<sup>19</sup>.

When a sound source is located to the left or right of the midline, the intensity will become louder in the near ear relative to the far ear. This interaural intensity difference (IID) is the cue for which pallid bat NSR neurons are selective. Within the NSR, there is a systematic map of IIDs, described by the IID at which the neuron response is inhibited to 50% of the maximum response (the inhibitory threshold (IT)). When the IT is negative, the neuron is inhibited when sounds are louder in the IL ear. There is a map in the rostralateral to caudomedial direction with a gradient of negative to more positive IID ITs. This arrangement creates a map of systematically increasing area of active cortex as a sound source moves IL to CL (Figure 4.6). Similar to studies of subcortical binaural selectivity<sup>22,23,31</sup>, the slope of the binaural selectivity function is the basis for the population code used in computing sound source locations.

The results presented here suggest that this spread of active cortex will be constrained by the elevation-frequency interactions. This activity will be constrained on the tonotopic axis, which is orthogonal to the IID IT axis (Figure 4.6). For a broadband sound originating from low elevations ( $-30^\circ$ ; Figure 4.6), the low frequency portion of the tonotopic map will be more active than the high frequency portion. As the sound source rises, the ear directionality features suggest that higher frequency sounds will be amplified by the external ear<sup>32</sup> (Chapter 2 of this dissertation). Thus, the neurons with higher CFs will become more activated, without a necessary loss of low-CF neuron firing rate, due to their broad elevation tuning. Moving the sound source from IL to CL locations will recruit more of the neurons along the IID IT axis. Therefore, the overlap of

IID IT and CF axes will constrain the extent of active cortex in an azimuth/elevation-dependent manner, yielding a code for 2D spatial coordinates (Figure 4.6).

IID selectivity of NSR neurons is expected to shape both the azimuth selectivity<sup>28</sup> and the CF-elevation relationship. Pallid bat ear directionality demonstrates that IIDs of low frequencies is relatively elevation invariant<sup>32</sup> (see Chapter 2 of this dissertation). As the frequency is increased, the directionality also increases, explaining the narrower elevation tuning in the high-CF neurons of the NSR relative to the broad tuning of low-CF neurons. This phenomenon arises due to the combined effects of sound frequency, ear directionality, and IID selectivity of the NSR neurons<sup>16</sup>. The finding that there is no correlation between CF and centroid azimuth (Figure 4.4C) or IID/azimuth selectivity<sup>13</sup> are consistent with previous reports that isofrequency contours contain spatial information across CL azimuths<sup>3</sup>. The CF-dependent elevation code we propose is also in line with reports of the influence of spectral bandwidth on elevation perception<sup>33–37</sup>.

Together, these results demonstrate a potential encoding strategy for 2D sound source location, represented in the extent of active cortical area. Future studies aim to test the necessity of these neural populations during a sound localization behavioral task.

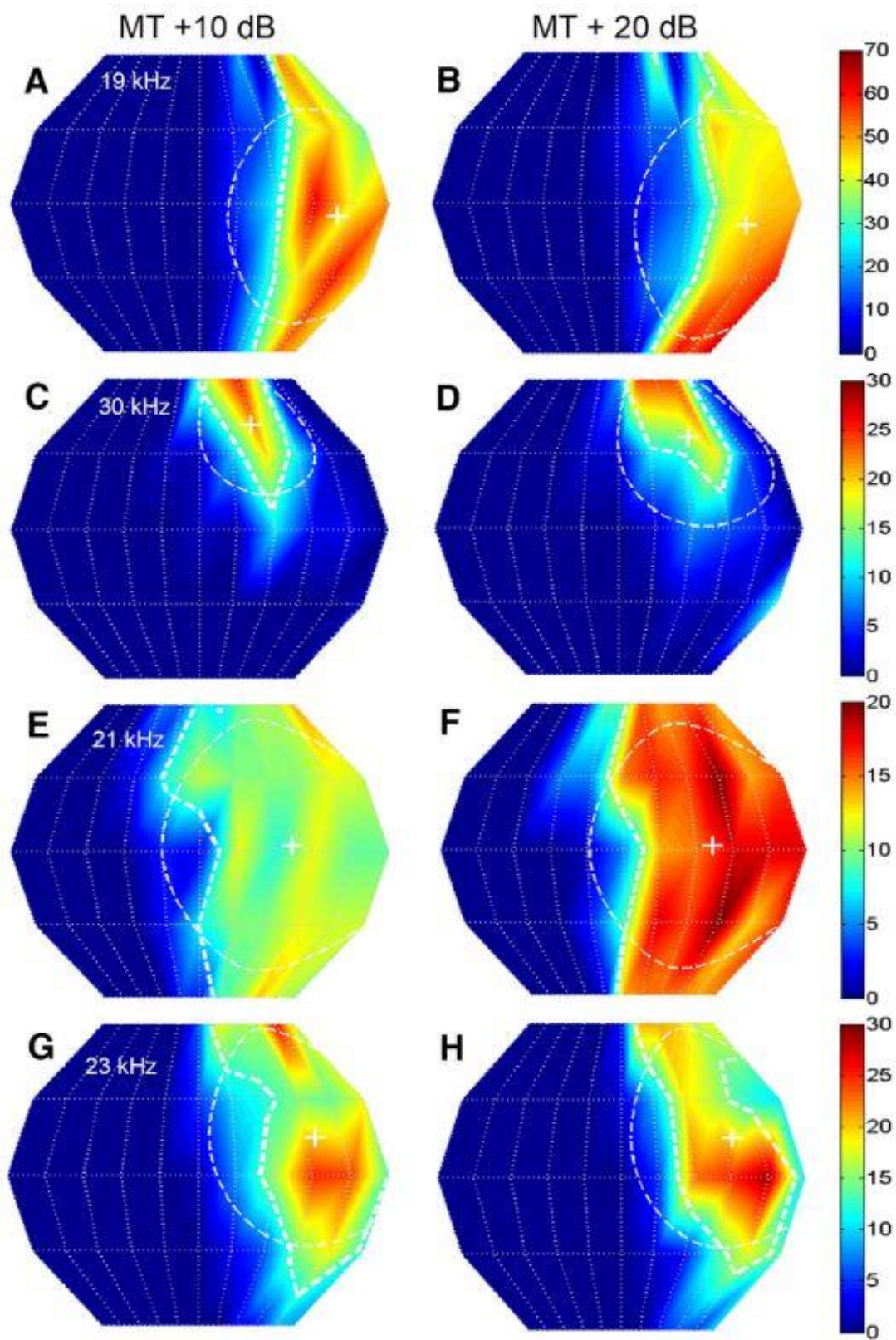


Figure 4.2. (previous page). SRF of 4 example neurons demonstrates stable properties as sound level is increased within the behaviorally relevant range. Left column, Responses measured for noise presented at MT + 10 dB. Right column, Responses measured for noise presented at MT + 20 dB. The color scale to the right corresponds to both MT+ 10 and +20 db plots. **(A-B)** Neuron #41B05, CF = 19 kHz. The centroid azimuth for MT + 10 dB stimulation was 54° and the azimuth for MT +20 dB was 53°. The centroid elevation for the same two sound levels was -5° and -9°. The gyradii were 44° and 46°, respectively. **(C-D)** Neuron #70C02, CF = 30 kHz. Centroid azimuth = 28°, 35°. Centroid elevation = 42°, 37°. Gyradius = 28°, 36°. **(E-F)** Neuron #83A01, CF = 21 kHz. Centroid azimuth = 36°, 36°. Centroid elevation = 3°, 2°. Gyradius = 51°, 50°. **(G-H)** Neuron #78B03, CF = 23 kHz. Centroid azimuth = 47°, 48°. Centroid elevation = 15°, 15°. Gyradius = 43°, 43°. (Figure 2 from <sup>35</sup>).

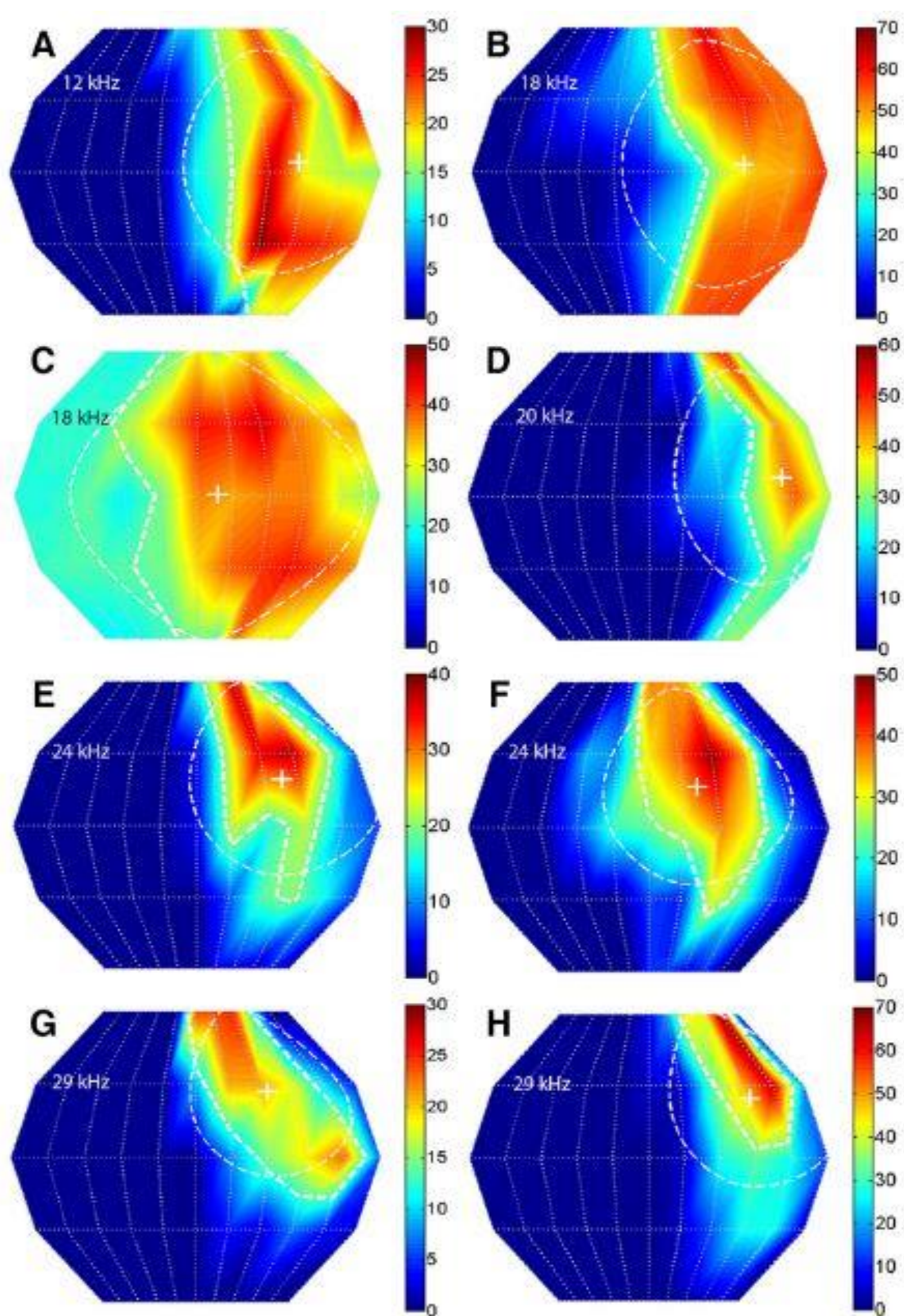


Figure 4.3. The relationship between SRF centroid elevation and CF is demonstrated in 8 example neurons of various CFs. Centroid elevation increases and gyradius decreases as CF increases. **(A)** Neuron #87A01: CF = 12 kHz, centroid azimuth =  $42^\circ$ , centroid elevation =  $3^\circ$ , gyradius =  $47^\circ$ . **(B)** Neuron #68B04: CF = 18 kHz, centroid azimuth =  $40^\circ$ , centroid elevation =  $3^\circ$ , gyradius =  $52^\circ$ . **(C)** Neuron #93B03: CF = 18 kHz, centroid azimuth =  $9^\circ$ , centroid elevation =  $0^\circ$ , gyradius =  $61^\circ$ . **(D)** Neuron #41B03: CF = 20 kHz, centroid azimuth =  $55^\circ$ , centroid elevation =  $8^\circ$ , gyradius =  $45^\circ$ . **(E)** Neuron #40A01: CF = 24 kHz, centroid azimuth =  $37^\circ$ , centroid elevation =  $19^\circ$ , gyradius =  $40^\circ$ . **(F)** Neuron #34A01: CF = 24 kHz, centroid azimuth =  $21^\circ$ , centroid elevation =  $17^\circ$ , gyradius =  $41^\circ$ . **(G)** Neuron #40B01: CF = 29 kHz, centroid azimuth =  $32^\circ$ , centroid elevation =  $27^\circ$ , gyradius =  $35^\circ$ . **(H)** Neuron #41A01: CF = 29 kHz, centroid azimuth =  $46^\circ$ , centroid elevation =  $24^\circ$ , gyradius =  $37^\circ$ . (Figure 7 from<sup>35</sup>).

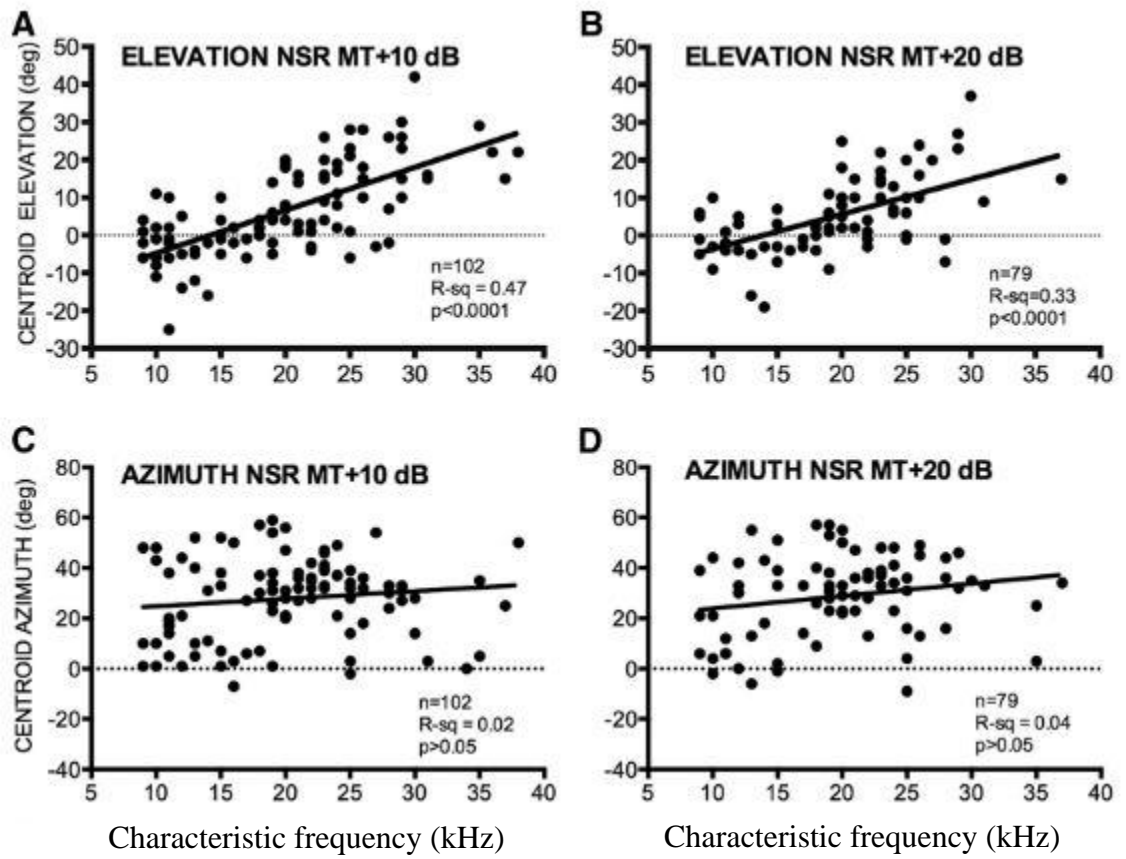


Figure 4.4. The correlation between centroid (A-B) azimuth or (C-D) elevation and CF is demonstrated in scatter plots. Each scatter point is a single neuron. Centroid elevation increases in a positive correlation with CF at both (A, C) +10 and (B, D) +20 dB above MT. (Figure 8 from <sup>35</sup>).

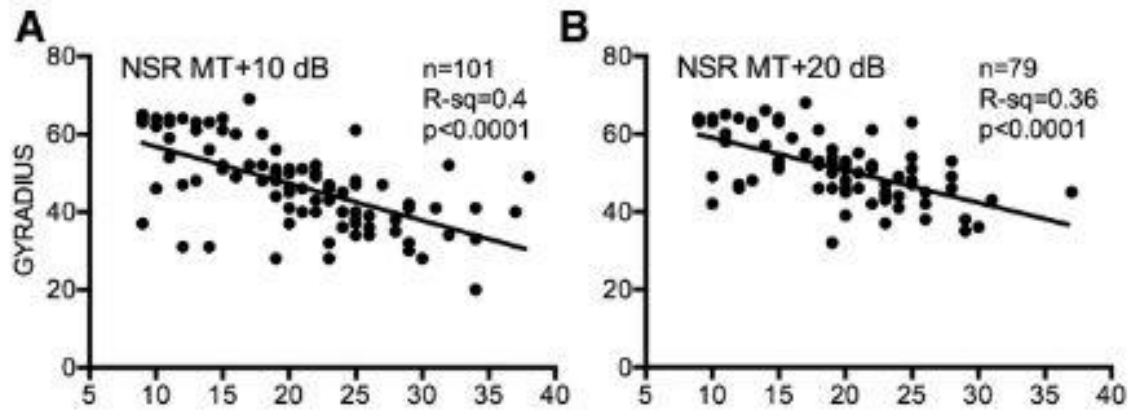


Figure 4.5. The correlation between gyradii and CF is demonstrated in scatter plots. Each scatter point is a single neuron. Gyradius decreases in a negative correlation with CF at both **(A)** +10 and **(B)** +20 dB above MT. (Figure 9A-B from <sup>35</sup>).

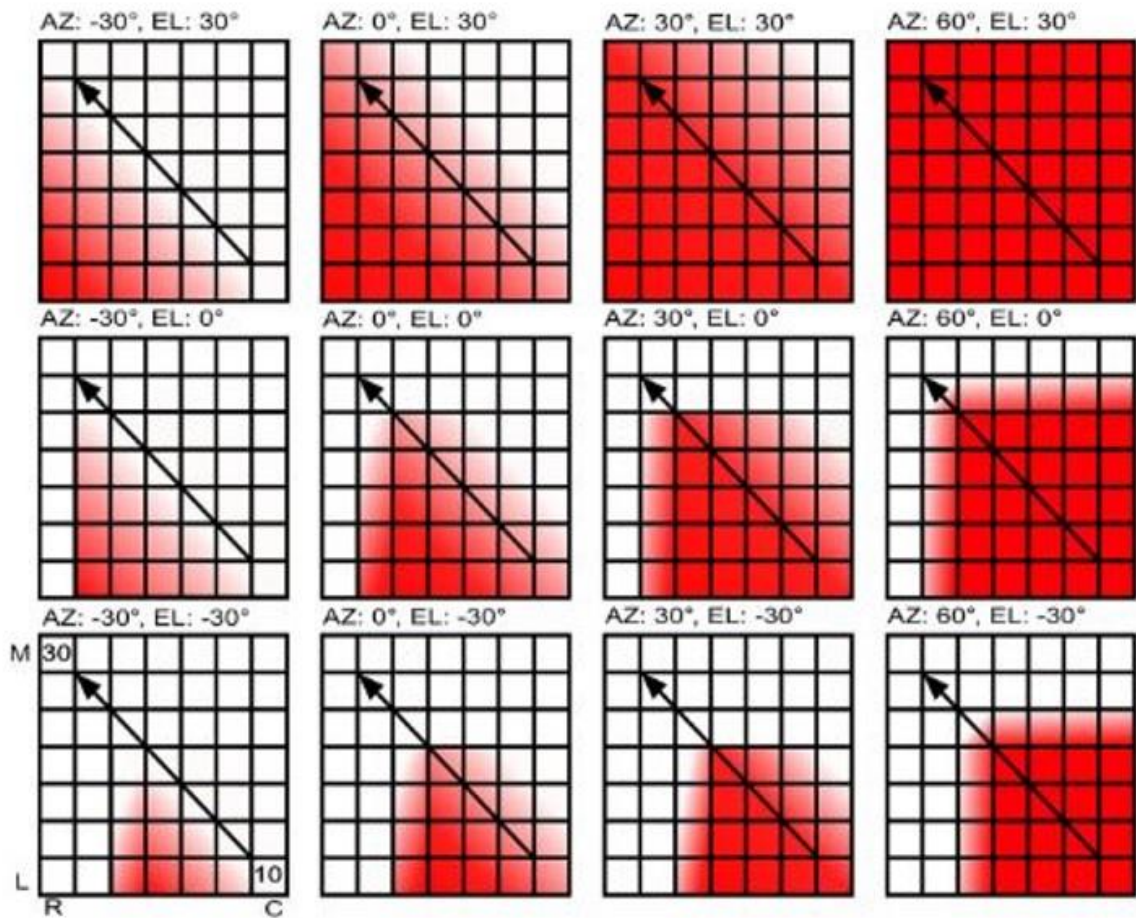


Figure 4.6. Model of the systematic representation of 2D space in the extent of active pallid bat A1, introduced in Chapter 1, Figure 1.8. Each box represents a cortical state of the pallid bat EI cluster, corresponding to a broadband sound source from in a distinctive spatial location. The location of the sound source is written above each box. AZ = azimuth, CL = contralateral, and EL = elevation. L = lateral and M = medial. R = rostral and C = caudal. The tonotopic axis is presented by the black arrow moving rostro-medially across each box. Red regions indicate active areas and the shading represents the level of activity, with the darkest shades representing the most active state for that cell. From left to right, on any row, the extent of activity will be seen to increase perpendicular to the tonotopic gradient (the isofrequency axis). From top to bottom, the extent of activity will be restrained down the tonotopic axis. The extent of activity in the isofrequency axis is constrained by sound source azimuth, while the activity is further constrained down the tonotopic axis by sound source elevation. This extent of activation is a model for 2D sound localization encoding at the cortex of the pallid bat.

1. Whitfield, I. Auditory space and the role of the cortex in sound localization. in *Psychophysics and Physiology of Hearing* (eds. Evans, E. & Wilson, J.) 1–9 (Academic, 1977).
2. Malhotra, S., Hall, A. J. & Lomber, S. G. Cortical Control of Sound Localization in the Cat: Unilateral Cooling Deactivation of 19 Cerebral Areas. *J. Neurophysiol.* **92**, 1625–1643 (2004).
3. Jenkins, W. M. & Merzenich, M. M. Role of cat primary auditory cortex for sound-localization behavior. *J. Neurophysiol.* **52**, 819–47 (1984).
4. Jenkins, W. M. & Masterton, R. B. Sound localization: effects of unilateral lesions in central auditory system. *J. Neurophysiol.* **47**, 987–1016 (1982).
5. Kavanagh, G. L. & Kelly, J. B. Contribution of auditory cortex to sound localization by the ferret (*Mustela putorius*). *J. Neurophysiol.* **57**, 1746–66 (1987).
6. Heffner, H. E. The Role of Macaque Auditory Cortex in Sound Localization. *Acta Otolaryngol* **532**, 22–27 (1997).
7. Bizley, J. K., Nodal, F. R., Parsons, C. H. & King, A. J. Role of Auditory Cortex in Sound Localization in the Midsagittal Plane. *J. Neurophysiol.* **98**, 1763–1774 (2007).
8. Middlebrooks, J. C. & Pettigrew, J. D. Functional classes of neurons in primary auditory cortex of the cat distinguished by sensitivity to sound location. *J. Neurosci.* **1**, 107–120 (1981).
9. Rajan, R., Aitkin, L. M. & Irvine, D. R. Azimuthal sensitivity of neurons in primary auditory cortex of cats. II. Organization along frequency-band strips. *J. Neurophysiol.* **64**, 888–902 (1990).
10. Nakamoto, K. T., Zhang, J. & Kitzes, L. M. Response Patterns Along an Isofrequency Contour in Cat Primary Auditory Cortex (AI) to Stimuli Varying in Average and Interaural Levels. *J. Neurophysiol.* **91**, 118–135 (2004).
11. Stecker, G. C., Harrington, I. A. & Middlebrooks, J. C. Location Coding by Opponent Neural Populations in the Auditory Cortex. *PLoS Biol.* **3**, e78 (2005).
12. Miller, L. M. & Recanzone, G. H. Populations of auditory cortical neurons can accurately encode acoustic space across stimulus intensity. *Proc. Natl. Acad. Sci. U. S. A.* **106**, 5931–5 (2009).
13. Razak, K. A. Systematic representation of sound locations in the primary auditory

cortex. *J. Neurosci.* **31**, 13848–59 (2011).

14. Reale, R. A. & Brugge, J. F. Directional Sensitivity of Neurons in the Primary Auditory (AI) Cortex of the Cat to Successive Sounds Ordered in Time and Space. *J. Neurophysiol.* **84**, 435–450 (2000).
15. Xu, L., Furukawa, S. & Middlebrooks, J. C. Sensitivity to Sound-Source Elevation in Nontotopic Auditory Cortex. *J. Neurophysiol.* **80**, 882–894 (1998).
16. Mrsic-Flogel, T. D., King, A. J. & Schnupp, J. W. H. Encoding of Virtual Acoustic Space Stimuli by Neurons in Ferret Primary Auditory Cortex. *J. Neurophysiol.* **93**, 3489–3503 (2005).
17. Bell, G. P. Behavioral and ecological aspects of gleaning by a desert insectivorous bat *Antrozous pallidus* (Chiroptera: Vespertilionidae). *Behav. Ecol. Sociobiol.* **10**, 217–223 (1982).
18. Goerlitz, H. R., Greif, S. & Siemers, B. M. Cues for acoustic detection of prey: insect rustling sounds and the influence of walking substrate. *J. Exp. Biol.* **211**, 2799–806 (2008).
19. Razak, K. A. & Fuzessery, Z. M. Functional Organization of the Pallid Bat Auditory Cortex: Emphasis on Binaural Organization. *J. Neurophysiol.* **87**, 72–86 (2002).
20. Razak, K. A., Shen, W., Zumsteg, T. & Fuzessery, Z. M. Parallel thalamocortical pathways for echolocation and passive sound localization in a gleaning bat, *Antrozous pallidus*. *J. Comp. Neurol.* **500**, 322–338 (2007).
21. Razak, K. A. & Fuzessery, Z. M. GABA Shapes a Systematic Map of Binaural Sensitivity in the Auditory Cortex. *J. Neurophysiol.* **104**, 517–528 (2010).
22. Wise, L. Z. & Irvine, D. R. Topographic organization of interaural intensity difference sensitivity in deep layers of cat superior colliculus: implications for auditory spatial representation. *J. Neurophysiol.* **54**, 185–211 (1985).
23. Fuzessery, Z. M., Wenstrup, J. J. & Pollak, G. D. A representation of horizontal sound location in the inferior colliculus of the mustache bat (*Pteronotus p. parnellii*). *Hear. Res.* **20**, 85–89 (1985).
24. Razak, K. A., Yarrow, S. & Brewton, D. Mechanisms of Sound Localization in Two Functionally Distinct Regions of the Auditory Cortex. *J. Neurosci.* **35**, 16105–15 (2015).

25. del Campo, H. M., Measor, K. & Razak, K. A. Parvalbumin and calbindin expression in parallel thalamocortical pathways in a gleaning bat, *Antrozous pallidus*. *J. Comp. Neurol.* **522**, 2431–2445 (2014).
26. Razak, K. A. & Fuzessery, Z. M. Neural Mechanisms Underlying Selectivity for the Rate and Direction of Frequency-Modulated Sweeps in the Auditory Cortex of the Pallid Bat. *J. Neurophysiol.* **96**, 1303–1319 (2006).
27. Razak, K. A. & Fuzessery, Z. M. Facilitatory mechanisms underlying selectivity for the direction and rate of frequency modulated sweeps in the auditory cortex. *J. Neurosci.* **28**, 9806–16 (2008).
28. Razak, K. A. Mechanisms underlying azimuth selectivity in the auditory cortex of the pallid bat. *Hear. Res.* **290**, 1–12 (2012).
29. Holderied, M., Korine, C. & Moritz, T. Hemprich's long-eared bat (*Otonycteris hemprichii*) as a predator of scorpions: whispering echolocation, passive gleaning and prey selection. *J. Comp. Physiol. A* **197**, 425–433 (2011).
30. O'Shea, T. J. & Vaughan, T. A. Nocturnal and Seasonal Activities of the Pallid Bat, *Antrozous Pallidus*. *J. Mammal.* **58**, 269–284 (1977).
31. Tollin, D. J., Koka, K. & Tsai, J. J. Interaural Level Difference Discrimination Thresholds for Single Neurons in the Lateral Superior Olive. *J. Neurosci.* **28**, 4848–4860 (2008).
32. Fuzessery, Z. M. Monaural and binaural spectral cues created by the external ears of the pallid bat. *Hear. Res.* **95**, 1–17 (1996).
33. Blauert, J. Sound localization in the median plane. *Acta Acust. united with Acust.* **22**, 205–213 (1969).
34. Populin, L. C. & Yin, T. C. Behavioral studies of sound localization in the cat. *J. Neurosci.* **18**, 2147–60 (1998).
35. Tollin, D. J., Ruhland, J. L. & Yin, T. C. T. The role of spectral composition of sounds on the localization of sound sources by cats. *J. Neurophysiol.* **109**, 1658–1668 (2013).
36. Roffler, S. K. & Butler, R. A. Factors That Influence the Localization of Sound in the Vertical Plane. *J. Acoust. Soc. Am.* **43**, 1255–1259 (1968).
37. Butler, R. A. & Belendiuk, K. Spectral cues utilized in the localization of sound in the median sagittal plane. *J. Acoust. Soc. Am.* **61**, 1264–1269 (1977).

## **Chapter 5**

### **Preliminary Studies for Validating Chemogenetic DREADDs in the Pallid Bat**

#### **Abstract**

The auditory cortex is necessary for sound localization, but the mechanisms underlying space encoding at the cortex are unclear. To address this gap in the field, we have proposed a model of bicoordinate spatial representation in the cortex of the pallid bat. Pallid bat auditory cortex neurons encode space in the extent of active cortical area. There is a map of binaural selectivity approximately orthogonal to and overlapping with the tonotopic map. The extent of activity in the binaural map encodes azimuth selectivity. Because the CF of the NSR neurons correlates with the elevation of the center of their spatial receptive fields, the extent of activity in the tonotopic map encodes elevation. Now, we aim to develop the inhibitory DREADDs technique in the pallid bat model to test the validity of this model. We have found that the pallid bat auditory cortex expresses rAAV-GFPs in volume that indicates it can be constrained to subpopulations within the NSR. The inhibitory DREADD, hM4Di, exhibits a cellular expression pattern consistent with previous reports in the mouse CNS. Additionally, the synthetic drug, clozapine-N-oxide, which selectively activates the DREADDs receptor, does not affect measurements of the auditory cortex ERP or sound localization behavior after subcutaneous injection. These data provide support for the utility of new chemogenetic tools in a neuroethological model of sound localization.

## Introduction

The pallid bat, *Antrozous pallidus*, localizes and hunts prey by passive listening to prey-generated noise caused by walking, rustling leaves, etc (5-30kHz noise sounds)<sup>1,2</sup>. The success of this foraging strategy is heavily dependent on accurate sound localization. The neurobiological underpinnings of such sound localization abilities are only beginning to be understood. A consistent finding across studies in mammals is that the auditory cortex is necessary for sound localization on both the azimuth<sup>3-8</sup> and elevation<sup>9</sup> planes.

In the pallid bat, primary auditory cortex (A1) neurons selective for these noise sounds are separated into the noise-selective region (NSR). This region contains the low frequency neurons of the tonotopic region of A1, and is distinctive from the higher frequency region, which contains neurons tuned to the echolocation frequency range (30-60kHz)<sup>10,11</sup>. Mapping studies, described in detail in Chapters 1 and 4 of this dissertation, have discovered the functional separation of NSR neurons into binaural clusters<sup>10</sup>. One cluster (peaked) contains neurons tuned to sounds coming from the middle of frontal space, directly in front of the nose of the animal<sup>12,13</sup>. The second cluster (EI) contains that respond best to contralateral (CL) stimulation and are inhibited by increasingly ipsilateral (IL) sound sources. The location where the number of action potentials decreases to half of the maximum is the inhibitory threshold. EI cluster neurons are organized in a map of inhibitory thresholds, resulting in a systematic recruitment of EI neurons as the sound becomes more contralateral<sup>12</sup>. Furthermore, 2D spatial receptive fields (SRFs) of EI neurons, described in Chapter 4 of this dissertation, suggest an elevation-dependent constraint on the extent of this activity<sup>14</sup>. The resulting picture is one of the first and most

complete models for the encoding of 2D sound sources in the mammalian auditory cortex (see Figure 4.6 in this dissertation).

Considerable progress has been made in utilizing designed receptors exclusively activated by designed drugs (DREADDs) in assessing the necessity or sufficiency of CNS circuits to behavior<sup>15–19</sup>. Such experiments are essential to furthering our understanding of brain functions. Based on the 2D model of sound source encoding, experiments probing the necessity of pallid bat A1 cortical subpopulations to sound localization behavior can be tested using newly available chemogenetic tools. The success of these experiments is dependent on the validation and characterization of these techniques in the pallid bat, a species which has not undergone a study with the transgenic tools commonly used in many other mammalian species. Here, we report preliminary findings regarding a series of experiments relating to the validation of using adeno-associated virus (AAV) to deliver DREADDs to pallid bat A1.

Recombinant AAVs (rAAVs) have been used to successfully introduce various gene products to the CNS of various animals<sup>20–25</sup>, however bats are not yet included in this list. Furthermore, rAAVs that deliver the gene for the inhibitory chemogenetic DREADDs (hM4Di) have been used to test the necessity of CNS circuits in animal behavior<sup>15–19</sup>. As an initial step towards determining the necessity of the NSR neurons to sound localization behavior, we evaluated the transfection efficiency of three rAAV serotypes. We also show that the hM4Di DREADD expresses within pallid bat cortical cells. In addition, we show that the synthetic drug that activates DREADDs has no significant effect on neural signals or behavior in control animals. Together, these studies

lay the groundwork for future studies to address the question of whether the 2D space encoding neurons in the pallid bat auditory cortex are necessary for sound localization.

## **Methods**

Pallid bats netted from various sites in Arizona, California, and New Mexico were used in this study according to the procedures outlined in the animal welfare guidelines required by the National Institutes of Health and the Institutional Animal Care and Use Committee. Bats were housed in an 11x14 foot room at the University of California, Riverside. Bats were able to fly and were provided mealworms/crickets and water ad libitum, except for bats going through the behavior experiments. The room was maintained on a reversed 12 h light/dark cycle.

*Surgical procedures.* Adult aged, male and female pallid bats (n=14) were anesthetized with isoflurane inhalation followed by an injection of sodium pentobarbital (30  $\mu$ g/g body weight) and acepromazine (2  $\mu$ g/g body weight). For a detailed report of the surgical process see <sup>10,12</sup>. The head was placed into a custom designed bite bar, a midline incision was made on the scalp, and the temporal muscles were deflected. Bats were held in a Plexiglas device, custom designed for a typical pallid bat. A head pin was inserted through a bar stationed overhead, and dental cement attached the bar to the front of the skull. The cement and pin held the bat's head still for the duration of the recording or injection session. A1 location was determined based on the relative position of the midsagittal sinus and the location of the lateral blood vessel. An approximately 2mm

exposure was made in the skull above this location with a scalpel and the exposed surface was covered with paraffin oil to deter drying out. Each exposure/recording session, was made over the right A1.

*AAV injection procedure.* Following the procedure for creating the cortical exposure, some bats were injected with one of three AAV serotypes (AAV2-CMB-EGFP, UPenn; AAV8-ds-CBh-GFP, UPenn; AAV9 CAG-EGFP, UPenn), an AAV8 carrying the inhibitory chemogenetic DREADDs (pAAV8-CaMKIIa-hM4D(Gi)-mCherry), or saline (control bats for sound localization behavior). pAAV-CaMKIIa-hM4D(Gi)-mCherry were obtained from the Bryan Roth lab (Addgene plasmid # 50477).

A nanoinjector setup (Nanoinjector Stepper Motor Precision, Leica Biosystems #3946203) was attached to a gas-tight syringe (Model 1701 RN SYR, 10  $\mu$ L, Hamilton #7653-01). The glass capillary coupled to the gas tight syringe was pulled and broken to 20-30  $\mu$ m at the tip. This was mounted into the nanoinjector device and attached to a stereotaxic micromanipulator (Micro Manipulator, Kopf #1760). A small drop of AAV or saline was placed on Parafilm (Sigma-Aldrich #P7793-1EA) and the capillary was lowered until it touched the droplet. By waiting on the capillary action and providing some backflow via running the nanoinjector in reverse, the capillary was filled with  $\sim$ 3  $\mu$ L of solution. The capillary is then removed from the droplet and the nanoinjector was run forward quickly until outflow was achieved. After this, we confirmed the outflow would continue at 0.5  $\mu$ L/min flow rate, the rate used during the actual injection, by observing the tip under a microscope and noting whether product was escaping the tip. When this was the case, the capillary was lowered into the exposure to a depth of 500  $\mu$ m

and pulled back towards the cortical surface 10-15  $\mu\text{m}$ . This creates an empty pocket for the solution to flow out without as much resistance from the surround brain tissue.

Depending on the experiment, 2 or 0.75  $\mu\text{L}$  of solution was ejected from the tip at 0.5  $\mu\text{L}/\text{min}$ , and the capillary rested in place for 10 minutes after the injection protocol was finished to allow residual outflow. Bats then recovered under observation following the recovery procedures detailed previously. Experiments in these bats (Immunohistochemistry (IHC) or sound localization) commenced after 28 days post-surgery, ample time for AAV products to express<sup>22,32,33</sup>.

*Immunohistochemistry and Microscopy.* Although different antibodies were used, all standard procedures were reported previously in<sup>34</sup>. Briefly, all steps were completed at room temperature unless otherwise stated. Mice or bats were euthanized with a lethal dose of sodium pentobarbital and transcardially perfused with a peristaltic pump (Harvard Apparatus, MA, USA). Perfusions were carried out with 0.1M phosphate buffer saline (PBS) first, then 4% paraformaldehyde (PFA, pH = 7.4). Brains were removed from the skull and soaked in 4% PFA for 2 more hours. Brains were then moved to a 30% sucrose solution until they sank (~36 hours), at which point they were taken for cryosectioning (CM1860, Leica, IL, UK). Brains were sectioned in 40  $\mu\text{m}$  slices and stored in 0.1M PBS with 0.1% sodium azide. Because we were interested in the mCherry or GFP signal from the AAV product expression too, in some cases, images are from sections that were simply mounted after the cryosectioning step.

The following procedures were performed on free-floating sections in a well plate, and the well plate was placed on a gyrator for agitation. Sections were treated with

4% PFA for 2 hours, rinsed for 5 minutes in 0.1M PBS three times, 50 mM ammonium chloride for 15 minutes, rinsed in 0.1M PBS for 5 minutes, washed in 0.1% Triton-X for 10 mins, soaked in a blocking buffer (0.1M PBS, 5% goat normal serum, 1% bovine serum albumin) for 1 hour, and incubated overnight (~16-20 hours) at 4° C in a primary antibody solution, containing the primary antibody (1:1000 rabbit anti-GFAP, EMD Millipore #NF-AB5804), 1% goat normal serum, 0.5% bovine serum albumin, and 0.1% Tween. Slices were washed with 0.5% Tween three times for 10 minutes, incubated in the secondary antibody solution, containing the secondary antibody (1:500 Donkey anti-Rabbit IgG Alexa 647, Thermo Fisher Scientific #A-31573) in 0.1M PBS, for 1 hour. Slices were washed with 0.1M PBS, mounted on glass slides, coverslipped with Vectashield DAPI nuclei stain (Vector Labs, F2-135), and sealed at the edges before imaging with the Leica SP5.

A1 location was determined under the microscope (Leica SP5) by using the DAPI nuclear stain to identify the appropriate hippocampal landmarks. This method has been validated previously, using electrophysiology and dye placements<sup>26,35</sup> and follows rules used in other studies<sup>36,37</sup>. Z-stack images were captured through the full depth of the 40 µm sections in 2 µm steps, such that each stack was made of approximately 20 images. Images were either captured at 5x, to show whole brain scans, 20x, to focus on a single hemisphere auditory cortex, or 40x, to focus on a sample range of cells of interest. Because the auditory cortex is located temporally, all images were collected with A1 at an angle. These images were uncropped but rotated so that the pia is at the top of the image. In cases where the image is cropped to highlight only the cortical column, these

20x images were cropped to obtain as much of the cortex as possible without including areas outside of the edge of the region.

*Event-related potential recordings.* An event-related potential (ERP) recording was carried out in one control bat (Bat15). After the cortical exposure was made, the bat was situated in the anechoic chamber in the same way they were for the single-unit recordings (see Chapter 4 of this dissertation for details). The tungsten ERP electrode (125  $\mu$ M diameter, FHC) was mounted into a micropositioner (Kopf Instruments, Tujunga, CA) and contacted the cortical surface. Recordings were displayed using the BioPac system (BIOPAC Systems, Inc.). The BioPac MP150 acquisition system was used to filter the signal between 0.5-35 Hz. Stimuli were generated, and traces were observed in (Sparkle, Dr. Christine Portfors, Washington State University at Vancouver, Vancouver, WA). Once a signal was found, the ERP trace was measured at source locations 0°, 45°CL, and 90°CL. Stimulus types used were BBN, 10-50 kHz tones in 5 kHz steps, and 60-30 kHz downward frequency modulated (FM) sweep; all played at 10 ms duration and 50 dB SPL). Stimuli were repeated once every 2 seconds. Tones and FM sweeps were played once each, with a BBN stimulus played between each, such that the BBN signal was played 10 times at each position. All 20 traces (10 BBN and 1 each of the other stimulus types) were extracted in a 150 ms window around the peak by using a synthetic TTL pulse produced at the onset of each stimulus played. The 10 windows for BBN were averaged, and the resulting average BBN trace and N1 peak were used in the results along with the traces and N1 peaks for each stimulus type. The best azimuth was defined

as the azimuth the elicited the greatest average BBN trace. Each tone and FM sweep ERP peak is reported as an absolute value or as a value relative to the average BBN trace.

To determine whether the synthetic drug that activates DREADDs, clozapine N oxide (CNO), affects this signal, the BBN ERP signals were recorded once every 4 seconds for 70 minutes following subcutaneous injection of CNO (5 mg/kg). Because the time course of CNO indicates that the onset of their effect on neurons in the CNS is 20-30 minutes after injection, average traces over the first 15 minutes after CNO injection (assumed to be before CNO crossing the blood-brain barrier) were compared to the average traces over the last 51 minutes of the recording session<sup>38,39</sup>. Further investigation of the potential time course of the effect of CNO on A1 ERP signals was achieved by binning the 70-minute recording session into 10-minute time windows. The average N1 peak and FFT of BBN-elicited ERP was calculated during each time window. All ERP traces, N1 peak amplitudes, and FFT plots were obtained from the signal analysis software package BrainVision Analyzer (Brain Products, Gilching, Germany).

*Sound localization behavior procedure.* The sound localization training and testing procedure is described in Chapter 3 of this dissertation and was performed with 3 bats following a sham surgery here. Briefly, the apparatus contained 11 speakers (Fostex FT17H) mounted in a semicircular pattern to the underside of a plywood board with holes cut out, that was elevated off the floor by 4x4s. Each speaker is mounted 18° from the next, so that the 11 speakers span the entire 180° of frontal space and covered with a wire mesh. A 10.5 x 19 x 8 inch (L x W x H) box was secured to the midpoint between the two extreme speakers, so that all speakers were equidistant (0.9 m) from one end of the

box. An opening in the box was cut into this end, so that our bats could enter the arena at this center point. All trials were recorded under infrared light (IRLamp6, Bat Management IR Kit), and the experimenter wore a red-light headlamp. All wire mesh either had a recently killed mealworm (target speakers) or a clay model (off target speakers).

Bats were conditioned to associate noise with a food reward. Because they don't approach speakers naturally<sup>40</sup>, a specific sequence had to be used on each bat. This sequence is described in detail in Chapter 3. The bats had to be trained to become comfortable with hunting for live mealworms on the apparatus, then worms were placed only at one sound producing speaker. The sound, 5-30 kHz BBN repeated at 1 Hz, played continuously until the bat found the reward. Quickly, bats learned to approach only the sound producing speaker, and walk through the box and wait at the end before doing so. At this point, sounds were played only once when the bat waited in the standard position and bat performance on an open loop task could be measured. Testing began when bats averaged less than 18° of error (missed by less than one speaker on average) over the course of 5 days. The bats were trained to not turn their heads while waiting for the sound.

Before testing each day, bats were anesthetized with isoflurane inhalation and injected subcutaneously with either saline or CNO. Whether the injected solution was saline or CNO was randomized each day. Trained bats were tested each day on their ability to localize a 200 ms BBN signal generated in Audacity and validated with an ultrasonic microphone (Sokolich Ultrasonic Probe Microphone System) to be flat 5-40

kHz, measured 10 cm above the speaker. The stimuli used were also randomized between 60-70 dB, based on these measurements, to reduce the possibility that the bats intensity as a cue to localize the sound source. Testing was complete when bats localized 15 trials at each speaker location, and the mutual information, percent of correct responses, and degrees of error are obtained for each condition, from each bat before running two-way repeated measures ANOVA to determine whether sound source location or CNO affects performance.

## **Results**

### *ii. Testing various AAV serotypes in pallid bat A1*

rAAV serotypes vary in spread from the injection site<sup>22,25</sup>. Since our end goal was to maintain delivery of rAAV and their gene products to within the NSR region, we aimed to find an injection volume that kept the spread from the injection site at less than 1 mm. This spread would restrict most of the expression of the genetic material within the pallid bat NSR<sup>10</sup>. Thus, our first goal was to inject 2  $\mu$ L of each product, which produced expression volumes that spread within 1 mm of the injection site for various rAAV serotypes injected into the mouse brain<sup>22</sup>.

2  $\mu$ L of rAAV serotypes 2, 8, and 9 were injected approximately halfway down the cortical column (500  $\mu$ m) of pallid bat A1 at a rate of 0.5  $\mu$ L/min. After allowing the AAVs 28 days to transfect cells and express GFP, the reporter signal was expressed robustly throughout the cortical column. rAAV2-CMV-EGFP was expressed relatively

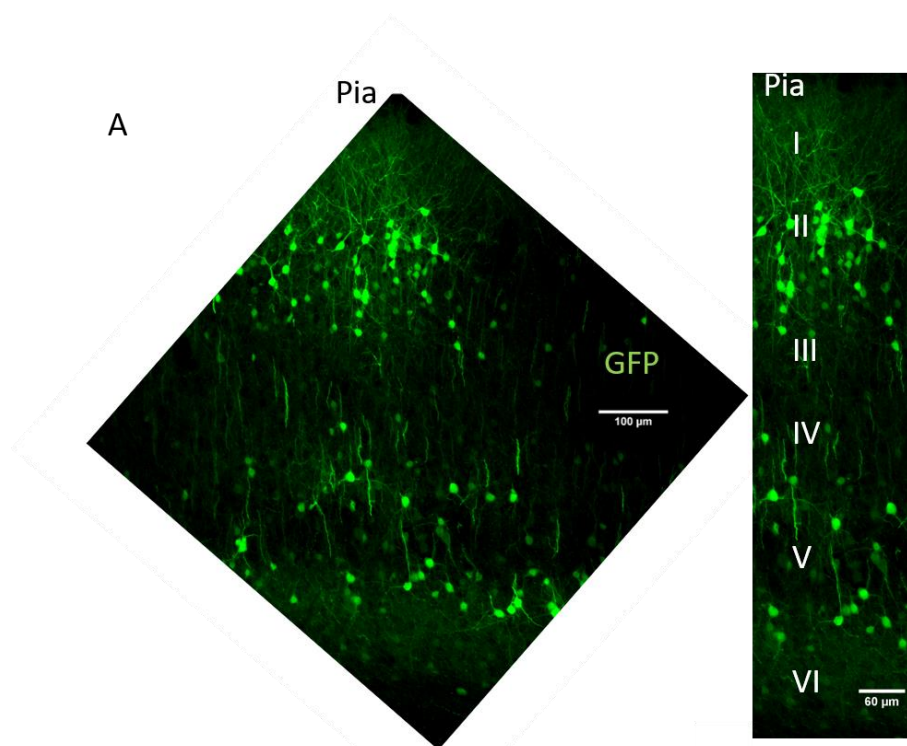
equally throughout layers I-VI (Figure 5.1A). This contrasted with rAAV9-CAG-GFP and rAAV8-ds-CBh-GFP. While these serotypes were expressed throughout the column, GFP delivered by rAAV9 expressed much more robustly in the deep cortical layers (Figure 5.1B), while GFP delivered by rAAV8 expressed more robustly in the superficial layers (Figure 5.2A). While these are qualitative observations based on a few animals, these preliminary observations set the stage for a more comprehensive analysis of various serotypes.

While it is desirable to find an injection paradigm that exhibits robust expression throughout the cortical column, it is also essential to restrict expression spread from the injection site so that the transfection does not extend outside of the desired cortical area. In both cases of 2  $\mu$ L injections rAAV2 and rAAV9, the spread of GFP expression exceeded 3 mm (data not shown). Here, GFP expression was defined as at least one visible cell filled with GFP signal and spread refers to the total rostral-caudal distance such expression was observed. Examples of cells with dim yet entirely filled cells are shown in Figure 5.2B (white arrowheads). Because we aimed to proceed to using the inhibitory hM4D(Gi) DREADD, and the available serotype delivering this genetic material was rAAV8, we further examined the rostral-caudal extent of cellular transfection and expression of GFP in conditions of varying rAAV8 injection volume. Two such conditions are shown in Figure 5.2. When we injected 2  $\mu$ L of rAAV8 the expression spread again exceeded 3 mm in the rostral-caudal direction. However, reducing this injection volume to 0.75  $\mu$ L resulted in transfection spread of 2.72 mm total. Furthermore, restricting our definition of GFP expression to only include sections

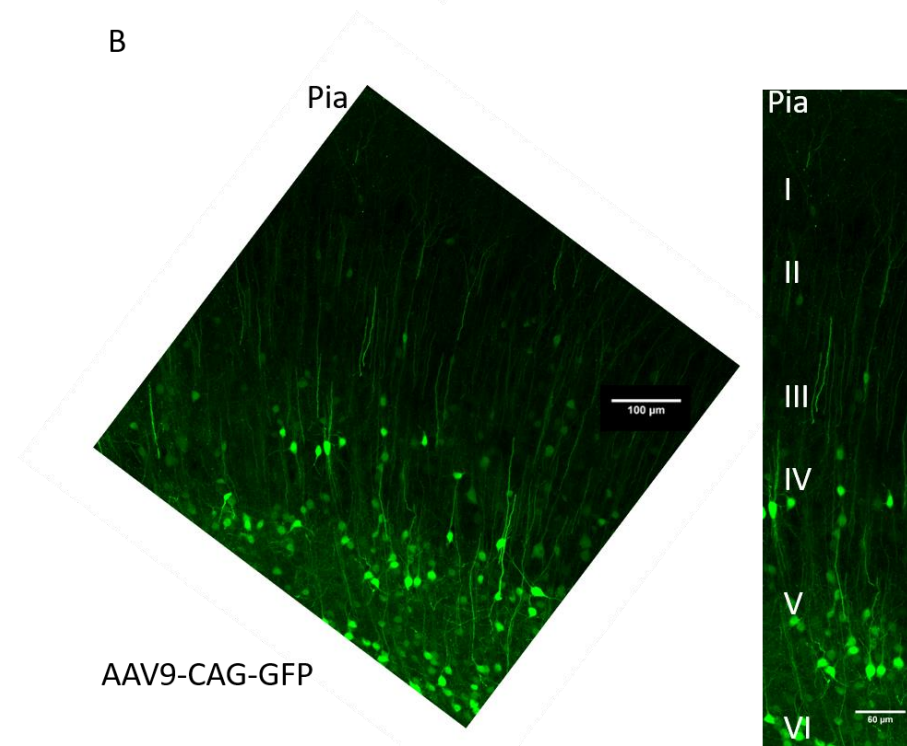
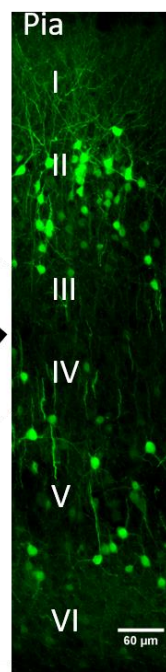
containing cells filled with GFP throughout the cortical column indicated an injection spread of 1.6 mm. Figure 5.2B shows an example of the expression after 0.75  $\mu$ L injections of rAAV8. Like the expression pattern after 2  $\mu$ L injections, the expression is more robust in the superficial layers. However, the GFP filled cells can still be seen in the deep layers of the cortex. Thus, our injection protocol was sufficient to procure rAAV8-GFP transfection and expression throughout the auditory cortex of the pallid bat. Based on these results, we aimed to characterize the expression of the rAAV8 serotype carrying the genetic material coding for the inhibitory DREADD (hM4Di).

*iii. rAAV8-hM4Di expression in pallid bat A1*

0.75  $\mu$ L of rAAV8-CaMKIIa-hM4Di-mCherry was injected into pallid bat A1 following the results of the rAAV8-GFP experiment. Figure 5.3A shows an image of a whole brain section from near the injection site, taken 28 days post injection. Injections were made in the right cortex and a faint red signal is observed in the right A1 region (white box, right side of image). Zooming into both the left (Figure 5.3B) and right (Figure 5.3C) boxes of Figure 5.3A reveals a very small region of hM4Di-mCherry expression in the right cortex (white arrow) compared to no expression in the left cortex. The expression was only observable in two sections, indicating that the spread from the injection site was  $<120 \mu\text{m}$ , a 10-fold reduction in transfection of the same volume of rAAV8-ds-CBh-GFP. Although the expected spread was not observed, individual cells express hM4Di-mCherry in a pattern matching the signal of expression in mice (compare white arrowheads of Figure 5.3D here to the center image of top row of Figure 5.2A from <sup>33</sup>). This expression is clearly not high enough to inhibit the activity of many neurons.



AAV2-CMV-EGFP



AAV9-CAG-GFP

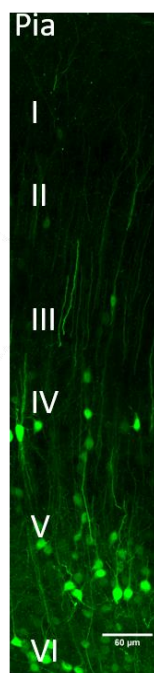


Figure 5.1. Sample images of the robust expression profile of different AAV serotypes. **(A)** AAV2-CMV-EGFP expression in pallid bat A1. Pia is at the top of each image, and most of the cortical column is observable in both images. The cropped image to the right is the center of the larger image, selected to clarify the extent of expression throughout the cortical column. Approximate position of cortical layers is determined from the DAPI nuclear stain in the ultraviolet channel (not shown). **(B)** AAV9-CAG-GFP expression in another pallid bat cortex. Volume of injection was 2  $\mu$ L in both (A) and (B). The green signal is GFP in all images.

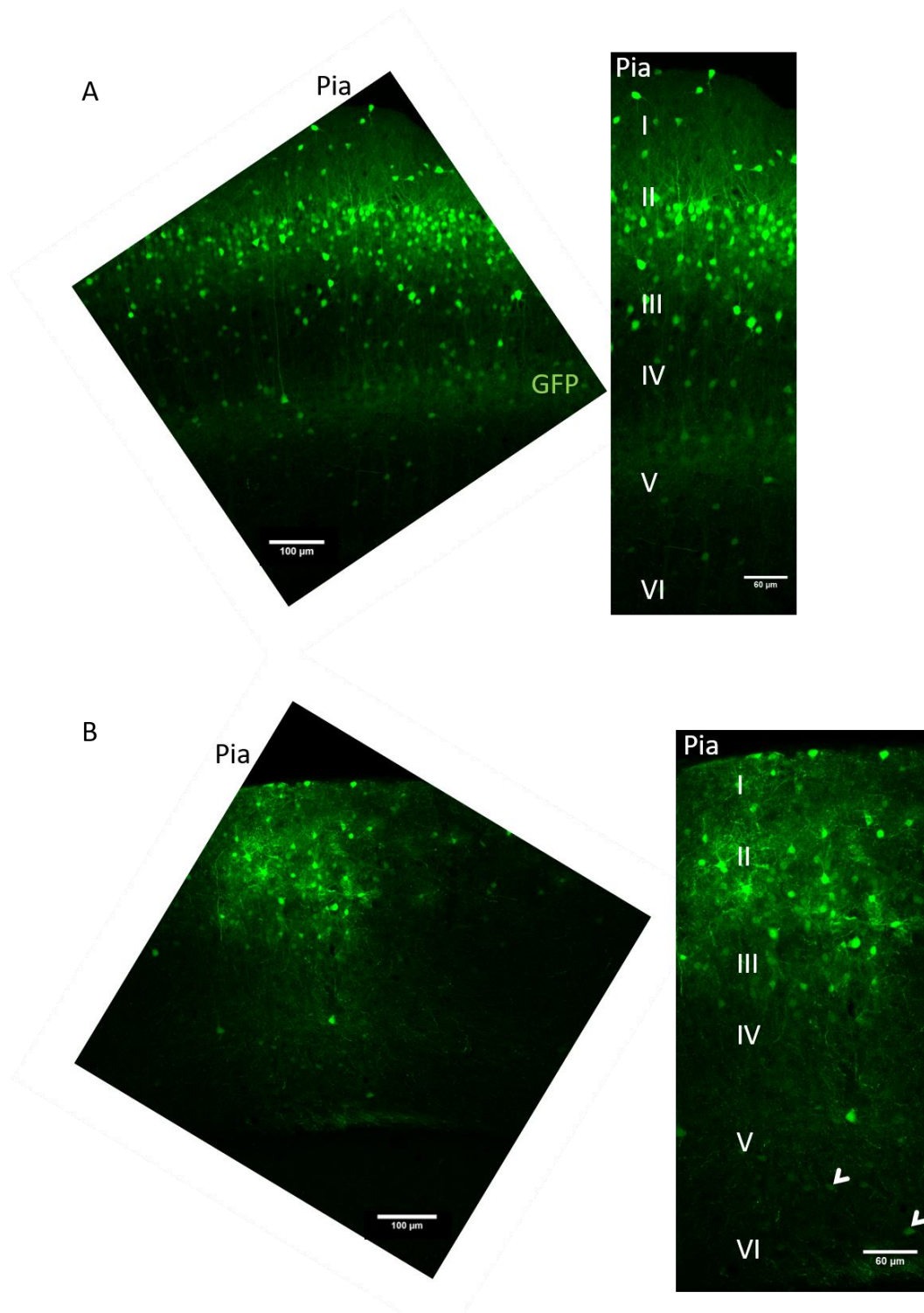


Figure 5.2. The expression profile of AAV8-ds-CBh-GFP 28 days after (A) 2  $\mu$ L of injection and (B) 0.75  $\mu$ L injection. White arrowheads highlight cellular expression of the rAAV delivered GFP in deep layers after a reduced volume injection. Pia and layers are displayed in the same way as Figure 5.1. The green signal is GFP in all images.

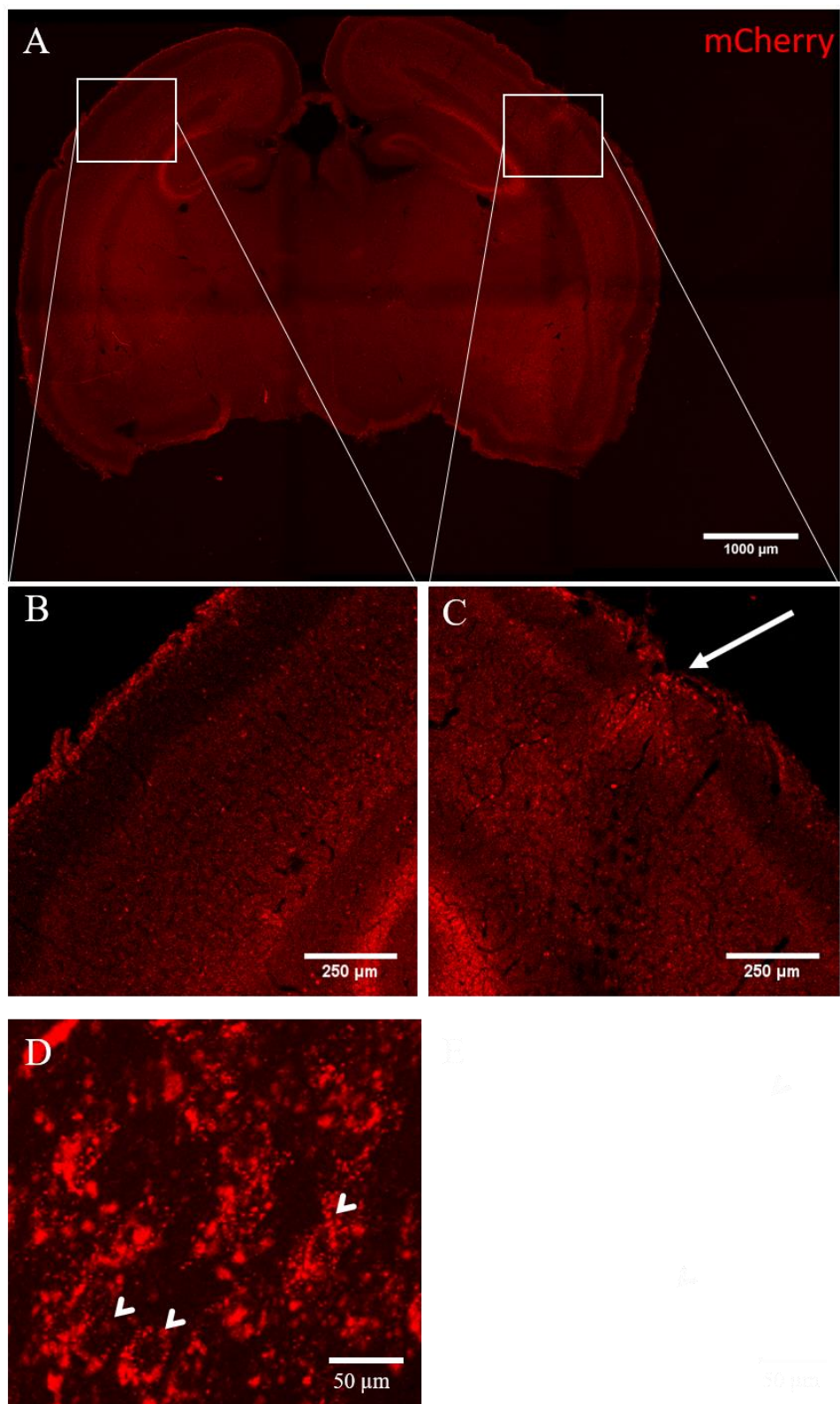


Figure 5.3. AAV8-CaMKii-hM4Di-mCherry expression in the pallid bat cortex 28 days after a 0.75  $\mu$ L injection. **(A)** Whole brain scan shows a stark contrast in expression of the hM4Di-mCherry compared to GFP (shown in Figure 8) carried by AAV8 (white boxes). Zoomed images of the cortex contralateral **(B)** and ipsilateral **(C)** to the injection site. Some expression of hM4Di-mCherry is observable (white arrow). **(D)** mCherry signal at the cellular level in the pallid bat demonstrates successful transfection and expression of hM4Di. The red signal is mCherry in all images.

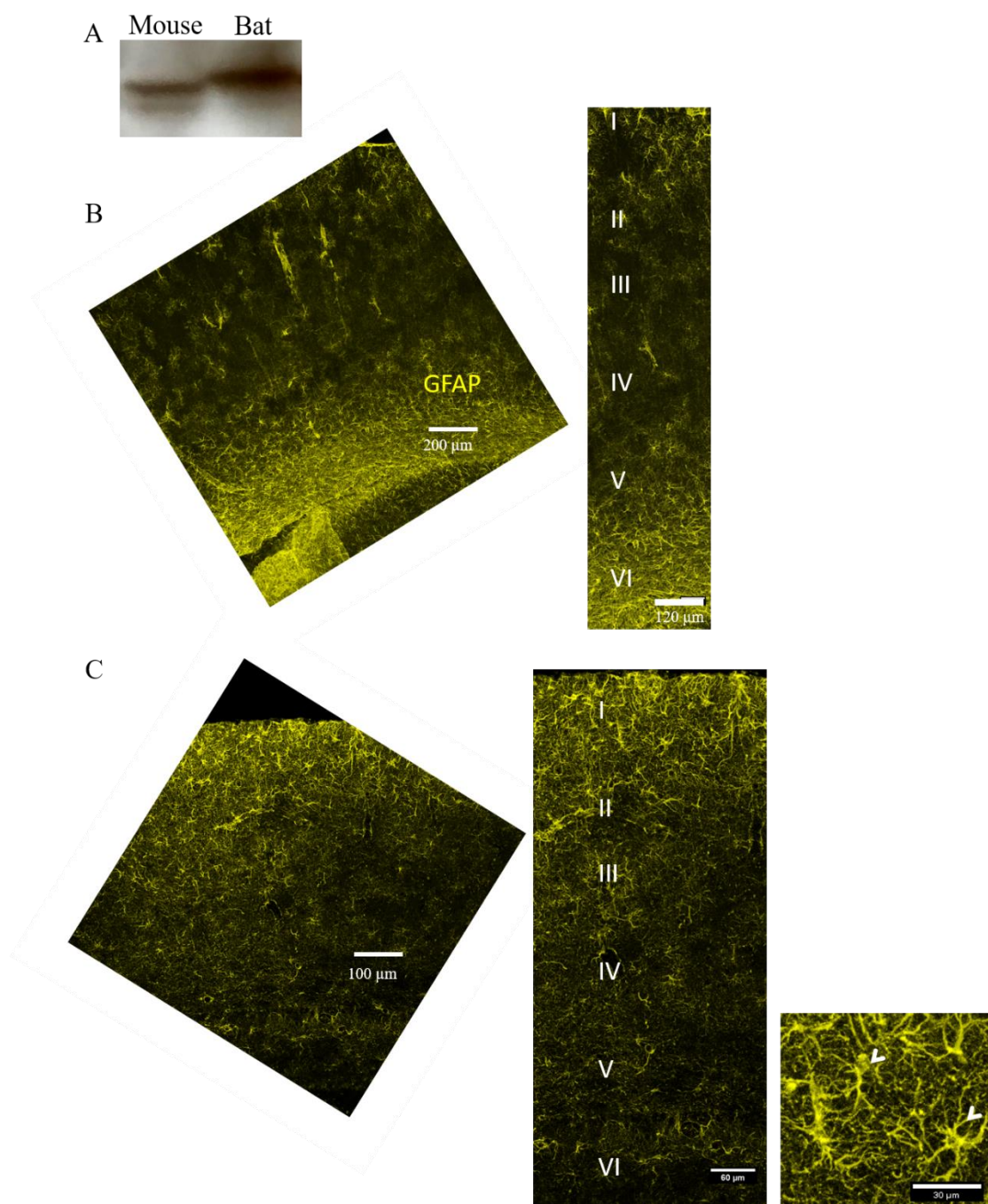


Figure 5.4. **(A)** Western blots showed an antibody that identifies GFAP signal in mice identifies GFAP in bats as well. **(B)** Mouse and **(C)** pallid bat cortex was successfully stained with GFAP antibody to demonstrate the cortical astrocytes. Layers are labeled as in Figure 5.1. Astrocytes were present throughout the cortex in both mice and pallid bat cortex. The farthest right image of **(C)** shows a zoomed in view of layer I astrocytes (white arrow heads) that stained the brightest in pallid bat cortex. The yellow signal is GFAP in all images.

Therefore, we plan to test larger injections and greater injection rates in the future.

However, the results do suggest that hM4Di is expressed in pallid bat auditory cortex cells, and the expression is well matched with the pattern of cellular expression that the same rAAV exhibited in the mouse brain<sup>33</sup>.

*iv. GFAP expression in pallid bat A1*

Because our AAV product was expressed in cortical cells, we want to eventually determine whether the promoter was working as intended by restricting expression of the inhibitory DREADDs to target cells. The CaMKIIa promotor was chosen to restrict expression to forebrain neurons. In the event of the injection spreading beyond our intended depth, this would maintain expression within the cortex. Additionally, this would prohibit hM4Di activity from interfering with glial function. To insure astrocytes were not expressing the hM4Di-mCherry, we tested a GFAP antibody in bats.

We compared the GFAP antibody stain in mouse auditory cortex to the same antibody signal in the pallid bat A1 (Figure 5.4). The Western blot GFAP antibody signal processed from bat tissue matched the signal in mouse tissue (Figure 5.4A), indicating that this antibody would be as selective and robust in bats as it is in mice. GFAP IHC in both mouse (Figure 5.4B) and pallid bat (Figure 5.4C) tissue support this conclusion. Bright GFAP signal was present in astrocytes (Figure 5.4C, white arrowheads) throughout the pallid bat cortex. Together, these data support the use of commercially available AAVs, DREADDs, and the astrocytic marker GFAP in pallid bats. More work

is necessary to determine optimal injection strategies for robust expression of hM4Di DREADDs, however.

*v. CNO does not affect pallid bat ERP signals or behavior*

A critical set of experiments that must be performed along with our future analyses using AAV-DREADDs are the experiments of injecting the synthetic drug, CNO, into control animals. Recent findings suggest that CNO administration can lead to increased clozapine levels<sup>41,42</sup>. Clozapine interacts with many endogenous neuroreceptors<sup>43,44</sup>. These findings have led to speculation that the injection of CNO may contribute to network changes, even in the absence of DREADDs. To test for this and to establish a recording paradigm in which DREADDs function might be tested in the future, we have recorded the ERP in the pallid bat A1 at various locations.

Figure 5.5A demonstrates the ERP signal of pallid bat A1 following stimulus presentation of BBN (5-40kHz, 10 ms duration) and a DFM sweep (60-30kHz, 5 ms duration). In this example, as well as at all other recording sites, the response to BBN was greater than for DFM sweeps (Figure 5.5B). We targeted the NSR region during the recording session. However, due to the poor spatial resolution of the ERP<sup>45</sup>, exact location is not possible to determine based on the absolute magnitudes presented in Figure 5.5B without single or multi-unit recordings from the same site<sup>46</sup>. We infer that we were positioned over the NSR in at least 3 of our recording positions (Pos 2, 3, and 4), based on a robust response to BBN and best frequencies below 40 kHz. Due to relatively

low signal strength for all acoustic stimuli tested at Pos 1, the electrode may have been placed adjacent to A1.

Because pallid bat A1 is topographical, with separate regions for FM selectivity and BBN selectivity, we hypothesized that the amplitude of the DFM sweep ERP signal relative to the ERP signal for BBN would change as the electrode position was moved. Supporting the hypothesis, the amplitude of DFM sweep ERPs relative to BBN ERPs at positions 1-3 were far larger than the same signal at position 4 (Figure 5.5C). Future studies should prioritize

measurements of single/multi-unit extracellular recordings in conjunction with the ERP recordings, to determine the electrode position within the cortical map with certainty.

ERP recordings were also made over the course of 71 minutes following subcutaneous injection of CNO. The signal amplitude before and after the assumed time(20 minutes<sup>38</sup>) of CNO penetrating the CNS were nearly identical (Figure 5.6A). Parsing the data into 10-minute time windows and plotting the average of each peak (P1, N1, and P2) amplitude or the average FFT of the ERP reveals a more detailed picture of signal changes over the time course following CNO injection (Figure 5.6B-C). We find that both the peak amplitude and average ERP are stable throughout the 71 minutes.

This doesn't prove that CNO will not affect the behavior of the animal in the absence of DREADDs. To address this gap, we trained a group of 3 pallid bats to localize BBN sounds, the same behavioral task described in Chapter 3 of this dissertation. 30

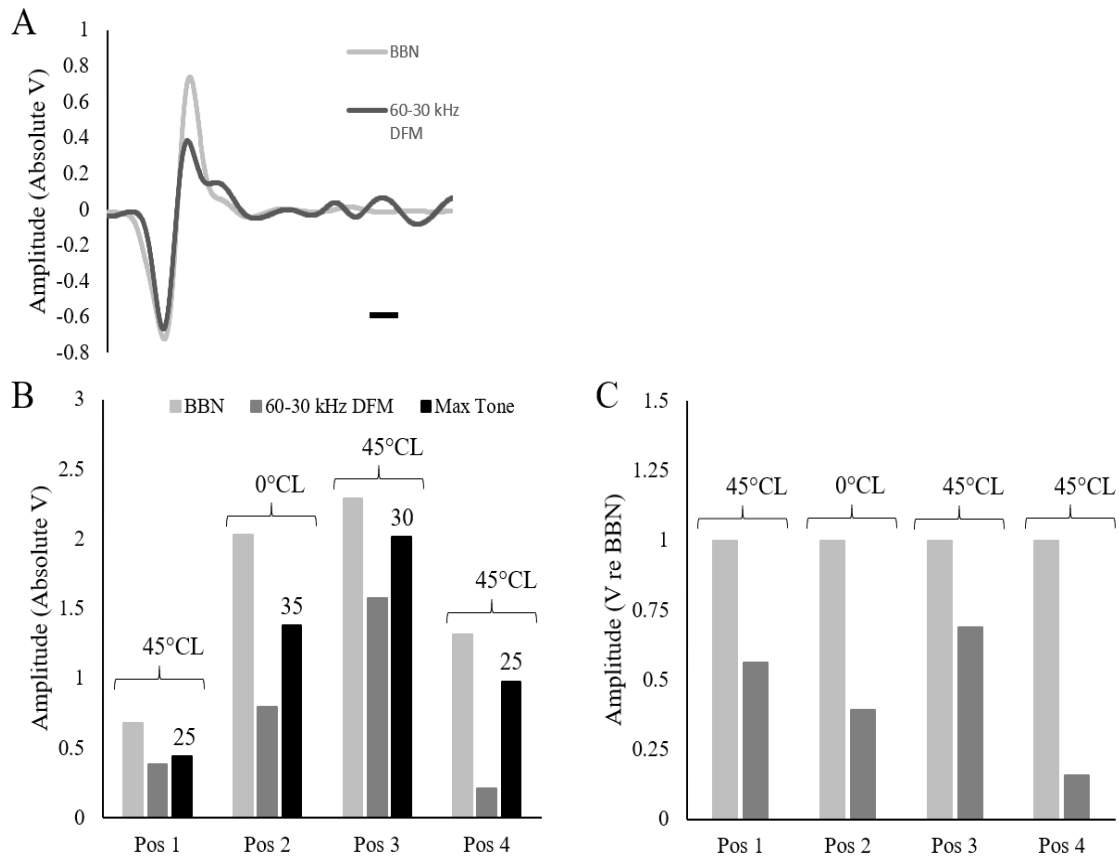


Figure 5.5. The ERP can be used to approximate electrode position in the pallid bat cortical map. (A) Example ERP from position 1 while sound source was located at 45°CL. BBN response always exceeded DFM response at all locations tested. The scale bar to the bottom right is 10 ms. (B) Absolute amplitudes of the maximum ERP signal following stimulations at various cortical positions and by various stimuli. Azimuthal positions above each set of bars are the location of greatest response to 5-40 kHz BBN. Numbers above the black bars indicate the tone that evoked the maximum ERP, interpreted as the approximate position in the tonotopic axis the electrode was placed at. (C) The amplitude of max ERP for various stimuli relative to the max ERP amplitude for BBN changes between positions. All notation follows the rules of (B).

minutes prior to testing each day, pallid bats were injected with either CNO or saline subcutaneously. There was not a significant difference in any of the three sound localization performance measurements when comparing the bats' performance after saline or CNO injection (Figure 5.7; mutual information:  $F = 0.311$ ,  $p = 0.633$ ; percent of

correct responses:  $F = 0.781$ ,  $p = 0.470$ ; degrees of error:  $F = 2.356$ ;  $p = 0.265$ ). Together, these data indicate that CNO alone does not impact the neural signals or behavior of the pallid bat.

## Discussion

*i. rAAV serotypes, ERPs, and tests of CNO in control animals suggest chemogenetic techniques may be viable in the pallid bat*

It is important to select the proper product for transfection when attempting to manipulate cortical circuits. rAAVs serotypes have a distinct tropism, infecting neurons with varying efficacies, and spreading from the injection site differently, as well<sup>22,23,25,32</sup>. In most cases, the serotype rAAV2 yields the worst and/or most variable transfection efficacy and viral spread, while rAAV8 and 9 delivered the product far from the injection site<sup>23,25,57</sup>.

Injections of rAAV2, 8, and 9 containing a GFP reporter protein demonstrated that pallid bat brain tissue interacts with the viral components robustly (Figures 6 and 7). The NSR region is approximately 2 mm<sup>2</sup><sup>10</sup>. In a previous report of AAV serotype tropism following a 2  $\mu$ L injection into the mouse CNS, rAAV2 spread approximately 1 mm in both the rostral and caudal directions<sup>22</sup>. Using the same injection protocol, we found that the spread was >3 mm total (>1.5 mm in either rostral or caudal direction) for all serotypes. This level of virus spread from the injection site is too much to maintain expression in the NSR region of the pallid bat.

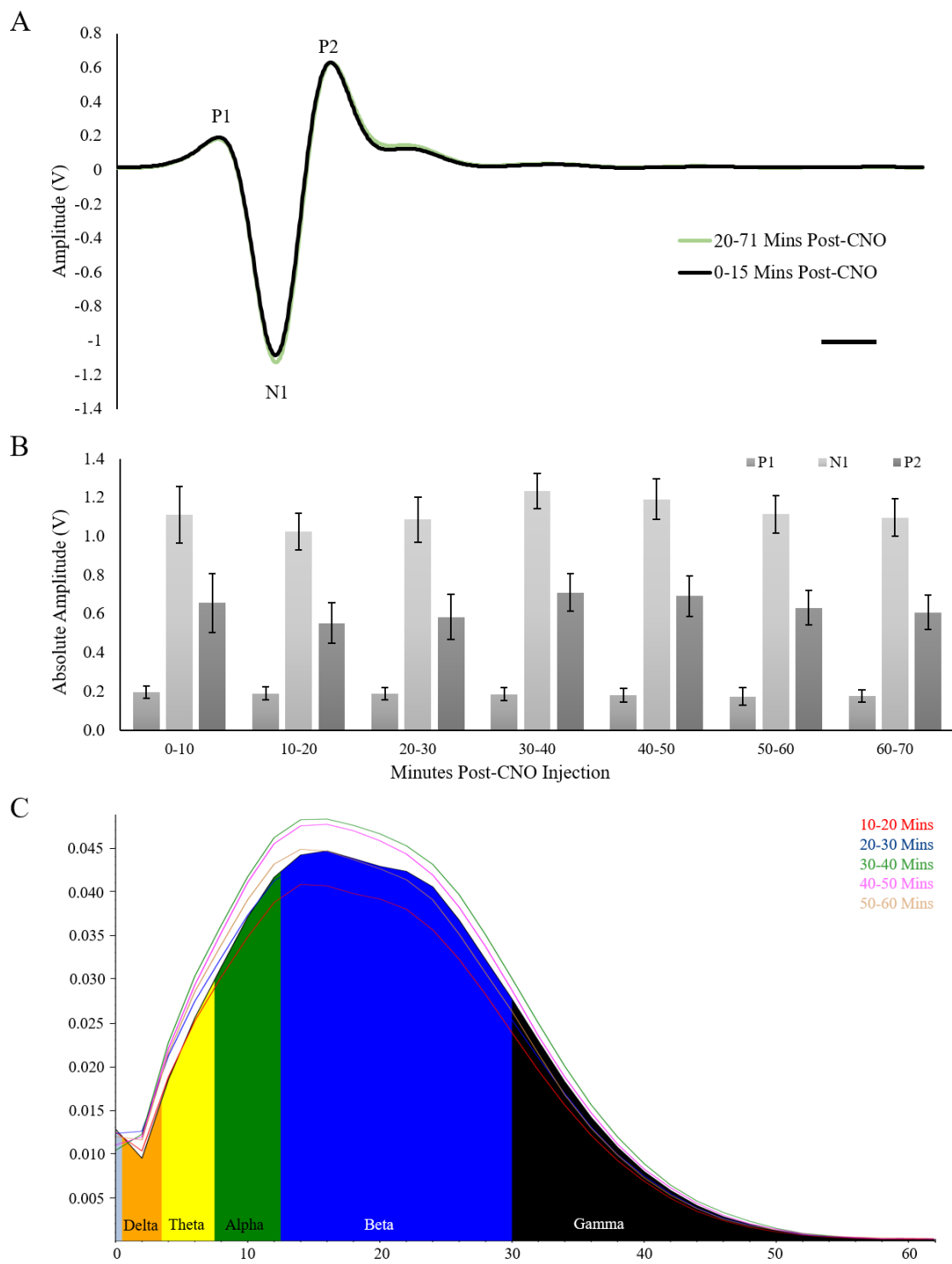


Figure 5.6. The ERP of one pallid bat is stable following subcutaneous administration of CNO. **(A)** Average ERP resulting from BBN stimulation during two different time periods following CNO injection intraperitoneally. The black line represents the average ERP for the first 15 minutes following CNO injections. The green line, which is nearly completely obfuscated by the black line, represents the average ERP for the last 56 minutes of the recording procedure. **(B)** The ERP amplitude after of each peak is shown as an average over time. Data are binned in 10-minute intervals, starting at 0-10 minutes after CNO injection. Error bars represent standard deviations. **(C)** The average FFT of the ERP following stimulation with BBN is shown for the various time windows following CNO injection. The signal was low-pass filtered at 30-Hz. The peak of each FFT after 0-10 minutes post-CNO injection are shown in the various colored lines. The FFT for time 0-10 minutes post-CNO is shown with all bandwidths separated by color (Delta = Orange, Theta = Yellow, etc.) In general, both the peak amplitudes of **(B)** and the bandwidth energy of **(C)** are not altered in any systematic way after CNO injection.

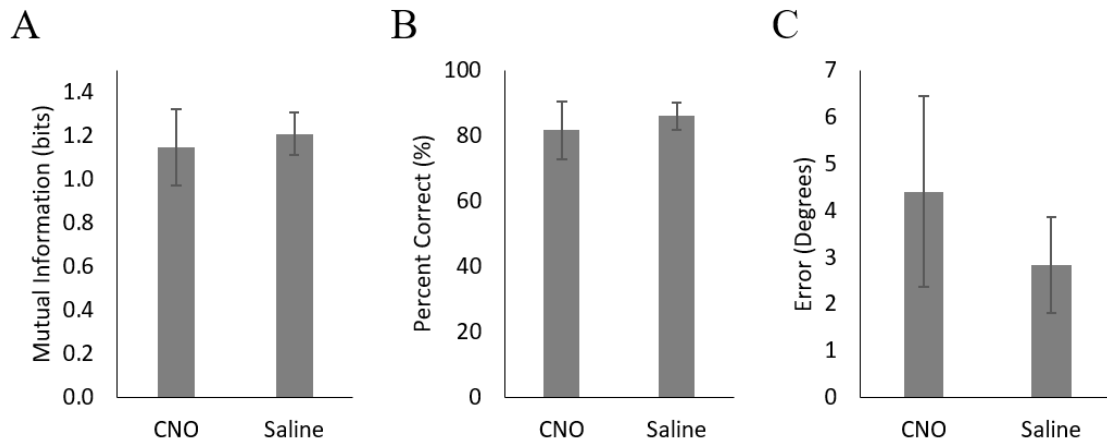


Figure 5.7. Pallid bat sound localization is unaffected by an injection of CNO compared to performance following saline injections. Average **(A)** mutual information, **(B)** percent of correct responses, and **(C)** degrees of error are all unaffected by the injection of CNO. Data are presented as means and error bars represent standard error.

Due to the availability of rAAV8-hM4D(Gi)-mCherry, we decided to focus on restricting rAAV8 within our accepted viral spread range. We injected 0.75  $\mu$ L of rAAV8-GFP and found that the viral spread was  $\sim 1$  mm spread from the injection site. This was closely matched to the spread observed in the marmoset cortex following a similar injection protocol<sup>23</sup>.

Utilizing the optimized injection protocol identified with rAAV8-GFP, we noticed a stark contrast in the expression of the rAAV8-CaMKII-hM4Di-mCherry vector gene products (Figure 5.3). Nonetheless, signatures of the injection site could be seen from the scan of the entire section near the injection site (Figure 5.3A), and individual cells were clearly labeled in the expected expression pattern. We take this to show that the hM4Di is likely expressed successfully in pallid bat cortex. A caveat to this interpretation lies in the fact that injections into the cortex necessarily involve trauma to the tissue. Such

procedures can result in inflammation at the site of injection, increasing the autofluorescent signal. Future studies should test for this possibility by injecting saline only, potentially into the opposite cortex of the same animal. Assuming this is not the case, future studies should begin with larger injection volumes and longer incubation time periods (>28 days).

It is important to the design of our experiments to restrict the inhibitory effects of the hM4Di DREADDs to cortical forebrain neurons. We chose a vector whose expression is under control of the CaMKII promoter for this reason. To demonstrate the degree to which this promoter constrains expression of the DREADDs products within neurons, we optimized an IHC protocol to show the expression profile of GFAP, an astrocytic marker (Figure 5.4). In these results, the pallid bat demonstrates robust astrocytic GFAP expression throughout the cortex. NeuN will be optimized for use in the pallid bat in the future. By co-staining NeuN and GFAP with the mCherry signal of the DREADDs, future studies would be able to demonstrate the restriction of DREADDs to cortical neurons by showing an overlap with of mCherry in the NeuN channel, but not in the GFAP channel.

Demonstrations of the effect of CNO on control and DREADDs expressing neurons are usually carried out via indirect methods. For instance, in vitro electrophysiology methods are used to show the effect after washing brain sections with CNO. Alternatively, the expression of the immediate early gene *cfos* is examined after subcutaneous or intramuscular CNO as a marker for DREADDs activation or inactivation by CNO. If the *cfos* signal is reduced (hM4Di) or increased (hM3Dq), it is attributable to

the DREADDs + CNO administration working as intended. In most circumstances, a combination of these methods is used<sup>15,58</sup>. One study had success measuring modulation of DREADDs expressing neurons using in vivo extracellular single-unit electrophysiology<sup>59</sup>. This method would be the most reliable one for determining where in the cortex the DREADDs were effectively expressed. We chose to measure the ERP over this method for a few reasons. First, sampling the activity across the relatively large area of the NSR would be much more time consuming with the in vivo single-unit recording method. Second, we are restricted to the size of the exposure in the populations of neurons we could sample from. Most importantly, single unit would restrict our ability to test how CNO is affecting the local circuit in a single experiment. We could only sample a single unit before subcutaneous injections of CNO. The problem is further compounded by the fact that we wouldn't know for certain whether the neuron expressed DREADDs in such a recording setup. By measuring the ERP, we are aiming to measure the effect of DREADDs + CNO on the entire NSR region.

The ERP approach is not without its own problems and considerations. It is difficult to know exactly where in the cortex we are recording without measuring single or multi-unit activity at the same recording positions, due to the poor spatial resolution of the large ERP electrodes<sup>45,46</sup>. Nevertheless, the spatial resolution may still be much smaller than necessary to resolve the separate cortical regions in pallid bat A1. A study investigating spatial resolution of the summed local field potential in primate visual cortex found that populations with a radius of 250  $\mu\text{m}$  could be resolved<sup>46</sup>. Recording sites such as position 4 support the notion that significant spatial resolution can be

achieved so as to record almost only from NSR neurons. Even if this is not the case, the relative amplitude could tell us about the populations that are being inhibited, assuming effective DREADDs transfection and expression can be achieved, and CNO is crossing the blood-brain barrier sufficiently. Once efficient hM4Di expression is achieved, ERP measurements in bats expressing the DREADD can be carried out with methods similar to those employed here to test this hypothesis.

Intramuscular or subcutaneous injections of CNO lead to increased CNO concentrations in the cerebrospinal fluid in monkeys<sup>38,39</sup>. CNO also metabolizes into clozapine, an endogenous compound that interacts with several CNS receptors<sup>41–44</sup>. The levels of CNO injected in these experiments have produced altered behaviors and neurotransmitter release in the CNS of rats<sup>42</sup>. To prepare for future experiments involving DREADDs, we wanted to make sure that CNO and the metabolism of CNO into clozapine would not affect the baseline ERP signal or the behavioral performance of animals that only received a saline injection into the cortex on the day of surgery (sham surgery). Our results suggest that CNO nor clozapine produce any effect on these measures, paving the way for the future experiments utilizing DREADDs to assess the necessity of the NSR to sound localization behavior.

Together, these results provide a foundation upon which future studies can further our understanding of auditory cortex function. Additionally, the continued validation of modern chemogenetic tools in a wild mammal, will provide a vital proof of concept to the field of neuroethology.

1. Bell, G. P. Behavioral and ecological aspects of gleaning by a desert insectivorous bat *Antrozous pallidus* (Chiroptera: Vespertilionidae). *Behav. Ecol. Sociobiol.* **10**, 217–223 (1982).
2. Goerlitz, H. R., Greif, S. & Siemers, B. M. Cues for acoustic detection of prey: insect rustling sounds and the influence of walking substrate. *J. Exp. Biol.* **211**, 2799–806 (2008).
3. Whitfield, I. Auditory space and the role of the cortex in sound localization. in *Psychophysics and Physiology of Hearing* (eds. Evans, E. & Wilson, J.) 1–9 (Academic, 1977).
4. Malhotra, S., Hall, A. J. & Lomber, S. G. Cortical Control of Sound Localization in the Cat: Unilateral Cooling Deactivation of 19 Cerebral Areas. *J. Neurophysiol.* **92**, 1625–1643 (2004).
5. Jenkins, W. M. & Merzenich, M. M. Role of cat primary auditory cortex for sound-localization behavior. *J. Neurophysiol.* **52**, 819–47 (1984).
6. Jenkins, W. M. & Masterton, R. B. Sound localization: effects of unilateral lesions in central auditory system. *J. Neurophysiol.* **47**, 987–1016 (1982).
7. Heffner, H. E. The Role of Macaque Auditory Cortex in Sound Localization. *Acta Otolaryngol.* **117**, 22–27 (1997).
8. Kavanagh, G. L. & Kelly, J. B. Contribution of auditory cortex to sound localization by the ferret (*Mustela putorius*). *J. Neurophysiol.* **57**, 1746–66 (1987).
9. Bizley, J. K., Nodal, F. R., Parsons, C. H. & King, A. J. Role of Auditory Cortex in Sound Localization in the Midsagittal Plane. *J. Neurophysiol.* **98**, 1763–1774 (2007).
10. Razak, K. A. & Fuzessery, Z. M. Functional Organization of the Pallid Bat Auditory Cortex: Emphasis on Binaural Organization. *J. Neurophysiol.* **87**, 72–86 (2002).
11. Razak, K. A., Shen, W., Zumsteg, T. & Fuzessery, Z. M. Parallel thalamocortical pathways for echolocation and passive sound localization in a gleaning bat, *Antrozous pallidus*. *J. Comp. Neurol.* **500**, 322–338 (2007).
12. Razak, K. A. Systematic representation of sound locations in the primary auditory cortex. *J. Neurosci.* **31**, 13848–59 (2011).
13. Razak, K. A. & Fuzessery, Z. M. GABA Shapes a Systematic Map of Binaural

- Sensitivity in the Auditory Cortex. *J. Neurophysiol.* **104**, 517–528 (2010).
14. Razak, K. A., Yarrow, S. & Brewton, D. Mechanisms of Sound Localization in Two Functionally Distinct Regions of the Auditory Cortex. *J. Neurosci.* **35**, 16105–15 (2015).
  15. Krashes, M. J. *et al.* Rapid, reversible activation of AgRP neurons drives feeding behavior in mice. *J. Clin. Invest.* **121**, 1424–8 (2011).
  16. Roth, B. L. DREADDs for Neuroscientists. *Neuron* **89**, 683–694 (2016).
  17. Kuhlman, S. J. *et al.* A disinhibitory microcircuit initiates critical-period plasticity in the visual cortex. *Nature* **501**, 543–546 (2013).
  18. Bender, F. *et al.* Theta oscillations regulate the speed of locomotion via a hippocampus to lateral septum pathway. *Nat. Commun.* **6**, 8521 (2015).
  19. DiBenedictis, B. T., Olugbemi, A. O., Baum, M. J. & Cherry, J. A. DREADD-Induced Silencing of the Medial Olfactory Tubercle Disrupts the Preference of Female Mice for Opposite-Sex Chemosignals. *eNeuro* **2**, ENEURO.0078-15.2015 (2015).
  20. McCown, T. J., Xiao, X., Li, J., Breese, G. R. & Jude Samulski, R. Differential and persistent expression patterns of CNS gene transfer by an adeno-associated virus (AAV) vector. *Brain Res.* **713**, 99–107 (1996).
  21. During, M. *et al.* In vivo expression of therapeutic human genes for dopamine production in the caudates of MPTP-treated monkeys using an AAV vector. *Gene Ther.* **5**, 820–827 (1998).
  22. Burger, C. *et al.* Recombinant AAV Viral Vectors Pseudotyped with Viral Capsids from Serotypes 1, 2, and 5 Display Differential Efficiency and Cell Tropism after Delivery to Different Regions of the Central Nervous System. *Mol. Ther.* **10**, 302–317 (2004).
  23. Watakabe, A. *et al.* Comparative analyses of adeno-associated viral vector serotypes 1, 2, 5, 8 and 9 in marmoset, mouse and macaque cerebral cortex. *Neurosci. Res.* **93**, 144–157 (2015).
  24. Xiao, X., Li, J., McCown, T. J. & Samulski, R. J. Gene Transfer by Adeno-Associated Virus Vectors into the Central Nervous System. *Exp. Neurol.* **144**, 113–124 (1997).
  25. Aschauer, D. F., Kreuz, S. & Rumpel, S. Analysis of Transduction Efficiency,

Tropism and Axonal Transport of AAV Serotypes 1, 2, 5, 6, 8 and 9 in the Mouse Brain. *PLoS One* **8**, e76310 (2013).

26. del Campo, H. M., Measor, K. & Razak, K. A. Parvalbumin and calbindin expression in parallel thalamocortical pathways in a gleaning bat, *Antrozous pallidus*. *J. Comp. Neurol.* **522**, 2431–2445 (2014).
27. Razak, K. A. & Fuzessery, Z. M. Neural Mechanisms Underlying Selectivity for the Rate and Direction of Frequency-Modulated Sweeps in the Auditory Cortex of the Pallid Bat. *J. Neurophysiol.* **96**, 1303–1319 (2006).
28. Razak, K. A. & Fuzessery, Z. M. Facilitatory mechanisms underlying selectivity for the direction and rate of frequency modulated sweeps in the auditory cortex. *J. Neurosci.* **28**, 9806–16 (2008).
29. Razak, K. A. Mechanisms underlying azimuth selectivity in the auditory cortex of the pallid bat. *Hear. Res.* **290**, 1–12 (2012).
30. Holderied, M., Korine, C. & Moritz, T. Hemprich's long-eared bat (*Otonycteris hemprichii*) as a predator of scorpions: whispering echolocation, passive gleaning and prey selection. *J. Comp. Physiol. A* **197**, 425–433 (2011).
31. O'Shea, T. J. & Vaughan, T. A. Nocturnal and Seasonal Activities of the Pallid Bat, *Antrozous pallidus*. *J. Mammal.* **58**, 269–284 (1977).
32. Zincarelli, C., Soltys, S., Rengo, G. & Rabinowitz, J. E. Analysis of AAV Serotypes 1–9 Mediated Gene Expression and Tropism in Mice After Systemic Injection. *Mol. Ther.* **16**, 1073–1080 (2008).
33. Chiou, C.-S. *et al.* Alleviating Bone Cancer-induced Mechanical Hypersensitivity by Inhibiting Neuronal Activity in the Anterior Cingulate Cortex. *Anesthesiology* **125**, 779–792 (2016).
34. Brewton, D. H., Kokash, J., Jimenez, O., Pena, E. R. & Razak, K. A. Age-related deterioration of perineuronal nets in the primary auditory cortex of mice. *Front. Aging Neurosci.* **8**, 270 (2016).
35. Martin del Campo, H. N., Measor, K. R. & Razak, K. A. Parvalbumin immunoreactivity in the auditory cortex of a mouse model of presbycusis. *Hear. Res.* **294**, 31–39 (2012).
36. Cruikshank, S. ., Killackey, H. . & Metherate, R. Parvalbumin and calbindin are differentially distributed within primary and secondary subregions of the mouse auditory forebrain. *Neuroscience* **105**, 553–569 (2001).

37. Anderson, L. A., Christianson, G. B. & Linden, J. F. Mouse auditory cortex differs from visual and somatosensory cortices in the laminar distribution of cytochrome oxidase and acetylcholinesterase. *Brain Res.* **1252**, 130–142 (2009).
38. Eldridge, M. A. G. *et al.* Chemogenetic disconnection of monkey orbitofrontal and rhinal cortex reversibly disrupts reward value. *Nat. Neurosci.* **19**, 37–39 (2016).
39. Raper, J. *et al.* Metabolism and Distribution of Clozapine-N-oxide: Implications for Nonhuman Primate Chemogenetics. *ACS Chem. Neurosci.* **8**, 1570–1576 (2017).
40. Fuzessery, Z. M., Buitenhoff, P., Andrews, B. & Kennedy, J. M. Passive sound localization of prey by the pallid bat (*Antrozous p. pallidus*). *J. Comp. Physiol. A* **171**, 767–777 (1993).
41. Jann, M. W., Lam, Y. W. & Chang, W. H. Rapid formation of clozapine in guinea-pigs and man following clozapine-N-oxide administration. *Arch. Int. Pharmacodyn. Ther.* **328**, 243–50 (1994).
42. MacLaren, D. A. A. *et al.* Clozapine N-Oxide Administration Produces Behavioral Effects in Long-Evans Rats: Implications for Designing DREADD Experiments. *eNeuro* **3**, ENEURO.0219-16.2016 (2016).
43. Ashby, C. R. & Wang, R. Y. Pharmacological actions of the atypical antipsychotic drug clozapine: A review. *Synapse* **24**, 349–394 (1996).
44. Selent, J., López, L., Sanz, F. & Pastor, M. Multi-Receptor Binding Profile of Clozapine and Olanzapine: A Structural Study Based on the New  $\beta_2$  Adrenergic Receptor Template. *ChemMedChem* **3**, 1194–1198 (2008).
45. Woodman, G. F. A brief introduction to the use of event-related potentials in studies of perception and attention. *Atten. Percept. Psychophys.* **72**, 2031–46 (2010).
46. Xing, D., Yeh, C.-I. & Shapley, R. M. Spatial spread of the local field potential and its laminar variation in visual cortex. *J. Neurosci.* **29**, 11540–9 (2009).
47. Wise, L. Z. & Irvine, D. R. Topographic organization of interaural intensity difference sensitivity in deep layers of cat superior colliculus: implications for auditory spatial representation. *J. Neurophysiol.* **54**, 185–211 (1985).
48. Fuzessery, Z. M., Wenstrup, J. J. & Pollak, G. D. A representation of horizontal sound location in the inferior colliculus of the mustache bat (*Pteronotus p.*

- parnellii). *Hear. Res.* **20**, 85–89 (1985).
49. Tollin, D. J., Koka, K. & Tsai, J. J. Interaural Level Difference Discrimination Thresholds for Single Neurons in the Lateral Superior Olive. *J. Neurosci.* **28**, 4848–4860 (2008).
  50. Fuzessery, Z. M. Monaural and binaural spectral cues created by the external ears of the pallid bat. *Hear. Res.* **95**, 1–17 (1996).
  51. Mrsic-Flogel, T. D., King, A. J. & Schnupp, J. W. H. Encoding of Virtual Acoustic Space Stimuli by Neurons in Ferret Primary Auditory Cortex. *J. Neurophysiol.* **93**, 3489–3503 (2005).
  52. Blauert, J. Sound localization in the median plane. *Acta Acust. united with Acust.* **22**, 205–213 (1969).
  53. Populin, L. C. & Yin, T. C. Behavioral studies of sound localization in the cat. *J. Neurosci.* **18**, 2147–60 (1998).
  54. Tollin, D. J., Ruhland, J. L. & Yin, T. C. T. The role of spectral composition of sounds on the localization of sound sources by cats. *J. Neurophysiol.* **109**, 1658–1668 (2013).
  55. Roffler, S. K. & Butler, R. A. Factors That Influence the Localization of Sound in the Vertical Plane. *J. Acoust. Soc. Am.* **43**, 1255–1259 (1968).
  56. Butler, R. A. & Belendiuk, K. Spectral cues utilized in the localization of sound in the median sagittal plane. *J. Acoust. Soc. Am.* **61**, 1264–1269 (1977).
  57. Klein, R. L. *et al.* Neuron-Specific Transduction in the Rat Septohippocampal or Nigrostriatal Pathway by Recombinant Adeno-associated Virus Vectors. *Exp. Neurol.* **150**, 183–194 (1998).
  58. Ferguson, S. M. *et al.* Transient neuronal inhibition reveals opposing roles of indirect and direct pathways in sensitization. *Nat. Neurosci.* **14**, 22–4 (2011).
  59. Teissier, A. *et al.* Activity of Raphé Serotonergic Neurons Controls Emotional Behaviors. *Cell Rep.* **13**, 1965–1976 (2015).

## **Chapter 6**

### **Age-Related Deterioration of Perineuronal Nets in the Primary Auditory Cortex of Mice**

#### **Abstract**

Age-related changes in inhibitory neurotransmission in sensory cortex may underlie deficits in sensory function. Perineuronal nets (PNNs) are extracellular matrix components that ensheath some inhibitory neurons, particularly parvalbumin positive (PV+) interneurons. PNNs may protect PV+ cells from oxidative stress and help establish their rapid spiking properties. Although PNN expression has been well characterized during development, possible changes in aging sensory cortex have not been investigated. Here we tested the hypothesis that PNN+, PV+ and PV/PNN co-localized cell densities decline with age in the primary auditory cortex (A1). This hypothesis was tested using immunohistochemistry in two strains of mice (C57BL/6 and CBA/CaJ) with different susceptibility to age-related hearing loss and at three different age ranges (1-3, 6-8 and 14-24 months old). We report that PNN+ and PV/PNN co-localized cell densities decline significantly with age in A1 in both mouse strains. In the PNN+ cells that remain in the old group, the intensity of PNN staining is reduced in the C57 strain, but not the CBA strain. PV+ cell density also declines only in the C57, but not the CBA, mouse suggesting a potential exacerbation of age-effects by hearing loss in the PV/PNN system. Taken together, these data suggest that PNN deterioration may be a key component of

altered inhibition in the aging sensory cortex, that may lead to altered synaptic function, susceptibility to oxidative stress and processing deficits.

## **Introduction**

Age-related decline in sensory function affects the quality of life in the elderly<sup>1-3</sup>. In the auditory realm, this is exemplified by the relationship between age-related hearing loss (presbycusis), speech recognition problems, social isolation, depression and cognitive decline<sup>4-9</sup>. Presbycusis affects ~35% of humans older than sixty-five and ~45% of humans older than seventy-five years<sup>10</sup>. Decline in sensory function in presbycusis likely reflects a combination of peripheral sensory organ deterioration and central aging<sup>11,12</sup>. The relative contributions of these factors to auditory processing deficits with presbycusis remain unclear.

A consistent finding across sensory cortex is a decline in inhibitory neurotransmission with age<sup>12-15</sup>. Processing of rapidly changing spectrotemporal cues, such as those present in speech, depends on interactions between excitatory and inhibitory components of the auditory neuron receptive field<sup>16-20</sup>. Reduced inhibition may, therefore, affect temporal and spectrotemporal processing, and cause speech processing deficits with age<sup>21-25</sup>. The cellular correlates of reduced inhibition in the auditory system remain incompletely characterized.

Of particular relevance to selectivity for fast spectrotemporal changes are rapid spiking cortical interneurons that express the calcium buffering protein, parvalbumin

(PV)<sup>26,27</sup>. These cells may shape inhibition in auditory cortical neurons that is necessary for some forms of spectrotemporal selectivity<sup>28</sup>. The number of PV+ cells in the primary auditory cortex (A1) declines with presbycusis<sup>29-32</sup> suggesting a cellular correlate of presbycusis-related decline in spectrotemporal processing.

The mechanisms underlying age-related reduction in the number of PV+ cells remain unclear but recent studies suggest that perineuronal nets (PNN) may play a major role. Many PV+ cells in A1 are ensheathed by PNN<sup>33,34</sup>. PNNs are specialized extracellular matrix components and consist of chondroitin sulfate proteoglycans (CSPG) that are found throughout the extracellular matrix but are highly dense around PV+ interneurons. PNNs may protect PV+ cells from oxidative stress that accumulate with age<sup>35,36</sup>. However, relatively little is known about changes to PNN with age in any sensory cortex. Therefore, the main aim of this study was to test the hypothesis that PNN deteriorates with age in A1. Because of the association between PV and PNN, we also examined if PV+, PNN+ and PV/PNN co-localized cell densities changed with age. We examined PV and PNN expression in two mouse strains. The C57BL/6 (C57) is a model for presbycusis with significant hearing deficits due to hair cell loss that begins at ~3 months of age<sup>37</sup>. The CBA/CaJ (CBA) mouse does not show significant hair cell loss with age even up to 18 months of age. Within the constraints imposed by differences in genetic backgrounds, comparison of these two strains will indicate if there is an overall age-related decline in PV, PNN and PV/PNN expression in A1 and if peripheral hearing loss exacerbates such a decline. The data show an age-related decline in PNN+ cell and PV/PNN co-localized cell density in both strains. However, an age-related decline in

PV+ cell density occurred only in the C57 mice. Moreover, in the cells that remain PNN+ in the old mice, there is a reduction in PNN intensity only in the C57 mice. Overall, these results suggest that changes in PNN and PV expression with age likely underlie altered inhibition in sensory cortex.

## **Methods**

*Experimental Groups.* All the mice used in this study were obtained from breeding triads purchased from Jackson Laboratories (Bar Harbor, ME). Littermates were housed in cages of 2-4 individuals on a 12:12 h light-dark cycle and fed *ad libitum*. Mice were housed and raised in the same vivarium under similar conditions. Data were collected from 3 age groups: young ('Y', 1-3 months old), middle aged ('M', 6-8 months old), and old ('O', 14-24 months old). The institutional Animal Care and Use Committee at the University of California, Riverside approved all procedures.

*Immunohistochemistry.* All steps were performed at room temperature unless stated otherwise. Mice were injected with a lethal dosage of sodium pentobarbital and then transcardially perfused using a peristaltic pump (Harvard Apparatus, MA) with 0.1M phosphate buffer saline (PBS) followed by 4% paraformaldehyde (PFA, pH 7.4). Brains were immediately removed and post-fixed in 4% PFA for 2 hours at 4°C. Following post-fixation, brains were placed in a 30% sucrose solution until they sunk (~36-48 hours at 4°C). Brains were sectioned into 40 µm slices on a cryostat (CM1860, Leica, IL) and

stored in a 0.1M PBS solution containing 0.1% sodium azide. Immunohistochemistry was performed on free-floating sections with agitation at room temperature, unless otherwise specified. Sections were pre-treated with 4% PFA for 2 hours, then rinsed for 5 minutes with 0.1M PBS solution two times. Sections were then treated with 50mM ammonium chloride for 15 minutes, followed by three rinses in 0.1M PBS for 5 minutes each. Sections were placed into a 0.1% Triton X solution for 10 minutes to permeabilize the lipid bilayer, and then treated with a blocking buffer (0.1M PBS, 5% goat normal serum (GNS), 1% bovine serum albumin (BSA) for 1 hour. Sections were incubated overnight at 4°C in the primary antibody solution containing a 1:750 ratio of 0.1M PBS to FITC conjugated *Wisteria Floribunda Agglutinin* (WFA, for labeling PNN; Vector Laboratories, FL-135), a 1:10,000 ratio of rabbit anti-PV (Swant, PV25), 1% GNS, 0.5% BSA and 0.1% Tween. After 16-20 hours in the primary antibody solution, sections were washed in 0.5% Tween buffer three times for 10 minutes each. The sections were then incubated in a 1:500 solution of secondary antibody (donkey anti-rabbit, AlexaFluor 647, Life Technologies, A31573) for 1 hour. Sections were washed once with 0.1M PBS for 5 minutes and mounted onto glass slides. Vectashield with a DAPI nuclei stain (Vector Labs, F2-135) was used as the mounting medium. Slides were cover-slipped and sealed prior to imaging on a Leica SP5 confocal microscope.

*Image capture, analysis, and data representation.* The location of the primary auditory cortex (A1) on coronal sections stained with DAPI was identified using the structure of the hippocampus. This method of identifying mouse A1 has been previously validated

with combined electrophysiology and dye placements<sup>30</sup> and cross-referenced with the Paxinos and Franklin, Mouse Brain Atlas (approximately Bregma  $-2.40$  to  $-3.40$ ) and other studies of the mouse auditory cortex<sup>38,39</sup>. Z-stack images were captured on a Leica SP5 confocal microscope in  $2\text{ }\mu\text{M}$  steps. Images were cropped so that the pia and deepest portions of the cortex were visible in a  $400\text{ }\mu\text{m}$  wide section, oriented with the pia to the left (e.g., Figure 6.2). Cell counts and intensity measurements were obtained with ImageJ software (NIH). PV+, PNN+, and co-localized (PV/PNN) cells were manually counted in each image. Only PV+ cells containing immunofluorescence throughout the soma, with the exception of the nucleus, met the criteria for being included in the count.

To reduce the potential influence of random and punctate autofluorescence on the PV+ cell counting procedure, images were filtered with the minimum filter function in ImageJ at a setting of 2 pixels. With this filter, all pixels were replaced with the minimum pixel intensity value in that pixel's neighborhood ( $\leq 2$  pixels away). The smallest objects, such as autofluorescent puncta, were erased or nearly erased by the filter, and cell-sized staining areas were slightly reduced in size while maintaining their shape, as only the edges were eroded. This procedure was used for PV stained sections across all age groups.

For PNN analysis, only cells with a clearly formed PNN ring around the soma were included. The PV+ and PNN+ channels were separated for counting in each image. Each cell, either PV+ or PNN+, was marked on their respective image, and the overlap of the two was used to determine the co-localized cell population. Counting bias was avoided by including all cells entirely within the boundaries of the image and those that

were in contact with the top border of the image. Those that were in contact with the lower border of the image were excluded from the count. The total area of the cortex was then used to calculate cell densities (cells/mm<sup>2</sup>) of each cell type.

There are layer-specific differences in responses to broadband noise between young and old rat A1 neurons, in a manner suggestive of greater loss of inhibition in superficial than deeper cortical layers (Hughes et al., 2010). Superficial (I-IV) and deep (V-VI) cortical layers are differentially susceptible to loss of PV+ cells in the aging C57 mouse<sup>30</sup>. To determine if PNN cell density also declined differentially with depth, the superficial and deep layers were separately analyzed. Layer IV typically terminates at approximately 50% of the depth of the cortex from the pia<sup>30,38</sup>, so this value was used to delineate between the two. Any cells contacting the line separating these two cortical sections were included in the layer I-IV cell populations.

In order to determine if the overall cell density changes with age in A1, cell counts were obtained from DAPI stained sections. The cortical column was split into eight sections, each 50  $\mu$ m wide, and in each image a random number generator was used to determine which of the eight sections to count. This cell density value was multiplied by 8 to estimate the total number of cells within the 400  $\mu$ m wide section of cortex.

Deterioration of PNN may manifest as changes in intensity without a loss of PNN+ cell density<sup>40</sup>. To determine PNN intensity throughout A1 and at the single cell level, images were converted into 8-bit format (where 0 is total absence of PNN). The average intensity of the cortex was determined with the 'Plot Profile' function in ImageJ. To accomplish this, a rectangle (width of 400  $\mu$ m and depth extending from pia to end of

layer VI) was drawn on the cortical section. Running the plot profile function on this rectangle yields a plot of depth through the cortex *versus* average gray scale intensity at that depth. These intensity values were averaged to obtain an average PNN intensity for an individual image. To determine if intensity was different between superficial and deep layers, all values from the first half of this data set were averaged for superficial and the second half was averaged for deep layers.

We also developed a method to analyze PNN intensity around individual cells. PNN intensity at the cellular level was determined by cropping a  $40\ \mu\text{m}^2$  square region centered on randomly selected PNN+ cells. Each cell was assigned a number and a random number generator was used to determine which of the cells would be analyzed. Fifteen cells in each image were randomly chosen for intensity analysis. The intensity was plotted as a function of the distance along the midline of the  $40\ \mu\text{m}^2$  region using the Plot Profile function (ImageJ). This resulted in a bimodal peaked scatter plot with the two peaks corresponding to the locations where the line intersected the most intense part of the PNN ring structure on both sides of the cell (e.g., Figure 6.7A). In order to account for possible differences in cell size, a custom Matlab script was used to find the pixel at which the intensity drops to 90% of the peak values on either side of the cell. The intensity values within these two cutoff points were averaged for each cell and every cell average within an image was averaged to obtain a single value of PNN+ cell intensity per image. These data were used in the statistical tests. In order to account for differences in background intensity, a  $40\ \mu\text{m}^2$  square was placed in layer I of A1 which is devoid of

PNN. The average value of this region was then subtracted from all PNN intensity measurements before making final comparisons.

*Data Analysis.* For the PV, PNN and PV/PNN cell density and across-A1 PNN intensity analyses, each image contributed a single value for each measure. The means of these values were compared across age using One Way ANOVA with post-hoc pairwise comparisons. We consider sections drawn from an individual mouse to be independent samples because the sections are a minimum of 160  $\mu\text{m}$  from each other and therefore likely cover parts of A1 with different response selectivity. For the cell-specific PNN intensity analysis, each image provided an average intensity value from up to 15 randomly selected cells (see above). The means of these values were compared across age using One Way ANOVA and post-hoc pairwise comparisons.

Table 6.1 provides the details on each mouse's age (column 2), strain (column 3) and the number of sections on which IHC was performed (column 4). An outlier analysis was done on the available images based on PV and PNN cell densities. Outliers were identified as images in which the values for cell density was above the value given from the equation,  $Q3 + IQR * 1.5$  or below the value given from equation.  $Q1 - IQR * 1.5$ , where  $Q1$  is the cutoff of the first quartile of the data set range,  $Q3$  is the cutoff of the third quartile of the dataset, and  $IQR$  (Interquartile Range) =  $Q3 - Q1$ <sup>41,42</sup>. Based on this analysis, the following PNN IHC images were excluded: 3 images (out of 34) from the old C57 dataset, 1 image (out of 25) from the young C57 group, 3 images (out of 14) from the middle-aged CBA group and 2 images (out of 23) from the O CBA group. The

right-most column of Table 6.1 indicates the number of images that were used for the PNN statistical analyses. None of the PV images were excluded.

It can also be noted from Table 6.1 that in terms of age groups, the Y and the M were relatively well matched between the two strains. However, in the O group, 3 out of 8 C57 mice were 24-month-old. All other O group mice were in the 13-15-month range. Due to the possibility that the C57 data may be inflated by the 24-month-old mice, a separate analysis was done in which the 24-month-old C57 mice were excluded. The major conclusions presented below in the Results section regarding age-related changes in the C57 mice were unchanged with the removal of the 24-month-old mice. Therefore, the Results section and figures to follow first present data from all the mice shown in Table 6.1. The last paragraph of the Results section presents the analyses with the 24-month-old C57 mice excluded.

*Statistical analyses.* All data sets were compared across age (3 levels, Y, M, and O) and within strain (either C57 or CBA). All statistical tests performed were One Way ANOVAs, unless stated otherwise. Typical One Way ANOVA was used when data were distributed normally and the Kruskal-Wallis One Way ANOVA on Ranks was used if data were not normally distributed, according to the Kolmogorov-Smirnov test. Statistical tests are reported with the F (ANOVA) or H (Kruskal-Wallis) for main effect of age. All pairwise multiple comparison procedures (Tukey test for the One Way ANOVA and Dunn's method for the Kruskal-Wallis test) were run subsequent to finding a main effect

( $p < 0.05$ ) in a data set. Multiple comparisons procedures statistics are reported as p-values for a specific comparison of age groups (e.g. Y-O:  $p < 0.05$ ).

## Results

Reduced inhibition is a consistent feature observed in sensory cortices of aging animals. To test the hypothesis that the cellular mechanisms of age-related reduction in inhibition includes the PV/PNN system, the main goal of this study was to examine PV+, PNN+ and PV/PNN co-localized cell density in A1 of two strains of mice (C57 and CBA) across three different age groups.

### *i. PNN cell density declines with age in A1 of both C57 and CBA mice*

The photomicrographs in Figure 6.1 illustrate the cells that were counted as PNN+ or PV/PNN co-localized cells. Each solid arrow or arrowhead points to a PNN+ with a complete or near complete ring structure. Arrowheads are PNN+ cells without PV+ immunofluorescence. The arrows in the merged image point to PV/PNN co-localized cells. The arrowheads in the merged image point to cells that were counted as PNN+. Qualitative observations of staining patterns show that PNN+ cells are found throughout A1, with a banding pattern of PNN+ cells and diffuse neuropil PNN staining in layer IV (Figure 6.2). Generally, more PNN+ cells were observed in layers IV-VI compared to layers I-III. PNNs frequently appeared around PV+ cells, especially within the layer IV band. However, a number of PNN+ cells were devoid of PV staining and *vice versa*. These observations were consistent across the mouse strains and age (see

Figure 6.2) and with previous studies of PNN expression in young mouse A1 (Happel et al., 2014; Fader et al., 2016).

Figure 6.3 shows PNN+, PV+ and PV/PNN co-localized cell density in A1 when all 6 layers of the cortex were considered. The PNN+ cell density decreased significantly with age in A1 of both the C57 mouse strain (Figure 6.3A,  $H(2,76) = 9.026$ ,  $p=0.011$ ) and CBA strain (Figure 6.3A,  $F(2,58) = 18.286$ ,  $p<0.001$ ). In the C57 group, the difference was only significant between Y and O mice (Tukey: Y-O  $p<0.05$ ). In the CBA mouse, PNN+ cell populations significantly decreased between Y *versus* O and M *versus* O (Dunn: Y-O, M-O  $p<0.05$ ), but not between Y *versus* M (Dunn: Y-O  $p=0.183$ ). In contrast to the decline of PNN+ cell density in both strains, PV+ cell density declined with age only in the C57 mouse (Figure 6.3B). The PV+ cell density declined with age in C57 mice ( $F(2,76) = 24.547$ ,  $p<0.001$ ) and the decrease was significant between each age group (Tukey: Y-M:  $p=0.004$ , Y-O:  $p<0.001$ , M-O:  $p=0.010$ ), but not in the CBA mice ( $F(2, 58) = 0.993$ ,  $p=0.377$ ). There was a significant age-related decline in PV/PNN co-localized cell density in both strains (Figure 6.3C; C57:  $H(2, 76) = 18.558$ ,  $p<0.001$ ; CBA:  $H(2, 58) = 16.018$ ,  $p<0.001$ ). This difference was observed only in the Y *versus* O comparison (C57: Dunn: Y-O:  $p<0.05$ ; CBA: Dunn: Y-O:  $p<0.05$ ). We further compared the PV+ cell density between the young mice of each strain. Interestingly, there were more PV+ cells in the Y C57 than Y CBA mice (Mann Whitney Rank Sum t-Test,  $U(47) = 524$ ,  $p<0.001$ ). This indicates strain-specific differences in PV expression in young mouse A1. There were no age-related differences in the total number of cells based on DAPI staining for either mouse strain (C57:  $F(2, 76) = 2.381$ ,  $p=0.106$ ; CBA:

Mouse	Age (months)	Strain	All Sections	PNN Sections
PM007	2	C57	4	4
PM008	2	C57	4	4
PM011	2	C57	4	4
PM034	3	C57	5	5
PM035	3	C57	4	3
PM036	3	C57	4	4
PM006	7	C57	4	4
PM025	8	C57	2	2
PM037	6	C57	5	5
PM038	6	C57	5	5
PM039	6	C57	4	4
PM001	13	C57	3	3
PM002	13	C57	3	3
PM003	13	C57	5	5
PM026	24	C57	4	4
PM027	24	C57	4	4
PM028	24	C57	4	3
PM046	14	C57	4	2
PM048	14	C57	7	7
PM052	1	CBA	5	5
PM053	1	CBA	4	4
PM054	2	CBA	4	4
PM055	2	CBA	3	3
PM056	2	CBA	2	2
PM057	2	CBA	3	3
PM058	2	CBA	3	3
PM029	6	CBA	2	2
PM030	6	CBA	2	2
PM031	6	CBA	5	3
PM032	6	CBA	3	3
PM033	6	CBA	2	1
PM040	15	CBA	3	3
PM041	15	CBA	4	2
PM042	15	CBA	4	4
PM043	15	CBA	4	4
PM044	15	CBA	4	4

Table 6.1. From left to right, the columns represent the mouse identifier, age in months, strain, the number of sections stained, and the number of sections used for PNN data analysis following outlier analysis.

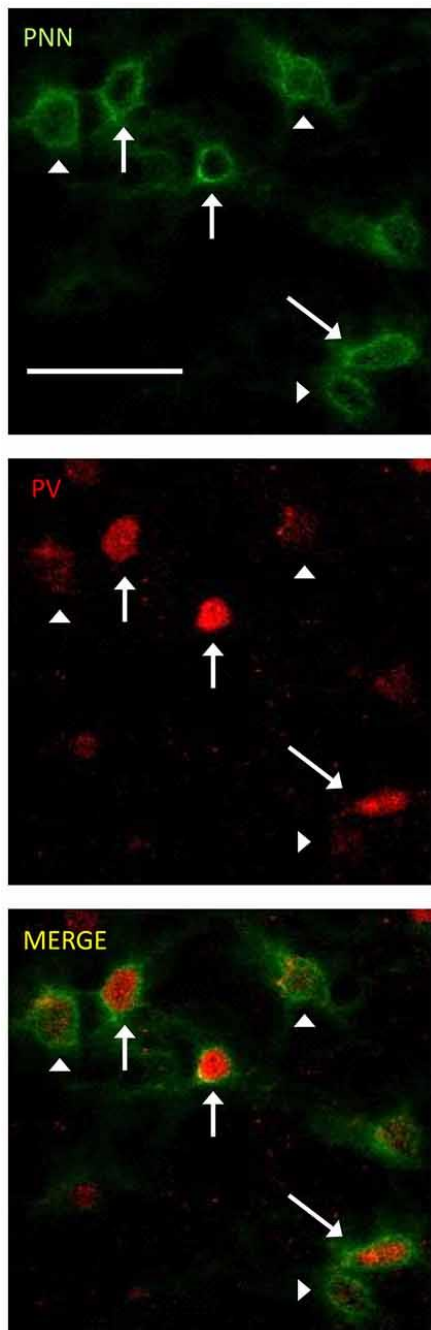


Figure 6.1. Representative examples of PNN+ and PV/PNN co-localized cells are shown. PNN+ cells (green channel) were identified by their complete or near complete ring structure, with relatively less intense staining in the area corresponding to the soma. PV+ cells (red channel) were identified by a staining pattern throughout most of the soma. PNN+ cells without PV are marked with arrowheads. PV+/PNN+ co-localized cells are indicated with a solid arrow. These labels are preserved when the images are separated out into the two channels and when the images are merged. The scale bar is 50  $\mu\text{m}$  and applies to all images.

$H(2, 58) = 3.606, p=0.165$ ). This indicates that the observed decline in PV and PNN is not due to non-specific changes in cell density with age. Taken together, these data indicate strain and age specific differences in PV and PNN expression in A1.

Consistent across both strains was the observed age-related decline in PNN cell density and PV/PNN co-localized cell density in A1.

*ii. Deep and superficial layers were similarly susceptible to age-related PNN deterioration*

Although some exceptions were seen, the general observation was that both superficial and deep layers were similarly susceptible (Figure 6.4). In the C57 mice, the significance in PNN density changes was lost when the data were sub-divided into the

layers. However, the trend towards reduction is preserved (Figure 6.4A-B, Layers I-IV:  $H(2, 76) = 4.1$ ,  $p=0.12$ . Layers V-VI:  $H(2, 76) = 4.629$ ,  $p=0.09$ ). In the CBA mice, data from all cortical layers showed a reduction in PNN cell density with age (Figure 6.3). This difference was also seen in the layer specific analysis of A1 (Figure 6.4A-B, Layers I-IV:  $F(2, 58) = 9.453$ ,  $p<0.001$ ; Layers V-VI:  $F(58, 2) = 9.96$ ,  $p=0.007$ ). The decrease in both layer sub-divisions was apparent in the old age group (Layers I-IV: Tukey: Y-O, M-O:  $p<0.05$ ; Layers V-VI: Tukey: Y-O:  $p<0.05$ ).

Layer specific analysis of PV+ cell density in C57 mice showed an age-related decline in both superficial (Layers I-IV:  $F(2, 76) = 16.917$ ,  $p<0.001$ ), and deep layers (Layers V-VI:  $F(2, 76) = 16.525$ ,  $p<0.001$ ) (Figure 6.4C-D). In the superficial layers, this reduction in PV+ density was seen in the O mouse group (Tukey: Y-O, M-O:  $p<0.05$ ) (Figure 6.4C), whereas the reduction in the deep layers occurred earlier, appearing in the M group (Tukey: Y-O, Y-M:  $p<0.05$ ) (Figure 6.4D). There was no age-related change in PV+ cell density in the CBA mice in either the superficial or deep layers. Counter-intuitively however, there was a significant increase from young to middle age in PV+ cell density in the superficial layers (Figure 6.4C-D, Layers I-IV:  $H(2, 58) = 7.801$ ,  $p=0.020$ ; Dunn: M-Y:  $p<0.05$ ; Layers V-VI:  $H(2, 58) = 5.613$ ,  $p=0.06$ ).

Finally, layer-specific PV/PNN co-localization was characterized in both mouse strains. The decline in PV/PNN co-localized cell density that appears across cortical layers in O C57 and O CBA mice is present in both the superficial and deep cortical layers (Figure 6.4E-F, C57: Layers I-IV:  $F(2, 76) = 11.502$ ,  $p<0.001$ ; Tukey: Y-O, M-O:

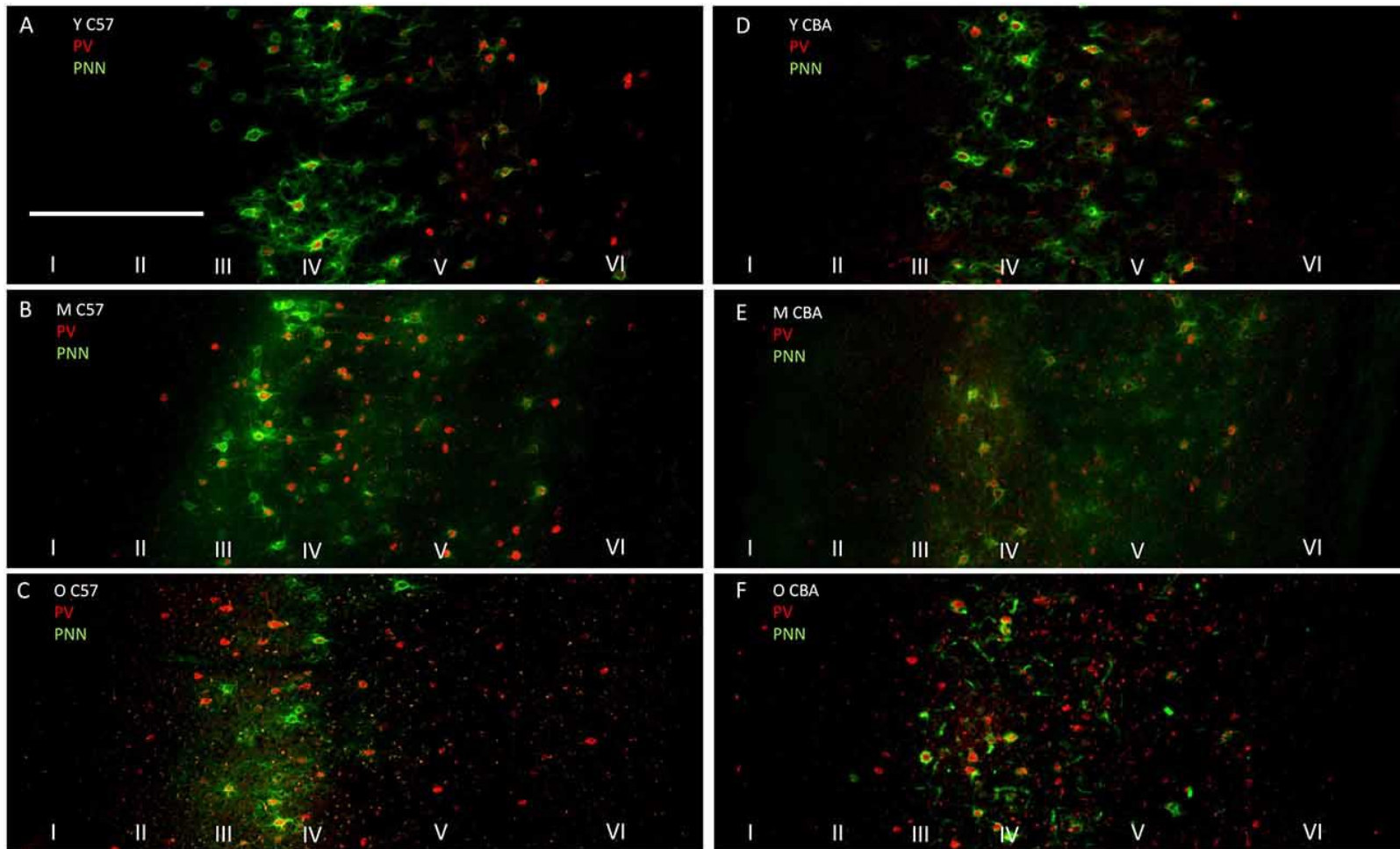


Figure 6.2. Representative photomicrographs through A1 from Young (A), Middle (B) and Old C57 mice (C) and Young (D), Middle (E) and (F) Old CBA mice. The scale bar in (A) is 250  $\mu$ m and applies to all images.

$p < 0.05$ ; Layers V-VI:  $H(2, 76) = 7.519$ ,  $p = 0.023$ ; Dunn: Y-O, Y-M:  $p < 0.05$ . CBA: Layers I-IV:  $F(2, 58) = 7.216$ ,  $p = 0.002$ ; Tukey: Y-O, M-O:  $p < 0.05$ ; Layers V-VI:  $F(2, 58) = 5.607$ ,  $p = 0.006$ ; Tukey: Y-O:  $p < 0.05$ ). Taken together, these data reveal an overall similarity between layers I-IV and layers V-VI in their susceptibility to age-related changes in PV and PNN cell densities. Some exceptions to this rule include the earlier susceptibility of C57 deep layers to PV+ cell decline and the increase in PV+ cell density in superficial layers in CBA mice.

### *iii. PNN Intensity Analysis*

Previous studies suggest that a decline in PNN intensity may reflect changes in PNN organization, and due to their role in buffering ions and stabilizing synaptic contacts, may lead to changes in excitation/inhibition balance. This change in PNN intensity may occur independent of changes to overall PNN+ cell density<sup>43</sup>. Therefore, we analyzed PNN intensity in A1. Representative images of PNN staining are shown in Figure 6.5 to illustrate the age-related decline in PNN staining. In the C57 mice, the average PNN intensity is reduced for the Y-O comparison (Figure 6.6,  $H(2, 76) = 9.619$ ,  $p = 0.008$ ; Y-O:  $p < 0.05$ ). Layer specific analysis showed that this age-related reduction in PNN intensity is only observed in the deep cortical layers of O C57 A1 (Layers I-IV:  $F(2, 76) = 1.040$ ,  $p = 0.346$ ; Layers V-VI:  $H(2, 76) = 18.360$ ,  $p < 0.001$ , Dunn: Y-O:  $p < 0.05$ ). Conversely, in the CBA mouse A1, there was no significant difference in PNN intensity with age (Figure 6.6;  $H(2, 58) = 2.060$ ,  $p = 0.357$ ). Comparison of PNN cell density

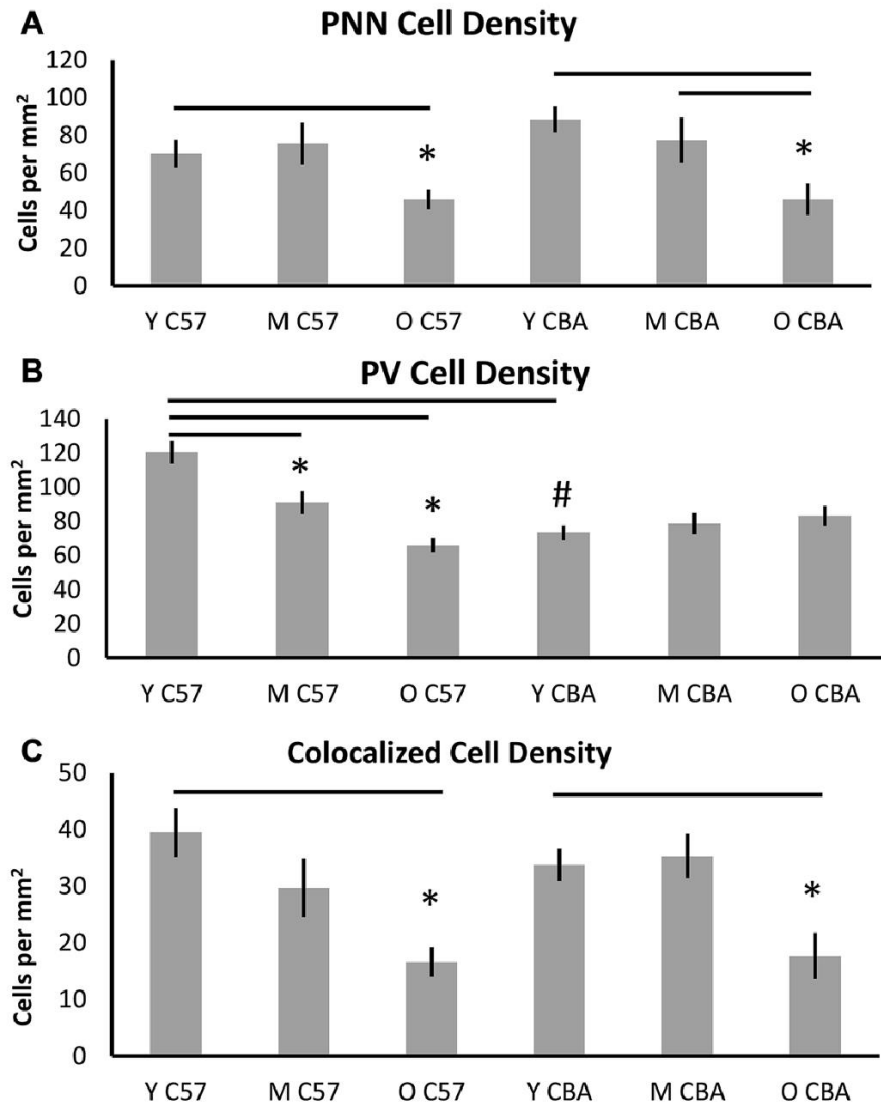


Figure 6.3. Density (cells per mm<sup>2</sup>) of (A) PNN+, (B) PV+, and (C) PV/PNN co-localized cells in A1 (all 6 layers combined) are shown. Asterisks indicate a significant difference from the Y group within the same strain. The '#' indicates a significant difference between age-matched groups across strains ( $p < 0.05$ ).

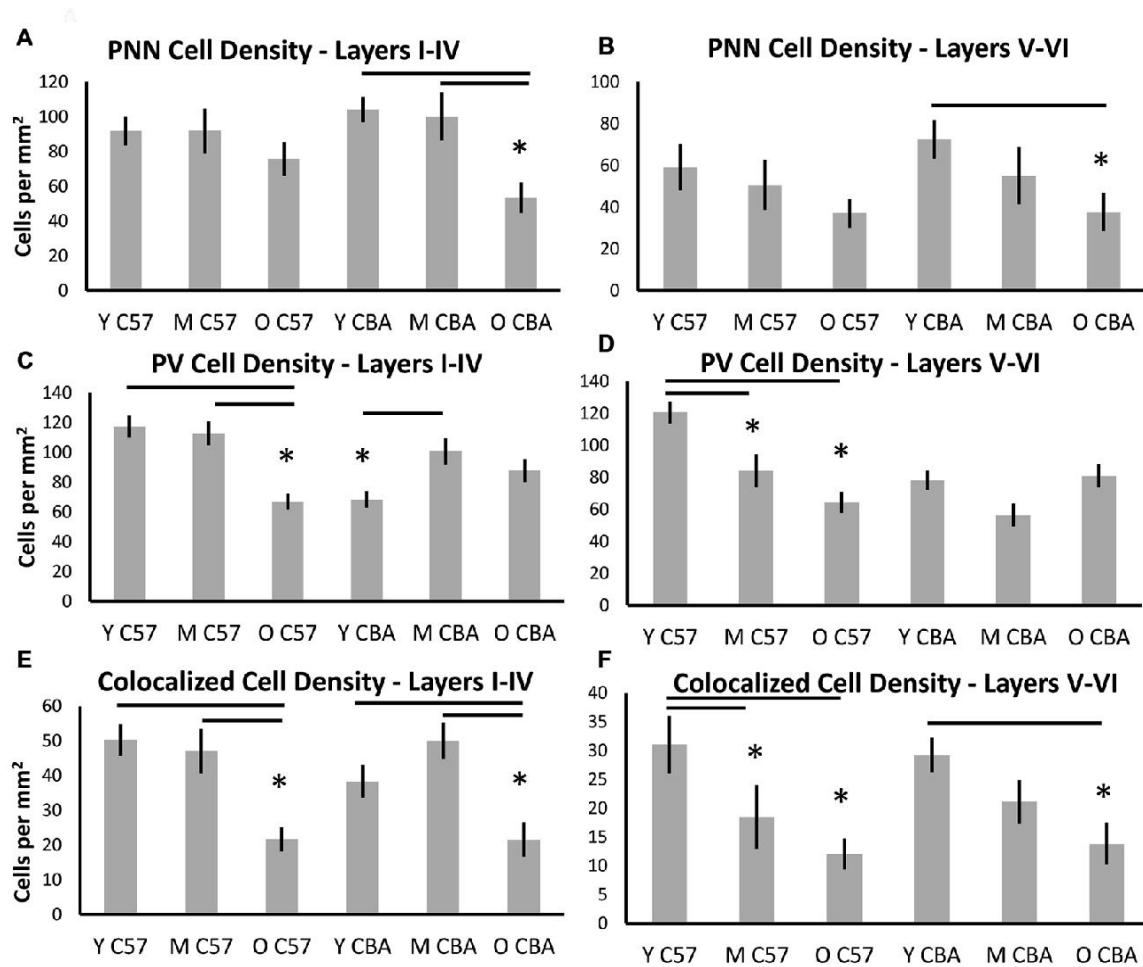


Figure 6.4. Density (cells per mm<sup>2</sup>) of (A-B) PNN+, (C-D) PV+, and (E-F) PNN+/PV+ cell types in superficial layers (layers I-IV) and deep layers (layers V-VI) of the auditory cortex. Asterisks indicate a significant difference from the Y group within the same strain ( $p < 0.05$ ).

*versus* PNN intensity (Figures 4 and 6) indicate that in C57 mouse A1, there is a decline in PNN+ cell density and the remaining PNN+ cells show reduced intensity. On the other hand, in the CBA mouse A1, there is a decline in PNN+ cell density, but the remaining PNN+ cells do not show a significant change in PNN staining intensity.

While the above analysis provides information about PNNs across the entire depth of A1, studies of epileptogenesis and songbird brain development<sup>44,45</sup> have suggested the integrity of PNN around the cell may provide more subtle markers of changes to PNN. Therefore, we developed a method to analyze PNN intensity in individual cells and compared A1 neurons across the three age groups. Analysis of PNN intensity at the individual cell level showed data that were consistent with the age-related changes in the average PNN intensity across all cortical layers. That is, there was a decrease in average single cell intensities in the C57 A1 (Figure 6.7B;  $F(2, 76) = 3.559$ ,  $p=0.034$ ) and the difference is significant between Y and O C57 mice (Tukey: Y-O:  $p<0.05$ ). No age-dependent change is observed in CBA A1 average cellular PNN intensity (Figure 6.7B;  $H(70, 2) = 4.937$ ,  $p=0.085$ ).

PNNs form most prominently around PV+ cells in A1, but they also form around other cells, which do not express PV. Previous studies have shown that PV cells with enwrapped PNNs are less susceptible to oxidative stress<sup>35</sup>. Age-related changes in PV and PNN expression may occur in specific subsets of cells that are identifiable with PV and/or PNN. Therefore, we quantified PNN intensity across the following cell types (Figure 6.8): (A) PNN+ cells with no PV, (B) PNN cells with PV, (C) PNN+ cells in layers I-IV of A1, and (D) PNN+ cells in layers V-VI of A1. The decline in average

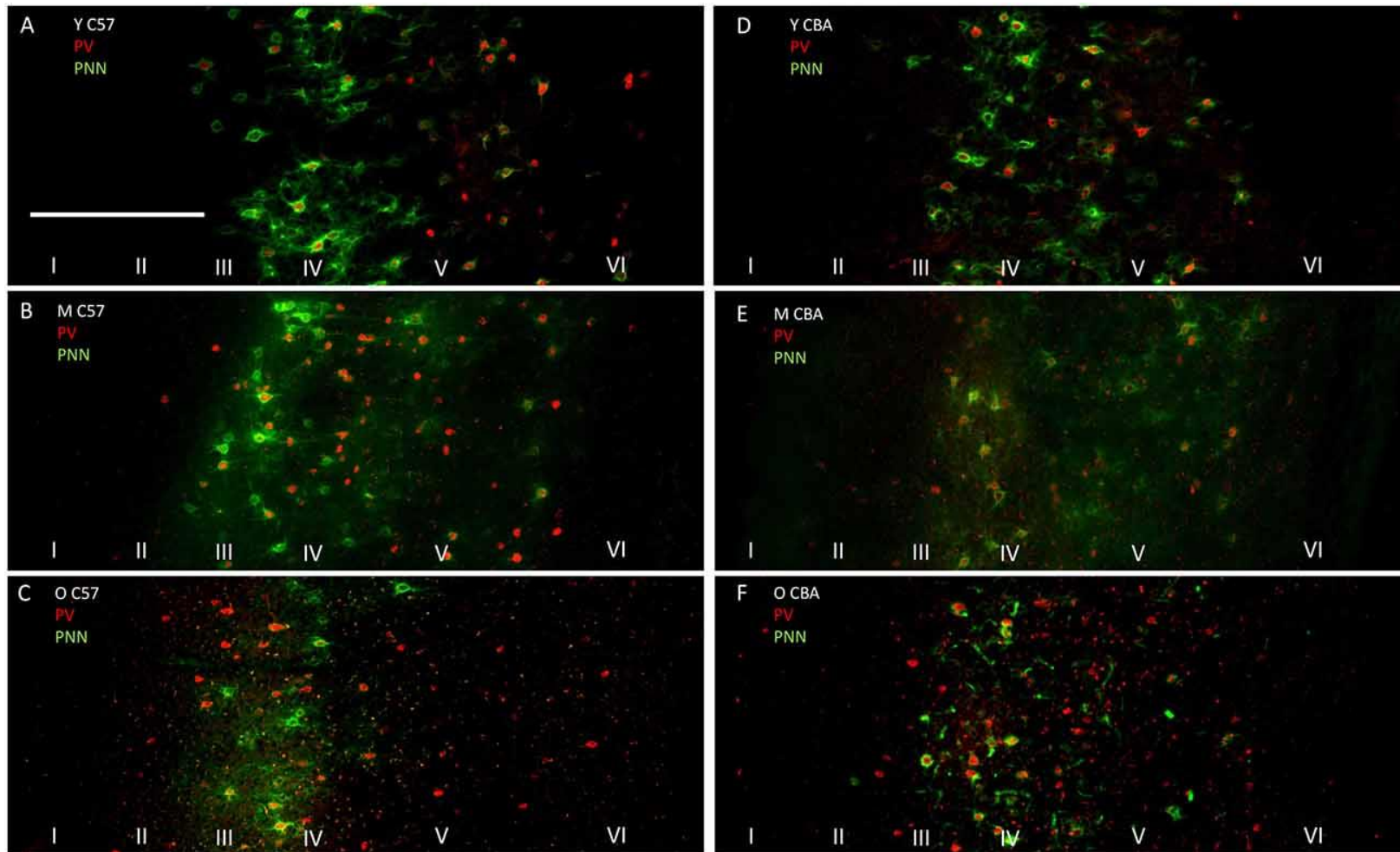


Figure 6.5. Representative examples of PNN images used for analyzing labeling intensity at the whole A1 level. (A, B) show young and old C57 mouse PNN examples, respectively. (C, D) show young and old CBA PNN staining examples, respectively. The scale bar in (A) is 250  $\mu$ m and applies to all images.

PNN+ cell intensity with age in the C57 strain is lost when subdividing PNN+ cells into PV+ or PV- subpopulations (Figure 6.8A, B, PV+ PNN:  $F(2, 76) = 1.34$ ,  $p=0.269$ ; PV- PNN:  $F(2, 76) = 1.902$ ,  $p=0.157$ ). When subdividing PNN+ cells into superficial and deep layer cells, there was an age-related decline in the average cellular PNN intensities of cells in both depths (Figure 6.8C, D Layers I-IV:  $F(2, 76) = 3.096$ ,  $p=0.051$ ; Layers V-VI:  $F(2, 76) = 5.355$ ,  $p=0.007$ ; Tukey: Y-M, Y-O:  $p<0.05$ ). No significant differences in PV+/PNN ( $F(70, 2) = 0.61$ ,  $p=0.547$ ) or PV-/PNN ( $H(70, 2) = 4.152$ ,  $p=0.125$ ) cell intensities were observed between age groups in CBA mice. Likewise, no significant differences in PNN+ cell intensity were observed for cells residing in Layers I-IV ( $F(70, 2) = 0.531$ ,  $p=0.591$ ) or in Layers V-VI ( $H(70, 2) = 5.079$ ,  $p=0.079$ ) between age groups in the CBA mouse strain. This was to be expected given that there was no difference in average PNN cell intensities with age in the CBA mice (Figure 6.6, 7).

Given that there were three 24-month-old C57 mice, but no CBA mice in that age range, there was a possibility our findings were influenced by the relative difference in age ranges between the two 'O' groups (Table 6.1). To account for this, the analyses were performed with the 24-month-old animals excluded from the O C57 group. All main effects of age in the C57 strain remained. Specifically, no changes were observed in the decline of PNN+, PV+, or PV/PNN co-localized cell densities with age in C57 (PNN+:  $H(2, 64) = 8.077$ ,  $p=0.018$ ; PV+:  $F(2, 64) = 23.479$ ,  $p<0.001$ ; Co-localized cells:  $H(2, 64) = 16.829$ ,  $p<0.001$ ). The effect of age on PNN intensity at the level of the entire A1

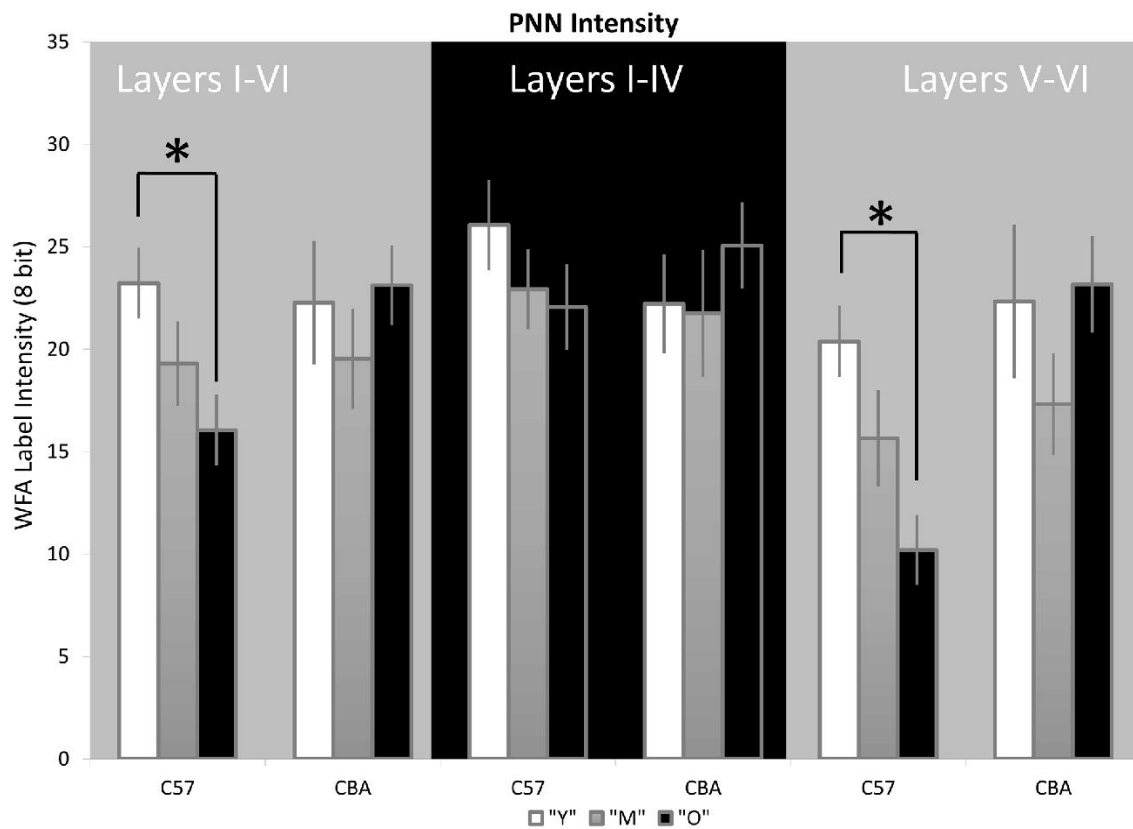


Figure 6.6. PNN staining intensity declines in A1 in C57, but not CBA, mice. The average WFA intensity is shown for the entire depth of A1 (left set of bars), superficial layers (middle) and deep layers (right). Asterisks indicate significant difference ( $p < 0.05$ ).

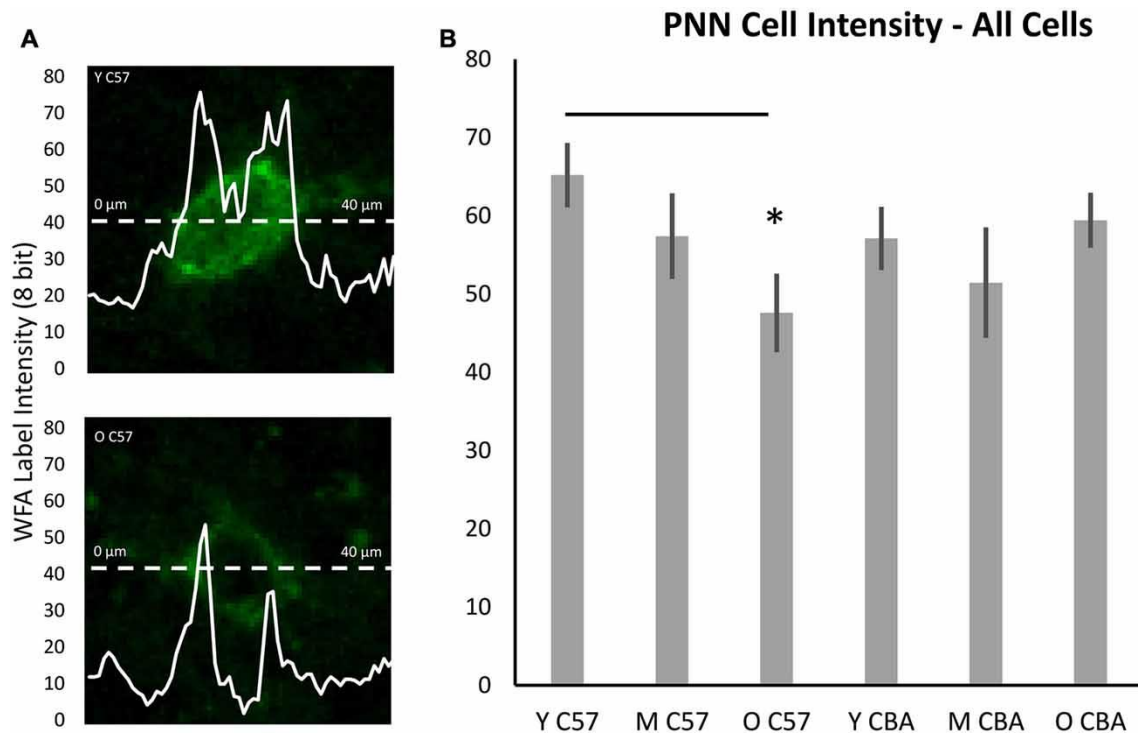


Figure 6.7. Cellular PNN intensity analysis. **(A)** Example images for analysis of PNN intensity around a cell. The dashed line represents the points at which the PNN gray scale intensity was measured. The double peaked curve shows the intensity at each point on the dashed line. In A, the upper image is from a young C57 mouse and the bottom image is from an old C57 mouse. These examples illustrate the decline in cellular PNN intensity shown in **(B)**. **(B)** Average of all cellular PNN intensity plots for each age group and strain. Asterisks indicate a significant difference from the Y group ( $p < 0.05$ ).

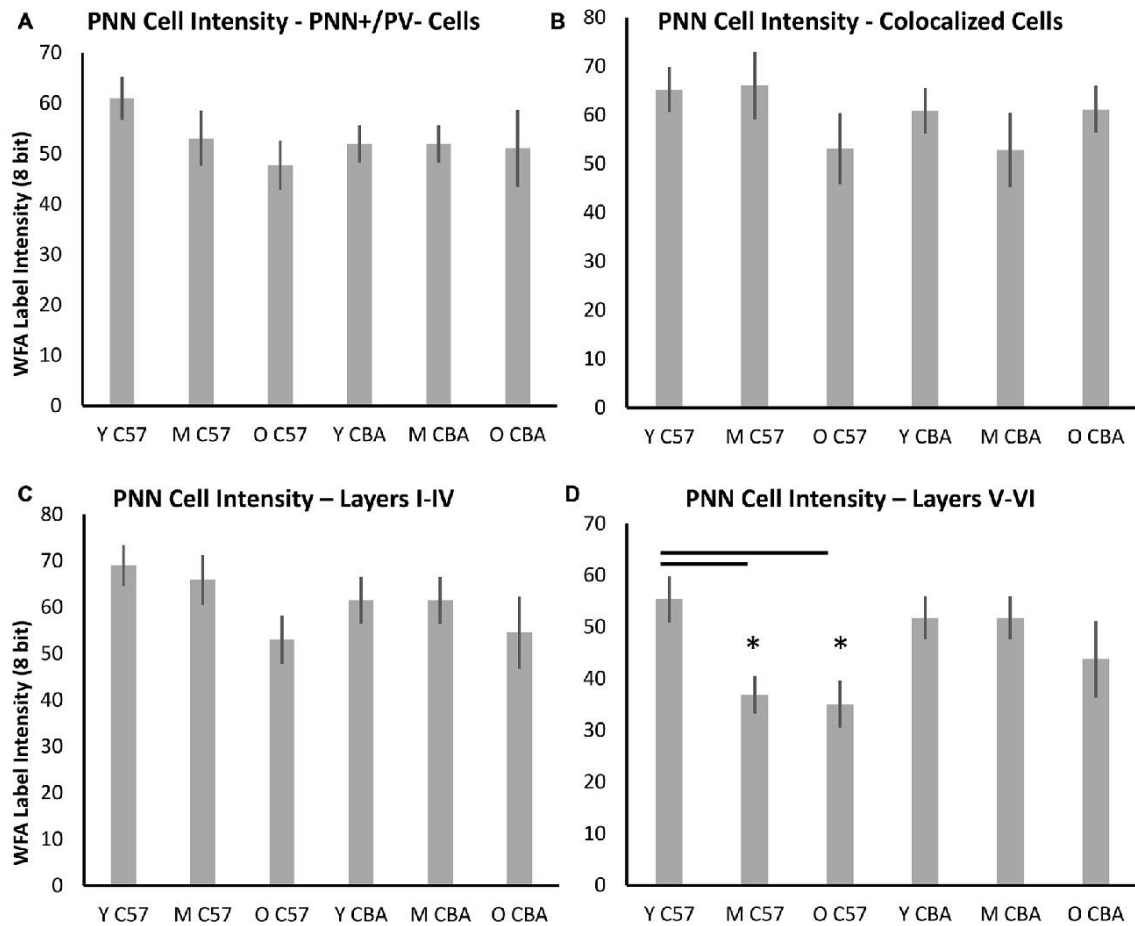


Figure 6.8. Changes in cellular PNN intensity in specific types of PNN cells. **(A)** Cellular PNN intensity in PNN+ cells that do not co-localize with PV. **(B)** Cellular PNN intensity in PNN+ cells that co-localize with PV. **(C)** Cellular PNN intensity in PNN+ cells in layers I-IV of A1. **(D)** Cellular PNN intensity in PNN+ cells in layers V-VI of A1. Asterisks indicate a significant difference ( $p < 0.05$ ) from the Y group.

column and at the individual cell level also remained significant (Layers I-VI:  $H(2, 64) = 16.120$ ,  $p < 0.001$ ; PNN cell intensity:  $F(2, 64) = 9.578$ ,  $p < 0.001$ ). The only change observed by removing the 24-month-old C57 mice was in the statistical difference observed in the PNN cell intensities of M and O C57 mice that was not seen when the oldest C57 mice were included (Tukey:  $p < 0.05$  for Y-O C57 and for M-O C57 comparisons).

## Discussion

The main findings of this study in relation to aging are summarized in Table 6.2. We show that PNN+ and PV/PNN co-localized cell densities decline with age in A1 of both C57 and CBA mice. PNN staining intensity was also reduced in the C57 mouse A1. The decline in PV+ cell density in aging C57 mice was consistent with a previous study<sup>30</sup>, but there was no change in PV+ cells density in CBA mice.

### *i. PNN expression in young mouse A1*

Although the expression of PNN and its association with specific cell types have been well characterized in rodent visual and somatosensory cortex<sup>46–49</sup> and subcortical auditory areas<sup>50</sup>, the expression patterns in A1 are only beginning to be described<sup>51</sup>. The relationship between PV and PNN expression in A1 has not been previously characterized. Consistent with previous papers on mouse A1, PNN expression was seen in layers II-VI, with a particularly high concentration in layer IV<sup>33,34</sup>. The PNN+ cell density was similar in C57 and CBA mice. A strong association between PV+ and PNN+

Analysis type	C57 Young → Old	CBA Young → Old
PNN+ cell density	Decrease	Decrease
PV+ cell density	Decrease	No change
PV/PNN co-localized cell density	Decrease	Decrease
Average PNN intensity across layers	Decrease	No change
Average PNN cellular intensity	Decrease	No change

Table 6.2: Summary of the main changes in expression of PV and PNN in A1 of C57 and CBA mice. Comparisons are only shown for all layers of A1 and only between young and old mice. Layer-specific changes and middle-aged data are omitted for clarity and can be found in the Results section.

cells in A1 was seen as reported in a number of other brain regions<sup>49,52–55</sup> is also present in A1. Approximately 35% of the PV+ cells in the C57 mouse A1 and 50% of PV+ cells in the CBA mouse A1 were also PNN+ (ratio of data in Figure 6.2C and 2B). Future studies are needed to classify the various types of neurons that express PNN in A1.

## *ii. Age-related changes in PNN and PV expression*

The main result of the current study is that PNN deteriorates in A1 with age. As far as we are aware, this is the first study to examine age-related changes in PNN expression in sensory cortex. PNN deterioration with age manifested as both a reduction in PNN+ cell density in C57 and CBA mice, and decreased PNN intensity across A1 and around cell bodies in C57 mice. Layer-specific comparisons do not provide support for deep *versus* superficial layers being more or less susceptible. In both strains, the PV/PNN co-localized cell density also declines significantly with age. The percentage of PV+ cells that also express PNN drops to ~25% in old mice of both strains. Age-related

decline of PV+ cells was observed only in the C57 mice. The PV+ changes are analogous to those observed in aging rats<sup>32</sup>. The Long-Evans rat (normally aging) did not show a loss in PV+ cell density in A1 with age while the Fisher F344 rat (presbycusis) showed a significant loss. Together, the PV/PNN system appears to be more susceptible in the C57 mice A1 compared to the CBA mice. The major age-related trends in the PV/PNN data were not affected regardless of whether the 3 oldest (24 months) C57 mice were included or not. Although the sample size is small, this suggests that much of the PV/PNN change in C57 mice occurs before 14 months of age. Henry and Chloe (1980) showed that most of the threshold shifts and hair cell loss in C57 mice occur by 15 months of age<sup>56</sup>. Further loss in 25-month-old C57 mice was relatively small. Willott (1986) showed a similar trend for inferior colliculus tuning curve thresholds with most of the change seen by 14 months<sup>57</sup>. On the other hand, CBA mice younger than 15 months were similar to young mice in thresholds and hair cell counts. With the caveat that these may simply be strain-specific differences, these data suggest that hearing loss that occurs between 2-14 months in the C57 mice exacerbates age-related changes in inhibitory systems in A1. Future studies will investigate this suggestion more directly by controlled induction of hearing loss during aging in the CBA mouse.

PNNs are highly structured extracellular matrix components around cell bodies and proximal dendrites. Components of PNN include chondroitin sulfate proteoglycans (CSPGs), hyaluronan, tenascin-R, link proteins, Reelin and semaphorin 3A. The main CSPGs in PNN are aggrecan, neurocan, brevican, versican and phosphacan. This study used the lectin WFA to stain PNN because it is the most widely used method to study

PNN expression with an extensive literature that supports the specificity of WFA for CSPGs. WFA binds specifically to N-acetyl-D-galactosamine. However, the specific CSPGs detected by WFA are unclear. Therefore, the interpretation that PNN deteriorates with age must be considered with the caveat that the results may be due to a change in the composition of PNN detected by WFA. Likewise, the reduction in PNN intensity seen in C57 A1 may reflect changes in CSPG protein levels and composition and/or hyaluronan synthase levels.

*iii. Mechanisms and implications for auditory function with presbycusis*

PV and PNN deterioration with age may result in abnormal synaptic regulation and firing properties of PNN-ensheathed PV+ neurons<sup>58,59</sup>. PNNs surround mostly GABAergic neurons in sensory cortex with preference for PV+ neurons. PNN deterioration may leave PV+ cells vulnerable to damage oxidative stress damage<sup>35</sup>. PV+ cells are susceptible to oxidative stress<sup>60</sup>. This suggests that the deterioration of PNN with age may impact auditory function by contributing to decreasing cortical inhibition mediated by PV+ cells. This notion is supported by findings of Shah and Lodge (2013) who showed that degradation of PNN enhances hippocampus activity<sup>61</sup>. The PV+ cells may shape inhibitory components of receptive fields and responses to rapid spectrotemporal cues<sup>26,28</sup>. Reduced inhibition may underlie spectrotemporal processing and speech recognition deficits with age<sup>19,21–25</sup>.

Strong evidence also suggests that PNNs provide stability to the excitation-inhibition balance during development and that adult plasticity can be promoted by

breaking down PNNs<sup>48</sup>. The deterioration of PNN with age may open up the cortical circuit to altered excitation-inhibition balance. The age-related decline in PNN density (C57 and CBA), intensity (C57) and PV cell density (C57) seen in the present study may result from decreasing afferent excitation with age and hearing loss and underlie a compensatory decrease in inhibition. Such reduced inhibition with age may be one of the steps in causing an increase in cortical gain and potentially, pathological activity (e.g. tinnitus). Evidence for such pathological activity correlated with changes in PNN comes from studies of epileptogenesis and schizophrenia<sup>44,62</sup>.

While the co-occurrence, and age-related loss, of PV and PNN have been discussed above primarily from the view of reduced inhibition, alternate explanations are possible. One is that the loss of PNN actually increases excitability of PV+ inhibitory neurons<sup>44</sup>. From this perspective, age-related decline of PV in GABAergic neurons in auditory cortex occurs independent of PNN changes. The loss of PNN may then be a homeostatic mechanism that compensates for altered PV neuron function. At present, it is still unclear how PNN contributes to PV/GABA neuron function. The alternate hypotheses proposed above could be addressed by future electrophysiology studies that compare activity of PV neurons with and without PNN and compare activity of PV/PNN neurons before and after enzymatic degradation of PNN.

The events leading up to PNN deterioration with age may include changes to matrix metalloproteases (MMP) and cartilage link proteins (e.g., Ctr11). MMP-9 is an endopeptidase that cleaves extracellular matrix including PNN<sup>63,64</sup>. MMP-9 levels are regulated by activity and high MMP-9 levels lead up to increased breakdown of PNN.

This suggests the hypothesis that MMP-9 levels increase with age. Carulli et al. (2010) showed that mice lacking Ctrl1, a PNN component, show attenuated PNNs including reduced intensity<sup>43</sup>. The attenuated PNN promoted cortical plasticity in adults. Thus, future studies of aging A1 will analyze expression levels of MMP-9 and Ctrl1 to identify the various players in age-related decline in auditory function and identify potential therapeutic avenues to delay or prevent the decline.

#### *iv. Conclusions*

These data show for the first time that PNN declines in aging sensory cortex. These changes likely contribute to altered inhibitory neurotransmission, which can then lead to impaired spectrotemporal processing. In humans, this leads to impaired speech recognition abilities. An age-related decline in PNN cell density is present in both the C57 and CBA primary auditory cortex, but a decrease in PNN intensity is seen only in the C57 mice suggesting a possible exacerbation with hearing loss in addition to aging. Future studies will examine the specific proteoglycans and other components of PNN that are susceptible to aging and whether an up-regulation of MMP-9 precedes the changes in PNN. Future studies should investigate if age-related decline in PNN density and intensity is present in other sensory cortical regions.

1. Carabellese, C. *et al.* Sensory Impairment and Quality of Life in a Community Elderly Population. *J. Am. Geriatr. Soc.* **41**, 401–407 (1993).
2. Dalton, D. S. *et al.* The Impact of Hearing Loss on Quality of Life in Older Adults. *Gerontologist* **43**, 661–668 (2003).
3. Guthrie, D. M., Declercq, A., Finne-Soveri, H., Fries, B. E. & Hirdes, J. P. The Health and Well-Being of Older Adults with Dual Sensory Impairment (DSI) in Four Countries. *PLoS One* **11**, e0155073 (2016).
4. Weinstein, B. E. & Ventry, I. M. Hearing Impairment and Social Isolation in the Elderly. *J. Speech Lang. Hear. Res.* **25**, 593 (1982).
5. Gordon-Salant, S., Yeni-Komshian, G. H., Fitzgibbons, P. J. & Barrett, J. Age-related differences in identification and discrimination of temporal cues in speech segments. *J. Acoust. Soc. Am.* **119**, 2455–2466 (2006).
6. Panza, F., Solfrizzi, V. & Logroscino, G. Age-related hearing impairment—a risk factor and frailty marker for dementia and AD. *Nat. Rev. Neurol.* **11**, 166–175 (2015).
7. Wayne, R. V. & Johnsrude, I. S. A review of causal mechanisms underlying the link between age-related hearing loss and cognitive decline. *Ageing Res. Rev.* **23**, 154–166 (2015).
8. Deal, J. A. *et al.* Hearing Impairment and Incident Dementia and Cognitive Decline in Older Adults: The Health ABC Study. *Journals Gerontol. Ser. A Biol. Sci. Med. Sci.* **72**, glw069 (2016).
9. Peelle, J. E. & Wingfield, A. The Neural Consequences of Age-Related Hearing Loss. *Trends Neurosci.* **39**, 486–497 (2016).
10. Gates, G. A. & Mills, J. H. Presbycusis. *Lancet* **366**, 1111–1120 (2005).
11. Frisina, D. R. & Frisina, R. D. Speech recognition in noise and presbycusis: relations to possible neural mechanisms. *Hear. Res.* **106**, 95–104 (1997).
12. Syka, J. The Fischer 344 rat as a model of presbycusis. *Hear. Res.* **264**, 70–78 (2010).
13. Leventhal, A. G., Wang, Y., Pu, M., Zhou, Y. & Ma, Y. GABA and its agonists improved visual cortical function in senescent monkeys. *Science* **300**, 812–5 (2003).

14. Caspary, D. M., Ling, L., Turner, J. G. & Hughes, L. F. Inhibitory neurotransmission, plasticity and aging in the mammalian central auditory system. *J. Exp. Biol.* **211**, 1781–91 (2008).
15. Hickmott, P. & Dinse, H. Effects of Aging on Properties of the Local Circuit in Rat Primary Somatosensory Cortex (S1) In Vitro. *Cereb. Cortex* **23**, 2500–2513 (2013).
16. Zhang, L. I., Tan, A. Y. Y., Schreiner, C. E. & Merzenich, M. M. Topography and synaptic shaping of direction selectivity in primary auditory cortex. *Nature* **424**, 201–205 (2003).
17. Razak, K. A. & Fuzessery, Z. M. Neural Mechanisms Underlying Selectivity for the Rate and Direction of Frequency-Modulated Sweeps in the Auditory Cortex of the Pallid Bat. *J. Neurophysiol.* **96**, 1303–1319 (2006).
18. Razak, K. A. & Fuzessery, Z. M. Facilitatory mechanisms underlying selectivity for the direction and rate of frequency modulated sweeps in the auditory cortex. *J. Neurosci.* **28**, 9806–16 (2008).
19. Razak, K. A. & Fuzessery, Z. M. GABA Shapes Selectivity for the Rate and Direction of Frequency-Modulated Sweeps in the Auditory Cortex. *J. Neurophysiol.* **102**, 1366–1378 (2009).
20. Trujillo, M., Carrasco, M. M. & Razak, K. Response properties underlying selectivity for the rate of frequency modulated sweeps in the auditory cortex of the mouse. *Hear. Res.* **298**, 80–92 (2013).
21. Walton, J. P., Frisina, R. D. & O'Neill, W. E. Age-related alteration in processing of temporal sound features in the auditory midbrain of the CBA mouse. *J. Neurosci.* **18**, 2764–76 (1998).
22. Mendelson, J. R. & Ricketts, C. Age-related temporal processing speed deterioration in auditory cortex. *Hear. Res.* **158**, 84–94 (2001).
23. Šuta, D., Rybalko, N., Pelánová, J., Popelář, J. & Syka, J. Age-related changes in auditory temporal processing in the rat. *Exp. Gerontol.* **46**, 739–746 (2011).
24. Parthasarathy, A. & Bartlett, E. L. Age-related auditory deficits in temporal processing in F-344 rats. *Neuroscience* **192**, 619–630 (2011).
25. Trujillo, M. & Razak, K. A. Altered cortical spectrotemporal processing with age-related hearing loss. *J. Neurophysiol.* **110**, 2873–2886 (2013).

26. Atencio, C. A. & Schreiner, C. E. Spectrotemporal processing differences between auditory cortical fast-spiking and regular-spiking neurons. *J. Neurosci.* **28**, 3897–910 (2008).
27. Moore, A. K. & Wehr, M. Parvalbumin-expressing inhibitory interneurons in auditory cortex are well-tuned for frequency. *J. Neurosci.* **33**, 13713–23 (2013).
28. Wu, G. K., Arbuckle, R., Liu, B., Tao, H. W. & Zhang, L. I. Lateral Sharpening of Cortical Frequency Tuning by Approximately Balanced Inhibition. *Neuron* **58**, 132–143 (2008).
29. de Villers-Sidani, E. *et al.* Recovery of functional and structural age-related changes in the rat primary auditory cortex with operant training. *Proc. Natl. Acad. Sci. U. S. A.* **107**, 13900–5 (2010).
30. Martin del Campo, H. N., Measor, K. R. & Razak, K. A. Parvalbumin immunoreactivity in the auditory cortex of a mouse model of presbycusis. *Hear. Res.* **294**, 31–39 (2012).
31. Ouellet, L. & de Villers-Sidani, E. Trajectory of the main GABAergic interneuron populations from early development to old age in the rat primary auditory cortex. *Front. Neuroanat.* **8**, 40 (2014).
32. Ouda, L., Profant, O. & Syka, J. Age-related changes in the central auditory system. *Cell Tissue Res.* **361**, 337–358 (2015).
33. Happel, M. F. K. *et al.* Enhanced cognitive flexibility in reversal learning induced by removal of the extracellular matrix in auditory cortex. *Proc. Natl. Acad. Sci. U. S. A.* **111**, 2800–5 (2014).
34. Fader, S., Imaizumi, K., Yanagawa, Y. & Lee, C. Wisteria Floribunda Agglutinin-Labeled Perineuronal Nets in the Mouse Inferior Colliculus, Thalamic Reticular Nucleus and Auditory Cortex. *Brain Sci.* **6**, 13 (2016).
35. Cabungcal, J.-H. *et al.* Perineuronal nets protect fast-spiking interneurons against oxidative stress. *Proc. Natl. Acad. Sci.* **110**, 9130–9135 (2013).
36. Suttkus, A., Morawski, M. & Arendt, T. Protective Properties of Neural Extracellular Matrix. *Mol. Neurobiol.* **53**, 73–82 (2016).
37. Willott, J. F., Aitkin, L. M. & McFadden, S. L. Plasticity of auditory cortex associated with sensorineural hearing loss in adult C57BL/6J mice. *J. Comp. Neurol.* **329**, 402–411 (1993).

38. Anderson, L. A., Christianson, G. B. & Linden, J. F. Mouse auditory cortex differs from visual and somatosensory cortices in the laminar distribution of cytochrome oxidase and acetylcholinesterase. *Brain Res.* **1252**, 130–142 (2009).
39. Cruikshank, S. ., Killackey, H. . & Metherate, R. Parvalbumin and calbindin are differentially distributed within primary and secondary subregions of the mouse auditory forebrain. *Neuroscience* **105**, 553–569 (2001).
40. Enwright, J. F. *et al.* Reduced Labeling of Parvalbumin Neurons and Perineuronal Nets in the Dorsolateral Prefrontal Cortex of Subjects with Schizophrenia. *Neuropsychopharmacology* **41**, 2206–2214 (2016).
41. Weber, A., Loui, A., Jochum, F., Bühner, C. & Obladen, M. Breast milk from mothers of very low birthweight infants: variability in fat and protein content. *Acta Paediatr.* **90**, 772–775 (2007).
42. Leys, C., Ley, C., Klein, O., Bernard, P. & Licata, L. Detecting outliers: Do not use standard deviation around the mean, use absolute deviation around the median. *J. Exp. Soc. Psychol.* **49**, 764–766 (2013).
43. Carulli, D. *et al.* Animals lacking link protein have attenuated perineuronal nets and persistent plasticity. *Brain* **133**, 2331–2347 (2010).
44. Dityatev, A. *et al.* Activity-dependent formation and functions of chondroitin sulfate-rich extracellular matrix of perineuronal nets. *Dev. Neurobiol.* **67**, 570–588 (2007).
45. Balmer, T. S., Carels, V. M., Frisch, J. L. & Nick, T. A. Modulation of perineuronal nets and parvalbumin with developmental song learning. *J. Neurosci.* **29**, 12878–85 (2009).
46. Pizzorusso, T. *et al.* Reactivation of ocular dominance plasticity in the adult visual cortex. *Science* **298**, 1248–51 (2002).
47. McRae, P. A., Rocco, M. M., Kelly, G., Brumberg, J. C. & Matthews, R. T. Sensory deprivation alters aggrecan and perineuronal net expression in the mouse barrel cortex. *J. Neurosci.* **27**, 5405–13 (2007).
48. Takesian, A. E. & Hensch, T. K. Balancing Plasticity/Stability Across Brain Development. *Prog. Brain Res.* **207**, 3–34 (2013).
49. Liu, H. *et al.* Expression of Perineuronal Nets, Parvalbumin and Protein Tyrosine Phosphatase  $\sigma$  in the Rat Visual Cortex During Development and After BFD. *Curr. Eye Res.* **38**, 1083–1094 (2013).

50. Beebe, N. L., Young, J. W., Mellott, J. G. & Schofield, B. R. Extracellular Molecular Markers and Soma Size of Inhibitory Neurons: Evidence for Four Subtypes of GABAergic Cells in the Inferior Colliculus. *J. Neurosci.* **36**, 3988–99 (2016).
51. Sonntag, M., Blosa, M., Schmidt, S., Rübsamen, R. & Morawski, M. Perineuronal nets in the auditory system. *Hear. Res.* **329**, 21–32 (2015).
52. Kosaka, T. & Heizmann, C. W. Selective staining of a population of parvalbumin-containing GABAergic neurons in the rat cerebral cortex by lectins with specific affinity for terminal N-acetylgalactosamine. *Brain Res.* **483**, 158–163 (1989).
53. Celio, M. R. Perineuronal Nets of Extracellular Matrix Around parvalbumin-containing neurons of the hippocampus. *Hippocampus* **3**, 55–60 (1993).
54. Pantazopoulos, H., Lange, N., Hassinger, L. & Berretta, S. Subpopulations of neurons expressing parvalbumin in the human amygdala. *J. Comp. Neurol.* **496**, 706–722 (2006).
55. Yamada, J., Ohgomori, T. & Jinno, S. Perineuronal nets affect parvalbumin expression in GABAergic neurons of the mouse hippocampus. *Eur. J. Neurosci.* **41**, 368–378 (2015).
56. Henry, K. R. & Chole, R. A. Genotypic Differences in Behavioral, Physiological and Anatomical Expressions of Age-Related Hearing Loss in the Laboratory Mouse: Original Papers Travaux originaux. *Int. J. Audiol.* **19**, 369–383 (1980).
57. Willott, J. F. Effects of aging, hearing loss, and anatomical location on thresholds of inferior colliculus neurons in C57BL/6 and CBA mice. *J. Neurophysiol.* **56**, 391–408 (1986).
58. Lucas, E. K. *et al.* Parvalbumin deficiency and GABAergic dysfunction in mice lacking PGC-1alpha. *J. Neurosci.* **30**, 7227–35 (2010).
59. Berretta, S., Pantazopoulos, H., Markota, M., Brown, C. & Batzianouli, E. T. Losing the sugar coating: Potential impact of perineuronal net abnormalities on interneurons in schizophrenia. *Schizophr. Res.* **167**, 18–27 (2015).
60. Powell, S. B., Sejnowski, T. J. & Behrens, M. M. Behavioral and neurochemical consequences of cortical oxidative stress on parvalbumin-interneuron maturation in rodent models of schizophrenia. *Neuropharmacology* **62**, 1322–1331 (2012).
61. Shah, A. & Lodge, D. J. A loss of hippocampal perineuronal nets produces deficits

in dopamine system function: relevance to the positive symptoms of schizophrenia. *Transl. Psychiatry* **3**, e215–e215 (2013).

62. McRae, P. A., Baranov, E., Rogers, S. L. & Porter, B. E. Persistent decrease in multiple components of the perineuronal net following status epilepticus. *Eur. J. Neurosci.* **36**, 3471–3482 (2012).
63. Ethell, I. M. & Ethell, D. W. Matrix metalloproteinases in brain development and remodeling: Synaptic functions and targets. *J. Neurosci. Res.* **85**, 2813–2823 (2007).
64. Reinhard, S. M., Razak, K. & Ethell, I. M. A delicate balance: role of MMP-9 in brain development and pathophysiology of neurodevelopmental disorders. *Front. Cell. Neurosci.* **9**, 280 (2015).

## Conclusions

The pallid bat sound localization studies described in this dissertation build on previous work aimed at understanding how external sound source location are encoded internally. In addition, these studies provide valuable insight into how the mechanisms underlying sound localization behavior can be tested in future studies.

In order to understand mechanisms for sound source encoding within the CNS, one needs to understand the stimuli being input to the CNS from various sound sources. Thus, we described how the ear shapes incoming sounds, by acting as a space-specific filter on a broad bandwidth of relevant frequencies in Chapter 2. More specifically, we find that the tragus of the pallid bat external ear is responsible for generating the correlation between spectral notch frequency and elevation. Future studies aim to assess behavior on an elevation localization task to determine whether the tragus is necessary for sound source perception too.

Chapter 3 of this dissertation delves into the sound localization behavior of the pallid bat. This series of experiments has yielded a controlled setting in which sound localization performance can be measured. A novel impact of this experimental paradigm lies in the ability to measure head position, so that the incoming sound source is a known variable. With this level of control over the incoming sound stimulus, we are able to say with certainty that pallid bats are excellent sound localizers, exhibiting an acuity of  $\sim 4^\circ$  near the midline, which is better than most mammals tested. While the pallid bat ear provided a broad low-frequency (5-20 kHz) gain (Chapter 2), pallid bats required

significant energy in the higher frequency bandwidth (20-30 kHz) for best localization performance. This corresponds well with the directional properties of the external ear, indicating that the significant directionality for frequencies in this bandwidth is useful to a bat while localizing.

In Chapter 4, the putative mechanisms underlying sound source encoding at the level of the cortex are described. Previous work had characterized the azimuth selectivity of noise-selective region (NSR) neurons in the pallid bat auditory cortex and found that the azimuthal sound source could be encoded in the extent of active cortical area. Results from measurements of spatial receptive fields (SRFs), testing for the 2D selectivity of NSR neurons, found that the characteristic frequency of the NSR neuron predicted the elevation of the sound source. The same population of neurons that become increasingly active with more contralateral sound sources was found to be constrained by the elevation (or, presumably, the frequency content) of the sound source. The proposed model can now be tested with novel genetic techniques that have only recently become available.

With the controlled assessment of sound localization performance described in Chapter 3, we can begin considering manipulations to the cortical maps to determine their contributions to pallid bat behavior. In Chapter 5 of this dissertation, we describe preliminary data indicating the validity of using the inhibitory DREADDs system in pallid bats. AAVs have been utilized in several mammalian species but had not yet been characterized in any bat species. Here, we show that several AAV serotypes exhibit robust expression of their genetic material. We also show that the GFAP molecule is effective at labelling astrocytes in the pallid bat auditory cortex, a necessary step to show

that AAV product expression is being properly controlled to the appropriate cells. In one bat, we also showed successful expression of hM4D(Gi), the inhibitory DREADD. Future studies will focus on expression of this DREADD within subpopulations of the NSR region. By reversibly inhibiting only the low- or high-frequency neurons, or only the peaked or binaurally inhibited neurons (described in Chapter 1 and 4 in detail), we can systematically test the model of bicoordinate sound encoding and localization.

Before starting the series of investigations into pallid bat sound localization, I carried out an analysis of the age-related changes into inhibitory network structures in the auditory cortex of two different mice strains. CBA mice and C57 mice were compared to distinguish the effects of accelerated and normal age-related hearing loss on CNS structural changes. Specifically, inhibitory network markers, parvalbumin (PV) and perineuronal nets (PNN), were counted and measured for intensity in both strains at three different age groups. We found that mice undergoing accelerated hearing loss (C57) show deficits in both the number of all inhibitory network structures and in cortical PNN intensity, while mice undergoing normal aging (CBA) only exhibit a decline in the number of PNN cells. Because PNNs may provide a protective effect to the PV cells they surround, these changes may lead to the altered inhibition observed with age. Our findings also suggest that the age-related deterioration of the sensory epithelium exacerbates these effects dramatically. Future studies aimed at testing these hypotheses will electrophysiologically characterize PV cells with and without PNNs following hearing loss.